



## City Research Online

### City, University of London Institutional Repository

---

**Citation:** Brittain, R. H. (1988). An investigation of non-uniformly excited, wide-band, ultrasonic transducers. (Unpublished Doctoral thesis, The City University)

This is the accepted version of the paper.

This version of the publication may differ from the final published version.

---

**Permanent repository link:** <https://openaccess.city.ac.uk/id/eprint/34303/>

**Link to published version:**

**Copyright:** City Research Online aims to make research outputs of City, University of London available to a wider audience. Copyright and Moral Rights remain with the author(s) and/or copyright holders. URLs from City Research Online may be freely distributed and linked to.

**Reuse:** Copies of full items can be used for personal research or study, educational, or not-for-profit purposes without prior permission or charge. Provided that the authors, title and full bibliographic details are credited, a hyperlink and/or URL is given for the original metadata page and the content is not changed in any way.

CONTENTS

	<u>PAGE</u>
LIST OF TABLES	5
LIST OF FIGURES	6
ACKNOWLEDGEMENTS	15
COPYRIGHT	16
ABSTRACT	17
LIST OF SYMBOLS	18
LIST OF ABBREVIATIONS	23
GLOSSARY OF TERMS AS USED IN THIS THESIS	25
INTRODUCTION	27
CHAPTER 1 PIEZOELECTRIC TRANSDUCERS	31
1.1 Ferroelectricity	34
1.2 Piezoelectric ceramics	38
1.2.1 Piezoelectricity	39
1.2.2 Electro-mechanical coupling	44
1.3 Lead Zirconate Titanate $Pb(Ti,Zr)O_3$ (PZT)	43
1.4 Lead (Zr) Niobate $Pb(Zr,Nb)O_3$ (PZN)	51
1.5 Production of ceramics	56
1.6 Applications	60
CHAPTER 2 ULTRASONIC TRANSDUCERS	60
2.1 Transducer Models	62
2.1.1 RLC equivalent circuit model	63
2.1.2 Plane-wave model	66
2.2 Impulse Response Method	68
2.2.1 Graded solutions	72
2.2.2 Principle of reciprocity	74
2.3 Non-Uniformly Excited Sources	76
2.3.1 Plane-wave only (PW) sources	78
2.3.2 Edge-wave only (EW) sources	80
2.4 Practical Wide-Band Transducers	83

A thesis submitted for the degree of

DOCTOR OF PHILOSOPHY

at

THE CITY UNIVERSITY

(London)

School of Electrical Engineering and Applied Physics

(Department of Physics)

CONTENTS

	<u>PAGE</u>
LIST OF TABLES	5
LIST OF FIGURES	6
ACKNOWLEDGEMENTS	15
COPYRIGHT DECLARATION	16
ABSTRACT	17
LIST OF SYMBOLS	18
LIST OF ABBREVIATIONS	23
GLOSSARY OF TERMS AS USED IN THE THESIS	25
INTRODUCTION	27
CHAPTER 1 PIEZOELECTRIC CERAMICS	31
1.1 Ferroelectricity	34
1.2 Piezoelectric Ceramics	38
1.2.1 Piezoelectric relations	39
1.2.2 Electromechanical coupling	44
1.3 Lead Zirconate Titanate $\text{Pb}(\text{Ti}, \text{Zr})\text{O}_3$ (PZT)	48
1.4 Lead (meta) Niobate $\text{PbNb}_2\text{O}_6$ (PMN)	51
1.5 Production of Ceramics	56
CHAPTER 2 ULTRASONIC TRANSDUCERS	60
2.1 Transducer Models	62
2.1.1 KLM equivalent circuit model	63
2.1.2 Plane- and edge-wave model	66
2.2 Impulse Response Method	68
2.2.1 Graphical solutions	72
2.2.2 Principle of reciprocity	74
2.3 Non-Uniformly Excited Sources	76
2.3.1 Plane-wave only (PWO) sources	78
2.3.2 Edge-wave only (EWO) sources	80
2.4 Practical Wide-Band Transducers	83

CHAPTER 3 EXPERIMENTAL METHODS	87
3.1 Electromechanical Coupling Measurement	88
3.2 Photofabrication of electrode patterns	89
3.3 Poling Apparatus	94
3.4 Transmitting Transducers	99
3.5 Excitation and Receiving System	107
CHAPTER 4 RESULTS	110
4.1 Computer Calculated Results	111
4.1.1 Pressure waveforms and spectra for circular transducers	114
4.1.2 Transmit-receive mode responses and spectra for circular transducers	116
4.1.3 Pressure beam profiles for circular transducers	118
4.1.4 Transmit-receive mode beam profiles for circular transducers	120
4.2 Poling and Fabrication of Transducers	122
4.2.1 Thermal depoling of piezoelectric ceramics	123
4.2.2 Resistance-temperature characteristics of piezoelectric ceramics	125
4.2.3 Poling and electromechanical coupling factor	127
4.2.4 Effect of backing characteristics on pulse shape and reproducibility	129
4.2.5 Calibration of miniature probes to measure electromechanical coupling factor	133
4.3 Field Measurements in Water	135
4.3.1 Pressure waveform measurements	136
4.3.2 Transmit-receive mode measurements	139
4.3.3 Beam profiles	143
4.4 B-Scan Results	147

## FURTHER WORK

## REFERENCES

- 1-1 The definitions for the direct and converse piezoelectric constants using the four main piezoelectric constants  $d, e, g,$  and  $h$ .
- 1-2 The definitions of the four main piezoelectric constants  $d, e, g,$  and  $h$  together with their mks units.
- 1-3 The piezoelectric equations of state for a ceramic disc with an infinite-fold symmetry axis.
- 1-4 The basic actions of a piezoelectric disc together with the relevant piezoelectric, elastic and dielectric constants.
- 1-5 A summary of some of the physical properties of PZT and PZN relating to their use in non-uniformly excited wide-band transducers.
- 1-6 The ideal fraction of single crystal polarization that can be realized in a ceramic.
- 2-1 Conditions of temperature, electric field strength and time used to pole transducer elements made of ceramic PZT and PZN.

## LIST OF TABLES

### Table

- 1-1 Equations for the direct and converse piezoelectric effect using the four main piezoelectric constants  $d, e, g,$  and  $h$ .
- 1-2 The definitions of the four main piezoelectric constants  $d, e, g,$  and  $h$  together with their mks units.
- 1-3 The piezoelectric equations of state for a ceramic disc with an infinite-fold symmetry axis.
- 1-4 The basic actions of a piezoelectric disc together with the relevant piezoelectric, elastic and dielectric constants.
- 1-5 A summary of some of the physical properties of PZT and PMN relating to their use in non-uniformly excited wide-band transducers
- 1-6 The ideal fraction of single crystal polarization that can be realised in a ceramic
- 3-1 Conditions of temperature, electric field strength and time used to pole transducer elements made of ceramic PZT and PMN
- 3-2 The impedance of a piezoelectric resonator against frequency near a fundamental resonance showing the resonant and anti-resonant frequencies  $f_r$  and  $f_a$  respectively. The difference in these two frequencies is used to measure the electromechanical coupling factors such as  $k_p$  (Jaffe et al, 1971)
- 3-3 The planar electromechanical coupling factor ( $k_p$ ) against composition for lead zirconate-titanate (PZT). The most sensitive composition can be clearly seen in the region where there is approximately 48%  $PbZrO_3$  and 52%  $PbTiO_3$  by atomic % (Jaffe et al, 1954)
- 3-4 A schematic projection of the potassium tungsten bronze type structure on the (001) plane showing the perovskite units within the structure (Frenkel and Lewis, 1958)
- 3-5 The KIN equivalent circuit (Krimholtz et al, 1970; Lewis et al, 1971) for a circular, thickness-expander mode, transducer showing:  
a) A circular, thickness-expander mode transducer element with its major face electrodes  
b) The KIN equivalent circuit of the transducer shown in a). Note: The front and back acoustic parts represent the front and back faces of the element shown in a). Energy (either acoustic or electrical) enters or leaves the network through the ports
- 3-6 A schematic diagram showing the plane and edge-wave from a circular source. Note: The directivity of the edge-wave is not accurately represented

## LIST OF FIGURES

### FIGURE

- I-1 A schematic picture of a transmit-receive mode NDT situation showing the range resolution. One transducer is used to both send and receive pulses of ultrasound
- 1-1 A classification of the crystal classes by symmetry - only materials which possess an inherent asymmetry in their crystal structure can exhibit asymmetric properties such as ferroelectricity and piezoelectricity
- 1-2 A dielectric hysteresis loop for a ferroelectric material showing the hysteresis in the polarization-field relationship (Jona and Shirane, 1962)
- 1-3 The equivalent circuit of a piezoelectric element near a fundamental resonance (Jaffe et al, 1971). The left hand branch of the circuit ( $R, L, C_1$ ) represents the mechanical behaviour of the element whilst the right hand branch ( $C_0$ ) represents its electrical behaviour. These two branches are connected in parallel where:-  
R represents the mechanical damping of the element  
L represents the mass of the element  
 $C_1$  represents the elastic compliance of the element  
 $C_0$  represents the electrical capacitance of the element
- 1-4 The impedance of a piezoelectric resonator against frequency near a fundamental resonance showing the resonant and anti-resonant frequencies  $f_r$  and  $f_a$  respectively. The difference in these two frequencies is used to measure the electromechanical coupling factors such as  $k_p$  (Jaffe et al, 1971)
- 1-5 The planar electromechanical coupling factor ( $k_p$ ) against composition for lead zirconate-titanate (PZT). The most sensitive composition can be clearly seen in the region where there is approximately 40%  $PbZrO_3$  and 60%  $PbTiO_3$  by atomic % (Jaffe et al, 1954)
- 1-6 A schematic projection of the potassium tungsten bronze type structure on the (001) plane showing the perovskite units within the structure (Francombe and Lewis, 1958)
- 2-1 The KLM equivalent circuit (Krimholts et al, 1970; Leedom et al, 1971) for a circular, thickness-expander mode, transducer showing:-  
a) A circular, thickness-expander mode transducer element with its major face electrodes  
b) The KLM equivalent circuit of the transducer shown in a). Note: The front and back acoustic ports represent the front and back faces of the element shown in a). Energy (either acoustic or electrical) enters or leaves the network through the ports
- 2-2 A schematic diagram showing the plane and edge-waves from a circular source. Note: The directivity of the edge-wave is not accurately represented

- 2-3 Pressure vectors and polar diagrams for diametrically opposite points on a circular EWO source (Weight, 1982a) showing the directivity of the edge-wave which compensates for the spreading of the wavefront. This results in (ideally) constant peak pressure at all axial ranges
- 2-4 The modulus of the axial pressure of a circular source under conditions of continuous excitation - the range is shown as multiples of the transducer radius  $a$  and  $a = 10\lambda$
- 2-5 The geometry of the equidistant arc on the surface of a source (Bess, 1970).  $Q'$  is the perpendicular projection of the general field point  $Q$  on the source
- 2-6 The graphical solution of the impulse-response for the axial pressure of a circular source (Robinson, 1974) showing:-
- the projection of the field point  $Q$  and the equidistant arcs at successive time intervals on the surface of the source. These are shown by  $Q'$  and the broken lines respectively
  - the velocity function
  - the velocity potential impulse response  $\phi$
  - the impulse pressure  $P_i$
  - the pressure found by convolving the impulse pressure from d) with the velocity function from b) i.e.  $P = P_i * v(t)$
- 2-7 The graphical solution of the impulse-response for the pressure at a point in the geometrical beam region of a circular source (Robinson, 1974) showing:-
- the projection of the field point  $Q$  and the equidistant arcs at successive time intervals on the surface of the source. These are shown by  $Q'$  and the broken lines respectively
  - the velocity function
  - the velocity potential impulse response  $\phi$
  - the impulse pressure  $P_i$
  - the pressure found by convolving the impulse pressure from d) with the velocity function from b) i.e.  $P = P_i * v(t)$
- 2-8 The graphical solution of the impulse-response for the pressure at a point outside the geometrical beam region of a circular source (Robinson, 1974) showing:-
- the projection of the field point  $Q$  and the equidistant arcs at successive time intervals on the surface of the source. These are shown by  $Q'$  and the broken lines respectively
  - the velocity function
  - the velocity potential impulse response  $\phi$
  - the impulse pressure  $P_i$
  - the pressure found by convolving the impulse pressure from d) with the velocity function from b) i.e.  $P = P_i * v(t)$
- 2-9 The form of velocity weighting function required to produce a PWO transducer. The function is a form of shifted cosine "bell" (Weight, 1982b)
- 2-10 The form of piezoelectric apodisation required to produce an EWO transducer. The excitation falls off from a maximum at the outer edge of the element to nothing a small distance in from the edge in a smooth Gaussian fashion (Weight, 1982a)

- 2-11 The time-base waveforms for a linear display of target range (Weight, 1982b) using:-  
 a) a conventional transducer  
 b) an EWO transducer
- 2-12 A schematic view of the near field of a circular, ceramic transducer showing the head waves
- 3-1 The circuit for measuring the planar Electromechanical coupling factor ( $k_p$ ) of a piezoelectric, ceramic disc in accordance with the standards of the IEEE (1978)
- 3-2 A vacuum operated jig used for holding thin ceramic elements by their back faces whilst aligning the masks on the photoresist coated front faces for exposure to UV light
- 3-3 The jig used for handling ceramic elements by their edges whilst developing the photoresist pattern on one of their major faces - based on devices used during the manufacture of integrated circuits to hold the silicon wafers
- 3-4 A schematic diagram of the temperature controlled oil bath used for poling ceramic elements during the fabrication of non-uniformly excited transducers
- 3-5 The jig used during poling to apply the poling potential(s) to the transducer elements and provide strain relief so that the wires carrying these potential(s) did not detach areas of the transducer electrode
- 3-6 The centrifuging jig used to apply the tungsten loaded epoxy resin backing to the ceramic element during the fabrication of wide-band transducers
- 3-7 A schematic illustration of a typical wide-band transducer showing the backing applied to prevent the element from resonating and the layer applied to the front face for protection and matching
- 3-8 A schematic illustration of the wide-band, excitation and receiving system used to make measurements of the pressure waveforms, transmit-receive responses and associated spectra of both conventional, uniformly excited transducers and non-uniformly excited transducers
- 4-1 Using the principal of superposition any axisymmetrically non-uniform source can be considered to be made up from the sum or difference of a number of concentric circular sources with various radii moving in phase but with different amplitudes. For example:-  
 a) a simple annular excitation built up by subtraction of one source from another  
 b) a stepwise approximation to a curve built up by the addition of several small sources

- 4-2 Points in the field of a circular source where calculated or measured results were made. These points are described by their range and distance off axis. At each point the result given has its axes (i.e. pressure or transducer output against time or frequency) superimposed on the grid. The axisymmetrical nature of a circular source means that the results in this plane alone are enough to fully describe the field of the source
- 4-3 Computer calculated results at points in the field of an ideal, uniformly-excited transducer radiating a short pulse into water showing:-  
a) pressure waveforms b) pressure spectra
- 4-4 Computer calculated results at points in the field of a non-uniformly excited PWO type transducer radiating a short pulse into water showing:-  
a) pressure waveforms b) pressure spectra
- 4-5 Computer calculated results at points in the field of an ideal EWO type transducer radiating a short pulse into water showing:-  
a) pressure waveforms b) pressure spectra
- 4-6 Computer calculated results at points in the field of an annular EWO type transducer radiating a short pulse into water showing:-  
a) pressure waveforms b) pressure spectra
- 4-7 Computer calculated results at points in the field of a non-uniformly excited, EWO type transducer radiating a short pulse into water showing:-  
a) pressure waveforms b) pressure spectra
- 4-8 Computer calculated transmit-receive mode results for an ideal, uniformly excited transducer interrogating a small target in water showing:-  
a) transmit-receive mode responses  
b) transmit-receive mode spectra
- 4-9 A schematic representation of the transmit-receive mode responses produced by transducers with various excitations interrogating a small (point-like), axial target in the near field in water for:-  
a) a conventional, uniformly-excited transducer  
b) a non-uniformly-excited PWO type transducer  
c) a non-uniformly-excited EWO type transducer
- 4-10 Computer calculated transmit-receive mode results for a non-uniformly excited PWO type transducer interrogating a small target in water showing:-  
a) transmit-receive mode responses  
b) transmit-receive mode spectra
- 4-11 Computer calculated transmit-receive mode results for an ideal EWO type transducer interrogating a small target in water showing:-  
a) transmit-receive mode responses  
b) transmit-receive mode spectra

- 4-12 Computer calculated transmit-receive mode results for an annular EWO type transducer interrogating a small target in water showing:-  
 a) transmit-receive mode responses  
 b) transmit-receive mode spectra
- 4-13 Computer calculated transmit-receive mode results for a non-uniformly excited EWO type transducer interrogating a small target in water showing:-  
 a) transmit-receive mode responses  
 b) transmit-receive mode spectra
- 4-14 Computer calculated pressure beam profiles for an ideal, uniformly-excited transducer, radiating a short pulse into water
- 4-15 Computer calculated pressure beam profiles for a non-uniformly excited, PWO type transducer, radiating a short pulse into water
- 4-16 Computer calculated pressure beam profiles for an ideal, EWO type transducer, radiating a short pulse into water
- 4-17 Computer calculated pressure beam profiles for an annular, EWO type transducer, radiating a short pulse into water
- 4-18 Computer calculated pressure beam profiles for a non-uniformly excited, EWO type transducer, radiating a short pulse into water
- 4-19 Computer calculated transmit-receive mode beam profiles for an ideal, uniformly excited transducer, interrogating a small target in water
- 4-20 Computer calculated transmit-receive mode beam profiles for a non-uniformly excited, PWO type transducer, interrogating a small target in water
- 4-21 Computer calculated transmit-receive mode beam profiles for an ideal, EWO type transducer, interrogating a small target in water
- 4-22 Computer calculated transmit-receive mode beam profiles for an annular, EWO type transducer, interrogating a small target in water
- 4-23 Computer calculated transmit-receive mode beam profiles for a non-uniformly excited, EWO type transducer, interrogating a small target in water
- 4-24 Planar electromechanical coupling factor( $k_p$ ) against depoling temperature for PZT ceramic (type PC5)
- 4-25 Resistance against temperature for a sample of PZT (type PC5) 15mm in diameter by 10MHz equivalent thickness
- 4-26 Resistance against temperature for a sample of PMN (type K83) 20mm in diameter by 10MHz equivalent thickness
- 4-27 Resistivity against temperature for PZT (type PC5)

- 4-28 Resistivity against temperature for PMN (type K83)
- 4-29 Resistivity against temperature for PZT (type PC5) and PMN (type K83)
- 4-30 Resistance against area for PMN 10MHz thickness (type K83)
- 4-31 Planar electromechanical coupling factor ( $k_p$ ) against poling field for PZT (type PC5) under conditions of constant poling temperature and time (150°C and 20 minutes respectively)
- 4-32 Transmit-receive mode responses and spectra for PZT transducers (type PC5, 19mm diameter by 5MHz equivalent thickness) with various backings at a range of 20mm from a large, plane, aluminium-reflector in water showing the effect of backing characteristics on pulse shape for:-
- a soft backing (90% CY208 resin and 10% MY750 by volume)
  - a medium hard backing (equal parts of resins CY208 and MY750 by volume)
  - a hard backing (10% CY208 resin and 90% MY750 by volume)
- 4-33 Transmit-receive mode responses and spectra for transducers (19mm diameter by 5MHz equivalent thickness) at a range of 20mm from a large, plane, aluminium-reflector in water showing the pulse shape for:-
- a PZT transducer with a medium hard backing (equal parts of resins CY208 and MY750 by volume)
  - a high quality commercial transducer made of PMN
  - is the pressure spectrum of b) shown at greater magnification to emphasise the shape of the frequency response
- 4-34 Transmit-receive mode responses and spectra for two PZT transducers (type PC5 19mm diameter by 5MHz equivalent thickness) made by identical methods but in different batches at a range of 20mm from a large, plane aluminium-reflector in water demonstrating reproducibility of pulse shape for:-
- the transducer from batch 1 (with a medium hard backing)
  - the transducer from batch 2 (with a medium hard backing)
- 4-35 Transmit-receive mode responses and spectra for PMN transducers (type K83, 19mm diameter by 10MHz equivalent thickness) with various backings at a range of 20mm from a large, plane, aluminium-reflector in water showing the effect of backing characteristics on pulse shape for:-
- a soft backing (90% CY208 resin and 10% MY750 by volume)
  - a medium hard backing (equal parts of resins CY208 and MY750 by volume)
  - a hard backing (10% CY208 resin and 90% MY750 by volume)
- 4-36 Transmit-receive mode responses and spectra for two PMN transducers (type K83 19mm diameter by 10MHz equivalent thickness) made by identical methods but in different batches at a range of 20mm from a large, plane aluminium-reflector in water demonstrating reproducibility of pulse shape for:-
- the transducer from batch 1 (with a medium hard backing)
  - the transducer from batch 2 (with a medium hard backing)

- 4-37 Transmit-receive mode responses and spectra for PMN transducers (type K83, 19mm diameter by 10MHz equivalent thickness) with various backings at a range of 20mm from a large, plane, aluminium-reflector in water showing the effect of backing characteristics on pulse shape for:-
- a soft backing (90% CY208 resin and 10% MY750 by volume)
  - a medium hard backing (equal parts of resins CY208 and MY750 by volume)
  - a hard backing (10% CY208 resin and 90% MY750 by volume)
  - a high quality commercial transducer made of PMN
- 4-38 Acoustic pressure as measured by a miniature receiving probe in water against electromechanical coupling factor for PZT
- 4-39 Acoustic pressure as measured by a miniature receiving probe in water against poling field for PZT (type PC5) under conditions of constant poling temperature and time (150°C and 20 minutes respectively)
- 4-40 Pressure waveforms and spectra measured on the axis of a conventional, uniformly-excited, circular transducer 19mm diameter by 10MHz equivalent thickness (Panametrics V3289) with a miniature (point-like) receiver in water at ranges of:-
- 20mm
  - 60mm
  - 100mm
  - 140mm
- 4-41 Pressure waveforms and spectra measured on the axis of an EWO transducer 19mm diameter by 10MHz equivalent thickness) with a miniature (point-like) receiver in water at ranges of:-
- 20mm
  - 60mm
  - 100mm
  - 140mm
- 4-42 Axial Pressure waveforms for a conventional, uniformly-excited, circular transducer and an EWO transducer (both 19mm diameter by 10MHz equivalent thickness) made with a miniature (point-like) receiver in water at ranges of:-
- 20mm
  - 60mm
  - 100mm
  - 140mm
- 4-43 Pressure waveforms and spectra measured 2mm off the axis of a conventional, uniformly-excited, circular transducer, 19mm diameter by 10MHz equivalent thickness (Panametrics V3289) with a miniature (point-like) receiver in water at ranges of:-
- 20mm
  - 60mm
  - 100mm
  - 140mm
- 4-44 Pressure waveforms and spectra measured 2mm off the axis of an EWO transducer, 19mm diameter by 10MHz equivalent thickness with a miniature (point-like) receiver in water at ranges of:-
- 20mm
  - 60mm
  - 100mm
  - 140mm
- 4-45 Pressure waveforms 2mm off axis for a conventional, uniformly-excited, circular transducer and an EWO transducer (both 19mm diameter by 10MHz equivalent thickness) made with a miniature (point-like) receiver in water at ranges of:-
- 20mm
  - 60mm
  - 100mm
  - 140mm

- 4-46 Transmit-receive mode responses and spectra for a conventional, uniformly-excited, circular transducer (19mm diameter by 10MHz equivalent thickness) interrogating a small brass target approximately 0.8mm in diameter in water at axial ranges of:-  
 a) 20mm b) 60mm c) 100mm d) 140mm
- 4-47 Transmit-receive mode responses and spectra for an EWO transducer (19mm diameter by 10MHz equivalent thickness) interrogating a small brass target approximately 0.8mm in diameter in water at axial ranges of:-  
 a) 20mm b) 60mm c) 100mm d) 140mm
- 4-48 Axial transmit-receive mode responses for a conventional, uniformly-excited, circular transducer and an EWO transducer (both 19mm diameter by 10MHz equivalent thickness) interrogating a small brass target approximately 0.8mm in diameter in water at ranges of:-  
 a) 20mm b) 60mm c) 100mm d) 140mm
- 4-49 Transmit-receive mode responses and spectra for a conventional, uniformly-excited, circular transducer (19mm diameter by 10MHz equivalent thickness) interrogating a small brass target approximately 0.8mm in diameter 2mm off axis in water at ranges of:-  
 a) 20mm b) 60mm c) 100mm d) 140mm
- 4-50 Transmit-receive mode responses and spectra for an EWO transducer (19mm diameter by 10MHz equivalent thickness) interrogating a small brass target approximately 0.8mm in diameter in water 2mm off axis at ranges of:-  
 a) 20mm b) 60mm c) 100mm d) 140mm
- 4-51 Transmit-receive mode responses 2mm off the axis of a conventional, uniformly-excited, circular transducer and an EWO transducer (both 19mm diameter by 10MHz equivalent thickness) interrogating a small brass target approximately 0.8mm in diameter in water at ranges of:-  
 a) 20mm b) 60mm c) 100mm d) 140mm
- 4-52 The electrode patterns and poling fields used in an early attempt (at the beginning of this project) to produce non-uniform excitation in the form of:-  
 a) a simple, step-like annulus at the edge of a disc of PZT  
 b) a simple step in the centre of a disc of PZT
- 4-53 Beam profiles, electrode patterns and poling fields for non-uniformly excited PZT transducers 15mm diameter by 5MHz equivalent thickness:-  
 a) a simple EWO b) a simple PWO  
 c) a step-wise approximation to an EWO  
 d) a step-wise approximation to a PWO
- 4-54 Results for a non-uniformly excited, EWO type transducer, 19mm diameter by 10MHz equivalent thickness made of PMN (type K83), showing:-  
 a) beam profile b) electrode pattern c) poling field

- 4-55 Measured pressure beam profiles at various ranges in water for a non-uniformly excited, EWO type transducer, 19mm in diameter by 10MHz equivalent thickness made of PMN (type K83)
- 4-56 Measured and calculated pressure beam profiles at various ranges in water for a non-uniformly excited, EWO type transducer:-  
 a) measured      b) calculated
- 4-57 Measured transmit-receive mode beam profiles at various ranges in water for a non-uniformly excited, EWO type transducer, 19mm in diameter by 10MHz equivalent thickness made of PMN type (K83)
- 4-58 Measured and calculated transmit-receive mode, beam profiles at various ranges in water from a small (point-like) target for a non-uniformly excited, EWO type transducer:-  
 a) measured      b) calculated
- 4-59 To scale schematic of the target imaged in the B-scans shown in figure 4-60
- 4-60 B-scan images of a number of 2mm diameter, flat-bottomed holes drilled into a block of mild steel imaged in water with:-  
 a) a conventional transducer of 13mm diameter  
 b) an EWO type transducer of 19mm diameter
- 4-61 To scale schematic of the target imaged in the B-scans shown in figure 4-62
- 4-62 B-scan images of the target shown in figure 4-61 imaged in water with:-  
 a) a conventional transducer of 13mm diameter  
 b) an EWO type transducer of 19mm diameter
- 4-63 B-scan images of a group 0.2mm diameter nylon threads, held in a plastic jig to produce a matrix pattern that gives rise to the words TCU (top row) and PHYSICS (bottom row). These are imaged in water using:-  
 a) a conventional transducer of 19mm diameter  
 b) an EWO type transducer of 19mm diameter
- 5-1 A photograph showing a non-uniformly excited, EWO type transducer, together with a uniformly-excited, top quality, commercial probe of the same diameter  
 a) a conventional, uniformly-excited, top quality, commercial probe  
 b) a non-uniformly excited EWO type transducer

### ACKNOWLEDGEMENTS

I would like to express my sincere gratitude to Professor A F Brown for supervising this project and for making it possible for me to study at The City University. Special thanks are also due to Dr J P [REDACTED] for his continuous supply of ideas and practical help.

I'am indebted to [REDACTED] for allowing me to use some of the measurements he made on the non-uniformly excited transducers which I made during the course of this work.

The encouragement and academic support received from Professor L Finkelstein the head of the Department of Physics and Dean of the School of Electrical Engineering and Applied Physics is gratefully acknowledged.

The help received from other members of the University is much appreciated, in particular [REDACTED] for his technical assistance and enthusiasm and the late [REDACTED] the Ultrasonics group technician who unfortunately did not live to see the completion of this project, for his assistance with the photography.

Financial support for this work was provided by the British Technology Group and is gratefully acknowledged.

The help received from outside sources including Brighton Polytechnic Department of Applied Physics, Middlesex Polytechnic Microelectronics Centre and Chelsea College Department of Electronics is gratefully acknowledged as are the samples kindly provided by Du Pont Chemicals Ltd, Shipley Europe Ltd and Multicore Solders Ltd amongst others.

In conclusion I would like to acknowledge the financial and moral support of my parents.



# THE CITY UNIVERSITY

Northampton Square London EC1V 0HB  
telephone: 01-253 4399 telex: 263896

SCHOOL OF ELECTRICAL ENGINEERING  
AND APPLIED PHYSICS

Dean of the School  
Professor L. Finkelstein  
Professor of Measurement and Instrumentation

### COPYRIGHT DECLARATION

I grant powers of discretion to the University Librarian to allow this thesis (AN INVESTIGATION OF NON-UNIFORMLY EXCITED, WIDE-BAND ULTRASONIC TRANSDUCERS) to be copied in whole or in part without further reference to me. This covers only single copies made for study purposes, subject to normal conditions of acknowledgment.

R H BRITTAIN



LONDON 1988

### ABSTRACT

An ultrasonic transducer converts acoustic signals into electrical signals and vice versa. Here practical attempts at fabricating non-uniformly excited, wide-band ultrasonic transducers are presented.

New transducers to directly replace conventional, uniformly-excited, wide-band transducers were produced by varying the piezoelectric excitation of transducer elements as a function of their radius i.e. apodisation. To do this it was necessary to re-examine the technology of poled ferroelectric or piezoelectric ceramics of PZT and PMN.

The construction of wide-band transducers is analysed in terms of the KLM transmission line model and their acoustic fields are described by the plane- and edge-wave model. The impulse response method is applied to transducers and useful forms of non-uniform excitation are described.

Details are given of measuring the planar electromechanical coupling factor of a piezoelectric element and of how standard photofabrication methods using photoresist were adapted to cope with the comparatively rough surfaces of ceramics working right up to and including the edges of the substrates. The poling apparatus designed to apply various poling regimes under conditions of constant temperature and time are detailed. Fabrication methods for producing wide-band transducers based on using a centrifuge to apply the required damping are given. The wide-band excitation and receiving system is described.

Computer-calculated results illustrate the effect of various types of transducer excitation ranging from the theoretical to the practically-attainable. Measured results confirm these calculations and also present some of the physical characteristics of the piezoelectric ceramics. Both uniformly and non-uniformly excited transducers are considered.

The thesis concludes that it is possible to make non-uniformly excited transducers by controlling the strength of the piezoelectric excitation within the transducer element.

**Keywords:** ultrasonic transducer, wide-band transducer, plane- and edge-wave model, non-uniform excitation, piezoelectric element, poled ferroelectric ceramics, transducer fabrication

LIST OF SYMBOLS

- a source radius
- $a_p, b_p, c_p$  lattice parameters (axes)
- A area
- $A_i, B_i$  ions
- c velocity of sound
- $c^D, c_{ij}^D$  elastic stiffness (constant dielectric displacement)
- $c^E$  elastic stiffness (constant electric field)
- $c_{ij}, c_{jh}$  elastic stiffness
- C carbon ion
- Ca calcium ion
- $C_C$  Curie constant
- $C_0$  electrical capacitance (clamped)
- $C_1$  capacitance representing mechanical compliance
- d, e, g, h piezoelectric constants
- $d_{ih}, d_{ij}, e_{ij}, g_{ij}, h_{ij}$  piezoelectric constants
- D dielectric displacement
- $D_1, D_2, D_3$  dielectric displacement in direction 1(x), 2(y) or 3(z)
- $D_m$  mechanical dissipation factor
- E electric field
- $E_1, E_2, E_3$  electric field in direction 1(x), 2(y) or 3(z)
- E(t) transducer output voltage
- $E_a$  electric field experienced
- $E_{app}$  applied electric field
- $E_C$  coercive field
- $E_i, E_i(r, t)$  impulsive receiver output voltage
- $E_{iax}(t)$  axial, impulsive receiver output voltage
- $E_p, E_p(t)$  receiver output voltage
- f frequency
- $f_a$  anti-resonant frequency

$f_m$  frequency of minimum impedance  
 $f_{max}$  maximum frequency  
 $f_n$  frequency of maximum impedance  
 $f_o$  continuous frequency  
 $f_p$  parallel resonance frequency  
 $f_r$  resonant frequency  
 $f_s$  series resonance frequency  
Fe iron ion  
h number (integer)  
H hydrogen ion  
j  $(-1)^{1/2}$   
 $J_1$  Bessel function of the first kind  
k wavenumber  
 $k_{ij}, k_f$  electromechanical coupling factor  
 $k_p$  planar electromechanical coupling factor  
 $k_t$  thickness electromechanical coupling factor  
K potassium ion  
 $K_r$  constant of proportionality  
 $K_3$  relative dielectric constant along the 3(z) axis  
l dimension (length)  
L inductance  
 $L_r$  radius of equidistant arc  
n number of dipoles per unit volume  
N nitrogen ion  
 $N_p$  number of data points  
Na sodium ion  
Nb niobium ion  
O oxygen ion  
p constant  
P,  $P(\theta)$ ,  $P(r,t)$ ,  $P(r,t,y)$  pressure

$P_{ax}$  axial pressure  
 $P_b$  lead ion  
 $P_i, P_i(r,t), P_i(r,t,y)$  impulse pressure  
 $P_{iax}(t), P_{iax}(r,t)$  axial impulse pressure  
 $P_{max}$  maximum pressure  
 $P_o$  normalising pressure  
 $P_p$  dielectric polarization  
 $P_r$  remanent polarization  
 $P_s$  saturation polarization  
 $P_w(r,t)$  pressure (weighted source)  
 $P_{wax}(r,t)$  axial pressure (weighted source)  
 $Q$  field point  
 $Q'$  projected field point  
 $Q_c$  charge  
 $Q_e$  electrical quality factor  
 $Q_m$  mechanical quality factor  
 $r$  range  
 $R$  electrical resistance  
 $R_{Ai}, R_{Bi}, R_o$  ionic radii  
 $R_{bk}$  equivalent mechanical load (back face)  
 $R_{ft}$  equivalent mechanical load (front face)  
 $R_{opt}$  optimum equivalent mechanical load  
 $R_t$  terminating resistance  
 $s$  constant of proportionality (area)  
 $s_{ij}^D, s^D$  elastic compliance (constant dielectric displacement)  
 $s_{ij}^E, s^E$  elastic compliance (constant electric field)  
 $s_{ij}, s_{ji}$  elastic compliance  
 $S$  strain  
 $S_1, S_2, S_3$  strain in direction 1(x), 2(y) or 3(z)  
 $Si$  silicon

$t$  time  
 $t_G$  Goldschmitt (1926) tolerance factor  
 $T$  stress  
 $T_C$  Curie point  
 $T_1, T_2, T_3$  stress in direction 1(x), 2(y) or 3(z)  
 $T_4, T_5, T_6$  stress in the 4(yz), 5(xz) or 6(xy) plane  
 $T_i$  titanium ions  
 $T_O$  Curie-Weiss Temperature  
 $T_P$  temperature  
 $v$  velocity  
 $\underline{v}$  particle velocity  
 $v(t), v(y), v(t,y)$  velocity function  
 $v_r(t), v_r(t - r/c)$  radial velocity  
 $v_n$  normal velocity  
 $v_O$  maximum velocity  
 $v_{sw}$  surface wave velocity  
 $V_1, V_2$  force  
 $V(t)$  time-base voltage waveform  
 $W$  tungsten ion  
 $x$  axial range  
 $X_S$  reactance (series)  
 $y$  distance off axis (radial)  
 $y_u$  initial distance (radial)  
 $y_v$  final distance (radial)  
 $Z$  impedance  
 $Z_O$  characteristic impedance  
 $Zr$  zirconium ion  
 $\alpha$  atomic polarizability  
 $\gamma$  constant  
 $\delta$  delta function

$\delta f$  frequency interval  
 $\delta t$  time interval  
 $\epsilon_{ij}$  absolute permittivity  
 $\epsilon_0$  permittivity of a vacuum  
 $\epsilon_r$  relative permittivity  
 $\epsilon^S$  permittivity (constant strain)  
 $\epsilon_3^S$  permittivity (constant strain) in the 3(z) direction  
 $\epsilon^T$  permittivity (constant stress)  
 $\epsilon_1^T, \epsilon_3^T$  permittivity (constant stress) in direction 1(x) or 3(z)  
 $\epsilon_1, \epsilon_2, \epsilon_3$  permittivity in direction 1(x), 2(y) or 3(z)  
 $\theta$  angle  
 $\lambda$  wavelength  
 $\pi$  constant  
 $\rho$  density  
 $\sigma$  Poisson's cross contraction ratio  
 $\Sigma$  summation  
 $\tau, \tau(y)$  delay time  
 $\tau_e$  delay time (edge-wave)  
 $\phi, \phi(r,t)$  velocity potential  
 $\phi_i, \phi_i(r,t)$  velocity potential impulse response  
 $\psi$  frequency dependent turns ratio  
 $\omega$  angular frequency  
 $\omega_0$  resonant angular frequency  
 $\Omega(r)$  included angle of equidistant arc  
 $\nabla$  grad

LIST OF ABBREVIATIONS

ac	alternating current
ADP	ammonium dihydrogen phosphate
BNC	bayonet nut connector
BTG	British technology group
cm	centimetre
cw	continuous wave
dB	decibel
dc	direct current
DVM	digital voltmeter
eht	extra high tension
EWO	edge-wave only
FFT	fast Fourier transform
IC	integrated circuit
IEEE	Institution of Electrical and Electronic Engineers
kpps	kilo pulses per second
kHz	kiloHertz
kV	kilovolt
k $\Omega$	kilohm
KDP	potassium dihydrogen phosphate
KLM	Krimholtz, Leedom and Mathaei
led	light emitting diode
mks	metres kilograms seconds
ml	millilitre
mm	millimetre
ms	millisecond
mV	millivolt
MHz	Megahertz
MOSFET	metal-oxide semiconductor field-effect transistor
NDT	non-destructive testing

ns	nanosecond
pF	picofarad
pp	peak to peak
ppm	parts per million
PCB	printed circuit board
PMN	lead meta niobate
PRF	pulse repetition frequency
PTFE	polytetrafluoroethylene
PVDF	poly(vinylidene flouride)
PWO	plane-wave only
PZT	lead zirconate-titanate
rf	radio frequency
rms	root mean square
rpm	revolutions per minute
swg	standard wire gauge
SAW	surface acoustic wave
THD	total harmonic distortion
TTL	transistor-transistor logic
UV	ultra violet
UK	United Kingdom
USA	United States of America
USSR	United Soviet Socialist Republics
$\mu$ s	microsecond
$^{\circ}$ C	degrees Celsius

GLOSSARY OF TERMS AS USED IN THE THESIS

- Apodisation - varying the strength of excitation of a circular acoustic source as a function of its radius.
- Calcination - heating of solids to an elevated temperature below their melting point to bring about thermal decomposition and/or recombination or phase transitions other than melting
- Ceramic - a material consisting of an agglomeration of many fine particles of a substance formed by sintering.
- Edge-wave - a toroidal wave with a special directivity pattern and phase relationship with the plane-wave (where present). In terms of rays it appears to emanate from the edge of the source but in fact is made up of all the Huygens-type wavelets from the whole area of the source.
- Far-field - the acoustic field at ranges of greater than approximately  $a^2/\lambda$  (for continuous waves) where Fraunhofer diffraction conditions exist.
- Ferroelectric - a substance which possess a permanent dipole moment which may be changed in direction (reversed) by an electric field. This dipole moment is due to the asymmetric arrangement of charge within the unit cell of the substance.
- Frit - a glaze consisting of very fine particles of glass and metal (silver in this case) together with some fluxes in the form of a water based paste. This is applied to the surface of ceramics and then fired to provide the conductive electrodes.
- Head-wave - a wave found in the near field of a transducer which is produced by a surface wave running across a transducer from the edge to the centre.
- Near-field - the acoustic field at ranges of less than approximately  $a^2/\lambda$  (for continuous waves) where Fresnel diffraction conditions exist.

Plane-wave - wave (often originating from the front face of a transducer) in which all points on the wavefront are in phase and possess a uniform amplitude.

Poling - inducing piezoelectric properties in ferroelectric materials by the application of high electric fields at elevated temperatures.

Port - an entry or exit point on an electrical network through which energy (electrical or acoustic) may be feed or withdrawn

Sintered - formed into a coherent body from many fine particles of a substance which have been compacted together and then subjected to an elevated temperature below their melting point.

Transducer - a device for converting a non-electrical signals (such as ultrasound) into an electrical signal or vice versa

## INTRODUCTION

Uniformly-excited, circular, ultrasonic transducers are used in a vast majority of applications. The pulse-echo technique is commonly employed in ultrasonic non-destructive testing (NDT) and medical diagnostics. This technique utilizes one ultrasonic transducer to both send and receive pulses of ultrasound. Figure I-1 illustrates the technique where the transducer is directly coupled to a block of material containing a crack.

When conventional, uniformly-excited transducers are used in this application it is possible to get an accurate idea of the depth of the crack, as the range resolution is primarily controlled and limited by the duration of the pulse. This is illustrated in figure I-1. However, it is very difficult to relate the amplitude of the reflections shown on the display to the lateral dimensions of the crack. There are two reasons for this:- firstly, the lateral resolution of the transducer is of the order of its diameter (for a circular transducer) and secondly, the amplitude of the pulse produced by the transducer changes with range, making image processing much more difficult.

At present, the best attempts at solving these problems use either small transducers, which suffer from reduced sensitivity and increased beam divergence or focussed transducers and arrays, which have a complicated construction and only work well at, or near, their particular focal length. What is really needed are transducers which produce pulses of short duration and with (ideally) constant amplitude at all ranges.

The variations in the amplitude and shape of the pulses produced by a uniformly excited transducer can be explained in terms of two components which emanate from the transducer. These may be considered to originate from the face and edge of the transducer respectively though both, in fact, consist of the sum of all the Huygens-type

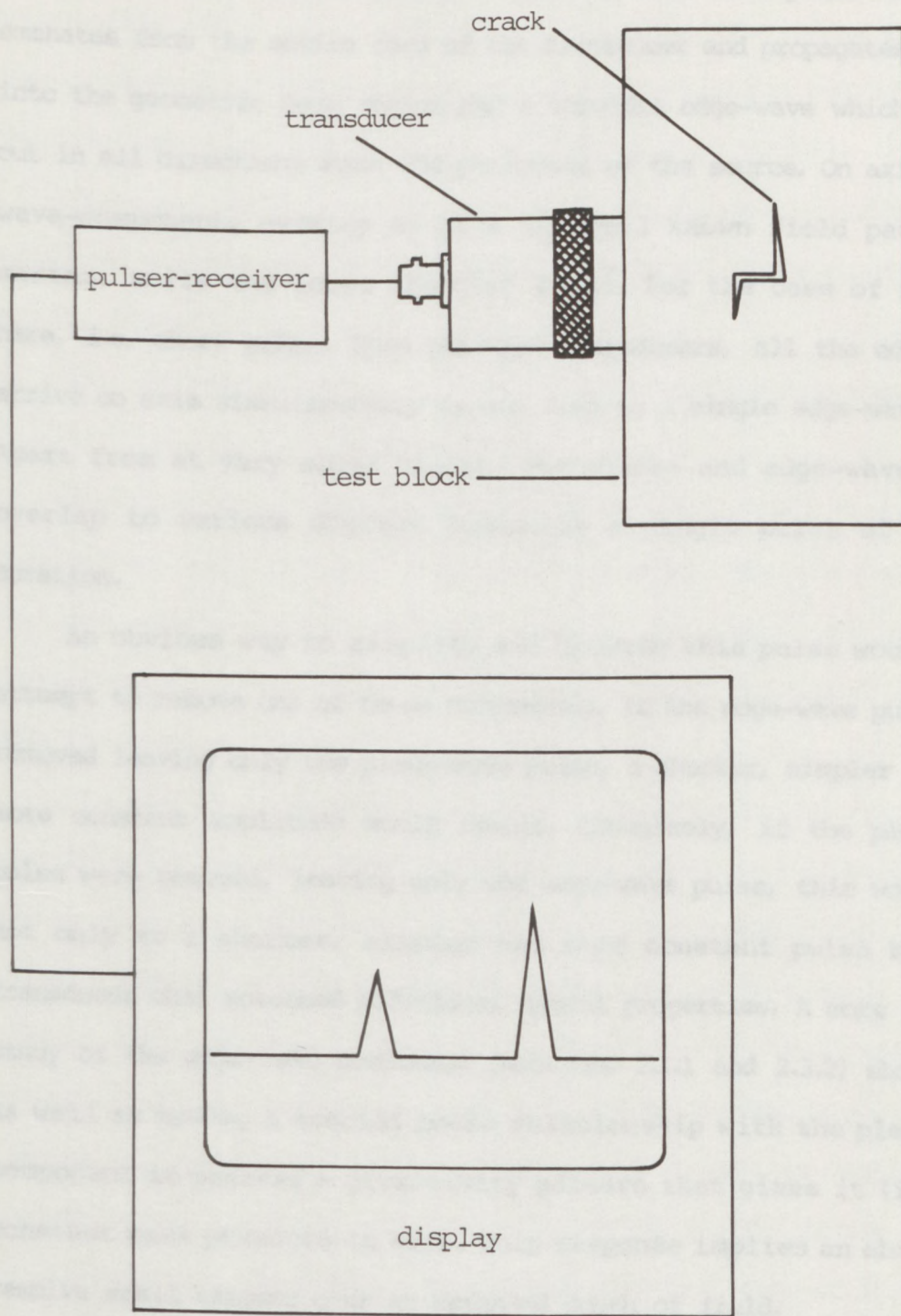


**Figure I-1** A schematic picture of a transmit-receive mode NDT situation showing the range resolution. One transducer is used to both send and receive pulses of ultrasound

wavelets from the whole face of the transducer. In the case of continuous waves these components take the form of a plane-wave which emanates from the entire face of the transducer and propagates forward into the geometric beam region and a toroidal edge-wave which spreads out in all directions from the perimeter of the source. On axis, these wave-components overlap to give the well known field pattern of maxima, nulls and lobes (section 2.1.1). For the case of interest here, i.e. short pulses from circular transducers, all the edge-waves arrive on axis simultaneously giving rise to a single edge-wave pulse. Apart from at very close ranges, the plane- and edge-wave pulses overlap to various degrees producing a single pulse of varying duration.

An obvious way to simplify and shorten this pulse would be to attempt to remove one of these components. If the edge-wave pulse were removed leaving only the plane-wave pulse, a shorter, simpler pulse of more constant amplitude would result. Conversely, if the plane-wave pulse were removed, leaving only the edge-wave pulse, this would lead not only to a shorter, simpler and more constant pulse but to a transducer that possessed additional useful properties. A more detailed study of the edge-wave component (sections 2.1.1 and 2.3.2) shows that as well as having a special phase relationship with the plane-wave component it possess a directivity pattern that gives it (ideally) constant peak pressure on axis. This response implies an ability to resolve small targets over an extended depth of field.

The fabrication of transducers with predominantly plane- or edge-wave only characteristics depends upon being able to produce a controlled, axisymmetrical variation in the excitation of the transducer element. This process is known as apodising. As both the plane- and edge-wave components are made up of the sum of all the wavelets from the whole face of the transducer it is impossible to

remove either component completely by this method. However, by varying the excitation of a transducer as a function of its radius it should be possible to reduce drastically the relative size of either of these components. The exact nature of the variation required to do this is discussed in chapter 2 (sections 2.3.1 and 2.3.2).

There are three fundamental ways in which non-uniformly excited wide-band transducers may possibly be produced. These employ one of the following:-

- (i) Shaped elements
- (ii) Apodised driving fields
- (iii) Apodised transducer elements

If shaped elements were employed (method (i)) the simple geometry of a disc element would be lost. This would probably introduce complicated resonant modes making damping (section 3.4) more difficult and precluding the use of direct coupling, the actual effect(s) depending upon which face(s) were shaped.

The use of an apodised driving field (method (ii)) implies the need for some type of divider network. This would need to be placed in series with the electrical connection to the transducer. It could be placed either between the driving signal and the back face or "hot" side of the transducer or between the front face or "cold" side of the transducer and the common or earth side of the driving signal. As the damping in contact with the back face of the element is nearly always conductive due to the high density of tungsten there (section 3.4), it is unlikely that any attempt to apodise the "hot" side of the driving field would be successful. The front face of the transducer is generally connected to earth for safety and screening purposes. Therefore, the insertion of a network between this face and earth would probably lead to the capacitive coupling of unwanted r.f. noise into the high-impedance, high-gain, wide-band electronics used with this type of transducer. A transducer of this construction would also

be unsuitable for use in contact applications

Method (iii) relies upon altering the sensitivity of a transducer element. This is possible as the elements are in fact isotropic ceramics of a ferroelectric material (sections 1.1 and 1.2) which are rendered piezoelectric by poling (sections 1.5 and 3.3). This involves subjecting the isotropic ceramic to high d.c. fields at an elevated temperature. The degree of poling achieved in a given time depends upon temperature and applied field. By maintaining suitable conditions of time and temperature the degree of poling effectively becomes a function of applied field alone. Using the high quality electrodes supplied on the elements it should be possible to produce various step-wise approximations to the required poling regimes.

These considerations effectively leave method (iii) as the only practicable option. This method therefore formed the basis of the work reported in this project. The object of this work was to fabricate non-uniformly excited wide-band ultrasonic transducers using non-uniformly polarized, piezoceramic elements and to see whether they possessed the properties predicted by the plane- and edge-wave model.

## CHAPTER 1

### PIEZOELECTRIC CERAMICS

In order to fabricate non-uniformly excited, wide-band, ultrasonic transducers it was necessary to re-examine the technology of poled ferroelectric or piezoelectric ceramics from which they are commonly constructed. The results of this work are collected together in this chapter.

The piezoelectric effect is the phenomenon whereby charges appear on the surface of certain substances in response to the mechanical strain produced by the application of external stress. The same materials exhibit the converse effect in that they experience strain (deformation) under the influence of an applied electric field. The charge or strain produced is directly proportional in magnitude and sense to the stress or electric field applied, provided that the material is not strained beyond its elastic limit.

The piezoelectric effect was discovered by the Curie brothers Pierre and Jacques whilst working on single crystals of quartz ( $\text{SiO}_2$ ) at the Sorbonne in France (1880). This effect should not be confused with the phenomenon of electrostriction which is present to a varying extent in all dielectric substances. Under electrostriction a substance becomes strained in the presence of an electric field but in proportion to even powers of the field. This produces a quadratic as opposed to a linear effect which is independent of the field sense (Cady, 1946).

Initially the piezoelectric effect was considered as a novelty confined to certain single crystals with little potential for practical application. The first major practical use of the piezoelectric effect was in early sonar. When the First World War started the French Government commissioned the development of a submarine detector. In 1918 Paul Langevin (Mason, 1971) constructed a

sonar system using quartz sandwiched between steel plates to generate and detect sound waves. Subsequently Cady, Anderson and Nicolson (Mason,1971) developed a sonar system for the United States navy based on the more readily available Rochelle salt or potassium sodium tartrate ( $\text{KNaC}_4\text{H}_4\text{O}_6 \cdot 4\text{H}_2\text{O}$ ), previously known as Seignette salt. During the feasibility and characterisation tests on Rochelle salt it was found to possess an unusually high dielectric constant and a dielectric hysteresis.

These anomalies were explained by Valasek (1921-24) when he described the ferroelectric properties of Rochelle salt. The name ferroelectricity was coined to describe this dielectric analogue of ferromagnetism even though it has no link with the element iron. The terms:- Curie point, coercive field and paraelectric phase also originate from this analogy.

The link between ferroelectricity and piezoelectricity led to a boom in scientific interest and the discovery of the ferroelectric phosphates and arsonates by Busch and Scherner (1935). Prime examples are potassium dihydrogen phosphate (KDP) and ammonium dihydrogen phosphate (ADP). The latter was used extensively in high power, piezoelectric, sonar-transducers during the Second World War.

The next ferroelectrics to be discovered were oxides, starting with Barium titanate ( $\text{BaTiO}_3$ ). This research originated from the discovery of its abnormally high dielectric constant. The peak in the dielectric constant versus temperature relationship was found independently in the USA, USSR, UK (Jackson and Reddish,1945; Megaw,1945; Rooksby,1945; Coursey and Brand,1946) and Japan in about 1948 (Miyake and Ueda,1946). The peak was shown to be due to its ferroelectric nature almost simultaneously by Von Hippel (1946) in the USA and Wul and Goldman (1945) in the USSR.

Barium titanate was the first ferroelectric substance to be

prepared in a ceramic form. This combined a piezoelectric sensitivity comparable with that of Rochelle salt and a chemical stability approaching that of quartz. Other advantages of the ceramic form include:-

- (i) Cheaper manufacture
- (ii) Increased mechanical strength
- (iii) The ability to produce piezoelectric elements in shapes unobtainable in single crystal form
- (iv) The option of choosing the poling direction and therefore the operating mode.

During the 1950s piezoelectric lead zirconate-titanate (PZT) (Jaffe et al,1954; Berlincourt et al 1964; Land et al 1964; Berlincourt,1964) and lead (meta)niobate (PMN) (Goodman,1952-3) were discovered and studied. Since then careful doping and processing have been used to develop piezoelectric ceramics for use in applications ranging from igniting domestic gas appliances to image storage and display devices (Maldonado et al,1971; Percy and Land,1981).

## 1.1 Ferroelectricity

All crystalline materials may be classified into one of 32 crystal classes according to the symmetry elements they possess (figure 1-1). Only materials which possess an inherent asymmetry in their crystal structure can exhibit asymmetric properties such as ferroelectricity and piezoelectricity. Each of the crystal classes represents a type of unit cell. Eleven of these classes have a centre of symmetry and one has an effective centre provided by a combination of symmetries. The remaining twenty have no centre of symmetry and are piezoelectric. Ten of these have a unique polar axis which allows the appearance of a spontaneous and temperature-dependent polarization. This is called pyroelectricity. Pyroelectric substances release charges on heating as well as under mechanical stress. A small number of pyroelectric substances also have the property of being ferroelectric. This means that all ferroelectrics are pyroelectric and piezoelectric. However, the converse is not true i.e. a pyroelectric material is not necessarily ferroelectric whilst a piezoelectric material need not necessarily be either pyroelectric or ferroelectric. Ferroelectrics have been the subject of many reviews see for example:- Devonshire,1954; Jona and Shirane,1962; Fatuzzo and Merz,1967; Burfoot,1967; Mason,1971.

The characteristic properties of a ferroelectric substance are:-

- (i) A spontaneous polarization which may be changed in orientation and/or reversed by an electric field.
- (ii) A sharp Curie point at which the relative permittivity shows a peak and above which the spontaneous polarization disappears.
- (iii) A dielectric hysteresis.
- (iv) A ferroelectric domain structure.

The non-centro-symmetric, spatial arrangement of the ions within

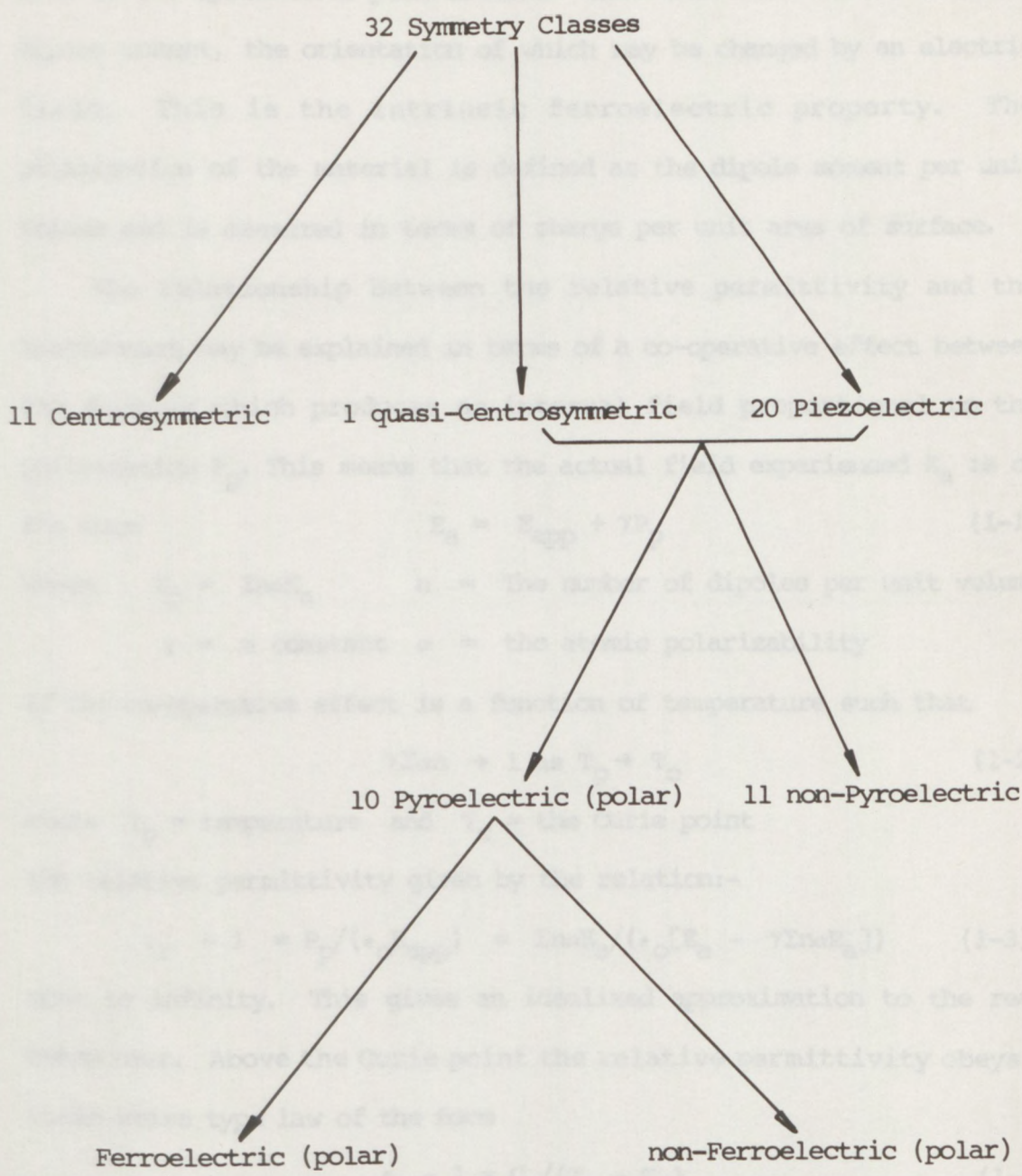


**Figure 1-1** A classification of the crystal classes by symmetry - only materials which possess an inherent asymmetry in their crystal structure can exhibit asymmetric properties such as ferroelectricity and piezoelectricity

the unit cell of a ferroelectric material below its Curie point gives rise to its spontaneous polarization. Each unit cell has an electric dipole moment, the orientation of which may be changed by an electric field. This is the intrinsic ferroelectric property. The polarization of the material is defined as the dipole moment per unit volume and is measured in terms of charge per unit area of surface.

The relationship between the relative permittivity and the temperature may be explained in terms of a co-operative effect between the dipoles which produces an internal field proportional to the polarization  $P_p$ . This means that the actual field experienced  $E_a$  is of the form

$$E_a = E_{app} + \gamma P_p \quad (1-1)$$

where  $P_p = \Sigma n \alpha E_a$        $n =$  The number of dipoles per unit volume  
 $\gamma =$  a constant       $\alpha =$  the atomic polarizability

If the co-operative effect is a function of temperature such that

$$\gamma \Sigma \alpha n \rightarrow 1 \text{ as } T_p \rightarrow T_c \quad (1-2)$$

where  $T_p =$  temperature and  $T_c =$  the Curie point

the relative permittivity given by the relation:-

$$\epsilon_r - 1 = P_p / (\epsilon_o E_{app}) = \Sigma n \alpha E_a / (\epsilon_o [E_a - \gamma \Sigma n \alpha E_a]) \quad (1-3)$$

goes to infinity. This gives an idealized approximation to the real behaviour. Above the Curie point the relative permittivity obeys a Curie-Weiss type law of the form

$$\epsilon_r - 1 = C_c / (T_p - T_o) \quad (1-4)$$

where  $C_c$  and  $T_o$  are constants known as the Curie constant and the Curie-Weiss temperature respectively.

The dielectric hysteresis shown schematically in figure 1-2 results from the ability of the individual dipoles to directionally respond to an electric field. When a low field is applied to a specimen in which the dipoles are orientated randomly the polarization initially increases linearly with the field and then saturates (path oa). If the field is then reduced to zero the polarization follows the

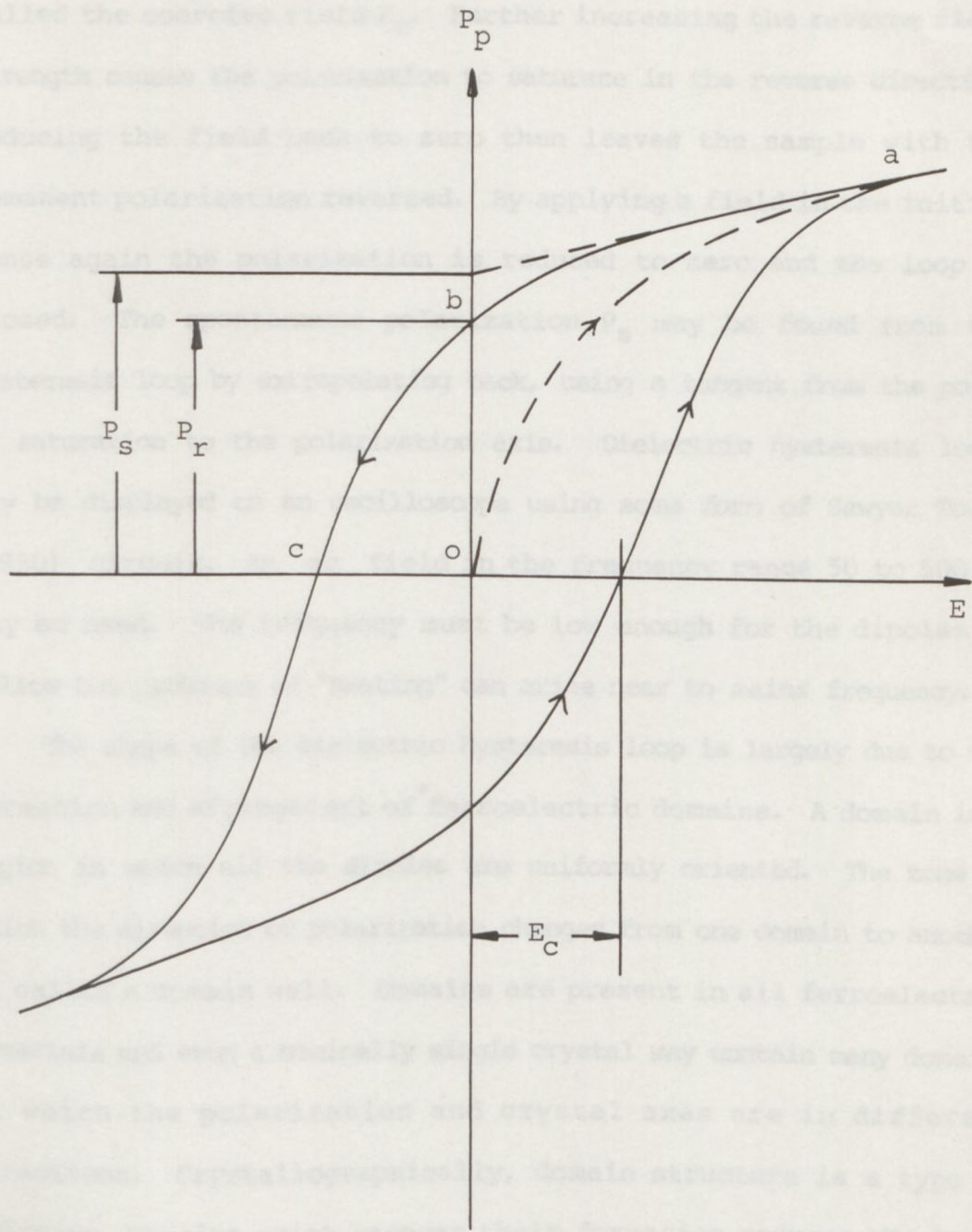


**Figure 1-2** A dielectric hysteresis loop for a ferroelectric material showing the hysteresis in the polarization-field relationship (Jona and Shirane, 1962)

path  $ab$  and the material retains a remanent polarization  $P_r$ . To return the polarization to zero a reverse field  $oc$  is required. This is called the coercive field  $E_c$ . Further increasing the reverse field strength causes the polarization to saturate in the reverse direction. Reducing the field back to zero then leaves the sample with the remanent polarization reversed. By applying a field in the initial sense again the polarization is reduced to zero and the loop is closed. The spontaneous polarization  $P_s$  may be found from the hysteresis loop by extrapolating back, using a tangent from the point of saturation to the polarization axis. Dielectric hysteresis loops may be displayed on an oscilloscope using some form of Sawyer Tower (1930) circuit. An ac field in the frequency range 50 to 500 Hz may be used. The frequency must be low enough for the dipoles to follow but problems of "beating" can arise near to mains frequency.

The shape of the dielectric hysteresis loop is largely due to the formation and arrangement of ferroelectric domains. A domain is a region in which all the dipoles are uniformly oriented. The zone in which the direction of polarization changes from one domain to another is called a domain wall. Domains are present in all ferroelectric materials and even a nominally single crystal may contain many domains in which the polarization and crystal axes are in different directions. Crystallographically, domain structure is a type of twinning. Domains exist because their formation reduces the large anisotropy energy present in ferroelectric substances. This is achieved by preventing the existence of free poles and by the formation of domains in which as many dipoles as possible point in opposite directions across a  $180^\circ$  wall. By doing this space-charge effects and internal fields are minimised. The linear relationship between electric field and polarization found at the beginning of a hysteresis loop is explained by the absence of domain switching for

fields less than  $E_c$ . For fields greater than  $E_c$  domain switching occurs and the polarization increases rapidly until saturation. The sharp onset of domain switching means that polarization reversal occurs over a narrow field range giving rise to the very rectangular shape of the hysteresis loop.

Theoretical explanations for the physical behaviour of ferroelectrics fall into two main categories, phenomenological theories based upon thermodynamic considerations (Devonshire, 1954) and dynamic theories (Born and Huang, 1956) based upon the dynamic theory of the crystal lattice (Ginzberg, 1961; Anderson, 1960; Cochran, 1961).

When a ferroelectric ceramic behaves like a piezoelectric, the polar axis of the individual domains must be preferentially aligned, a process known as "poling" (see also 1.5 and 3.3).

Once a ferroelectric ceramic has been poled, it retains a residual polarization on a semi-permanent basis, making it strongly piezoelectric and anisotropic. This gives it properties akin to those of a piezoelectric crystal and by common convention poled ceramics are referred to as piezoelectric ceramics (Devi, 1964; Grew et al., 1964; Debye et al., 1960; Jaffe et al., 1971; Van Turnhout and Genter, 1964). The electro-mechanical response of poled ferroelectric ceramics in the common range of applied stress or electric field has been shown to be in essence due to true piezoelectric effects in the poled domains, rather than domain switching effects (Casper, 1964).

The piezoelectric nature of poled ferroelectric ceramics allows a connection between strain and electric field allowing them to be used for the generation and detection of sound waves (see also Jaffe and Berlincourt, 1964; Cross et al., 1977-81).

## 1.2 Piezoelectric Ceramics

The ceramic form of a ferroelectric substance (Born and Huang, 1956; Ginzberg, 1961) is an agglomeration of very many fine ferroelectric crystallites 1-150  $\mu$  x  $10^{-6}$  in size. Each crystallite is randomly placed with respect to the others and contains a number of domains which are randomly distributed in their orientation between the permitted crystallographic directions.

As a result, the ceramic is completely isotropic and shows a net strain of zero when subjected to electric fields. This is due to the piezoelectric effects in adjacent domains cancelling each other out. To make a ferroelectric ceramic behave like a piezoelectric, the polar axes of the individual domains must be preferentially aligned, a process known as "poling" (sections 1.5 and 3.3).

Once a ferroelectric ceramic has been poled, it retains a remanent polarization on a semi-permanent basis, making it strongly piezoelectric and anisotropic. This gives it properties akin to those of a piezoelectric crystal and by common convention poled ceramics are known as piezoelectric ceramics (Deri, 1966; Gruver et al, 1966; Berlincourt et al, 1960b; Jaffe et al, 1971; Van Randerat and Setterington, 1974). The electromechanical response of poled ferroelectric ceramics in the common range of applied stress or electric field has been shown to be in essence due to true piezoelectric effects in the individual crystallites, rather than domain switching effects (Caspari and Merz, 1950).

It is the piezoelectric nature of poled, ferroelectric ceramics that provides a connection between strain and electric field allowing them to be used for the generation and detection of sound waves (Mattiati, 1971; Jaffe and Berlincourt, 1964; Cross et al, 1977-81).

### 1.2.1 Piezoelectric relations

The electromechanical behaviour of piezoelectric elements is related to the mechanical quantities, stress  $T$  and strain  $S$ , and the electrical quantities, field  $E$  and displacement  $D$ , by up to six constants. These are:-

- (i)  $d_{ij}$  constants which relate the displacement produced to the stress applied in the direct effect and the strain produced to the field applied in the converse effect.

$$\text{thus:- } D = Q_c/A = dT \quad (\text{direct effect})$$

$$S = dE \quad (\text{converse effect})$$

$$\text{so } d = D/T = S/E$$

- (ii)  $e_{ij}$  constants which relate the stress produced to the field applied.

$$\text{thus:- } T = -eE$$

- (iii)  $g_{ij}$  constants which relate the field produced to the stress applied

$$\text{thus:- } E = -gT$$

- (iv)  $h_{ij}$  constants which relate the strain produced to the field applied

$$\text{thus:- } E = -hS$$

- (v)  $c_{ij}$  constants which describe the elastic stiffness

- (vi)  $\epsilon_{ij}$  constants which describe the absolute permittivity

As these constants depend upon the direction of the field, the displacement, the stress and the strain in a piezoelectric material, they are tensors with subscripts indicating directions added. The subscripts  $i$  and  $j$  may take values ranging integrally from 1 to 6. Numbers 1, 2 and 3 refer to orthogonal, right hand  $x$ ,  $y$  and  $z$  axes respectively as used in standard tensor notation (Nye, 1957). The numbers 4, 5 and 6 refer to shear about these axes in the  $yz$ ,  $xz$  and  $xy$  planes respectively.

For the piezoelectric constants  $d, e, g, h$  and the coupling factors  $k_{ij}$  the first subscript refers to the direction of the field whilst the second refers to the direction of the mechanical stress or strain. For the permittivity constant  $\epsilon_{ij}$  the first subscript refers to the direction of the dielectric displacement whilst the second refers to the direction of the field. The first subscript in the stiffness constants  $c_{ij}$  refer to the direction of the strain whilst the second refers to the direction of the stress.

Using the four piezoelectric constants  $d, e, g$  and  $h$  it is possible to write eight equations, four describing the direct piezoelectric effect and four describing the converse effect. Each pair of equations is formed by keeping one mechanical and one electrical variable constant. These are shown in table 1-1, simplified by omitting the tensor subscripts. The superscripts indicate the variables which are kept constant under boundary conditions for the purposes of definition and measurement. For example shorting the electrodes of a piezoelectric element would make the electric field constant at zero and the superscript E would be used.

Piezoelectric Constant	Direct Effect	Inverse Effect
$d$	$D = \epsilon^T E + dT \quad (1)$	$S = (1/c^E)T + dE \quad (2)$
$e$	$D = \epsilon^S E + eS \quad (3)$	$T = c^E S + eE \quad (4)$
$g$	$E = (1/\epsilon^T)D - gT \quad (5)$	$S = (1/c^D)T + gD \quad (6)$
$h$	$E = (1/\epsilon^S)D - hS \quad (7)$	$T = c^D S - hD \quad (8)$

Table 1-1 Equations for the direct and converse piezoelectric effect using the four main piezoelectric constants  $d, e, g,$  and  $h$ .

Using the equations in table 1-1 it is possible to define the piezoelectric constants d,e,g and h in two ways and assign them units in accordance with the rationalized mks system (see table 1-2).

Constant	Definition	mks Units
d	or $\frac{\text{Charge density developed}}{\text{Applied mechanical stress}}$ $\frac{\text{Strain developed}}{\text{Applied field}}$	$C N^{-1}$ $m V^{-1}$
e	or $\frac{\text{Charge density developed}}{\text{Applied mechanical strain}}$ $\frac{\text{Stress developed}}{\text{Applied field}}$	$C m^{-2}$ $N V^{-1} m^{-1}$
g	or $\frac{\text{Electric field developed}}{\text{Applied mechanical stress}}$ $\frac{\text{Strain developed}}{\text{Applied charge density}}$	$V m N^{-1}$ $m^2 C^{-1}$
h	or $\frac{\text{Electric field developed}}{\text{Applied mechanical strain}}$ $\frac{\text{Stress developed}}{\text{Applied charge density}}$	$V m^{-1}$ $N C^{-1}$

Table 1-2 The definitions of the four main piezoelectric constants d,e,g, and h together with their mks units.

The four piezoelectric constants are not independent, but related as follows

$$c_{ij} = \sum_h c_{jh} d_{ih}$$

$$h_{ij} = e_{ij} / \epsilon_{ij} \quad (1-5)$$

$$g_{ij} = d_{ij} / \epsilon_{ij}$$

The selection of piezoelectric materials for various applications depends upon the constants shown in table 1-2. The  $d_{ij}$  or piezoelectric charge constants are the most commonly used. These relate to motor actions such as vibration i.e. electromechanical

conversion. A high  $d_{ij}$  constant is desirable for piezoelectric elements intended for use in applications such as ultrasonic transducers.

Poled piezoelectric ceramics have cylindrical polar symmetry about their poling axis. This means that the poling axis is an infinite-fold symmetry axis. For the dielectric, piezoelectric and elastic constants a 6-fold symmetry axis is equivalent to this infinite-fold axis. Using this fact together with equations (1) and (2) from table 1-1 it is possible to get a set of specific equations of state describing a piezoelectric ceramic. These are given in table 1-3.

Equation of State	Effect
$D_1 = \epsilon_1 E_1 + d_{15} T_5$ $D_2 = \epsilon_1 E_2 + d_{15} T_4$ $D_3 = \epsilon_3 E_3 + d_{31}(T_1 + T_2) + d_{33} T_3$	Direct effect
$S_1 = s_{11}^E T_1 + s_{12}^E T_2 + s_{13}^E T_3 + d_{31} E_3$ $S_2 = s_{11}^E T_2 + s_{12}^E T_1 + s_{13}^E T_3 + d_{31} E_3$ $S_3 = s_{13}^E (T_1 + T_2) + s_{33}^E T_3 + d_{33} E_3$ $S_4 = s_{44}^E T_4 + d_{15} E_2$ $S_5 = s_{44}^E T_5 + d_{15} E_1$ $S_6 = s_{66}^E T_6$	Converse effect

$$\text{where } s_{ij} = 1/c_{ij}$$

Table 1-3 The piezoelectric equations of state for a ceramic disc with an infinite fold symmetry axis.

In keeping with convention the direction of positive polarization is taken to be that of the 3 or z axis. One subscript (field) is enough to describe the permittivity as oblique fields and forces are not found in ceramics. Each elastic constant describes a single stress

component whilst all the others are fixed - the condition of no lateral restraint. This means that the stress and strain are interchangeable i.e.  $s_{ij} = s_{ji}$ . The planar isotropy of a poled ceramic is given in the  $d$  constants by the equalities  $d_{32} = d_{31}$  and  $d_{24} = d_{15}$ . The first equality means that an electric field parallel to the poling axis interacts identically with stress along either the 2(y) or 1(x) axis. The second equality means that an electric field parallel to the 2(y) axis interacts in the same way with shear in the 4 (yz) plane as a field along the 1(x) axis interacts with a shear in the 6(xy) plane. A full account of the piezoelectric relations and crystal symmetry can be found in the work of Mason (1950). The basic actions of a ceramic piezoelectric disc as used for ultrasonic transducer elements are shown in table 1-4.

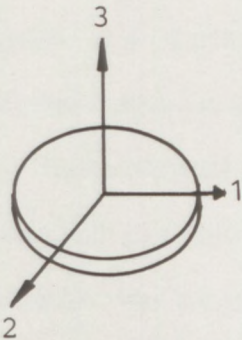
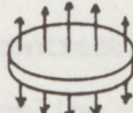
Axes	Action	Piezoelectric, Elastic and Dielectric Constants.
	<p style="text-align: center;"><b>RADIAL EXPANDER</b></p> <p>Poled      Field      Strain</p> <p>↓ or ↑      ↑↓      </p>	$d_{31}, g_{31}, k_p$ $s_{11}, c_{11}, \rho$ $K_3 (= \epsilon_3/\epsilon_0)$
	<p style="text-align: center;"><b>THICKNESS EXPANDER</b></p> <p>Poled      Field      Strain</p> <p>↓ or ↑      ↑↓      </p>	$d_{33}, g_{33}, k_{33}$ $s_{33}, c_{33}, \rho$ $K_3 (= \epsilon_3/\epsilon_0)$

Table 1-4 The basic actions of a piezoelectric disc together with the relevant piezoelectric, elastic and dielectric constants.

### 1.2.2 Electromechanical coupling

A good measure of the strength of the piezoelectric effect is the electromechanical coupling factor  $k_f$ . This measures the square root of the fraction of energy converted from the electrical to the mechanical form in an alternating cycle. The relation in terms of  $k_f^2$

$$\begin{aligned} \text{is :- } k_f^2 &= \frac{\text{electrical energy converted to mechanical energy}}{\text{input electrical energy}} \\ \text{or} & \\ k_f^2 &= \frac{\text{mechanical energy converted to electrical energy}}{\text{input mechanical energy}} \end{aligned} \quad (1-6)$$

As the conversion is never complete  $k_f^2$  is always less than 1 as is  $k_f$ . For the piezoelectric ceramics used in modern ultrasonic transducer elements the coupling is typically in the range 0.1 to 0.7. The unconverted energy is either stored (elastically or dielectrically) or dissipated as heat. In crystals the electromechanical coupling factor is a material constant. However, for ceramics it is a function of the degree of poling. Coupling factors derived from the equations of state that use  $d_{ij}$  constants (table 1-3) are the most useful, these include

$$\begin{aligned} k_{15} &= d_{15}/(s_{44}^E \epsilon_1^T)^{1/2} \\ k_{33} &= d_{33}/(s_{33}^E \epsilon_3^T)^{1/2} \\ k_{31} &= d_{31}/(s_{11}^E \epsilon_3^T)^{1/2} \\ k_p &= d_{31}/(2/[s_{11}^E + s_{12}^E] \epsilon_3^T)^{1/2} \\ &= k_{31}(2/[1 - \sigma])^{1/2} \\ k_t &= e_{33}/(\epsilon_3^S c_{33}^D)^{1/2} \end{aligned} \quad (1-7)$$

where  $\sigma = s_{12}^E/s_{11}^E$  is Poisson's cross-contraction ratio.

The planar electromechanical coupling factor  $k_p$  refers to the simultaneous application of equal stress along the 1(x) and 2(y) axes. This is equivalent to radial compression or tension in a plane normal to the poling axis. The thickness coupling factor  $k_t$  relates  $E_3$  and  $S_3$  in the absence of other strains. This coupling factor applies to thickness or longitudinal vibration in laterally clamped discs and

whilst referring to the same directions of field and stress as  $k_{33}$  it is much smaller.

The coupling factors in (1-7) relate the open and short-circuit elastic constants. By manipulating these coupling factors (1-7) with the equations given in table 1-3 it is possible to get the following relations

$$\begin{aligned} s_{44}^D &= s_{44}^E(1 - k_{15}^2) \\ s_{33}^D &= s_{33}^E(1 - k_{33}^2) \\ s_{11}^D &= s_{11}^E(1 - k_{31}^2) \\ s_{12}^D &= s_{12}^E - k_{31}^2 s_{11}^E \end{aligned} \quad (1-8)$$

To measure the coupling factor accurately and in accordance with the standards laid down (IEEE,1978; IRE,1949-61) specimens of different geometry must be used for the determination of different coupling factors. The piezoelectric discs extensively used in modern wide-band, ultrasonic transducers are only suitable for the measurement of  $k_p$  where the ratio of the diameter to the thickness should be equal to or greater than 6. The measurement of  $k_p$  for an ultrasonic transducer element is simplified by the fact that the dimensions commonly involved mean that frequencies in the lower r.f. region are used. Typical frequencies for radial resonance and antiresonance in a 15 mm diameter element are below 150 kHz.

Electromechanical coupling factors can be determined by using the piezoelectric effect to excite mechanical resonances in piezoelectric elements and measuring the frequencies at which maximum and minimum electrical impedance occur (section 3.1). The behaviour of a piezoelectric element near resonance can be modelled using an equivalent circuit as shown in figure 1-3 where:-

$C_0$  is the (clamped) capacitance of the element in the absence of mechanical strain

$L$  is the inductance representing the mass of the element

mechanical branch

electrical branch

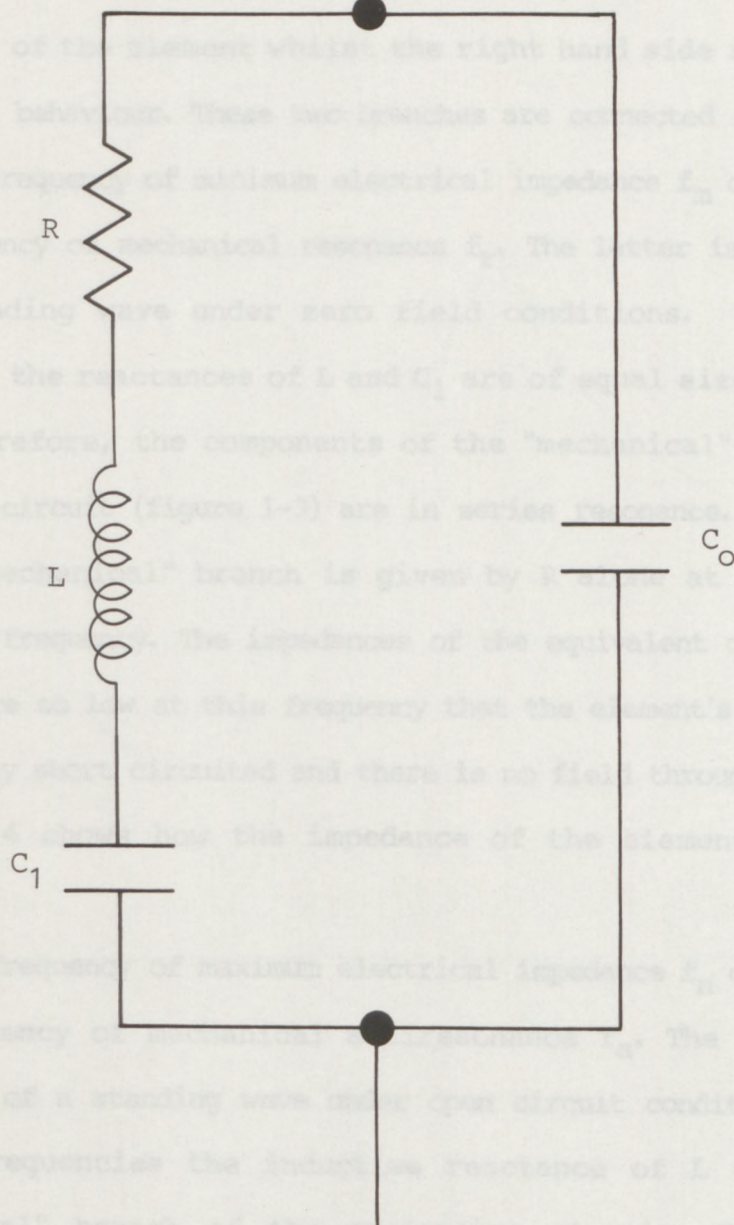


**Figure 1-3** The equivalent circuit of a piezoelectric element near a fundamental resonance (Jaffe et al, 1971). The left hand branch of the circuit ( $R, L, C_1$ ) represents the mechanical behaviour of the element whilst the right hand branch ( $C_0$ ) represents its electrical behaviour. These two branches are connected in parallel where:-  
 $R$  represents the mechanical damping of the element  
 $L$  represents the mass of the element  
 $C_1$  represents the elastic compliance of the element  
 $C_0$  represents the electrical capacitance of the element

$C_1$  is the capacitance representing the elastic compliance of the element

R is the resistance representing the mechanical damping of the element.

The left hand side of the circuit represents the mechanical behaviour of the element whilst the right hand side represents its electrical behaviour. These two branches are connected in parallel.

The frequency of minimum electrical impedance  $f_m$  occurs close to the frequency of mechanical resonance  $f_r$ . The latter is the frequency of a standing wave under zero field conditions. At about this frequency the reactances of L and  $C_1$  are of equal size but opposite sign. Therefore, the components of the "mechanical" branch of the equivalent circuit (figure 1-3) are in series resonance. The impedance of the "mechanical" branch is given by R alone at  $f_s$  the series resonance frequency. The impedances of the equivalent circuit and the element are so low at this frequency that the element's electrodes are effectively short circuited and there is no field through the element. Figure 1-4 shows how the impedance of the element varies with frequency.

The frequency of maximum electrical impedance  $f_n$  occurs close to the frequency of mechanical antiresonance  $f_a$ . The latter is the frequency of a standing wave under open circuit conditions. At these higher frequencies the inductive reactance of L dominates the "mechanical" branch of the equivalent circuit. Eventually the inductive reactance of this branch becomes equal in size but opposite in sign to the reactance of the electrical branch of the equivalent circuit  $C_0$ . At the frequency  $f_p$  the "mechanical" and electrical branches of the equivalent circuit are in parallel resonance and the field through the element is a maximum. The impedances of the equivalent circuit and the element are so high at this frequency that the element's electrodes are effectively open circuit.

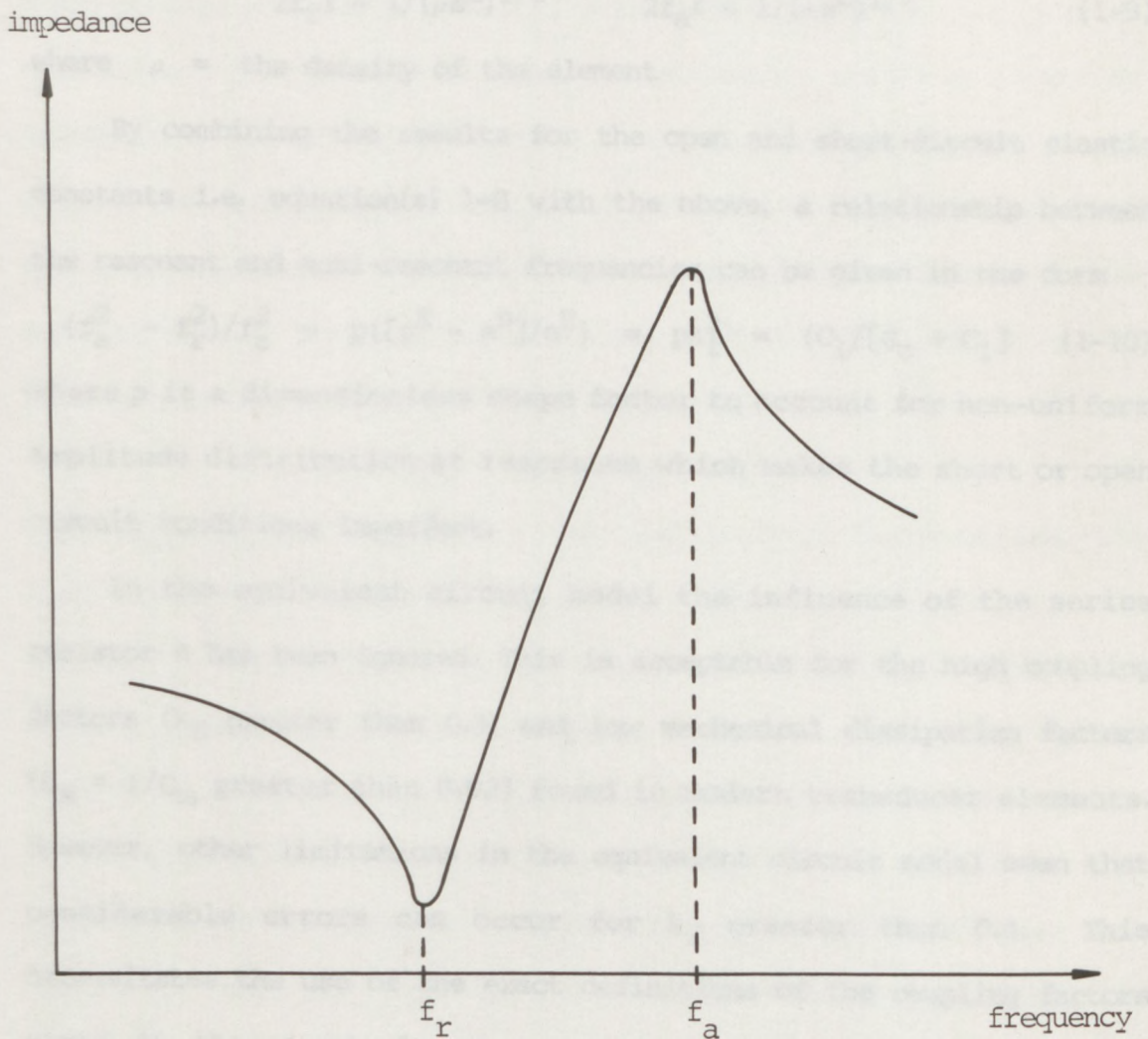


**Figure 1-4** The impedance of a piezoelectric resonator against frequency near a fundamental resonance showing the resonant and anti-resonant frequencies  $f_r$  and  $f_a$  respectively. The difference in these two frequencies is used to measure the electromechanical coupling factors such as  $k_p$  (Jaffe et al, 1971)

The relations between the fundamental resonant ( $f_r$ ) and antiresonant ( $f_a$ ) frequencies and the controlling dimension  $l$  are given in terms of the elastic compliance thus

$$2f_r l = 1/(\rho s^E)^{1/2} \quad 2f_a l = 1/(\rho s^D)^{1/2} \quad (1-9)$$

where  $\rho$  = the density of the element

By combining the results for the open and short-circuit elastic constants i.e. equation(s) 1-8 with the above, a relationship between the resonant and anti-resonant frequencies can be given in the form

$$(f_a^2 - f_r^2)/f_a^2 = p([s^E - s^D]/s^E) = pk_f^2 = (C_1/[C_0 + C_1]) \quad (1-10)$$

where  $p$  is a dimensionless shape factor to account for non-uniform amplitude distribution at resonance which makes the short or open circuit conditions imperfect.

In the equivalent circuit model the influence of the series resistor  $R$  has been ignored. This is acceptable for the high coupling factors ( $k_f$  greater than 0.3) and low mechanical dissipation factors ( $D_m = 1/Q_m$  greater than 0.02) found in modern transducer elements. However, other limitations in the equivalent circuit model mean that considerable errors can occur for  $k_f$  greater than 0.4. This necessitates the use of the exact definitions of the coupling factors given in the standards. For modern piezoelectric ceramics the frequency differences, normally in the order

$$(f_n - f_m) > (f_p - f_s) > (f_a - f_r) \quad (1-11)$$

are nearly equal. In practice the coupling factors (including  $k_p$ ) are easily found from measurements of the frequencies of minimum and maximum impedance ( $f_m$  and  $f_n$ ) and a graph of the coupling factor  $k_p$  against  $(f_p - f_s)/f_s$  (IRE, 1961).

### 1.3 Lead zirconate-titanate $Pb(Ti,Zr)O_3$ (PZT)

Lead zirconate-titanate or PZT compositions are part of an extensive range of substances that constitute the perovskite group. These possess the general chemical formula  $AiBiO_3$  where Ai is a large monovalent, divalent or trivalent metal cation and Bi is a smaller pentavalent, tetravalent or trivalent elemental cation. Members of the perovskite group possess the ideal perovskite structure or minor deviations from it. The ideal perovskite structure is that of the mineral itself i.e. calcium titanate ( $CaTiO_3$ ). This structure is described by the Goldschmitt (1926) tolerance factor

$$t_G = (R_{Ai} + R_O) / (2[R_{Bi} + R_O])^{1/2} \quad (1-12)$$

where  $R_{Ai}$ ,  $R_{Bi}$  and  $R_O$  are the ionic radii of the large cation, the small cation and the anion respectively. Structures whose tolerance factor ( $t_G$ ) lie in the range 0.95 to 1.0 are cubic centro-symmetric and not piezoelectric. Any structure that has a tolerance factor outside this range has a distorted cubic structure and structures where  $t_G$  is greater than 1.0 tend to be ferroelectric. Extensive studies of the chemistry and crystallography of the perovskites have been made and are reported in the literature (Galasso, 1969; Roth, 1957a; Megaw, 1946; Naray-Szabo, 1943).

PZT ceramics are prepared from solid solutions of lead zirconate ( $PbZrO_3$ ) and lead titanate ( $PbTiO_3$ ). They are characterized by the existence of an almost temperature independent phase boundary between the rhombohedral zirconium rich phase and the tetragonal titanium rich phase. The proportions of either constituent may be varied continuously from 0 to 100% giving a gradual change in physical properties from anti-ferroelectric lead zirconate to strongly ferroelectric lead titanate.

Lead titanate has a tetragonally distorted perovskite structure at room temperature and is ferroelectric. At the Curie point ( $490^\circ C$ )

it undergoes a phase transition to a paraelectric state of cubic symmetry. The lattice parameters of lead titanate have been studied by Shirane (Shirane and Hoshino,1951) and their variation as a function of temperature measured. Studies of the dielectric properties of ceramic lead titanate have been summarized by Ikegami and Ueda(1958).

Lead zirconate has an orthorhombic structure at room temperature and is antiferroelectric. The orthorhombic structure results from antiparallel displacement of lead ions along the  $\langle 110 \rangle$  directions. This gives rise to a superlattice of antiparallel dipoles which retain a centre of symmetry. Antiferroelectric substances have a dipole moment in each unit cell below the Curie point, however, in adjacent unit cells it points at  $180^\circ$  giving a zero net effect. Above the Curie point lead zirconate has a trigonal lattice structure (Sawaguchi et al,1951).

The addition of small amounts of lead titanate to lead zirconate can produce a ferroelectric rhombohedral structure (Shirane et al,1952). The variation in the piezoelectric strength (as indicated by the planar coupling factor  $k_p$ ) with composition (Jaffe et al,1954) is shown in figure 1-5. It is obvious that the most useful compositions for transducer elements lie in the region where there is approximately 40% lead zirconate and 60% lead titanate by atomic volume.

The PZT compositions employed in practice are very rarely unmodified i.e. consist of only lead zirconate and lead titanate. Most compositions are modified by doping with small quantities of alternative ions. The types of additives used may be broadly divided into four classes according to the manner in which they work. These classes are as follows:-

- (i) Isovalent substitution additives
- (ii) Compensating valence additives

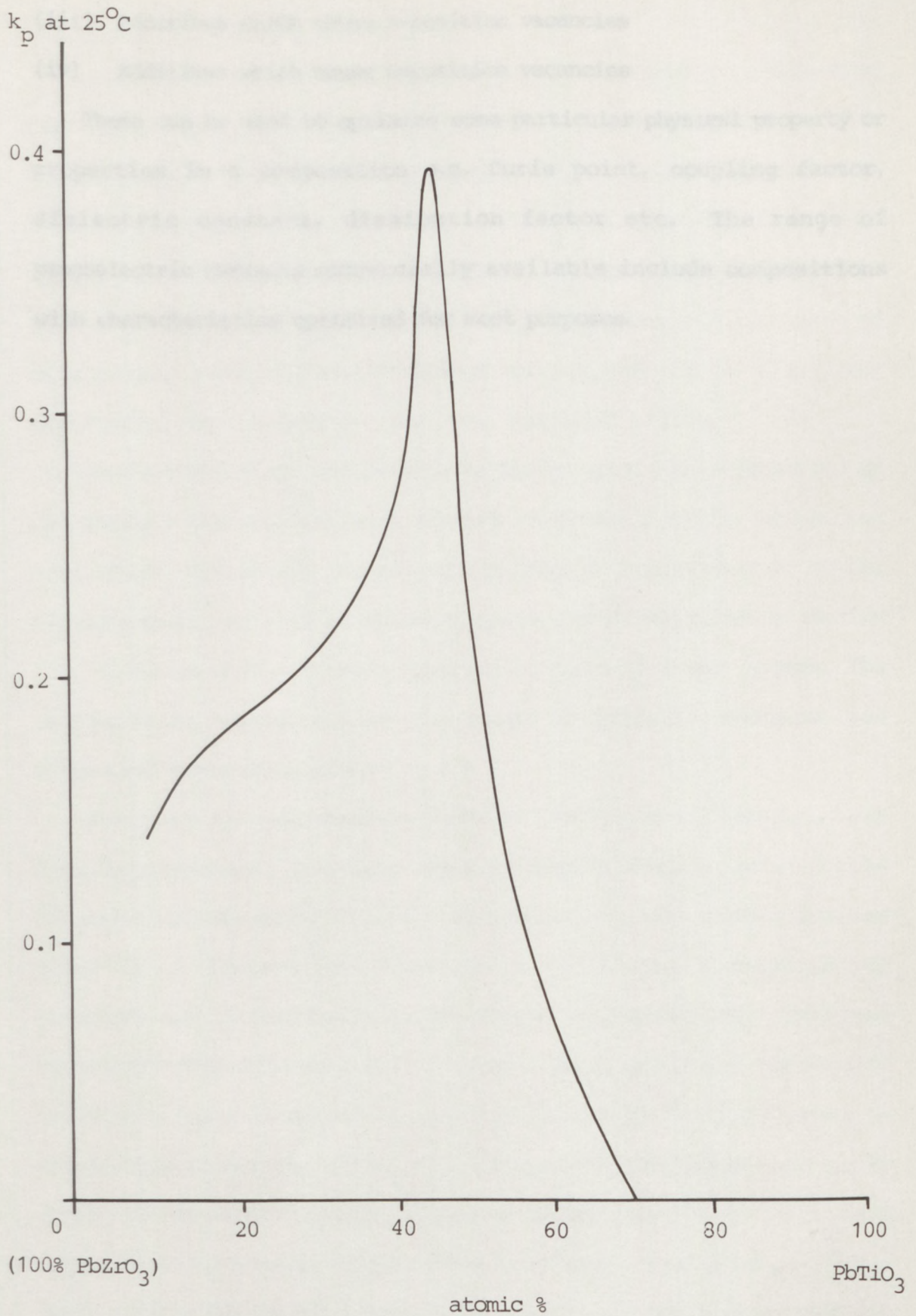


**Figure 1-5** The planar electromechanical coupling factor ( $k_p$ ) against composition for lead zirconate-titanate (PZT). The most sensitive composition can be clearly seen in the region where there is approximately 40% PbZrO<sub>3</sub> and 60% PbTiO<sub>3</sub> by atomic % (Jaffe et al, 1954)

(iii) Additives which cause A-position vacancies

(iv) Additives which cause O-position vacancies

These can be used to optimize some particular physical property or properties in a composition e.g. Curie point, coupling factor, dielectric constant, dissipation factor etc. The range of piezoelectric ceramics commercially available include compositions with characteristics optimized for most purposes.

are Al is a large monovalent, divalent or trivalent cation and Bi is a smaller pentavalent, tetravalent or trivalent, divalent cation.

more specifically, PMN belongs to the group of oxides described by the formula  $AiBi_2O_6$ . While a deeper study may give the impression that these oxides are completely different from the rest of the  $Ai_2Bi_2O_6$  group, as well as the  $Ai_2Bi_2O_6$  type oxides described in section 1.3, it is in fact, closely related to both of these groups. The similarities extend across the range of crystal, chemical and structural characteristics.

There are two polymorphic forms of lead niobate ( $PbNb_2O_6$ ), both have approximately the same density but different structures (Francis, 1956; Roth, 1959). By convention, the two forms are named after their discoverers. Franciscite (1956) has a rhombohedral structure and is non-ferroelectric whilst Goodenite (1952; 1953) has an orthorhombic structure and is ferroelectric below its Curie point ( $570^\circ\text{C}$ ). At room temperature equilibrium the Franciscite phase is stable with reversible transition to the Goodenite phase occurring at approximately  $125^\circ\text{C}$ . (Roth, 1959). The Goodenite (1952; 1953) phase is produced by carefully quenching lead niobate from temperatures above  $125^\circ\text{C}$  and may be further stabilized by the addition of suitable agents (Francis and Lewis, 1956; Sakata, 1960). This means that the Goodenite phase is only meta-stable at room temperature.

Above its Curie point lead niobate has a tetragonal structure

#### 1.4 Lead (meta)Niobate $PbNb_2O_6$ (PMN)

Lead meta-niobate or PMN was the first non-perovskite, oxide-type ferroelectric to be discovered (Goodman, 1952; 1953). It is one of a large group of double and complex oxides that does not crystallise with the perovskite structure and it displays a dielectric anomaly typical of oxide ferroelectrics. These non-perovskite oxides may be described by the general formula  $Ai_xBi_2O_6$  where Ai is a large monovalent, divalent or trivalent cation and Bi is a smaller pentavalent, tetravalent or trivalent, elemental cation.

More specifically, PMN belongs to the group of oxides described by the formula  $AiBi_2O_6$ . Whilst a cursory study may give the impression that these oxides are completely different from the rest of the  $Ai_xBi_2O_6$  group, as well as the  $AiBiO_3$  type oxides described in section 1.3, it is in fact, closely related to both of these groups. The similarities extend across the range of crystal, chemical and structural characteristics.

There are two polymorphic forms of lead niobate ( $PbNb_2O_6$ ), both have approximately the same density but different structures (Francombe, 1956; Roth, 1959). By convention, the two forms are named after their discoverers. Francombite (1956) has a rhombohedral structure and is non-ferroelectric whilst Goodmanite (1952; 1953) has an orthorhombic structure and is ferroelectric below its Curie point ( $570^\circ\text{C}$ ). At room temperature equilibrium the Francombite phase is stable with reversible transition to the Goodmanite phase occurring at approximately  $1250^\circ\text{C}$  (Roth, 1959). The Goodmanite (1952; 1953) phase is produced by carefully quenching lead niobate from temperatures above  $1250^\circ\text{C}$  and may be further stabilized by the addition of suitable dopants (Francombe and Lewis, 1958; Subbarao, 1960). This means that the Goodmanite phase is only meta-stable at room temperature.

Above its Curie point lead niobate has a tetragonal structure

(Roth, 1957b) and obeys the Curie-Weiss law. This paraelectric phase is isostructural with potassium tungsten bronze  $K_xWO_3$  where  $0.57 \geq x \geq 0.43$  (Magneli, 1949). This structure may be generally described as a collection of oxygen octahedra linked at their corners. This produces three types of holes, two of which normally contain the Ai ions whilst the Bi ions are inside the octahedra. In the simplest unit cell there are six Ai positions and ten octahedra. This means that the chemical formula of the unit cell is  $Pb_5Nb_{10}O_{30}$ .

As there are only five lead ions the A sites can only be 5/6th filled and it is presumed that the distribution of the ions amongst the sites is random. The rest of the structure is made up of corner-linked, distorted  $NbO_6^{-2}$  octahedrons. Figure 1-6 shows a schematic projection of the potassium tungsten bronze structure on the (001) plane using tetragonal axes (Francombe and Lewis, 1958). The configuration of the oxygen octahedra gives rise to a series of "cages" and "tunnels" (Wadsley, 1955) within the structure. The  $Pb^{2+}$  ions are shown as circles at  $z = 0$  located in either "tunnels" or "cages" at  $z = \pm 1/2$ . The "tunnels" are made up of five-member rings of  $NbO_6$  octahedra and run in parallel through the structure at a fixed orientation. These "tunnels" may be considered as continuous lines of interstitial sites some of which are open to guest atoms such as the 10 co-ordinated  $Pb^{2+}$  ions. The "cages" are made up of four membered rings of  $NbO_6$  octahedra and contain the 8 co-ordinated  $Pb^{2+}$  ions.

Whilst this structure is more complicated than the perovskite structure it exhibits many similarities. A common building block in many complex oxides of the transition metals is the  $BiO_6$  octahedron made up of oxygen ions surrounding a transition metal ion (Magneli, 1956). This unit is found in non-ferroelectric oxides such as the potassium tungsten bronzes (Hagg and Magneli, 1954) given by the general formula  $Ai_xWO_{3-x}$  (where A is an alkali metal) as well as in

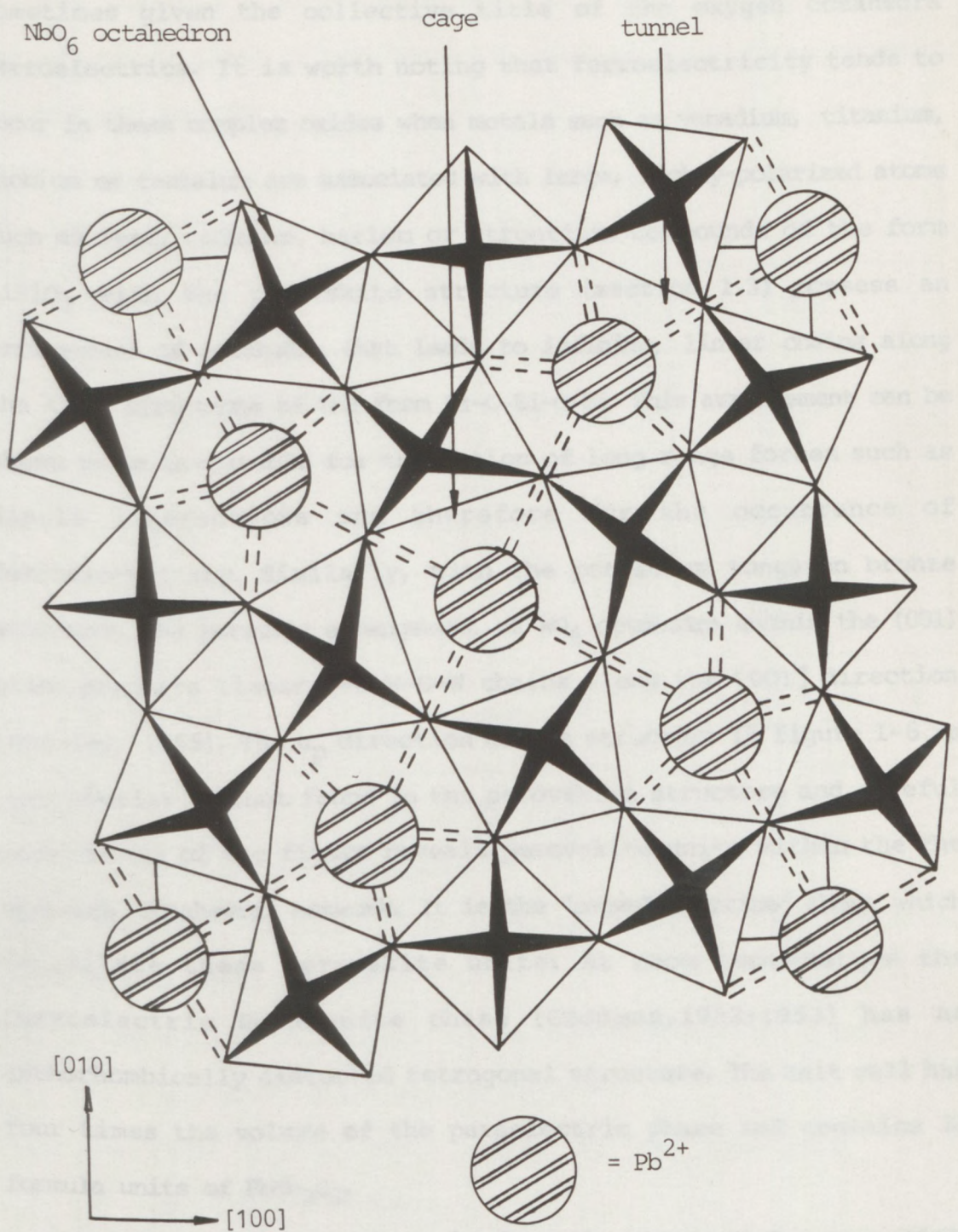


**Figure 1-6** A schematic projection of the potassium tungsten bronze type structure on the (001) plane showing the perovskite units within the structure (Francombe and Lewis, 1958)

both  $\text{AiBiO}_3$  and  $\text{AiBi}_2\text{O}_6$  type oxides. For this reason these are sometimes given the collective title of the oxygen octahedra ferroelectrics. It is worth noting that ferroelectricity tends to occur in these complex oxides when metals such as vanadium, titanium, niobium or tantalum are associated with large, highly-polarized atoms such as lead, cadmium, barium or strontium. Compounds of the form  $\text{AiBiO}_3$  with the perovskite structure (section 1.3) possess an arrangement of octahedra that leads to infinite, linear chains along the  $\langle 100 \rangle$  directions of the form Bi-O-Bi-O-Bi. This arrangement can be shown to be favourable for the action of long range forces such as dipole interactions and therefore for the occurrence of ferroelectricity. Similarly, with the potassium tungsten bronze structure, the periodic arrangement of  $\text{WO}_6$  octahedra within the (001) plane produces linear W-O-W-O-W chains along the [001] direction (Wadsley, 1955). The  $c_p$  direction of the structure in figure 1-6 is very similar to that found in the perovskite structure and careful examination of the figure reveals perovskite units within the the depicted, octahedral network. It is the "cages" described above which constitute these perovskite units. At room temperature the ferroelectric Goodmanite phase (Goodman, 1952; 1953) has an orthorhombically distorted tetragonal structure. The unit cell has four times the volume of the paraelectric phase and contains 20 formula units of  $\text{PbNb}_2\text{O}_6$ .

The large lattice constants in the  $a_p$ - $b_p$  plane are due to a slight monoclinic shear which results in a new choice of axes at  $45^\circ$  to the original set. Whilst there are no conclusive data on the value of the spontaneous polarization, its direction is thought to lie within the (001) plane parallel to the  $b_p$  axis. The slight elongation of the orthorhombic  $b_p$  axis is therefore in the polar direction and the ratio  $b_p/a_p = 1.033$  can be considered as a measure of the spontaneous

strain.

PMN (Keramos) is increasingly being used in wide-band, ultrasonic transducers in place of PZT. Table 1-5 summarises the characteristics of both PMN and PZT.

Physical Property	PZT	PMN
Curie Point	370°C	570°C
Planar Electromechanical Coupling Factor ( $k_p$ )	0.52 to 0.6	up to 0.35
Mechanical Quality Factor	approximately 500	approximately 11
Coercivity	high	very high
Conductivity	negligible	finite at poling temperature

Table 1-5 A summary of some of the physical properties of PZT and PMN relating to their use in non-uniformly excited wide-band transducers

PMN has many features which make it suitable for transducer applications. These include:-

- (i) The ability to tolerate temperatures approaching its very high Curie point without depoling.
- (ii) A large  $d_{33}/d_{31}$  ratio making it very responsive to hydrostatic pressure.
- (iii) A very low mechanical quality factor  $Q_m$ .

The low transverse response indicated by the  $d_{33}/d_{31}$  ratio is thought to be due to  $d_{31}$  and  $d_{32}$  being opposite in sign in each crystallite within the ceramic and therefore tending to cancel out. This low response is reflected in the planar coupling of PMN which is only about 17% of that found in PZT. It is the low coupling of

longitudinal excitation into transverse modes (including radial) that helps to reduce the generation of unwanted plate waves in PMN transducers (section 2.4).

The main disadvantages of PMN are its high coercivity and its conductivity at elevated temperatures substantially below its Curie point. These make it difficult to measure its ferroelectric polarization using its dielectric hysteresis (section 1.1) and difficult to pole (see sections 1.5. and 3.3).

The process begins with the mixing of their constituent oxides in the correct proportions. PZT is made from a mixture of lead zirconate 50% zirconium dioxide ( $ZrO_2$ ) and titanium dioxide ( $TiO_2$ ) whilst PMN is made from a mixture of lead zirconate 50% niobium oxide ( $Nb_2O_5$ ). The oxides are then calcinated to drive off impurities and cause the chemical reaction which forms solid solutions of PZT and PMN. After calcination the reacted material(s) are ground into a fine powder and pressed (usually by compaction) into bodies of the required shape. These bodies are then sintered and finished, usually by polishing before being electrode and poled (section 3.3).

Instantly attached, conductive electrodes are an essential part of any ceramic, piezoelectric transducer. The poling and subsequent driving of transducers (often with high voltages) rely on almost ideal electrode characteristics. Ideal electrodes should be very thin but porous, highly conductive, chemically inert and physically durable. It should also be possible to make good soldered connections to them. In practice not all these ideals can be met. Electrode adherence is critical as any gap between the electrode and a high dielectric constant ceramic forms a low voltage series capacitor. This severely lowers the overall capacitance of the transducer and can divide the poling and subsequently applied driving voltages. Most commercial electrodes are made by sintering a coat of fine silver

### 1.5 Production of Ceramics

The manufacturing process plays an important part in determining the electromechanical characteristics of a piezoelectric ceramic. Piezoelectric ceramics of PZT and PMN are conventionally manufactured from their constituent oxides by a series of eight main steps :-

- (i) Mixing            (ii) Calcination            (iii) Grinding            (iv) Forming  
(v) Sintering        (vi) Finishing            (vii) Electroding        (viii) Poling

Briefly, the manufacture of PZT ( $\text{Pb}[\text{Ti},\text{Zr}]\text{O}_3$ ) and PMN ( $\text{PbNb}_2\text{O}_5$ ) ceramics begins with the mixing of their constituent oxides in the correct proportions. PZT is made from a mixture of lead monoxide ( $\text{PbO}$ ), zirconium dioxide ( $\text{ZrO}_2$ ) and titanium dioxide ( $\text{TiO}_2$ ) whilst PMN is made from a mixture of lead monoxide and niobium oxide ( $\text{Nb}_2\text{O}_5$ ). The mixed oxides are then calcinated to drive off impurities and cause the thermal reaction which forms solid solutions of PZT and PMN. After calcination the reacted material(s) are ground into a fine powder and formed (usually by compaction) into bodies of the required shape. These bodies are then sintered and finished, usually by polishing before being electroded and poled (section 3.3).

Intimately attached, conductive electrodes are an essential part of any ceramic, piezoelectric transducer. The poling and subsequent driving of transducers (often with high voltages) rely on almost ideal electrode characteristics. Ideal electrodes should be very thin but continuous, highly conductive, chemically inert and physically durable. It should also be possible to make good soldered connections to them. In practice not all these ideals can be met. Electrode adherence is critical as any gap between the electrode and a high dielectric constant ceramic forms a low value, series capacitor. This severely lowers the overall capacitance of the transducer and can divide the poling and subsequently applied driving voltages. Most commercial electrodes are made by sintering a coat of fine silver

powder and glass (or glass former), dispersed in a liquid onto the appropriate surfaces. This forms a conductive glaze or frit which is well attached to the ceramic substrate and can be soldered to.

The final step in the production of a piezoelectric ceramic is poling. A high dc voltage is applied across the electrodes. Poling aligns a majority of the dipoles present in the individual unit cells, as well as causing whole domains to switch. This partially de-twins the ceramic by eliminating much of the domain structure. To allow the freedom necessary for movements during poling the temperature of the ceramic is usually raised. This is often done using an oil bath as the high dielectric strength of the oil helps to prevent arcing around the surface of the ceramic. The conditions of electric field, temperature and time required to "pole" a ceramic to saturation are composition dependent. However, the electric field strength must be in excess of the coercive field of the composition and yet below its dielectric breakdown strength. Within these limits the poling time may be, to a certain extent, traded off against the electric field strength and the temperature (see section 3.3).

Due to the large commercial interest in piezoelectric ceramics most of the information relating to poling is published in patents. Probably the most important patent covering PZT ceramics was issued to Berlincourt et al in (1960a). However, an excellent and comprehensive scientific study of the poling characteristics of PZT ceramics has been given by O'Callaghan (1974).

The tendency for dielectric breakdown and mechanical failure to occur during the poling of ferroelectric ceramics makes poling one of the most difficult operations in their production. A good poling medium is essential in the production of piezoelectric elements. Probably the best poling medium is silicone oil, however, vegetable oils are also used successfully. Arcing across the edges of specimens

during poling often results from deterioration of the poling media and is made worse by salt contamination of the ceramic through handling. Dielectric breakdown is accentuated by the inevitable presence of physical flaws such as voids and cracks. The greater the electrode area the greater the likelihood of there being a fault to initiate dielectric breakdown.

Mechanical distortion during poling may also cause failure. Ceramics are relatively weak in tension and some compositions distort up to 0.5% in the direction of the applied field and up to -0.2% in directions normal to it. In thick, curved or only partially electroded samples the tensile stresses experienced during poling can cause failure. Mechanical failure may precede electrical failure and be obscured by it.

Even without the problems of electrical or mechanical failure the maximum polarization attainable is limited. Due to the random orientation of the crystallographic axes within the grains of a ceramic the alignment of dipoles along the poling axis can never be as complete as in a single crystal. The fraction of the single crystal polarization that can be ideally realized in pseudocubic ceramics has been calculated by Baerwald (1957) and is shown in table 1-6.

Crystal Symmetry and Polar Axis	Number of Equivalent Directions	Fraction of Single Crystal Polarization that can be Realized Ideally
Tetragonal [001]	6	0.831
Orthorhombic [110]	12	0.912
Rhombohedral [111]	8	0.866

Table 1-6 The ideal fraction of single crystal polarization that can be realized in a ceramic.

In practice this figure is not realized due to many factors which tend to prevent domain switching. These include intergranular stresses and flaws which cause strains within individual grains.

The subject can be modelled using a variety of approaches. In this chapter both the design and construction of these transducers as well as the signals produced by them are considered mainly in terms of theory and experiment. However, the important practical features of transducers made from ceramic piezoelectric elements (chapter 4) are also considered.

As an aid to understanding the fabrication methods for wide-band transducers (section 3.4) and the important features of their physical operation a brief summary of the Cristofolini, London and Mitchell or LLM model is given. This models the transducer in terms of an element converting compression waves into an acoustic transmission line. From this an equivalent circuit can be developed which can be used to predict the effects of the loading and the front-face loading on the acoustic characteristics of a transducer.

The ultrasonic field produced by these transducers is interpreted in terms of the plane- and edge-wave model. Briefly, the field of a uniformly excited, wide-band, ultrasonic transducer consists of two components i.e. the plane- and edge-waves. These emanate from the face and the edge of the transducer respectively and propagate outward from it. Due to the varying amplitude, phase and degree of overlapping of these components the resulting acoustic field consists of several lobes which change in both amplitude and shape with range. The simplification of this field is then discussed in terms of removing or shading out one or other of these components.

The impulse response method is then used to further interpret the behaviour of both uniformly and non-uniformly excited transducers. Graphical solutions of the impulse response method are considered as is the principle of reciprocity.

Short-pulse, wide-band transducers of the type considered in this project can be modelled using a variety of approaches. In this chapter both the design and construction of these transducers as well as the fields produced by them are considered mainly in terms of theory and models. However, the important practical features of transducers made from ceramic, piezoelectric elements (chapter 1) are also considered.

As an aid to understanding the fabrication methods for wide-band transducers (section 3.4) and the important features of their physical construction a brief summary of the Krimholtz, Leedom and Matheai or KLM model is given. This models the transducers in terms of an element launching compression waves into an acoustic transmission line. From this an equivalent circuit can be developed which can be used to predict the effects of the backing and the front-face loading on the acoustic characteristics of a transducer.

The ultrasonic field produced by these transducers is interpreted in terms of the plane- and edge-wave model. Briefly, the field of a uniformly excited, wide-band, ultrasonic transducer consists of two components i.e. the plane- and edge-waves. These emanate from the face and the edge of the transducer respectively and propagate forward from it. Due to the varying amplitude, phase and degree of overlapping of these components the resulting acoustic field consists of several pulses which change in both amplitude and shape with range. The simplification of this field is then discussed in terms of removing or shading out one or other of these components.

The impulse response method is then used to further interpret the behaviour of both uniformly and non-uniformly excited transducers. Graphical solutions of the impulse response method are considered as is the principle of reciprocity.

2.1 Finally, the performance of practical transducers made from ceramic piezoelectric elements is discussed and the effect of the head waves they produce is explained in the context of the plane- and edge-wave model.

This utilizes transmission line theory to model the electrical and mechanical properties of ultrasonic transducers. As the lateral dimensions of the transducer element are large compared with the thickness, a one-dimensional analysis is possible, in which all quantities are assumed to vary only in the direction of the propagation. Starting with a general transmission line equivalent model, an equivalent T-network may be developed and from this an equivalent circuit. In a piezoelectric material the mechanical and electrical properties are coupled so the equivalent circuit must exhibit a complicated mixture of electrical and mechanical properties.

Wang (1963) derived one of the first one-dimensional equivalent circuits which described a transducer as an arbitrary transmission line of length (i.e. thickness)  $l$ . A circuit better suited to determining the optimum electrical and mechanical matching for broadband (i.e. pulsed) transducer operation is the Krimholtz (1970, 1971) and Nathaniel or IEM equivalent circuit model. Details of this are given in section 2.1.1. In this circuit the roles of the electrical and mechanical parts are clearly distinguished. The model retains the intrinsic transmission line character of the mechanical system but permits lumped circuit analysis of the electrical system.

The plane- and edge-wave model, used extensively here, models the transducer in terms of wave propagation ideas. The transducer is considered as a source of two wave components plane- and edge-waves which interact in the acoustic field to produce a characteristic diffraction pattern. Full details of this model and its useful properties for analyzing transducers are given in section (2.1.2).

## 2.1 Transducer Models.

Ultrasonic transducers may be modelled using two main approaches. The KLM equivalent circuit models the transducer as an acoustic transmission line. This utilizes transmission line theory to model the electrical and mechanical properties of ultrasonic transducers. As the lateral dimensions of the transducer element are large compared with the thickness, a one-dimensional analysis is possible, in which all quantities are assumed to vary only in the direction of the propagation. Starting with a general transmission line equivalent model, an equivalent T - network may be developed and from this an equivalent circuit. In a piezoelectric material the mechanical and electrical properties are coupled so the equivalent circuit must exhibit a complicated mixture of electrical and mechanical properties.

Mason (1948) derived one of the first one-dimensional equivalent circuits which described a transducer as an arbitrary transmission line of length (i.e. thickness)  $l$ . A circuit better suited to determining the optimum electrical and mechanical matching for broadband (i.e. pulsed) transducer operation is the Krimholtz (1970, Leedom (1971) and Matthaei or KLM equivalent circuit model. Details of this are given in section 2.1.1. In this circuit the roles of the electrical and mechanical parts are clearly distinguished. The model retains the intrinsic transmission line character of the mechanical system but permits lumped circuit analysis of the electrical system.

The plane- and edge-wave model, used extensively here, models the transducer in terms of wave propagation ideas. The transducer is considered as a source of two wave components (plane- and edge-waves) which interact in the ultrasonic field to produce a characteristic (diffraction) pattern. Full details of this model and its useful properties for analysing transducers are given in section (2.1.2).

### 2.1.1 KLM equivalent circuit model.

The Krimholtz (1970), Leedom (1971) and Mathaei or KLM equivalent circuit, models a piezoelectric transducer as a lossless mechanical transmission line of length  $l$ . This is coupled at its mid-point ( $l/2$ ) to a lumped-element electrical network. The circuit is shown in figure 2-1. It consists of an electrical network of frequency dependent components connected to the centre of an acoustic transmission line. The mechanical and electrical systems are linked through an ideal transformer of turns ratio  $1:\psi$  where  $\psi$  is a function of frequency and other physical parameters thus

$$\psi = [k_t(\pi/\omega_0 C_0 Z_0)^{1/2} \text{sinc}(\omega/2\omega_0)]^{-1} \quad (2-1)$$

where  $\text{sinc } x = \sin(\pi x)/\pi x$

$$\omega_0 = 2\pi f_0 \quad \text{the mechanical resonant frequency}$$

$$k_t^2 = \text{electromechanical coupling factor}$$

$$C_0 = \text{the clamped capacitance of the element}$$

$$\text{and } X_S = [k_t^2 \text{sinc}(\omega/\omega_0)]/C_0$$

Therefore  $\psi$  is an explicit function of both the frequency and electromechanical coupling factor.

$Z_0$  and  $v$  are the characteristic impedance and velocity respectively, associated with the acoustic transmission line. The line length  $l$  is equal to the transducer dimensions in the direction of acoustic wave propagation. The acoustic forces  $V_1$  and  $V_2$  appear directly across the transmission line terminals which allows clear distinction between the lumped element electrical behaviour and the wave acoustic behaviour of the transducer. This clearly distinguishes the roles of the electrical and mechanical ports of the transducer making it easy to see the effect of an arbitrary impedance connected to the electrical port. The useful features of this circuit include the ability to cope with transducers excited by non-uniform field distributions and/or non-uniform piezoelectric properties (Matthaei et

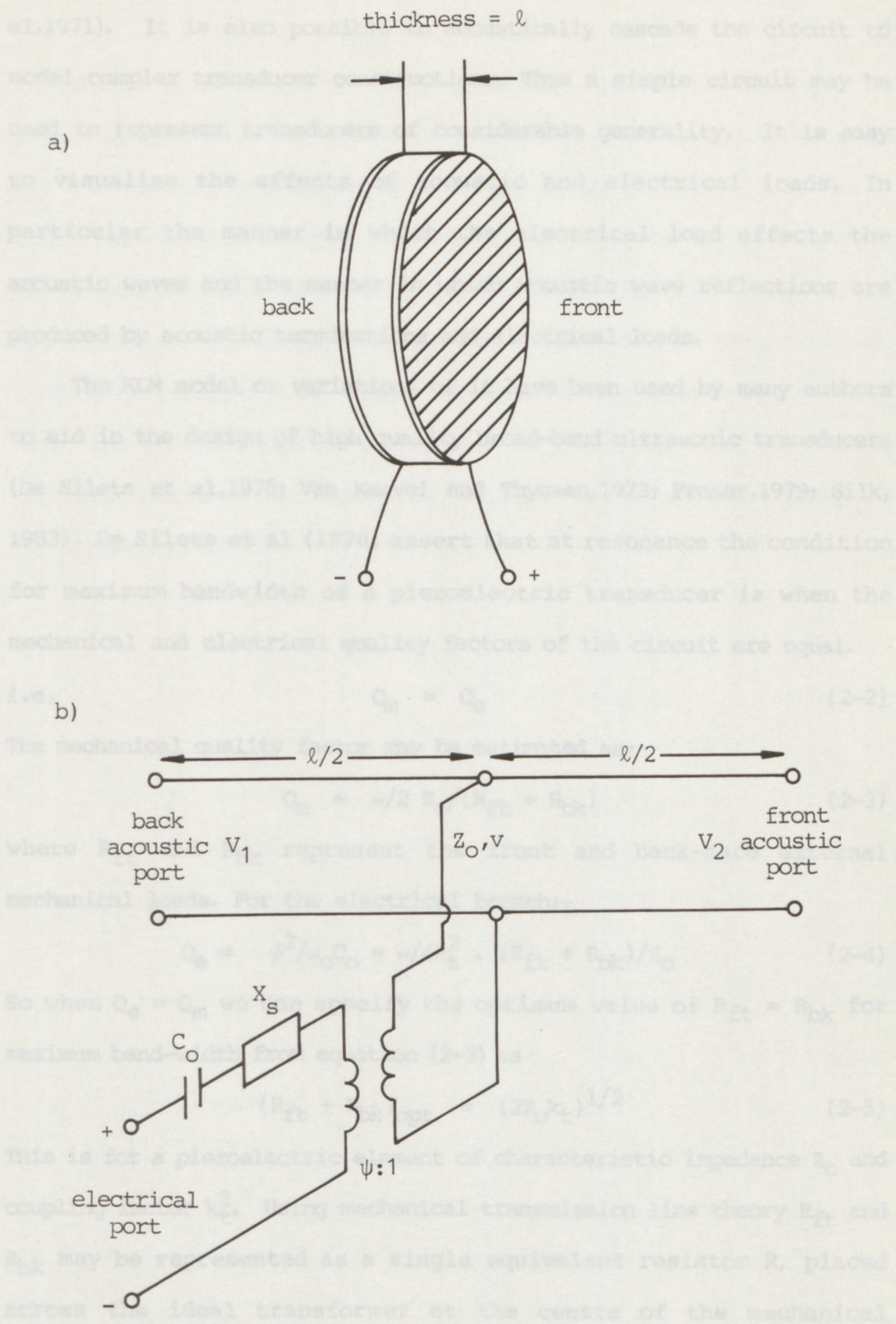


**Figure 2-1** The KLM equivalent circuit (Krimholts et al,1970; Leedom et al,1971) for a circular, thickness-expander mode, transducer showing:-  
 a) A circular, thickness-expander mode transducer element with its major face electrodes

b) The KLM equivalent circuit of the transducer shown in a).  
 Note: The front and back acoustic ports represent the front and back faces of the element shown in a). Energy (either acoustic or electrical) enters or leaves the network through the ports

al,1971). It is also possible to acoustically cascade the circuit to model complex transducer constructions. Thus a simple circuit may be used to represent transducers of considerable generality. It is easy to visualise the effects of acoustic and electrical loads. In particular the manner in which the electrical load effects the acoustic waves and the manner in which acoustic wave reflections are produced by acoustic terminations and electrical loads.

The KLM model or variations of it have been used by many authors to aid in the design of high quality broad-band ultrasonic transducers (De Silets et al,1978; Van Kervel and Thyssen,1973; Fraser,1979; Silk, 1983). De Silets et al (1978) assert that at resonance the condition for maximum bandwidth of a piezoelectric transducer is when the mechanical and electrical quality factors of the circuit are equal.

i.e. 
$$Q_m = Q_e \quad (2-2)$$

The mechanical quality factor may be estimated as:-

$$Q_m = \pi/2 Z_o / (R_{ft} + R_{bk}) \quad (2-3)$$

where  $R_{ft}$  and  $R_{bk}$  represent the front and back-face external mechanical loads. For the electrical branch:-

$$Q_e = \sqrt{2}/\omega_o C_o = \pi/4k_t^2 \cdot (R_{ft} + R_{bk})/Z_o \quad (2-4)$$

So when  $Q_e = Q_m$  we can specify the optimum value of  $R_{ft} = R_{bk}$  for maximum band-width from equation (2-3) as

$$(R_{ft} + R_{bk})_{opt} = (2Z_o k_t)^{1/2} \quad (2-5)$$

This is for a piezoelectric element of characteristic impedance  $Z_o$  and coupling factor  $k_t^2$ . Using mechanical transmission line theory  $R_{ft}$  and  $R_{bk}$  may be represented as a single equivalent resistor  $R$ , placed across the ideal transformer at the centre of the mechanical transmission line. The value of  $R$  is found from the parallel combination of  $R_{ft}$  and  $R_{bk}$  at the resonant frequency to give

$$R = Z_o^2 / (R_{ft} + R_{bk}) \quad (2-6)$$

Now  $R_{opt}$  the optimum value of  $R_{ft} + R_{bk}$  may be given as

$$R_{\text{opt}} = Z_0 / (2k_t)^{1/2} \quad (2-7)$$

In the case where an element of high characteristic acoustic impedance is radiating into a low impedance fluid like water the value obtained for  $R$  is usually much less than the  $R_{\text{opt}}$  value. To optimize the bandwidth the equivalent mechanical resistance  $R$  may be adjusted upwards using quarter-wave matching layers between the front face of the transducer and the propagating medium. The design of these may also be modelled using the KLM model. As well as the effects of front and back line acoustic loading the effects of electrical matching and the transient (impulse) response of transducers may be modelled using the KLM equivalent circuit.

face of the transducer into the geometric beam region whilst the edge-wave emanates from the periphery of the source and spreads in all directions (figure 2-2). Thus for a circular source the edge-wave has an almost toroidal wavefront. This wavefront has two important features which are essential to understand how the model can be used to explain the fields produced by ultrasonic transducers. Firstly, the portion of the "toroidal" edge-wave, which is propagating into the geometric beam region is  $\pi$  radians out of phase with the plane-wave whilst the portion propagating out of the geometric region is in phase with it. Secondly, the directivity of the edge-waves (figure 2-3) is such that on axis they appear as delayed, inverted replicas of the plane-wave with constant peak pressure on axis unlike a simple, toroidal wave where the peak pressure falls off as  $1/(r)^{-1/3}$ . It is this directivity which compensates for the spreading out of the wavefront with distance giving the constant peak pressure on axis.

In the case of continuous waves or of the plane- and edge-waves combine to give the well known axial field pattern of maxima and nulls shown in figure 2-6. This is a plot of the modulus of the axial pressure against range. For the case of interest here, i.e. short

### 2.1.2 Plane- and edge-wave model

Studies of the propagation of ultrasonic pulses in fluids and solids, at The City University, have confirmed that the field pattern produced by a rigid piston-like source undergoing longitudinal excitation can be explained as the combination of two components. These are known as plane- and edge-waves (Weight, 1982b; Weight and Hayman, 1978; Hayman and Weight, 1979). These may be considered to originate from the face and edge of the transducer respectively though both, in fact, consist of the sum of all the Huygens-type wavelets from the whole face of the transducer. The plane-wave propagates forward from the entire face of the transducer into the geometric beam region whilst the edge-wave emanates from the perimeter of the source and spreads in all directions (figure 2-2). Thus for a circular source the edge-wave has an almost toroidal wavefront. This wavefront has two important features which are essential to understand how the model can be used to explain the fields produced by ultrasonic transducers. Firstly, the portion of the "toroidal" edge-wave, which is propagating into the geometric beam region is  $\pi$  radians out of phase with the plane-wave whilst the portion propagating out of the geometric region is in phase with it. Secondly, the directivity of the edge-waves (figure 2-3) is such that on axis they appear as delayed, inverted replicas of the plane-wave with constant peak pressure on axis unlike a simple, toroidal wave where the peak pressure falls off as  $1/(r)^{-1/2}$ . It is this directivity which compensates for the spreading out of the wavefront with distance giving the constant peak pressure on axis.

In the case of continuous waves or cw the plane- and edge-waves combine to give the well known axial field pattern of maxima and nulls shown in figure 2-4. This is a plot of the modulus of the axial pressure against range. For the case of interest here, i.e. short

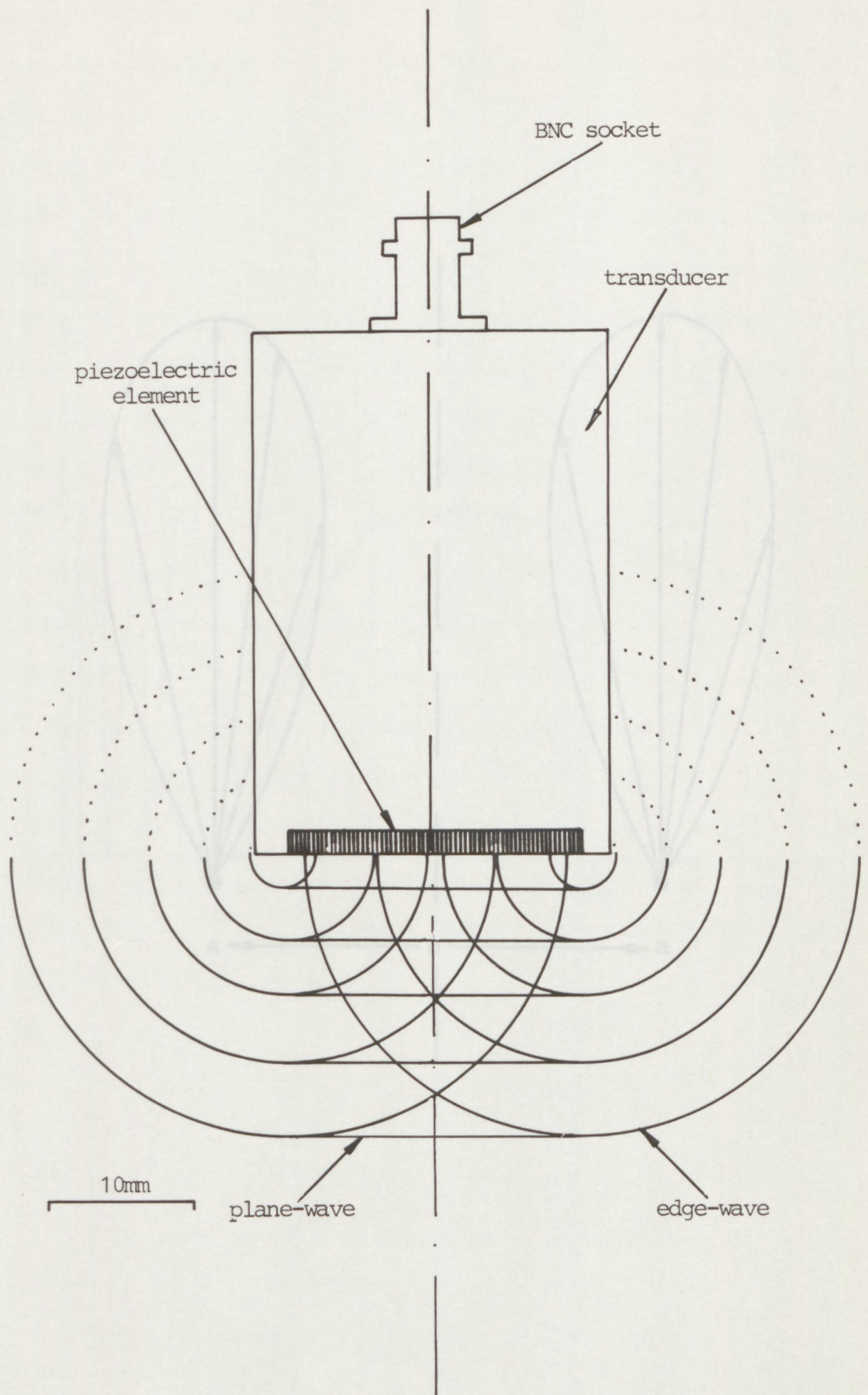
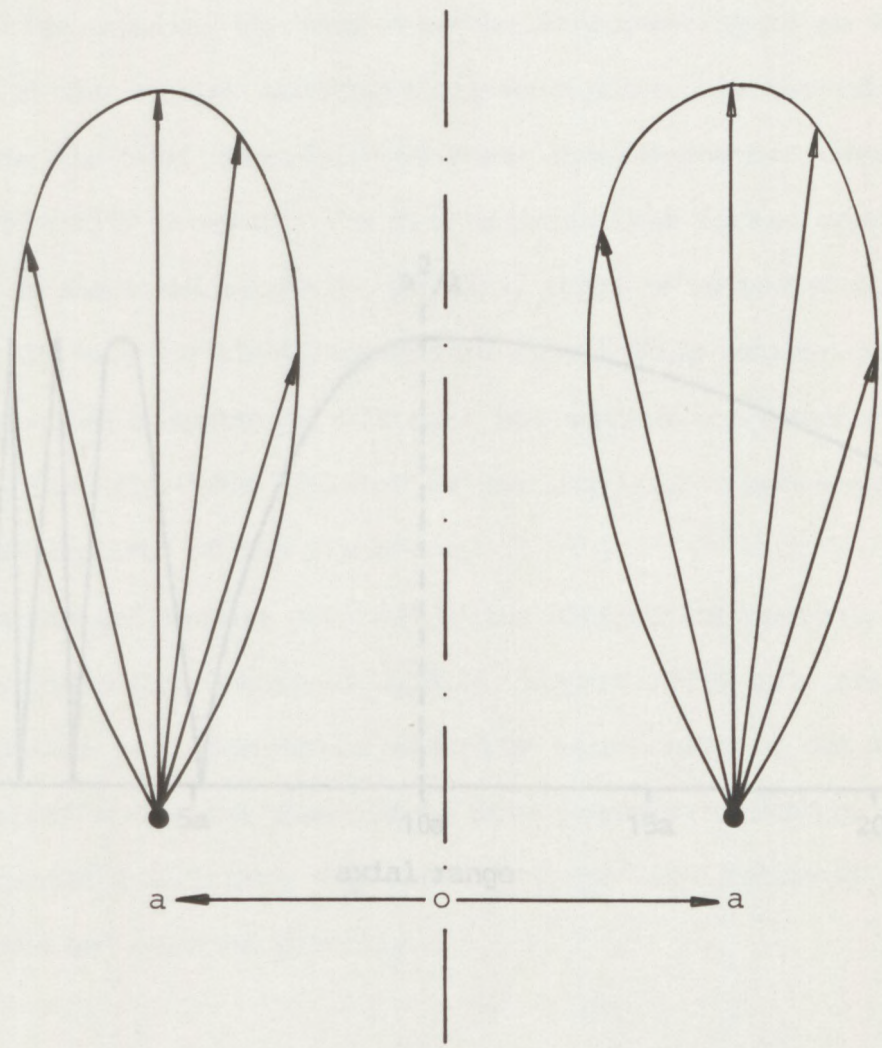


Figure 2-2 A schematic diagram showing the plane and edge-waves from a circular source. Note: The directivity of the edge-wave is not accurately represented



**Figure 2-3** Pressure vectors and polar diagrams for diametrically opposite points on a circular EWO source (Weight, 1982a) showing the directivity of the edge-wave which compensates for the spreading of the wavefront. This results in (ideally) constant peak pressure at all axial ranges

pulses from circular transducers, all the contributions from the source perimeter arrive on axis simultaneously giving rise to a single edge-wave pulse. At small axial ranges (e.g. less than 1 transducer diameter) the path difference between the plane- and edge-wave pulses is such that they can be clearly resolved from one another in the time domain, the edge-wave pulse appearing as an inverted replica of the earlier arriving plane-wave pulse. As the axial range increases, the time separation of these components decreases until they eventually overlap. The single pulse thus formed continuously changes in shape and length as the axial range is increased due to the continuing time separation between the plane- and edge-wave components off axis but within the geometric beam region, the edge-wave appears as two smaller, time-separated and distorted replicas of the plane-wave pulse.

Experimental results obtained by the ultrasonics research group at The City University (Wight, 1976, 1977b; Hayman, 1979) have shown that these plane- and edge-waves actually exist and are not a purely theoretical construct. Under suitable experimental conditions they may be time resolved from the plane-wave and observed directly.

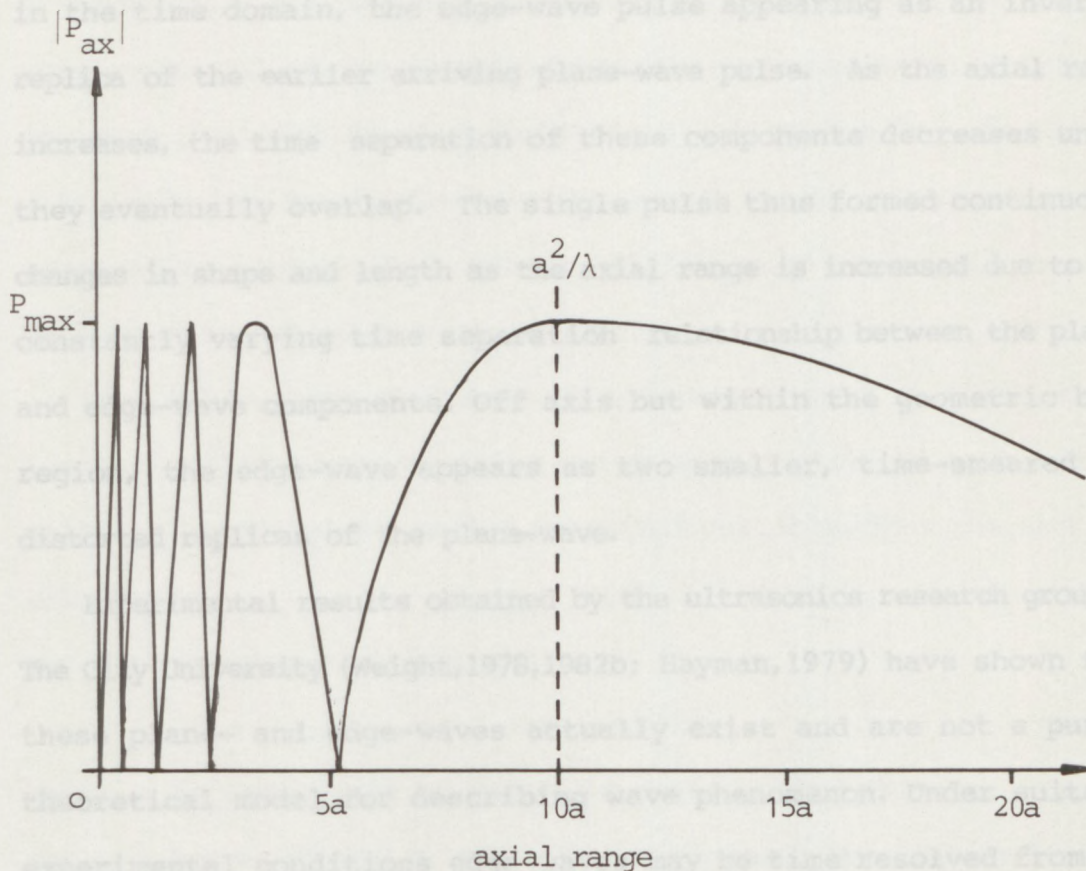


**Figure 2-4** The modulus of the axial pressure of a circular source under conditions of continuous excitation - the range is shown as multiples of the transducer radius  $a$  and  $a = 10\lambda$

pulses from circular transducers, all the contributions from the source perimeter arrive on axis simultaneously giving rise to a single edge-wave pulse. At small axial ranges (e.g. less than 3 transducer diameters) the path difference between the plane- and edge-wave pulses is such that they can be clearly resolved from one another in the time domain, the edge-wave pulse appearing as an inverted replica of the earlier arriving plane-wave pulse. As the axial range increases, the time separation of these components decreases until they eventually overlap. The single pulse thus formed continuously changes in shape and length as the axial range is increased due to the constantly varying time separation relationship between the plane- and edge-wave components. Off axis but within the geometric beam region, the edge-wave appears as two smaller, time-smeared and distorted replicas of the plane-wave.

Experimental results obtained by the ultrasonics research group at The City University (Weight, 1978, 1982b; Hayman, 1979) have shown that these plane- and edge-waves actually exist and are not a purely theoretical model for describing wave phenomenon. Under suitable experimental conditions edge-waves may be time resolved from the plane-wave and observed directly.

$$p(r,t) = \frac{1}{2} \iint_S p_0(\theta) \exp[i(kr - \omega t)] dA \quad (2-11)$$

where  $k = \omega/c$  (the wave number),  $c$  is wave velocity (compression),  $r$  is the distance from the field point to the surface element  $dA$  and  $\omega$  is the angular frequency. Generally this expression is insoluble apart from a few special cases such as the far field of a circular piston source (see 13.7). For this case the pressure variation across the beam  $p(r)$  (normalised by the average value  $p_0$ ) is given by

$$p(r)/p_0 = (2J_1(ka \sin \theta)) / (ka \sin \theta) \quad (2-12)$$

## 2.2 Impulse Response Method.

For the purposes of this treatment an ultrasonic transducer is considered as a rigid-piston type radiator mounted in an infinite baffle. This is analogous to an aperture illuminated by a plane-wave. When the source is emitting continuous sinusoidal waves into a fluid the pressure field produced corresponds to a diffraction pattern. The wavelengths and source dimensions typically encountered in ultrasonics are such that both Fresnel (near-field) and Fraunhofer (far-field) diffraction are found. Extensive literature exists on continuous wave propagation (Strutt, 1945; Hunter, 1957) so only a synopsis is given here as an introduction to pulse theory.

By taking the particle displacements in a fluid to be irrotational the wave equation can be simply given in terms of the velocity potential  $\phi$  a scalar potential variable. Thus the particle velocity is

$$\underline{v} = -\nabla\phi \quad (2-8)$$

and the instantaneous pressure is

$$P = \rho\partial\phi/\partial t \quad (2-9)$$

where  $\rho$  is the density of the fluid medium. The velocity potential due to a source of area  $A$  undergoing continuous sinusoidal motion with normal velocity

$$v_n = v_0 \exp^{j\omega t} \quad (2-10)$$

has been shown by Lord Rayleigh (Strutt, 1945) to be

$$\phi(r,t) = 1/2\pi \iint_A (v_0/r) \exp^{j(\omega t - kr)} dA \quad (2-11)$$

where  $k = \omega/c$  (the wave number),  $c$  is wave velocity (compression),  $r$  is the distance from the field point to the surface element  $dA$  and  $\omega$  is the angular frequency. Generally this expression is insoluble apart from in a few special cases such as the far field of a circular piston source (Bess, 1970). For this case the pressure variation across the beam  $P(\theta)$  (normalised by the on-axis value  $P_0$ ) is given by

$$P(\theta)/P_0 = (2J_1[kasin\theta])/(kasin\theta) \quad (2-12)$$

where  $a$  is the source radius,  $\theta = \tan^{-1}(y/r)$  and  $y$  is the distance of the field point from the axis. The intensity modulation across the beam is a series of rings surrounding a central maximum in the form of a Fraunhofer diffraction pattern. Close to the source, equation (2-11) can only be analytical solved on axis and gives the following result for the axial pressure  $P_{ax}(x)$  normalised by the maximum pressure  $P_{max}$

$$P_{ax}(x)/P_{max} = \sin(\pi/\lambda[(a^2 + x^2)^{1/2} - x]) \quad (2-13)$$

where  $\lambda =$  wavelength and  $x =$  axial range. It is notable that the amplitude of  $P_{max}$  is twice that of the emitted plane-wave. Figure 2-4 shows a plot of this axial solution for a source of radius  $10\lambda$ . Note that for a cw source, the near field extends to  $a^2/\lambda$ .

Continuous wave theory can often be used to describe the situation of quasi-continuous pulses containing several cycles during the period (if any) where steady state conditions apply. However, with short pulses the temporal shape of the wave fronts is not adequately described.

Rayleigh's equation must be solved in terms of an arbitrary source velocity in order to obtain a full transient solution giving the temporal waveforms at pressure points in the field. Theoretically this transient solution may be obtained by transforming steady-state harmonic solutions into the time domain. However, as mentioned earlier even steady-state solutions are not available for general field points.

Impulse response methods (Tupholme,1969; Beaver,1974; Bess,1970; Stepanishen,1971; Robinson et al,1974) have since been developed particularly by Stepanishen (1971). These allow the pressure due to an impulsive source velocity to be calculated. By making use of the theory of linear time invariant systems, the pressure for an arbitrary source motion may be found by convolving the source velocity with the pressure impulse response. Rayleigh's equation for arbitrary motion

of a source radiating into a fluid is

$$\phi(r,t) = 1/2\pi \iint_A v_n(t - r/c)/r \, dA \quad (2-14)$$

where  $v_n(t - r/c)$  represents the normal velocity of the surface element  $dA$  at a time  $r/c$  before  $\phi$  is estimated. The pressure is again given by equation (2-9) as  $P = \rho \partial \phi / \partial t$

so

$$P(r,t) = \rho/2\pi \partial/\partial t \iint_A v_n(t - r/c)/r \, dA \quad (2-15)$$

Defining an impulse response function  $\phi_i(r,t)$  for an impulsive motion of the source at a time  $(t - r/c)$  as

$$\phi_i = 1/2\pi \iint_A \delta(t - r/c)/r \, dA \quad (2-16)$$

where  $\delta$  represents a delta function and assuming a linear time invariant system the velocity potential for an arbitrary source motion  $v(t)$  is given by

$$\phi(r,t) = v(t) * \phi_i(r,t) \quad (2-17)$$

$$= v(t) * 1/2\pi \iint_A \delta(t - r/c)/r \, dA \quad (2-18)$$

Similarly the pressure (equation 2-15) for an arbitrary source motion may be expressed as a convolution thus:-

$$P(r,t) = v(t) * P_i(r,t) \quad (2-19)$$

where

$$P_i = \rho \partial \phi_i / \partial t \quad (2-20)$$

This is the impulse pressure response. Stepanishen (1971) and Robinson et al (1974) have shown that equation (2-16) may be integrated by using a change of variable.  $dA$  may be expressed in terms of angle and distance (figure 2-5) by treating the surface of the source as the sum of the circular segments  $dA$ . If all points on a segment are equidistant from the general field point  $Q$  and  $Q'$  is the perpendicular projection of  $Q$  on the source

$$\begin{aligned} dA &= \Omega(r) L_r \delta L_r \\ \text{since } r^2 &= x^2 + L_r^2, \quad rdr = L_r dL_r \end{aligned} \quad (2-21)$$

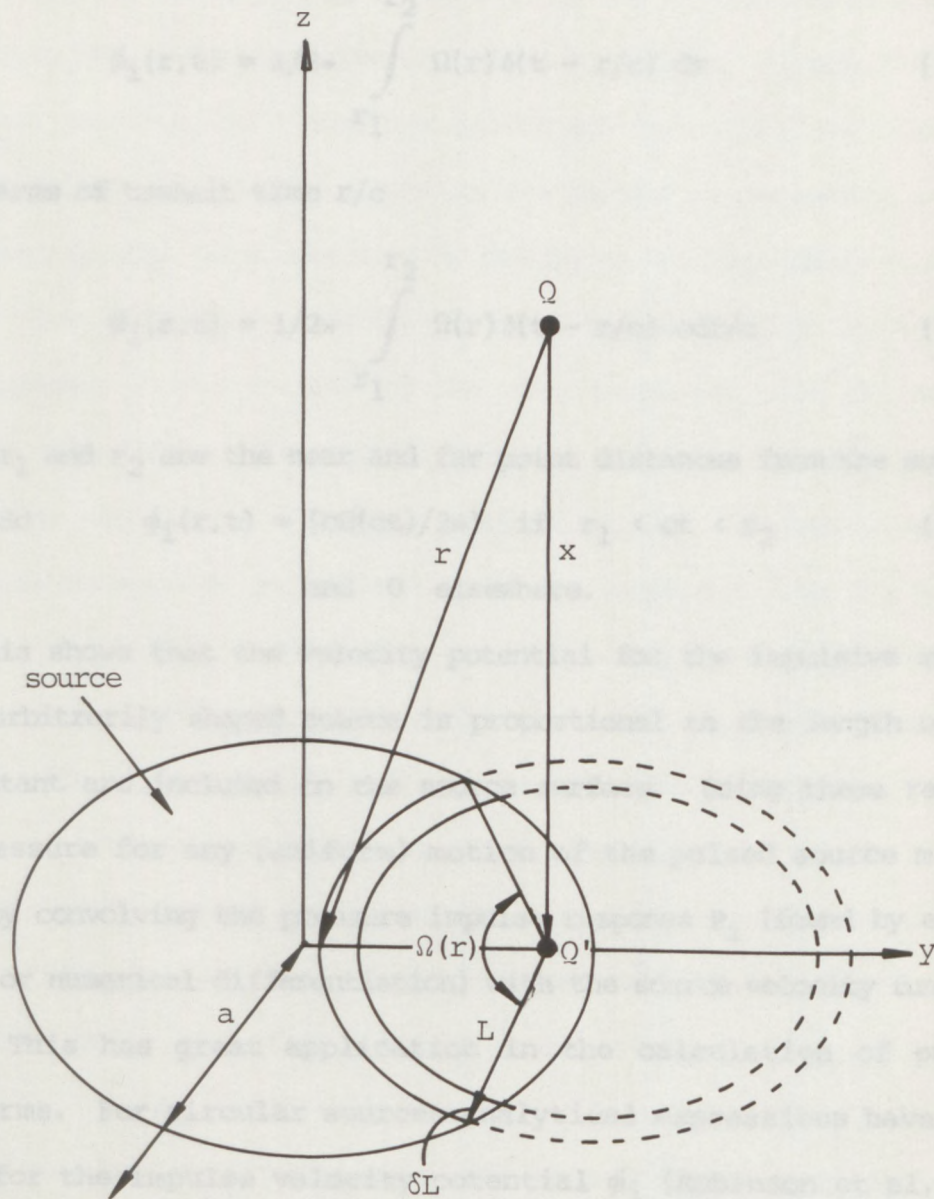


**Figure 2-5** The geometry of the equidistant arc on the surface of a source (Bess, 1970).  $Q'$  is the perpendicular projection of the general field point  $Q$  on the source

2-2-1  $dA = \Omega(r)rdr$

substituting in equation (2-16)

$$\phi_i(r,t) = 1/2\pi \int_{r_1}^{r_2} \Omega(r) \delta(t - r/c) dr \quad (2-22)$$

or in terms of transit time  $r/c$

$$\phi_i(r,t) = 1/2\pi \int_{r_1}^{r_2} \Omega(r) \delta(t - r/c) c dr/c \quad (2-23)$$

where  $r_1$  and  $r_2$  are the near and far point distances from the surface

to Q. So  $\phi_i(r,t) = (c\Omega(ct)/2\pi)$  if  $r_1 < ct < r_2$  (2-24)

and 0 elsewhere.

This shows that the velocity potential for the impulsive motion of an arbitrarily shaped source is proportional to the length of the equidistant arc included on the source surface. Using these results the pressure for any (uniform) motion of the pulsed source may be found by convolving the pressure impulse response  $P_i$  (found by either direct or numerical differentiation) with the source velocity function  $v(t)$ . This has great application in the calculation of pulsed waveforms. For circular sources analytical expressions have been given for the impulse velocity potential  $\phi_i$  (Robinson et al,1974; Lockwood and Willete,1973).

Figure 2-7 shows the situation off axis but inside the geometrical projection of the source. Again the velocity potential initially rises to a constant value at  $t_1$  but after  $t_2$  which now represents the transit time from the nearest source edge, the equidistant arc is no longer complete and  $\phi_i$  starts to fall. The fall is initially rapid but slows down for a period in the middle before speeding up again to reach zero at  $t_3$  the transit time from the

### 2.2.1 Graphical solution of the impulse-response method.

The usefulness of the impulse response method may be demonstrated by considering field points close i.e. in the near field of a source undergoing single-cycle, sinusoidal velocity motion. Figure 2-6 shows the axial solution for a circular piston source. Equidistant arcs at successive (arbitrary) time intervals are marked on the piston surface by broken lines. When the source undergoes an impulsive velocity motion the velocity potential  $\phi_i$  at Q rises sharply at time  $t_1$  corresponding to the arrival of the wave component from the nearest point on the source. The velocity potential  $\phi_i$  then remains constant whilst the equidistant arcs are complete circles and just after time  $t_2$ , which corresponds to the arrival of the component from the edge of the source, falls to zero. The corresponding impulse pressure is proportional to the time differential of  $\phi_i$  and consists of two equal and opposite delta functions. These are separated by the time between components arriving at Q from the nearest point on the source and the edge. When the piston motion is one cycle of a sine wave, the two pulse pattern is retained, the second pulse being an inverted replica of the first i.e. the axial pressure is given by

$$P_{ax}(r,t) = \rho c(v[t-t_1] - v[t-t_2]) \quad (2-25)$$

These two time resolved pulses are Young's plane and edge-waves respectively. At greater distances these would be closer together, eventually overlapping.

Figure 2-7 shows the situation off axis but inside the geometrical projection of the source. Again the velocity potential initially rises to a constant value at  $t_1$  but after  $t_2$ , which now represents the transit time from the nearest source edge, the equidistant arc is no longer complete and  $\phi_i$  starts to fall. The fall is initially rapid but slows down for a period in the middle before speeding up again to reach zero at  $t_3$  the transit time from the

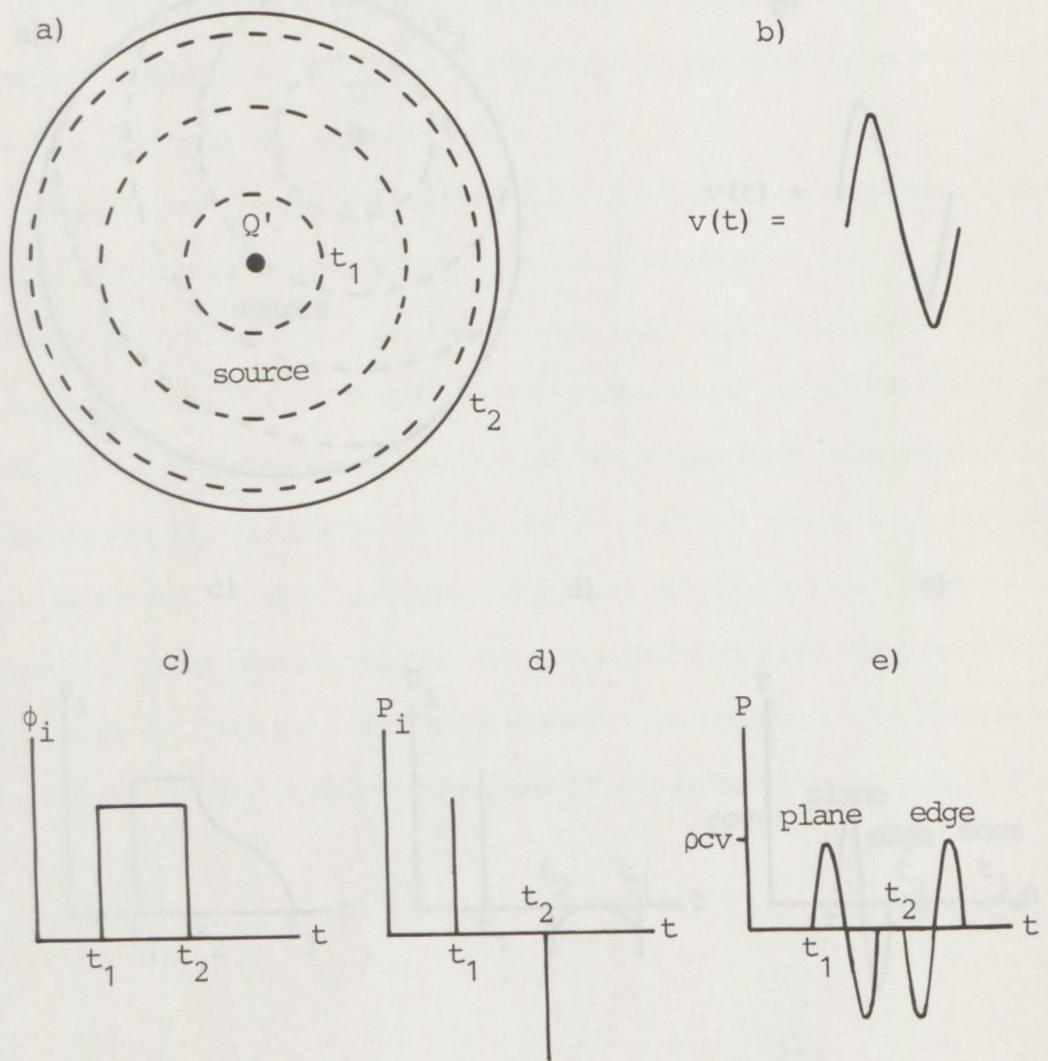


**Figure 2-6** The graphical solution of the impulse-response for the axial pressure of a circular source (Robinson, 1974) showing:-  
a) the projection of the field point  $Q$  and the equidistant arcs at successive time intervals on the surface of the source. These are shown by  $Q'$  and the broken lines respectively  
b) the velocity function  
c) the velocity potential impulse response  $\phi$   
d) the impulse pressure  $P_i$   
e) the pressure found by convolving the impulse pressure from d) with the velocity function from b) i.e.  $P = P_i * v(t)$

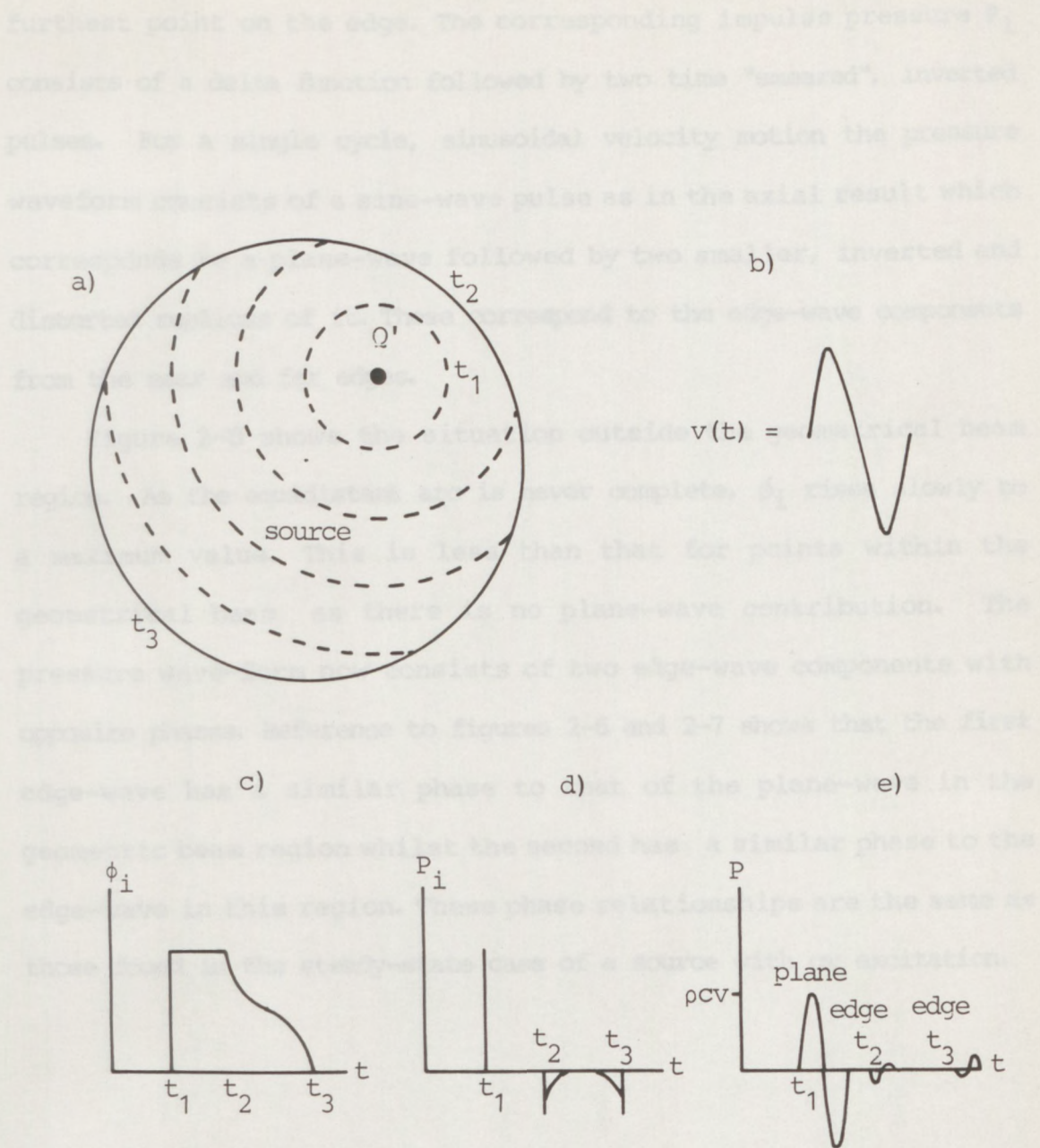


**Figure 2-7** The graphical solution of the impulse-response for the pressure at a point in the geometrical beam region of a circular source (Robinson, 1974) showing:-

- a) the projection of the field point  $Q$  and the equidistant arcs at successive time intervals on the surface of the source. These are shown by  $Q'$  and the broken lines respectively
- b) the velocity function
- c) the velocity potential impulse response  $\phi$
- d) the impulse pressure  $P_i$
- e) the pressure found by convolving the impulse pressure from d) with the velocity function from b) i.e.  $P = P_i * v(t)$

furthest point on the edge. The corresponding impulse pressure  $P_i$  consists of a delta function followed by two time "smeared", inverted pulses. For a single cycle, sinusoidal velocity motion the pressure waveform consists of a sine-wave pulse as in the axial result which corresponds to a plane-wave followed by two smaller, inverted and distorted replicas of it. These correspond to the edge-wave components from the near and far edges.

Figure 2-8 shows the situation outside the geometrical beam region. As the equidistant arc is never complete,  $\phi_i$  rises slowly to a maximum value. This is less than that for points within the geometrical beam as there is no plane-wave contribution. The pressure wave-form now consists of two edge-wave components with opposite phases. Reference to figures 2-6 and 2-7 shows that the first edge-wave has a similar phase to that of the plane-wave in the geometric beam region whilst the second has a similar phase to the edge-wave in this region. These phase relationships are the same as those found in the steady-state case of a source with cw excitation.

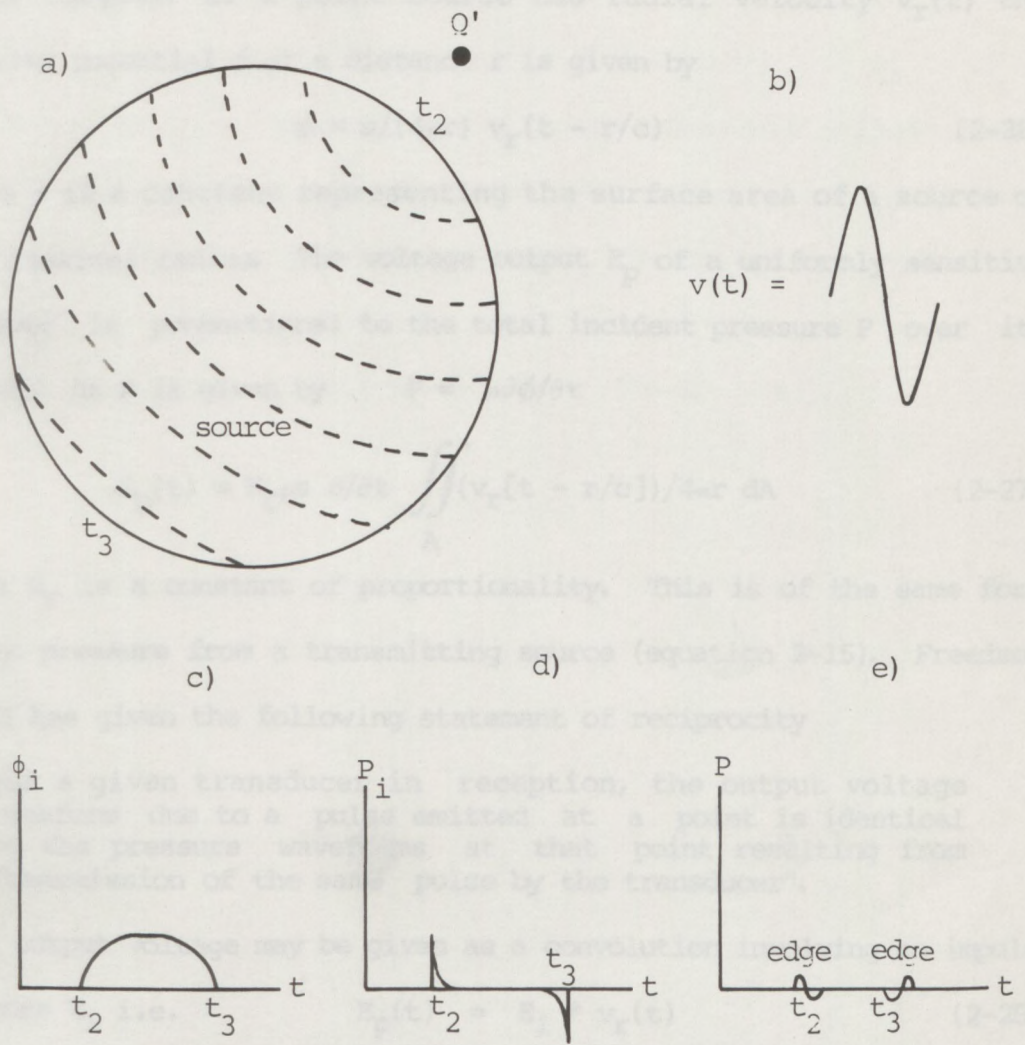


**Figure 2-8** The graphical solution of the impulse-response for the pressure at a point outside the geometrical beam region of a circular source (Robinson, 1974) showing:-

- a) the projection of the field point  $Q$  and the equidistant arcs at successive time intervals on the surface of the source. These are shown by  $Q'$  and the broken lines respectively
- b) the velocity function
- c) the velocity potential impulse response  $\phi$
- d) the impulse pressure  $P_i$
- e) the pressure found by convolving the impulse pressure from d) with the velocity function from b) i.e.  $P = P_i * v(t)$

### 2.2.2 Principle of reciprocity

The impulse response method may be extended to consider the principle of reciprocity and the transmit-receive mode responses from small targets. If a point source has radial velocity  $v_r(t)$  the velocity potential  $\phi$  at a distance  $r$  is given by

$$\phi = s/(4\pi r) v_r(t - r/c) \quad (2-26)$$

where  $s$  is a constant representing the surface area of a source of infinitesimal radius. The voltage output  $E_p$  of a uniformly sensitive receiver is proportional to the total incident pressure  $P$  over its surface. As  $P$  is given by

$$E_p(t) = K_r \rho s \frac{\partial}{\partial t} \iint_A (v_r[t - r/c]) / 4\pi r \, dA \quad (2-27)$$

where  $K_r$  is a constant of proportionality. This is of the same form as the pressure from a transmitting source (equation 2-15). Freedman (1970) has given the following statement of reciprocity

"For a given transducer in reception, the output voltage waveform due to a pulse emitted at a point is identical to the pressure waveforms at that point resulting from transmission of the same pulse by the transducer".

This output voltage may be given as a convolution involving an impulse response  $E_i$  i.e.

$$E_p(t) = E_i * v_r(t) \quad (2-28)$$

so the reciprocity relation may be stated as

$$E_i = (K_r s / 2) P_i \quad (2-29)$$

If the point source is replaced by a small rigid reflector which is assumed to have a reflection coefficient of  $-1$  and the incident wave is assumed to be locally plane the reflector may be treated as equivalent to a point source with velocity

$$v_r = -P/\rho c \quad (2-30)$$

Substituting for  $v_r(t)$  in equation (2-28) the electrical output from the receiver on receiving the reflected waveform is

$$E(t) = -(1/\rho c) E_i(r, t) * P(r, t) \quad (2-31)$$

using equations (2-19) and (2-29)

$$E(t) = - (K_T s / 2 \rho c) v(t) * P_i(r, t) * P_i(r, t) \quad (2-32)$$

On axis, the pressure impulse response  $P_{i\text{ax}}$  consists of delta functions only thus (from section 2.2.1)

$$P_{i\text{ax}}(r, t) = \rho c \delta(t) - \rho c \delta(t - \tau) \quad (2-33)$$

where the origin of the time scale is now taken as the instant when the plane wave arrives at the field point and  $\tau = t_2 - t_1$  the extra time taken by the edge-wave to arrive. The output voltage is then given by

$$E_{i\text{ax}}(t) = K_T s / 2 (\delta(t) - 2\delta[t - \tau] + \delta[t - 2\tau]) \quad (2-34)$$

### 2.3 Non-Uniformly Excited Sources.

Undesirable pressure fluctuations in the near field of uniformly excited sources emitting continuous or quasi-continuous waves have long been noted (Roderick,1951; Kossoff,1971). Sources emitting short pulses produce more uniform beams but the pulse shape varies considerably with field positions due to the diffraction effects already discussed. It has been shown (Szabo,1975; Pohlman et al,1977) that a cw source that has a Gaussian velocity profile across its diameter can produce a steady-state field containing no near-field minima or far-field side lobes. However, in general its sensitivity and lateral resolution are lower than a uniformly excited source of equal size. This is because any practical approximation to the Gaussian velocity cannot be truncated too much, otherwise near-field extrema may be re-introduced. Thus the collimation of the beam and, in turn, its sensitivity with range are reduced as only the centre of the source is strongly excited. The reduced length of the near-field region and beam spreading can spoil the lateral resolution. Weighting functions which attempt to compromise between improved pulse-shape and lower sensitivity and collimation have also been tried (Bradfield,1960; von Haselberg and Krautkramer,1959; Martin and Breazeale,1971; Kossoff,1971; Szabo,1975; Pohlman et al,1977).

It has also been found (Kondrat'ev and Karpel'son,1978; Burckhardt et al,1975; Shnyrev and Semiovova,1980) that a circular source which is excited more strongly towards its periphery can produce a narrow beam centred on the axis. Such a source compares favourably with a conventional focussed transducer in that it has a much greater depth of field but suffers from larger side lobes in the focal region.

More recently, non-uniformly excited pulsed sources have been investigated (Burckhardt et al,1975; Shnyrev and Semiovova,1980; Weyns,1980; Dietz et al,1979; Stepanishen,1981; Harris,1981) with a

great interest in the beam profile of arrays and high lateral-resolution transducers. The impulse response approach has been extended to non-uniformly excited sources and a simple approach using the principle of superposition is used here.

The pressure at a point in the field of a non-uniformly excited source of axial symmetry is considered to be due to the sum of concentric sources of varying radii, each of which undergoes uniform in-phase motion of arbitrary amplitude. The pressure from each source is given by equation (2-19) as

$$P(r,t,y) = v(t,y) * P_i(r,t,y) \quad (2-35)$$

Note that the source velocity  $v$  is now also a function of radial displacement  $y$ , so the total pressure due to a non-uniformly excited source of radius  $a$  is

$$P_w(r,t) = \int_0^a P(r,t,y) dy \quad (2-36)$$

which may be evaluated numerically. Considering the situation on axis, the pressure is given by equations (2-25) and (2-36) as

$$P_{wax}(r,t) = \rho c \int_0^a v(t,y) - v(t - \tau(y),y) dy \quad (2-37)$$

It should be noted that the time origin is offset to coincide with the arrival time of the wave component from the centre of the source and  $\tau(y)$  is the delay until the edge-wave components arrive. If the amplitude of  $v(t,y)$  is constant over a large central area,  $P_{wax}$  consists of a large plane-wave component (given by the first term of the integral) followed by a smeared out edge-wave component given by the second term. This is due to the first terms of the summation superimposing and each of the second being slightly time shifted. By reversing the situation so that the amplitude is zero at the centre of the source an approximation to an edge-wave only source may be made.

### 2.3.1 Plane-wave only (PWO) sources

The problem of producing a more uniform field from pulsed sources may be considered in terms of the plane- and edge-wave model. As many of the undesirable effects which cause the pulse produced by a transducer to extend in duration and change in shape are due to the interaction of the plane- and edge-wave pulses, removing the edge-wave pulse would seem an obvious method of producing a more uniform beam. However, there are major problems with this approach to producing a plane-wave only or PWO transducer. Firstly, if a uniform plane-wave were produced, edge-waves would be generated as soon as the wave started to propagate (c.f. an aperture illuminated by an infinite plane-wave). Secondly the directivity of the beam in a uniformly excited source may be considered to come from the plane- and edge-wave interaction. Therefore removing the edge-wave pulse would cause the beam to spread out with range. A practical source would have to produce a non-uniform plane-wave pulse which was strong in the centre falling off towards the edge. This would give simple pulse shapes but suffer from reduced sensitivity and lateral resolution due to beam spreading.

As the plane-wave pulse consists of all the Huygens-type wavelets from the whole face of the transducer it is necessary to apodise the response of the entire transducer face as some function of its radius in order to achieve the desired effect. The velocity weighting is chosen to effect a compromise between having a simple pulse shape and loss of directivity. A simple shifted cosine function (figure 2-9) as

$$\begin{aligned} \text{given by } v(y) &= 1, 0 < y \leq Y_u \\ v(y) &= (1 + \cos [\pi/Y_V][Y-Y_u]), Y_u \leq y \leq a \end{aligned} \tag{2-38}$$

provides a smooth transition from the central region of constant velocity to the zero velocity region at the edge. Computer simulation results (section 4.1) using the impulse response method have shown

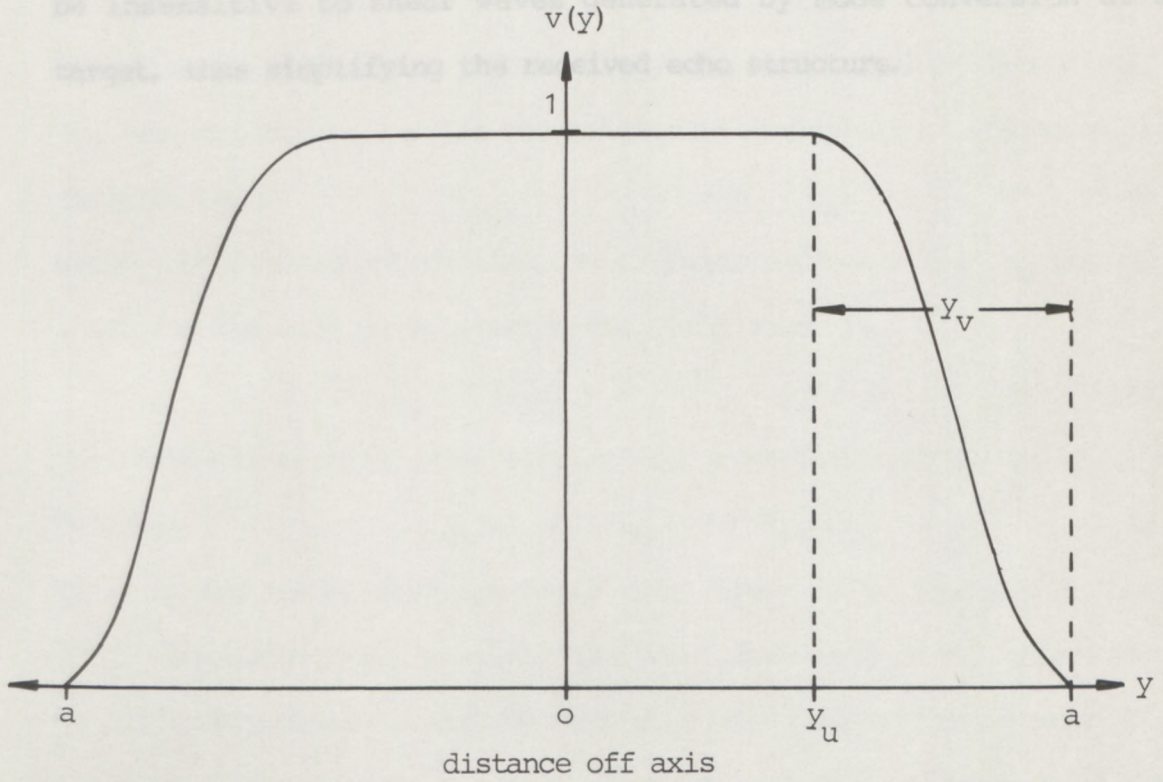


**Figure 2-9** The form of velocity weighting function required to produce a PWO transducer. The function is a form of shifted cosine "bell" (Weight, 1982b)

that if  $y_u = a/2$  so  $y_u = y_v$  (2-39)

good results are obtained.

So far only propagation in fluids has been discussed. However, a PWO transducer would also be useful when coupled to solids. This is because no shear waves would be generated and conversely it would also be insensitive to shear waves generated by mode conversion at a target, thus simplifying the received echo structure.

The axial pressure impulse response would consist of a single delta function thus  $P_{1ax}(t) = \delta(t - t_0)$  (2-40)

where the instant of excitation is taken as  $t = 0$  and  $t_0$  the time taken for the edge wave to reach the field point is

$$t_0 = \frac{1}{c} \sqrt{a^2 + x^2} \quad (2-41)$$

The transmit-receive axial response for a small target using section 2.2.2 is  $S_{1ax}(t) = P_{1ax}(t) * P_{1ax}(t)$  (2-42)

This reduces (using equation 2-40) to a single delta function at time  $2t_0$ . Equation (2-40) predicts that the sensitivity of the PWO source to small targets is similar to that of a uniformly excited source. Its range resolution is theoretically limited only by the duration of the excited pulse unlike a uniformly excited transducer where the near field resolution by instance is limited by diffraction effects and the lateral resolution by the extent of the plane-wave component of the source diameter. Unlike a conventionally focused source, its range sensitivity to targets is uniform. As the edge-wave pulse exhibits the sum of all the Rayleigh-type wavelets from the entire face of the transducer it is necessary to specify the response of the whole transducer face as some function of its radius in order to predict the desired type of response. Computer modelling (section 2.3) has shown that a circular transducer with the full excitation of the edge of the source to zero a small distance in, gives a good approximation to the desired response. This type of piezoelectric

### 2.3.2 Edge-wave only (EWO) sources.

Graphical solutions of the impulse response method have shown that for points on the axis of a circular source the edge-wave pulse is an inverted replica of the plane-wave pulse. The edge-wave pulse retains its amplitude at all axial ranges and splits into two smaller distorted replicas off axis. An ideal edge-wave only or EWO transducer would have a uniform response concentrated on its axis. The axial pressure impulse response would consist of a single delta function thus

$$P_{iax}(t) = -\delta(t - \tau_e) \quad (2-40)$$

where the instant of excitation is taken as  $t = 0$  and  $\tau_e$  the time taken for the edge wave to reach the field point is

$$\tau_e = 1/c(a^2 + x^2)^{1/2} \quad (2-41)$$

The transmit-receive mode response for a small target using section 2.2.2 is

$$E_{iax}(t) = P_{iax}(t) * P_{iax}(t) \quad (2-42)$$

This reduces (using equation 2-40) to a single delta function at time  $2\tau_e$ . Equation (2-40) predicts that the sensitivity of the EWO source to small targets is similar to that of a uniformly excited source. Its range resolution is theoretically limited only by the duration of the emitted pulse unlike a uniformly excited transducer where the near field resolution for instance is limited by diffraction effects and the lateral resolution by the extent of the plane-wave component i.e. the source diameter. Unlike a conventionally focussed source, its range sensitivity to targets is uniform. As the edge-wave pulse consists of the sum of all the Huygens-type wavelets from the entire face of the transducer it is necessary to apodise the response of the whole transducer face as some function of its radius in order to produce the desired type of response. Computer modelling (section 4.1) has shown that a smooth Gaussian fall off from full excitation at the edge of the source to zero a small distance in, gives a good approximation to the desired response. This type of piezoelectric

apodisation is shown in figure 2-10. A practical approximation to this type of transducer in the form of a fine annular source has already given promising results (Weight,1982a). These show good lateral resolution over a wide axial range. A better EWO source would have advantages over this device in that it would possess a greater depth of field and a simpler lobe structure due to its increased bandwidth. Equation (2-41) shows that, unlike the characteristics of a conventional source, there is a non-linear relationship between the time of flight of the echo pulse and the range of the target from the source plane. The target range is given by the expression

$$x(t) = (c^2t^2 - a^2)^{1/2} \quad (2-43)$$

where  $ct$  is the distance from the edge of the source to the target. To obtain a linear range display on an oscilloscope the time base waveform must be of the form given by equation 2-44 thus

$$V(t) = 2(c^2t^2 - a^2)^{1/2} \quad (2-44)$$

as shown in figure 2-11. If the start of the display is to represent zero target range the time base waveform must be delayed by  $2(a/c)$  before each sweep as  $ct = a$  at zero target range. The range resolution of conventional transducers in the near field is limited by the extra time taken for the edge-wave to arrive back at the edge of the transducer. In an EWO transducer the circular shape provides a built in delay equal to twice the transit time across the transducer radius. This reduces the dead time and therefore the size of the "dead zone" in front of the transducer in which there is no response to targets.

An EWO transducer has better short range resolution than a conventional transducer with similar sensitivity to targets of different sizes but at the expense of a non-linear range-time relationship. The positional error that results from using a linear time base sweep is less than 12% at ranges greater than  $2a$  and falls to approximately 3% at ranges from  $4a$ . So far for the sake of

piezoelectric polarisation

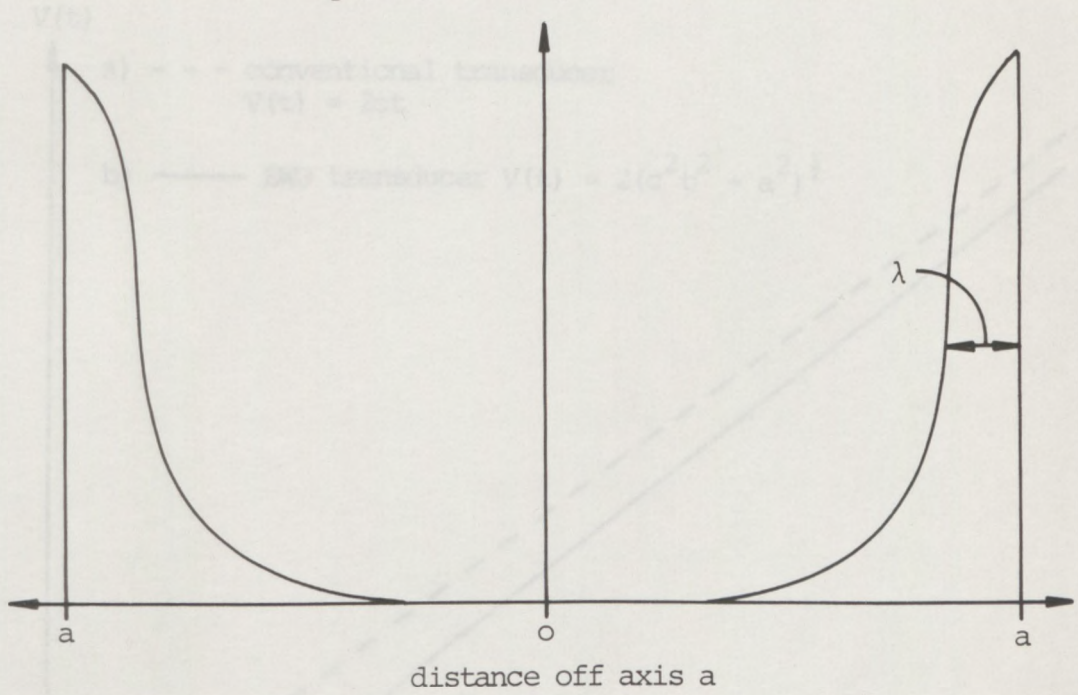


**Figure 2-10** The form of piezoelectric apodisation required to produce an EWO transducer. The excitation falls off from a maximum at the outer edge of the element to nothing a small distance in from the edge in a smooth Gaussian fashion (Weight, 1982a)

assumes only a linear time base has been used. The results presented in chapter 2 and particularly the 2-scale ranges given in section 4.4 require the analysis made above for EWO transducer. The effects of the non-linear range-time relationship are of course evident in the results.

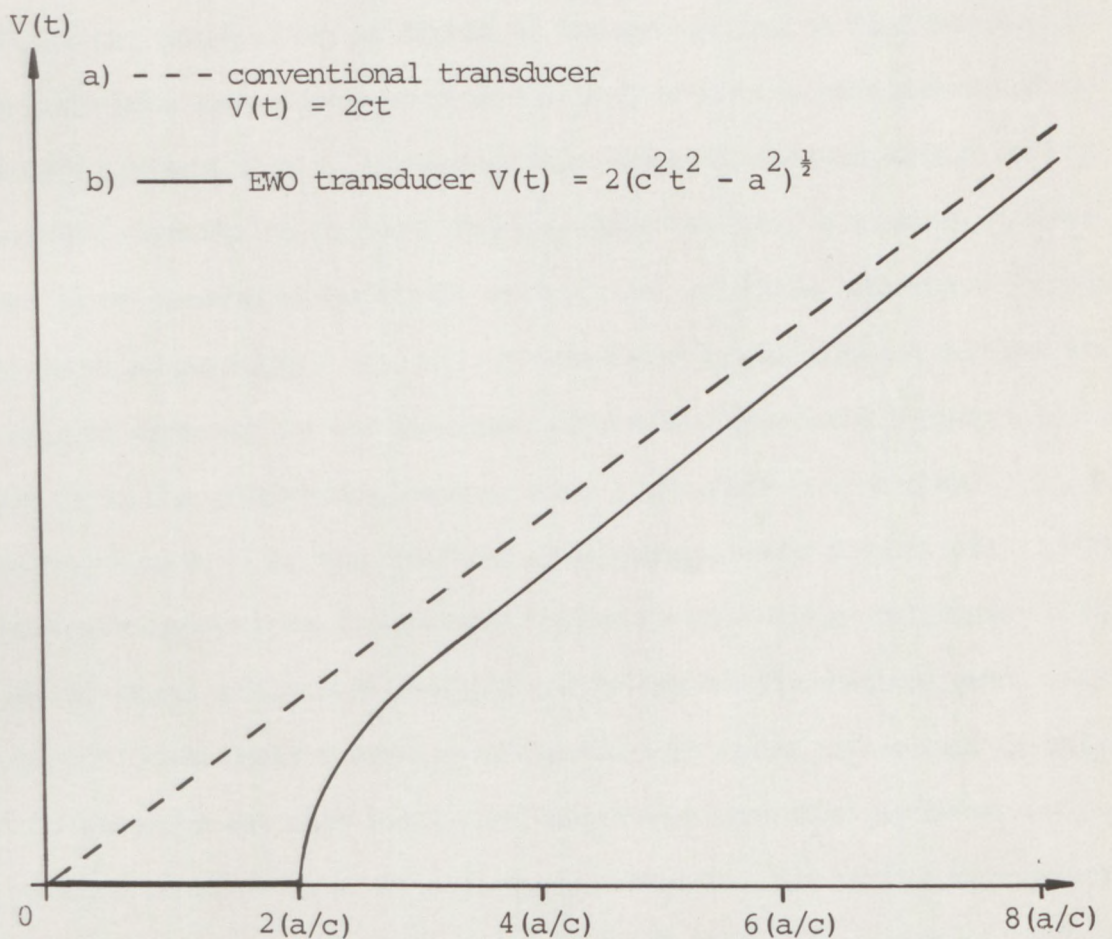


**Figure 2-11** The time-base waveforms for a linear display of target range (Weight, 1982b) using:-  
 a) a conventional transducer  
 b) an EWO transducer

convenience only a linear time base has been used. The results presented in chapter 4 and particularly the B-scan images given in section 4.4 confirm the claims made above for EWO transducer. The effects of the non-linear range-time relationship are of course evident in the results.

The major practical effect which is excited by the model when considering propagation in fluids is the generation of head waves. All the wide-band transducers considered in this work were constructed by bonding a thin disc of piezoelectric ceramic onto an acoustically impedance backing to provide damping (section 3.4). Ultrasonic pulses were then generated by shock excitation of these elements using electric pulses (section 3.5). These caused the element either to expand or contract in the thickness direction, launching a compression wave into the propagating medium with a pressure proportional to the source velocity. As the transducer elements were solids of finite volume it is obvious from their Poisson's ratio (approximately 0.3) that if their thickness changes their radial dimensions must also change to keep their volume approximately constant. The effect of this is to generate not only plane- and edge-waves but also plate waves.

Plate waves consist of a complex vibration that occurs throughout the thickness of thin (i.e. a few wavelengths thick) plates. These waves travel inwardly from the outer edge towards the centre and are damped by the transducer's backing. This causes their amplitude to decay exponentially. These waves are a type of incoherent wave in many ways and are a leak wave. They travel across the transducer element at a velocity somewhere between those of compression and shear waves. The radial velocity is a critical function of the geometry and dimensions of the element, its operating frequency, elastic constants and the boundary conditions which prevail. (1982) has given the plate

## 2.4 Practical Wide-Band Transducers

So far the ideal piston-source model of a pulsed transducer has been used. Whilst this has been shown to give an acceptable description of a transducer there are some differences between the behaviour of practical transducers (Weight, 1982b) and that predicted by this model.

The major practical effect which is omitted by the model when considering propagation in fluids is the generation of head waves. All the wide-band transducers considered in this work were constructed by mounting a thin disc of piezoelectric ceramic onto an acoustically absorbent backing to provide damping (section 3.4). Ultrasonic pulses were then generated by shock excitation of these elements using electric pulses (section 3.5). These caused the element either to expand or contract in the thickness direction, launching a compression wave into the propagating medium with a pressure proportional to the source velocity. As the transducer elements were solids of finite volume it is obvious from their Poisson's ratio (approximately 0.3) that if their thickness changes their radial dimensions must also change to keep their volume approximately constant. The effect of this is to generate not only plane- and edge-waves but also plate waves.

Plate waves consist of a complex vibration that occurs throughout the thickness of thin (i.e. a few wavelengths thick) plates. These travel inwardly from the outer edge towards the centre and are damped by the transducer's backing. This causes their amplitude to decay progressively. These waves are a type of interface wave in many ways akin to a Lamb wave. They travel across the transducer element at a velocity somewhere between those of compression and shear waves. The actual velocity is a critical function of the geometry and dimensions of the element, its operating frequency, elastic constants and the boundary conditions which prevail. Weight (1982b) has quoted the plate

wave velocities for PZT and PMN as  $3 \times 10^3$  m/s and  $4 \times 10^3$  m/s respectively. These results were obtained from experimental observations and are about 0.8 of compression wave velocities for these materials.

As these plate waves travel across the transducer element they cause a compression wave, known as a head wave, to be radiated into the propagating medium normal to the face of the transducer. They should also cause a head wave to be radiated outward from the edge of the transducer but in practice this wave is quickly absorbed by the material used to mount the backed element into its case. In travelling across the element, the plate wave causes the head wave to be launched into the propagation medium at an angle  $\theta$  with the transducer face. This angle depends upon the relative velocities of sound in the propagating fluid and the plate wave in the transducer element. It is given by

$$\theta = \sin^{-1}(c/v_{sw}) \quad (2-45)$$

where  $c = 1.5 \times 10^3$  m/s in water at  $20^\circ\text{C}$  and  $v_{sw}$  = lateral velocity of the plate wave. Figure 2-12 shows the development of these head waves in cross section.

It is the interference between the head wave and the edge-waves which leads to some departure from the behaviour predicted by the plane- and edge-wave model. Experiments with miniature probes interrogating uniformly excited transducers (Weight, 1982b) have shown that at certain axial ranges the amplitude of the edge-waves is much greater than expected, whilst at others the amplitude is below that predicted by theory. This effect, sometimes known as "edge-wave focusing" may be explained by considering the interaction between edge- and head-waves in more detail. At very short axial ranges the head waves converge and are time resolved from the edge-waves which arrive slightly later. However, at a slightly greater range these waves overlap and as they are in phase the head waves reinforce the

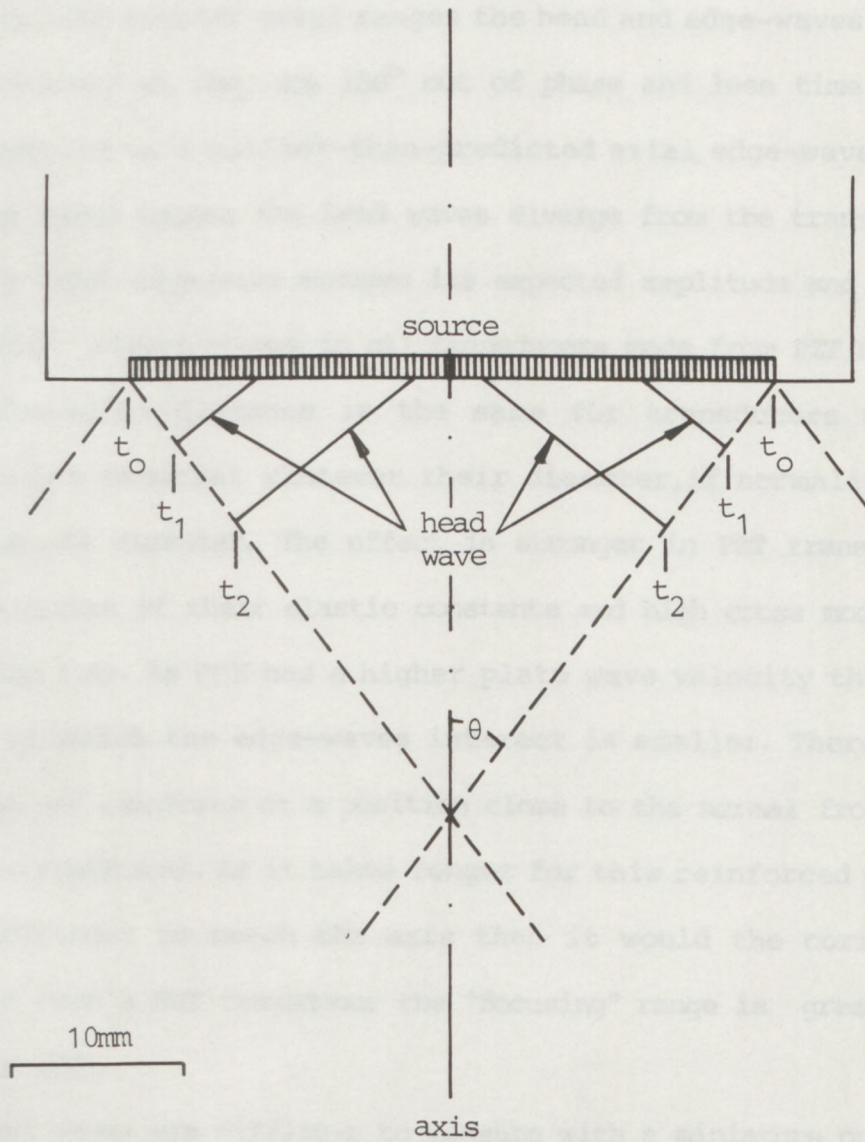


**Figure 2-12** A schematic view of the near field of a circular, ceramic transducer showing the head waves

edge-waves to produce the "focusing" effect. The head wave is quite strong at this range so the axial edge-wave can be nearly twice as large as expected in a PMN transducer and nearly four times its expected size in a PZT transducer. This enlarged, axial edge-wave may be distorted with a leading edge  $180^\circ$  out of phase with its expected polarity. At greater axial ranges the head and edge-waves interfere destructively as they are  $180^\circ$  out of phase and less time separated. This results in a smaller-than-predicted axial edge-wave. At still greater axial ranges the head waves diverge from the transducer axis and the axial edge-wave assumes its expected amplitude and shape. The "focusing" effect occurs in all transducers made from PZT and PMN and the "focusing" distance is the same for transducers made of a particular material whatever their diameter, if normalized by the transducer's diameter. The effect is stronger in PZT transducers due to the nature of their elastic constants and high cross mode coupling (section 1.4). As PMN has a higher plate wave velocity than PZT the angle at which the edge-waves interact is smaller. Therefore they overlap and reinforce at a position close to the normal from the edge of the transducer. As it takes longer for this reinforced portion of the wavefront to reach the axis than it would the corresponding portion from a PZT transducer the "focusing" range is greater in PMN than in PZT.

Head waves are difficult to measure with a miniature probe due to the obtuse angle of incidence of both the head and edge-waves at the range at which they are resolved. They are also difficult to visualize in a Schlieren system (Hayman, 1977) as their conical wavefront in water does not give rise to strong refraction of the incident illumination. However, by careful examination it is possible to observe them experimentally. Work done at The City University (Weight, 1982b) has revealed the head waves more strikingly by using square or

rectangular transducers so that the plate waves produce plane, compression head-waves in water which are more easily visualized and measured.

The effect of head waves on the characteristics of uniformly excited transducers has been discussed in some detail. However, head waves may also be generated in non-uniformly excited transducers. In EWO transducers head waves of reduced amplitude are likely to be generated and these will interfere with the edge-waves in the manner described above. This would lead to variations in the axial pressure in the near field of the transducer which should otherwise be constant with range (section 2.3.2). In PWO transducers no head waves should be generated, although at this stage it is unclear whether any other form of surface wave will be generated due to the form of excitation used to produce the PWO response. Recently more research has been done into the nature of head waves in ultrasonic transducers (Baboux et al, 1984), although, they have always been present in both thick, air-backed transducers and thin, highly damped transducers (Harris et al, 1982).

## CHAPTER 3

### EXPERIMENTAL METHODS

The equipment and methods described in this chapter were used to construct and characterize (Bredael, 1977) both uniformly and non-uniformly-excited, wide-band, ultrasonic, transducers.

Measurements of the electromechanical coupling coefficients of both PZT and PMN were made using equipment and methods as specified in the standards relating to piezoelectric measurements (IEEE,1978; IRE,1949-61).

Photofabrication methods based on the use of photoresist were used to produce the electrode pattern required for non-uniform poling. In order to make non-uniformly excited transducers it was necessary to develop methods for working right up to and including the edges of the substrates.

Whilst the method used to pole ceramics of both PZT and PMN had been established the poling apparatus was specially designed and commissioned for the production of non-uniformly excited transducers.

The apparatus and many of the methods used to construct the wide-band transmitting-transducers were developed especially for this project. Transmitting transducers were constructed from both uniformly-excited and non-uniformly excited piezoelectric elements. The methods used to produce wide-band characteristics are described.

The instrumentation used to make measurements including pressure waveforms, transmit-receive mode responses, frequency spectra, beam profiles and B-scans is outlined. The wide-band excitation and receiving system was designed and constructed within the ultrasonics group at The City University (Weight,1975,1982b). The specification of this system is given.

### 3.1 Electromechanical Coupling Measurement

The planar electromechanical coupling coefficient  $k_p$  was measured in accordance with the standards of the IEEE (1978; IRE, 1949-61). Figure 3-1 shows the circuit used and a schematic diagram of the apparatus. The matching network at the signal input stage was so arranged that the output impedance of the signal generator was always less than the impedance of the test specimens. The terminating resistor  $R_t$  was also kept below the impedance of the disc to avoid damping the peak current found at resonance. The resonant and anti-resonant frequencies  $f_r$  and  $f_a$  respectively for a disc vibrating in the radial mode were found by monitoring the current in the circuit with frequency. The current was measured as the voltage developed across  $R_t$ . At resonance ( $f_r$ ) the disc has a minimum electrical impedance so a large voltage (proportional to current) was developed across  $R_t$ . Conversely at anti-resonance ( $f_a$ ) the high impedance of the disc means that little current flows and there was a minimum voltage at that frequency. As the impedance of the disc is higher at  $f_a$  a higher value of  $R_t$  may be used to increase the sensitivity of the circuit.

The voltage was measured using a microvoltmeter (Solartron DVM model 7040 with a 70402 rf probe sub-unit) and the frequency of the signal generator (Wayne Kerr Video oscillator type 022B) was measured using a digital counter (Hewlett Packard model 5303B).

Connections to the discs were made either by small spring contacts or small soldered wires both of which were applied centrally so that they caused minimum interference with the resonance of the disc. Note: Discs in radial resonance have a node at the centre of their major faces. A typical signal strength of 50mV/mm (rms) was applied to the specimens.

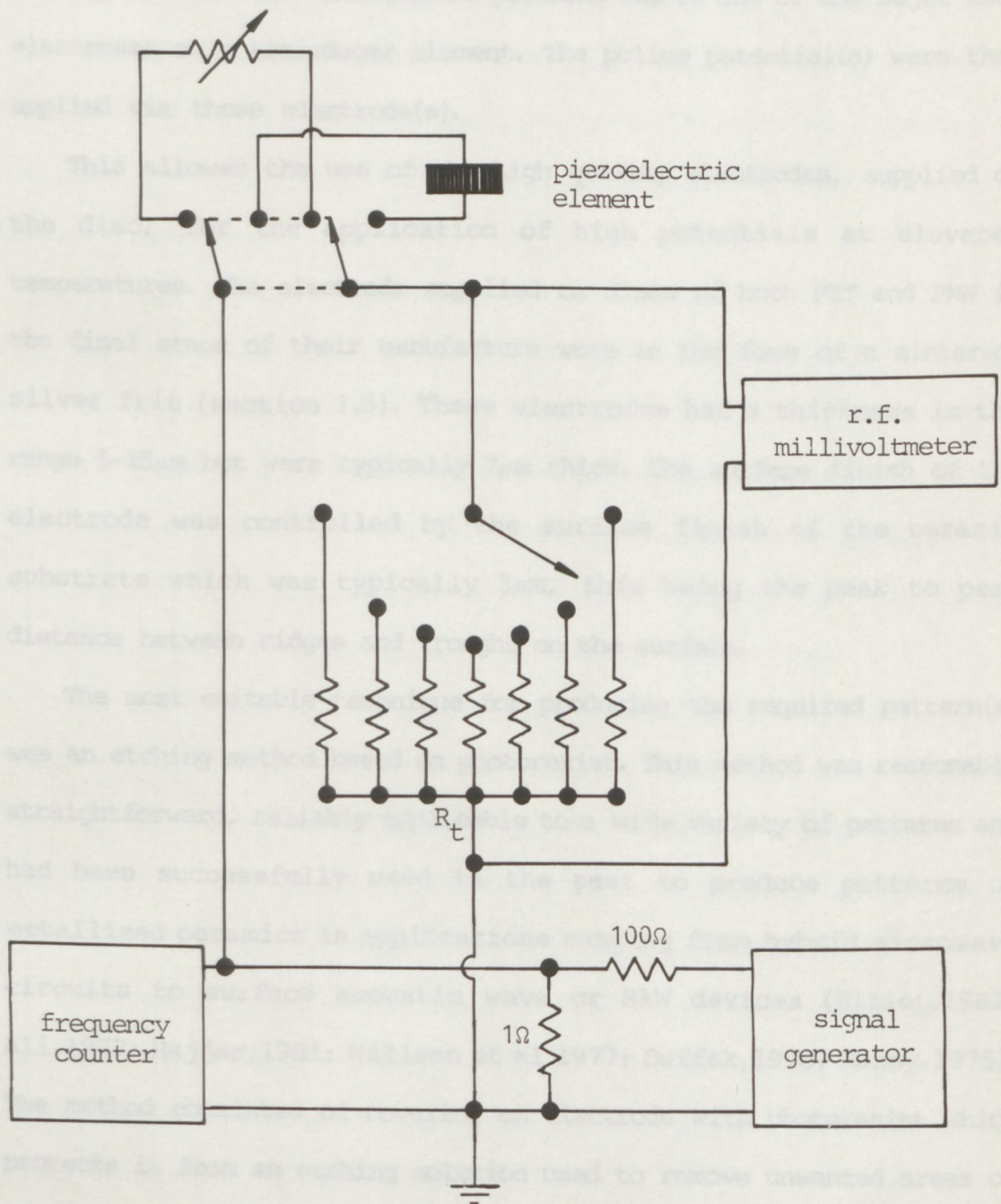


**Figure 3-1** The circuit for measuring the planar Electromechanical coupling factor ( $k_p$ ) of a piezoelectric, ceramic disc in accordance with the standards of the IEEE (1978)

### 3.2 Photofabrication of electrode patterns

Before poling, the field pattern needed to produce the required poling regime had to be set up. These field patterns were produced by etching suitable two-dimensional patterns out of one of the major face electrodes on a transducer element. The poling potential(s) were then applied via these electrode(s).

This allowed the use of the high quality electrodes, supplied on the disc, for the application of high potentials at elevated temperatures. The electrode supplied on discs of both PZT and PMN in the final stage of their manufacture were in the form of a sintered, silver frit (section 1.5). These electrodes had a thickness in the range 5-25 $\mu\text{m}$  but were typically 7 $\mu\text{m}$  thick. The surface finish of the electrode was controlled by the surface finish of the ceramic substrate which was typically 2 $\mu\text{m}$ , this being the peak to peak distance between ridges and troughs on the surface.

The most suitable technique for producing the required pattern(s) was an etching method based on photoresist. This method was reasonably straightforward, reliably applicable to a wide variety of patterns and had been successfully used in the past to produce patterns on metallized ceramics in applications ranging from hybrid microwave circuits to surface acoustic wave or SAW devices (Elliot,1982; Ali,1977; Hajjar,1981; Willson et al 1977; Duffek,1970; Kansy,1975). The method consisted of covering an electrode with photoresist which protects it from an etching solution used to remove unwanted areas of electrode. Photoresist is a solution of ultraviolet or UV light-sensitive resin in an organic solvent. By exposing it to UV light through a mask and then developing it in a suitable chemical the resist may be removed where required to allow the electrode to be etched. Exact details of the workings of photoresist may be found in the literature, see for example De Forest (1975).

Photoetching is a very common process used in applications ranging from the manufacture of semiconductor integrated circuits or IC's where resolution of the order of a  $1\mu\text{m}$  is sought to the manufacture of printed circuit boards or PCS's where resolution of the order of up to  $1\text{mm}$  may be acceptable. Whilst it might, at first, appear, that the resolution required in this application is trivial (of the order of  $100\mu\text{m}$ ) there are two major factors which conspire to make fabrication harder. These are :-

- (i) the surface roughness of the electrodes
- (ii) the fact that the discs are used right up to and including their edges.

Often the surface to be etched can be polished flat and the edges of the substrate discarded. However, as neither of these options were available in this application, special techniques had to be developed from the standard technologies of IC and PCB fabrication.

The photoresist used in this project was Microposit TF20 (Shipley Chemicals, COVENTRY) with Microposit 450cd developer. When required Microposit thinner was used to adjust the viscosity of the photoresist. Microposit TF20 is a novalak resin, diazo-oxide inhibited, positive working photoresist in an organic solvent system. It was a general purpose photoresist ideal in character for working on rough surfaces. This was found to be superior to the negative wet and dry photoresists used initially although it had the slight disadvantage of not being coloured.

The procedure for using the resist consisted of the following standard steps (De Forest, 1975; Kodak, 1979; Shipley, 1985):-

- (i) pretreatment
- (ii) coating
- (iii) softbake
- (iv) exposure
- (v) development
- (vi) postbake
- (vii) etching
- (viii) removal

The most serious contamination of the electrode surfaces was caused by finger prints. Therefore the pretreatment had to be rigorous enough to

remove these from the surface. Firstly the piezoelectric elements were soaked in an ultrasonically agitated aqueous surfactant (Neutracon - Decon Laboratories Ltd. BRIGHTON). The discs were then rinsed in tap water followed by distilled water and then dried by baking. Next they were thoroughly degreased in ultrasonically agitated "Arklone" (1-1-2-trichloro 1-2-2-trifluoro ethane stabilized for use in ultrasonic cleaners). Finally the discs were baked at 200°C for an hour to remove all traces of cleaner from their surfaces and allowed to cool down to room temperature in a desiccator before coating.

One of the major face electrodes was then coated with a thin, even layer of photoresist. Coating was effected using a spin coater (Headway Research - model EC101) which held the discs down by their back face using an inter-locked vacuum system whilst photoresist was spun onto the front face. The thickness and evenness of the layer was controlled by the speed and duration of the spinning as well as the acceleration of the substrate. Prior to spinning, the photoresist was applied to the disc by static flood using a dropping pipette. From the beginning of this stage until the photoresist was developed, great care was taken to ensure that the photoresist was not fogged by stray UV light. This meant that the working area (in this case a dark room) had to be illuminated by either tungsten filament bulbs or UV safe "gold" fluorescent tubes.

Once coated, the discs were softbaked on a temperature controlled hot plate (Gallenkamp HPL500-050M) at 95°C for 30 minutes. This removed the solvent from the photoresist and increased its adhesion to the electrode. After softbaking the elements were allowed to cool down to room temperature again before being exposed.

The photoresist was exposed through masks using a mercury discharge, ultraviolet lamp. The photoresist was most sensitive to long UV light in the range 365-405nm. The masks were made

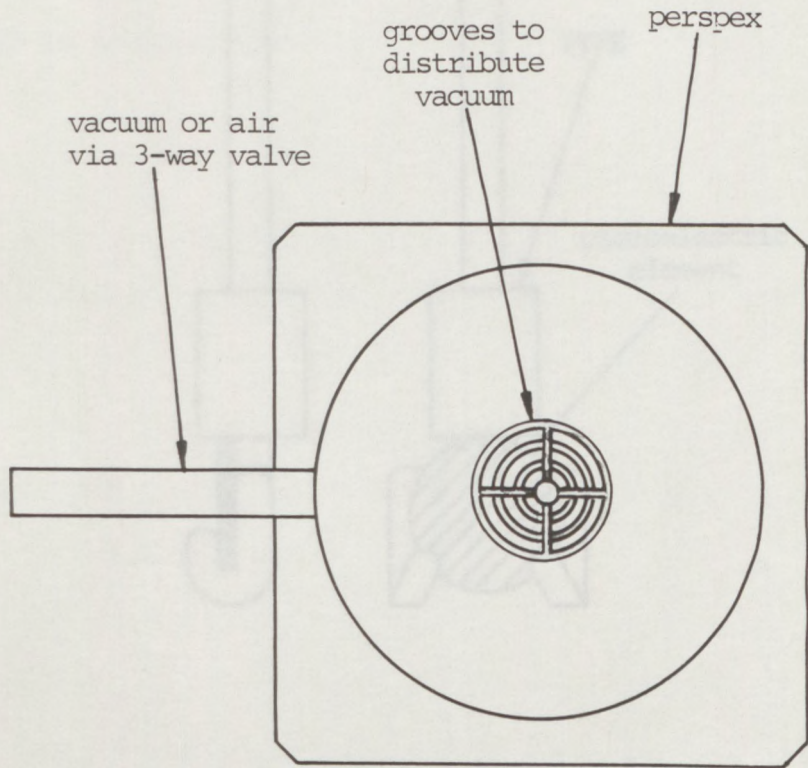
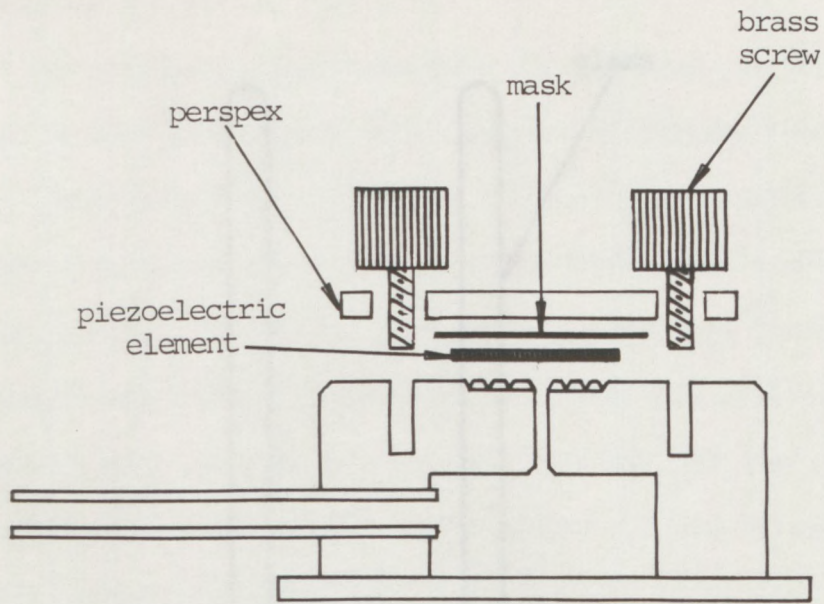
photographically from art work drawn ten times the required size on draughting film with high quality technical drawing pens. This was reduced and transferred on to line film (Kodalith ortho-film type 3) to make highly accurate masks. A specially constructed perspex jig (shown in figure 3-2) was used in conjunction with a light box to finely align the masks over the discs prior to exposure. The delicate discs were held in position on the jig using a rough vacuum in a manner similar to that used for holding silicon wafers during the manufacture of integrated circuits. Using this system the discs could be held or released simply by applying or releasing the vacuum using a three way valve. This was especially useful when handling large-diameter, 10MHz, discs.

The exposed photoresist was then developed in the appropriate developer until a clear image was obtained. After the photoresist had been developed it was thoroughly rinsed in water to remove any traces of unwanted resist before being postbaked.

Postbaking was achieved by baking the developed photoresist pattern on a temperature controlled hot plate. The purpose of this was to harden the photoresist and make it more resistant to attack from the etchant. The postbake was carried out at 120°C for 25 minutes. After postbaking the transducer elements were once again allowed to cool down to room temperature. The back face electrode was then painted with a coloured lacquer to protect it from the etchant.

The etching solution was 2M ferric nitrate ( $\text{FeN}_2\text{O}_3$ ) at 50°C. When the electrode had been etched it was rinsed in water and the photoresist and lacquer removed from the front and back faces using propane-2-one (acetone) as a stripper.

During the pretreatment, development, etching and stripping stages the piezoelectric elements were held by their edges in a custom made jig. This was made of PTFE and glass and is shown in figure 3-3.



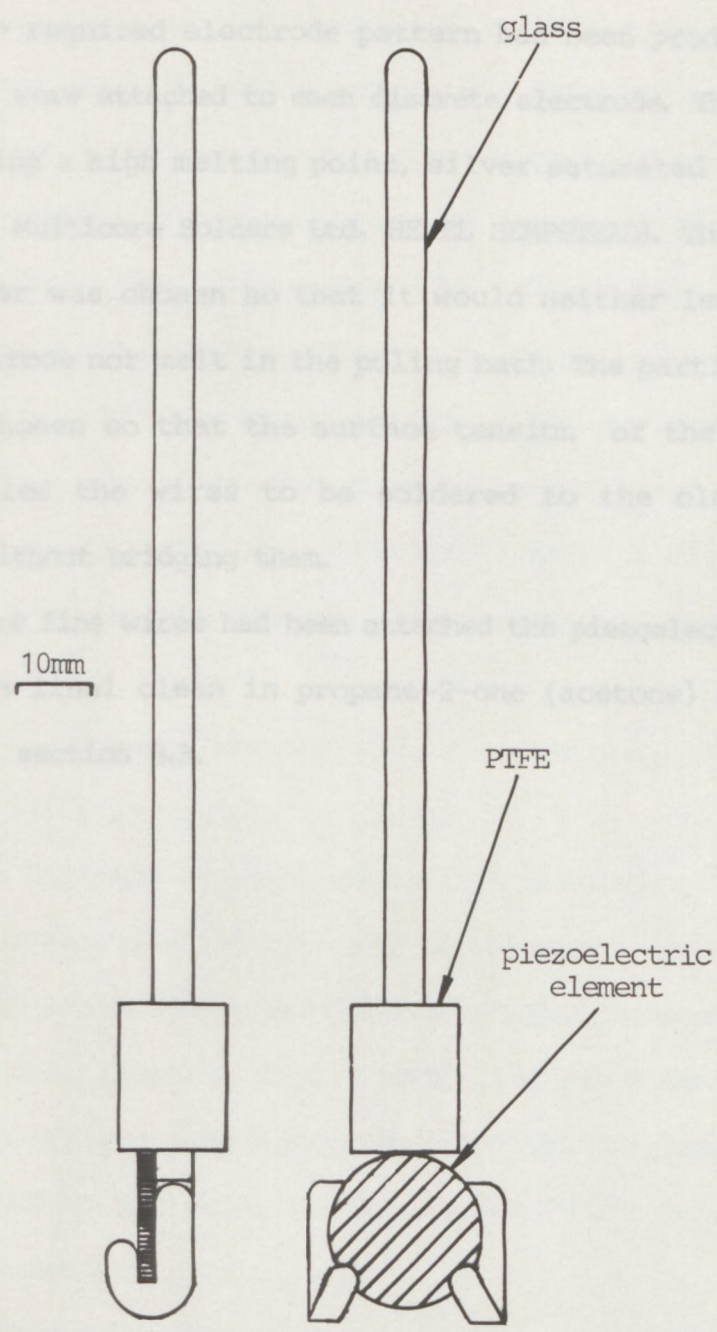
10mm

Figure 3-2 A vacuum operated jig used for holding thin ceramic elements by their back faces whilst aligning the masks on the photoresist coated front faces for exposure to UV light

The jig was based on a device used to hold silicon wafers during the manufacture of integrated circuits.

When the required electrode pattern had been produced, 40- $\mu$ m copper wires were attached to each electrode. The wires were attached using a high melting point, silver saturated solder cream (OSP 2000 - Sulphur Solder Ltd. BMS2000). The composition of the solder was chosen so that it would neither leach away the silver electrode nor melt in the boiling bath. The particle size and this were chosen so that the surface tension of the solder when molten enabled the wires to be attached to the closely spaced electrodes without bridging them.

Once these fine wires had been attached the piezoelectric elements were glued in place using a special (acetone) and poled as described in section 3.1.



**Figure 3-3** The jig used for handling ceramic elements by their edges whilst developing the photoresist pattern on one of their major faces - based on devices used during the manufacture of integrated circuits to hold the silicon wafers

The jig was based on a device used to hold silicone wafers during the manufacture of integrated circuits.

When the required electrode pattern had been produced, 40 swg copper wires were attached to each discrete electrode. The wires were attached using a high melting point, silver saturated solder cream (HMP PRAB3 - Multicore Solders Ltd. HEMEL HEMPSTEAD). The composition of the solder was chosen so that it would neither leach away the silver electrode nor melt in the poling bath. The particle size and flux were chosen so that the surface tension of the solder when molten enabled the wires to be soldered to the closely spaced electrodes without bridging them.

Once these fine wires had been attached the piezoelectric elements were given a final clean in propane-2-one (acetone) and poled as described in section 3.3.

PEP was used in these experiments as it was cheaper, more readily available and required less severe experimental conditions. For thermal depoling the discs had their two major faces abraded before being placed in a closed alumina crucible and baked in a temperature controlled box furnace (Galliskamp model P8655). Temperatures ranging from just below to just above the Curie point (370°C for PEP and 570°C for PZT) were used.

The field depoling was carried out using either dc fields applied in the opposite sense to that of the original poling field or ac fields. The dc fields were produced by a standard high voltage supply and the ac field was produced by a step up transformer fed from a mains voltage. A combination of field and temperature was achieved by using a temperature controlled oil bath (described below) in conjunction with the dc or ac fields. Electrical connections to the discs were made by either fine silvered wires or small spring

### 3.3 Poling Apparatus

The equipment described in this section was used to pole piezoelectric ceramics of PZT type PC5 and PMN type K83. Discs of these materials 15mm and 19mm in diameter by 5MHz and 10MHz equivalent thickness (about 0.5mm and 0.25mm respectively) were supplied by the manufacturers (Unilator Technical Ceramics Ltd. WREXHAM) already poled and electroded. The electroding and poling were carried out simultaneously during their manufacture in specially designed furnaces and it was not possible to obtain unpoled discs. As it was desired to use the high quality electrodes supplied on the discs (section 3.2) and as there were no facilities available to bake electrodes onto unpoled piezoelectric ceramics preliminary experiments concentrated on controlled depoling using:-

- (i) Thermal depoling
- (ii) Field depoling
- (iii) A combination of (i) and (ii)

PZT was used in these experiments as it was cheaper, more readily available and required less severe experimental conditions. For thermal depoling the discs had their two major faces shorted before being placed in a closed alumina crucible and baked in a temperature controlled box furnace (Gallenkamp model FR655). Temperatures ranging from just below to just above the Curie point ( $370^{\circ}\text{C}$  for PZT and  $570^{\circ}\text{C}$  for PMN) were used.

The field depoling was carried out using either dc fields applied in the opposite sense to that of the original poling field or ac fields. The dc fields were produced by a standard high voltage supply and the ac field was produced by a step up transformer fed from a mains variac. A combination of field and temperature was achieved by using a temperature controlled oil bath (described below) in conjunction with the dc or ac fields. Electrical connections to the discs were made by either fine soldered wires or small spring

contacts. The degree of poling was checked by measuring the planar electromechanical coupling factor  $k_p$  (sections 1.2.2 and 3.1).

Field depoling was soon abandoned as it became clear that the discs were suffering dielectric breakdown before depoling. However, attempts to depole the discs thermally were very successful except that the effect was of an "all or nothing" nature and took place over a very narrow temperature range due to the crystallographic basis of the piezoelectric effect (section 1.1). This made the production of the required poling regimes very difficult and also gave rise to the possibility of spoiling the discs by loss of certain chemical components at the elevated temperatures required.

Subsequently, controlled re-poling of thermally depoled discs proved to be much more effective. The degree of poling achieved in a given time depends upon temperature and applied field and of these only  $E$ , the applied field permits variations to give apodisation of the required precision.

Poling was effected by subjecting the piezoelectric ceramics to high dc fields at an elevated temperature and then cooling them to room temperature in the presence of the field. Once the required temperature had been reached the discs were kept at this temperature for about 30 minutes to reach thermal equilibrium. After this the poling field was applied for a set period known as the poling time. The discs were then cooled to room temperature in the presence of the field. Table 3-1 summarizes the poling schemes used for PZT and PMN.

In order to be able to view the piezoelectric elements whilst they were being poled and check for any visible problems a poling bath of novel design was constructed. Most conventional poling baths consist of a temperature controlled heating element, a stirrer and a cooling coil immersed in a heavily insulated tank of poling fluid. Whilst this design has proved effective it precludes the visual inspection of

Material	Curie Point (°C)	Poling Temperature (°C)	Poling Field (kV/mm)	Poling Time (Minutes)	Poling Medium
PZT (type PC5)	370	150	2	20	Safflower Oil
PMN (type K83)	570	210	2	30	Silicone Fluid (Dow Corning - 210H/100cs)

Table 3-1 Conditions of temperature, electric field strength and time used to pole transducer elements made of ceramic PZT and PMN specimens during poling. The poling bath constructed for this project was based upon a clear glass tank and used an external heater in addition to an immersion heater to compensate for the absence of heavy, external insulation.

It is worth noting that in all heating baths the input power per unit volume must be limited to prevent the thermal degradation of the poling oil immediately around the heat source(s). For this type of oil bath the maximum power per unit volume which may be used is around 100W/litre, the limit is set by the physical properties of the poling oil.

Figure 3-4 shows the poling apparatus schematically. A 1000ml, borosilicate glass beaker containing the poling oil was heated by a 350 watt immersion heater and/or a 1000 watt external hot plate. The temperature was sensed by a type K thermocouple (RS Components Ltd stock No 151-186) connected to a temperature sensing relay (RS Components Ltd stock No 348-144) which controlled the heating. The temperature was measured by another type K thermocouple connected to a cold junction compensating, thermocouple amplifier (RS Components Ltd stock No 301-779) and output to a digital, liquid crystal display. To maintain a constant temperature throughout the bath a small motor

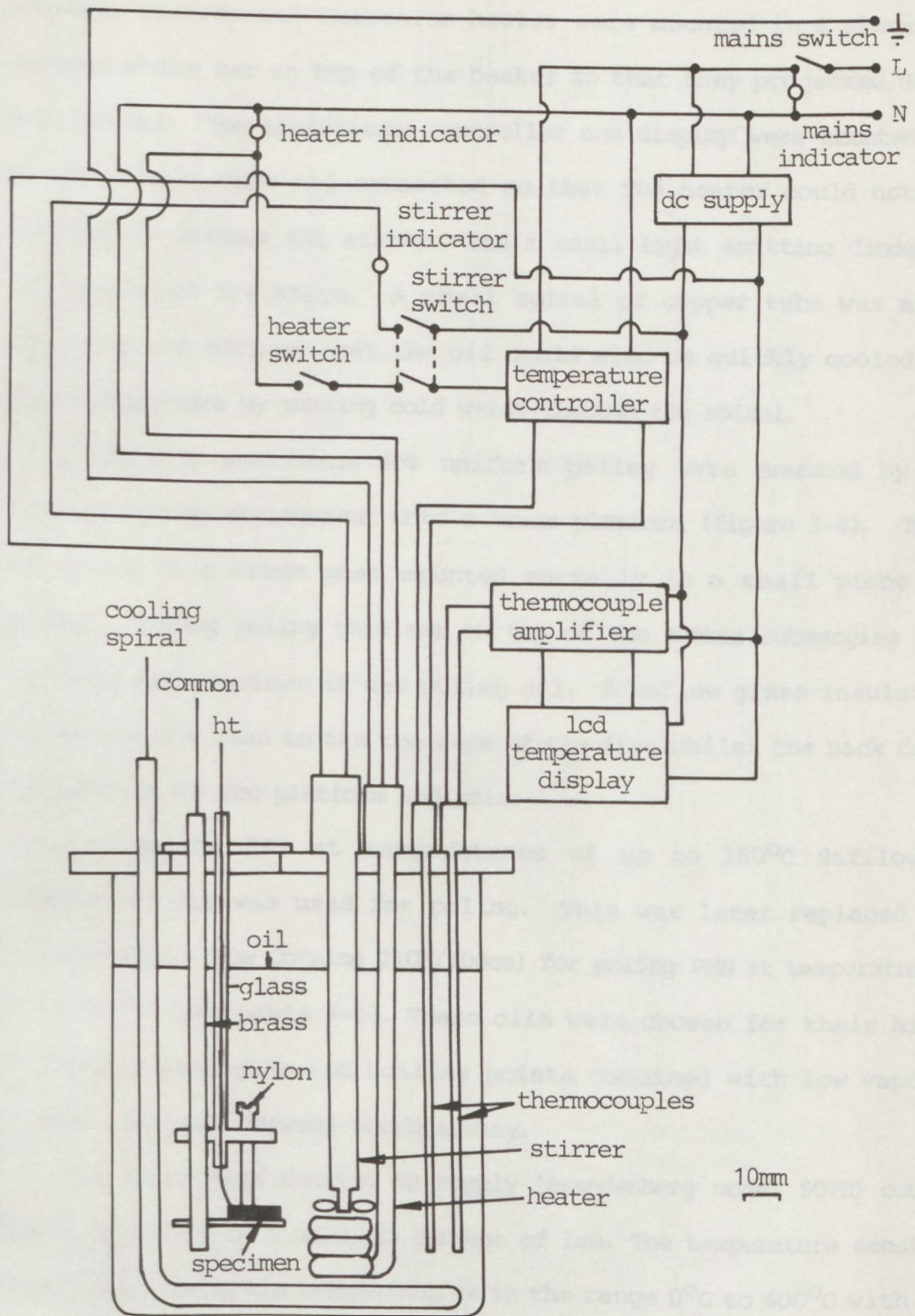


**Figure 3-4** A schematic diagram of the temperature controlled oil bath used for poling ceramic elements during the fabrication of non-uniformly excited transducers

driven stirrer was used to keep the poling oil circulating. The sensors, stirrer and immersion heater were mounted in a piece of perspex which sat on top of the beaker so that they projected down into the oil. The temperature controller and display were mounted in an instrument case and connected so that the heater could not be switched on without the stirrer, and a small light emitting diode or led indicated its state. A small spiral of copper tube was also fitted in the bath so that the oil could also be quickly cooled to room temperature by passing cold water through the spiral.

Initially specimens for uniform poling were mounted by an isolated spring arrangement onto a brass platform (figure 3-4). This was fixed to a brass post mounted normally in a small piece of perspex. During poling this sat on top of the beaker submerging the platform and specimen in the poling oil. A hollow glass insulator guided the eht lead to the top face of the disc whilst the back face was earthed via the platform and pole.

For poling PZT at temperatures of up to 150°C Safflower (vegetable) oil was used for poling. This was later replaced by silicone fluid (Dow Corning 210H/100cs) for poling PMN at temperatures up to 210°C (see table 3-1). These oils were chosen for their high dielectric strengths and boiling points combined with low vapour pressure and good thermal conductivity.

The extra high tension dc supply (Brandenberg model 507R) could supply up to 5kV at a maximum current of 1mA. The temperature sensing relay could maintain temperatures in the range 0°C to 400°C with an accuracy of  $\pm 2\%$ . A high tension, multi-tapped potential divider was used to provide several different potentials which could be applied to separate areas of electrode simultaneously. Wires from the potential divider taps were connected to the fine wires on the electrodes via the poling jig shown in figure 3-5. This consisted of a tube clip

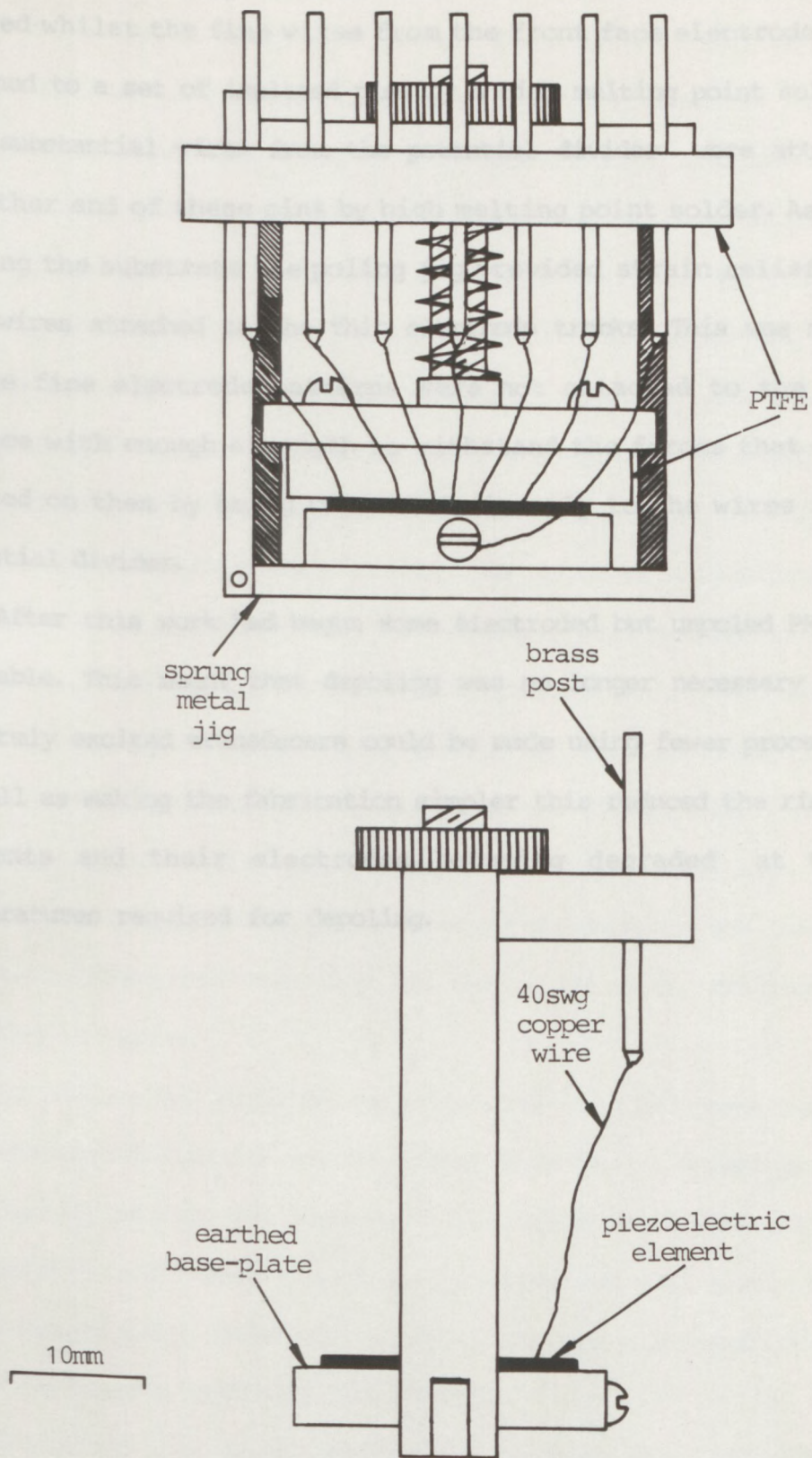


**Figure 3-5** The jig used during poling to apply the poling potential(s) to the transducer elements and provide strain relief so that the wires carrying these potential(s) did not detach areas of the transducer electrode

modified to allow the back electrode of a transducer element to be earthed whilst the fine wires from the front face electrode(s) were attached to a set of isolated pins by a high melting point solder. The more substantial wires from the potential divider were attached to the other end of these pins by high melting point solder. As well as holding the substrate the poling jig provided strain relief for the fine wires attached to the thin electrode tracks. This was necessary as the fine electrode patterns were not attached to the ceramic surface with enough strength to withstand the forces that would be exerted on them by being connected directly to the wires from the potential divider.

After this work had begun some electroded but unpoled PMN became available. This meant that depoling was no longer necessary and non-uniformly excited transducers could be made using fewer process steps. As well as making the fabrication simpler this reduced the risk of the elements and their electrodes becoming degraded at the high temperatures required for depoling.

### 3.4 Transmitting Transducers

The equipment described in this section was developed to make both uniformly and non-uniformly excited, wide-band, ultrasonic transducers. Ideally, these transducers produce ultrasonic pulses approximating to a single cycle of a sine wave at each excitation. In order to produce the simple pulse shapes required for pulsed mode testing and ultrasonic spectroscopy it was necessary to have transducers with a frequency response covering the range from approximately 1-10MHz. This response is conveniently produced by using unidirectional electric pulses to shock excite thin, heavily damped, ceramic, piezoelectric elements (section 3.5). The transducers used in this work were optimized to give a simple, well defined pulse shape rather than the widest attainable bandwidth, as it was their pulse shape and structure which was primarily of interest in this project. The transducers were mainly intended for immersion testing and therefore only a thin, protective front-layer was used. This had virtually no effect on the pulse shape or matching to the load as long as its thickness was less than  $\lambda/4$  (where  $\lambda/4$  is approximately 0.04mm at 10MHz in water).

To produce the required response from the transducer elements it was necessary to use damping to prevent them from resonating. This was affected by backing the elements with tungsten loaded epoxy resin. When excited with fast-rise time, unidirectional, electric pulses these transducers generated short, wide-band ultrasonic pulses with spectra extending typically from 1-8MHz.

A matched high impedance backing material and a suitable method of attaching it to the transducer element are essential in the fabrication of wide-band transducers (Low and Jones, 1984; Foster and Hunt, 1978). Backings such as cylinders of solid lead (DeSilets et al, 1975) - impedance  $22 \times 10^6$  mks Rayl i.e.  $\text{kgm}^{-2}\text{s}^{-1}$ ) unpoled PZT

(Low,1975) and filled plastics (Lees and Davison,1977) have been tried with some success. Cylindrical cones of impedance matched material such as PZT in contact with a PZT element and mounted in a highly attenuating material have also been tried (Swartz et al,1979). The loss mechanism in these materials appears to be by scattering the ultrasonic waves into incoherent compression waves which have very slow decay rates. This produces noise in the backing which in turn severely reduces the transducer's dynamic range or signal to noise ratio.

Tungsten-epoxy composites are commonly and successfully used to produce wide-band transducers. These have higher loss and much faster, multimode decay rates. This allows greater sensitivity and dynamic range. The acoustic impedance of PZT is about  $34(x10^6 \text{ mks Rayl})$  and impedances in the range  $8.5-40(x10^6 \text{ mks Rayl})$  have been produced using tungsten-epoxy composites (DeSilets et al,1975). The most reproducible results being in the range  $20-30(x10^6 \text{ mks Rayl})$ . A typical attenuation figure is better than  $10\text{dB/cm}$  at  $2.7\text{MHz}$  for a composite of impedance  $24(x10^6 \text{ mks Rayl})$ . Acoustic theory for composite materials is not yet firmly established and the agreement between theory and experiment is only over a limited range. Bainton and Silk (1980) have shown that the particle size and proportion of tungsten in the composite are essential for determining its acoustic properties. However, as long as the particle size is very much smaller than the acoustic wavelength at the frequencies of interest the acoustic properties of composite materials can be taken as independent of frequency (Fraser,1979). This makes them suitable for the construction of wide-band transducers. Backings and their effect on transducer performance have also been studied by Ying et al(1981) and others (Sayers and Tait,1984; Smith et al,1974) who agree that overall tungsten-epoxy components are the most suitable for the

construction of wide-band transducers. *been characteristics. Every*

Good acoustic contact between the transducer element and its backing is essential for good damping but not easy to obtain with a tungsten-epoxy composite. Methods of attaching the backing to the element include:- glueing (Low,1975) soldering (DeSilets et al,1975) and casting. Special techniques for minimising the bond thickness between the element and backing are needed to produce a good impedance match. Tungsten-epoxy composite backings may also be glued to the transducer element with a thin layer of the epoxy resin used to fabricate them. *this was cast onto the piezoelectric elements and*

Whilst every effort was made - by carefully controlling the materials and construction procedures - to ensure that the backing and mountings of every transducer element was similar, it is notoriously difficult to produce transducers without large variations in characteristics and performance. However the reproducibility of the results obtained was very good. *of silicon brass or stainless steel and*

Despite the apparently simple construction and engineering of transducers, inherent variations in the piezoelectric elements and subtle variations introduced by interactions at component interfaces can conspire to produce major variations in characteristics and performance. Variations are often produced by bad contact between the piezoelectric element and its backing. This may be caused by air gaps, delamination of the disc electrode and/or an uneven or excessively thick layer of adhesive between the disc and its backing. These can prevent good acoustic matching and lead to variable damping and performance. It has been suggested (Bainton and Silk,1980) that ideally this layer should be less than  $\lambda/200$  thick. Casting the backing onto the elements seems to avoid the worst of these effects. However, the parallelism and surface roughness of the discs themselves can also be a problem as can the spatial variation of the poling. All

of these tend to produce non-uniform beam characteristics. Every transducer is an engineering compromise (Posakony,1975) involving frequency(s) of operation, beam characteristics, dielectric constants, construction and application. Even well backed transducers can suffer from parasitic resonances in their housing, often caused by pulse excitation, which adversely affects the beam. This problem is usually cured by using a flexible resin to mount the backed disc in the housing.

The transducers used in this project were backed with a tungsten-epoxy mixture. This was cast onto the piezoelectric elements and centrifuged to remove any dissolved gas. This also compacted the tungsten powder increasing its acoustic impedance. To facilitate the construction of these transducers a special jig was designed and built. The jig, shown in figure 3-6, consisted of five parts:-

(i) body (ii) base plate (iii) plug (iv) cap (v) bush

The first four parts were made of either brass or stainless steel and the fifth part was made of PTFE. The bush fitted closely around the piezoelectric ceramic disc and tightly inside the body of the jig. Below the PTFE bush the base plate sat on a shelf around the inside of the body. Underneath the shelf the bottom of the body, which was open to allow the base plate to be pushed out from underneath, was sealed by a threaded plug. The protruding section of the plug had parallel flats machined onto it to facilitate its tightening and removal with a spanner. The PTFE bush and later the transducer housing/case were held in position by a knurled brass cap against the force of the fabricating resins during centrifuging. These were inserted and removed from the body of the jig using a small hand operated arbor press.

In order to minimise the leakage of backing material it was necessary for the PTFE bush to be a tight fit around the outside of

The silicon and the inside of the body. This material can be...  
 surfaces in series... and short circuit the plates...  
 of the transducer above. The sides of the... plug were...  
 covered with a thin layer of adhesive from (R S Components Ltd. stock...  
 No. 20000). The silicon was then... the shaft and placed to contain the...  
 resin over the...  
 The process...  
 The initial...  
 radius from...  
 their backing...  
 radius they were...  
 (bottom) and...  
 stabilised for...  
 allowed that...  
 thickness...  
 with...  
 A thin wire to...  
 12MP...  
 alternative...  
 that a...  
 uniform...  
 locally, was...  
 conductive...  
 insulation...  
 but still...  
 the back face...  
 base plate of the jig...  
 that each disc was backed with a mixture of low tungsten powder in...

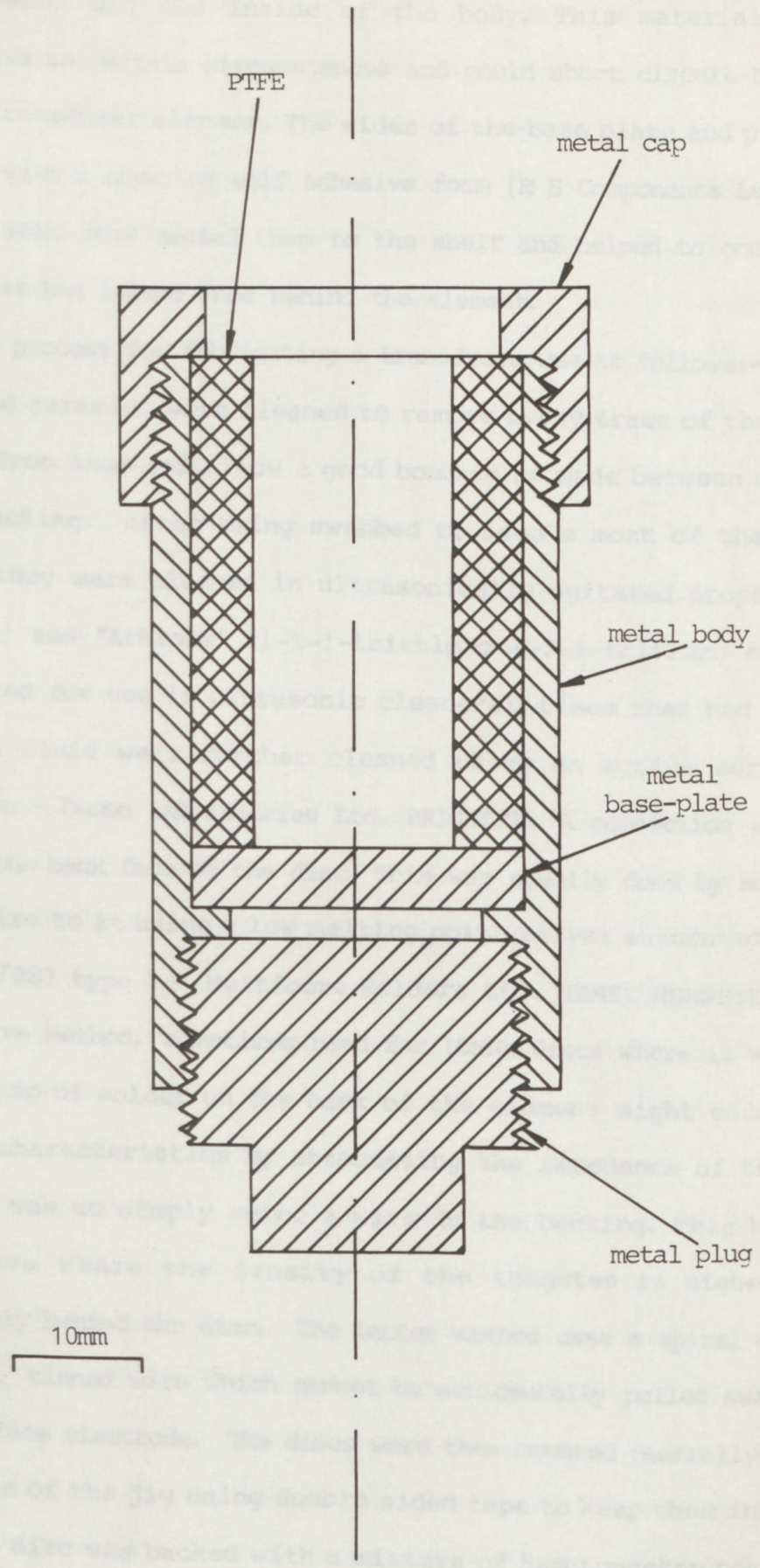


**Figure 3-6** The centrifuging jig used to apply the tungsten loaded epoxy resin backing to the ceramic element during the fabrication of wide-band transducers

the element and the inside of the body. This material can be conductive in certain circumstances and could short circuit the faces of the transducer element. The sides of the base plate and plug were covered with a layer of self adhesive foam (R S Components Ltd. stock No. 554-844). This sealed them to the shelf and helped to contain the resin that had leaked from behind the element.

The process for fabricating a transducer was as follows:- Firstly the poled ceramics were cleaned to remove every trace of the poling medium from them and allow a good bond to be made between them and their backing. After being swabbed to remove most of the poling medium they were cleaned in ultrasonically agitated propen-2 one (acetone) and "Arklone" (1-1-1-trichloro 1-2-2-trifluoro ethane - stabilized for use in ultrasonic cleaners). Discs that had been in silicone fluid were further cleaned using an active surfactant (Neutracon - Decon Laboratories Ltd. BRIGHTON). A connection was then made to the back face of the disc. This was usually done by soldering a fine wire to it using a low melting point, silver saturated solder (LMP 422/287 type 1 - Multicore Solders Ltd. HEMEL HEMPSTEAD). An alternative method, sometimes used for 10MHz discs where it was felt that a lump of solder on the back of the element might cause non-uniform characteristics by attenuating the impedance of the disc locally, was to simply embed a wire in the backing. This becomes conductive where the density of the tungsten is highest i.e. immediately behind the disc. The latter method uses a spiral of fine but stiff, tinned wire which cannot be accidentally pulled away from the back face electrode. The discs were then mounted centrally on the base plate of the jig using double sided tape to keep them in place. Next each disc was backed with a mixture of 5 $\mu$ m tungsten powder in epoxy resin. This was centrifuged onto the back of the discs at 4000rpm at a radius of about 150mm for 20 minutes using the jig. The

excess resin was then poured off and some granules of vermiculite foam were stirred into the less dense part of the backing. These scattered the lower frequency ultrasonic waves and reduced the chances of them appearing in the transducer's output. The jigs were then baked at 60°C for several hours to cure the epoxy resin. The centrifuging process produced a gradual change in the density and impedance of the backing such that they decreased with distance from the back of the disc. Close to the back of the disc the high impedance of the backing made it a good match to the disc allowing the easy transfer of energy from the disc to the backing. Further away its lower impedance and density made it highly attenuating. The nett effect was to produce an "infinite" transmission line into which transmitted acoustic energy was lost by dissipation as heat. The epoxy resin used was a 50:50 mixture by volume of Ciba-Geigy M750 resin and CY208 resin with a suitable quantity of HY951 hardener. The CY208 is a flexible resin which sets to a hardness similar to that of rubber whilst M750 is a basic resin which sets to a hardness similar to that of a hard plastic such as perspex. As these resins are completely miscible and use the same hardener (in different proportions) it was possible to produce a range of hardness in the cured mixture ranging continuously between the hardnesses of the two component resins.

Once a disc had been backed with the tungsten-epoxy mixture to produce a "slug" it was mounted in a suitable case. As well as protecting the element and making the transducer easy to handle, the case provided both electrical and mechanical isolation. The procedure for producing a finished transducer from a "slug" started by testing the "slug" for continuity and shorts using a multimeter. The tested "slugs" were then encapsulated in their cases using either a flexible polyurethane resin (R S Components Limited Stock No 555-106) or the same mixture of resins as was used in their backings. After attaching

the "slug" and case to the base plate of the jig with double sided tape the "slug", case and encapsulating resin were centrifuged in the jig at about 4000rpm at a radius of about 150mm for 5 minutes. This removed any dissolved air from the encapsulating resin and ensured that it filled the gap between the sides of the case and the "slug". When this resin had been cured by a further baking the mounted "slugs" were removed from their jigs and the earth connection made between the front face of the disc and the screen of a BNC socket. This was used to connect the transducer to the excitation source (section 3.4) via screened co-axial cable. The earth connection was made using either conductive paint (R S Components Limited stock No 555-156) or conductive epoxy resin (Johnson Matthey Limited type A520 or R S Stock No 555-673). Figure 3-7 shows a finished transducer. The outer case is usually made of earthed metal (stainless steel or brass) to provide screening. Some early transducers, however, were made using polyethylene specimen tubes for economy and convenience. The stainless steel case shown in figure 3-7 had a fine shoulder cut into its inner rim so that the material used to connect the front face electrode to the case could be lapped down flat using the rim of the case as a reference to produce a thin even layer. The transducers mounted in polyethylene cases had their front face electrodes connected to earth via a tinned wire which was soldered to the screen of their BNC socket and ran down the outside of the case until it reached the front where it was inserted into the flexible mounting. A connection was then made to this using either conductive paint or conductive epoxy resin.

Pulse shape tests in a water tank (section 4.2.4) showed that the 50:50 mixture by volume of epoxy resins gave the best compromise between pulse shape and dynamic range. Harder backings had higher acoustic impedances closer to that of the ceramic elements. These

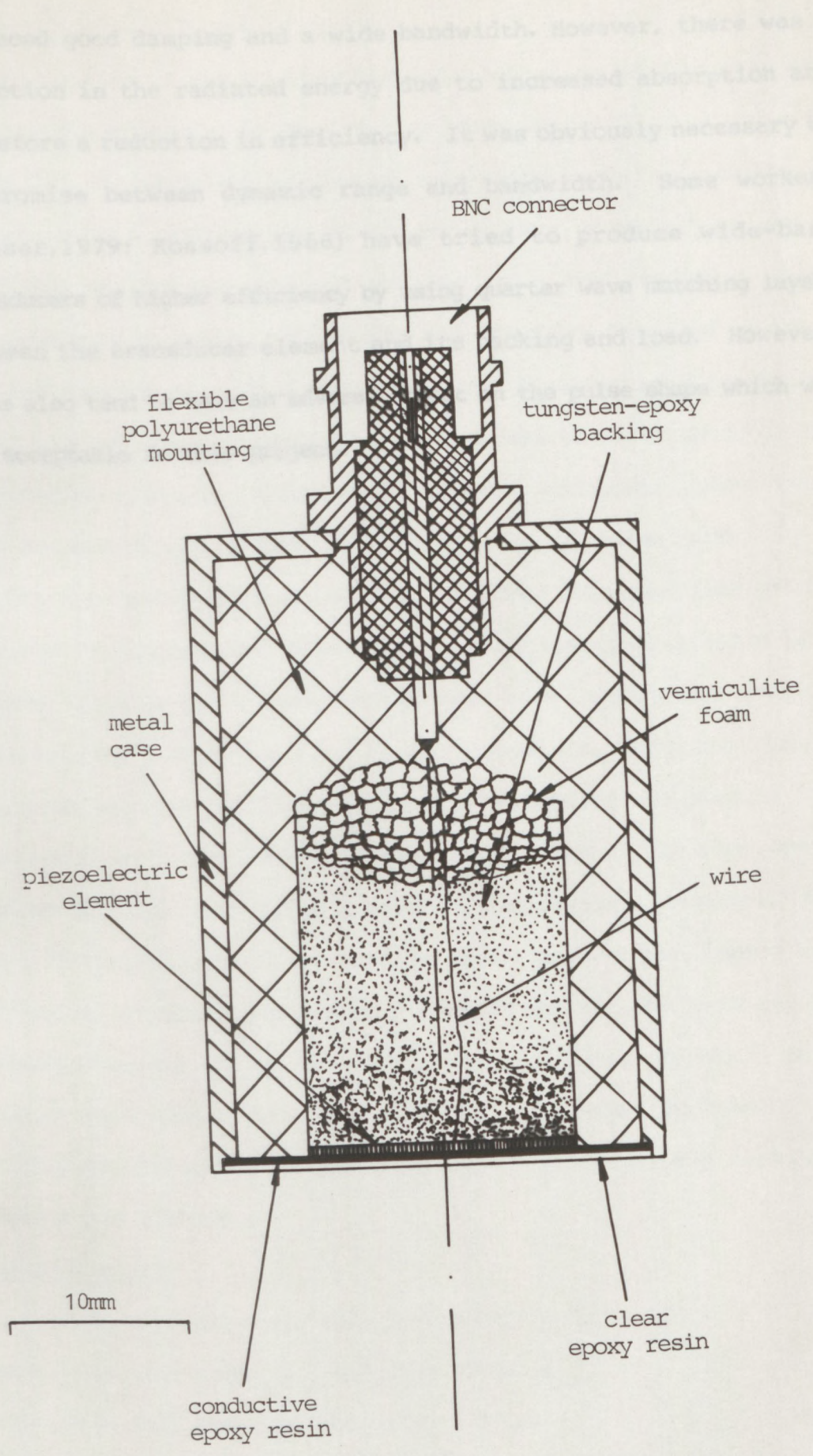


**Figure 3-7** A schematic illustration of a typical wide-band transducer showing the backing applied to prevent the element from resonating and the layer applied to the front face for protection and matching



### 3.5 Excitation and Receiving System

An outline of the electronic instrumentation used to make the measurements presented in chapter 4 is given by the block diagram in figure 3-8. The wide-band excitation and receiving system consists of the excitation source, the main amplifier, a wide-band gated amplifier, an analogue spectrum analyser and a head amplifier. These were developed by Weight (1975,1982b) and are fully described by him.

The excitation source produced short, unidirectional electrical pulses with adjustable amplitude, rise and fall times. These drove the transmitting transducer which produced short ultrasonic pulses which could be made to approximate to a single cycle of a sine wave.

The time and frequency domain outputs from main amplifier and the spectrum analyser were displayed on oscilloscopes. A gated peak detector (Metrtek MD702) was used to make beam profile measurements. Permanent records of the time domain responses, frequency domain responses and beam profiles were made by feeding the outputs to a chart recorder (Hewlett-Packard 7004). In the case of the time domain response this was done using a sampling oscilloscope (Tektronix 7063 with a 7514 sampling unit) to slow the signal down. B-scan images were produced by using a digital scan converter (Anaram 80). This was fed ultrasonic signals via an rf envelope detector (Metrotek MR101) and a standard video monitor was used to display the images produced.

The specification of the wide-band excitation and receiving system was as follows:-

#### Excitation Source

Output pulse amplitude: variable from 100-500V (into 50 $\Omega$ )

Output pulse rise time: variable from 30-200ns

Output pulse fall time: variable from 0.5-5 $\mu$ s

Triggering: internal - PRF set in range 200-1 kpps external

- negative edge min. 5V max. 20V

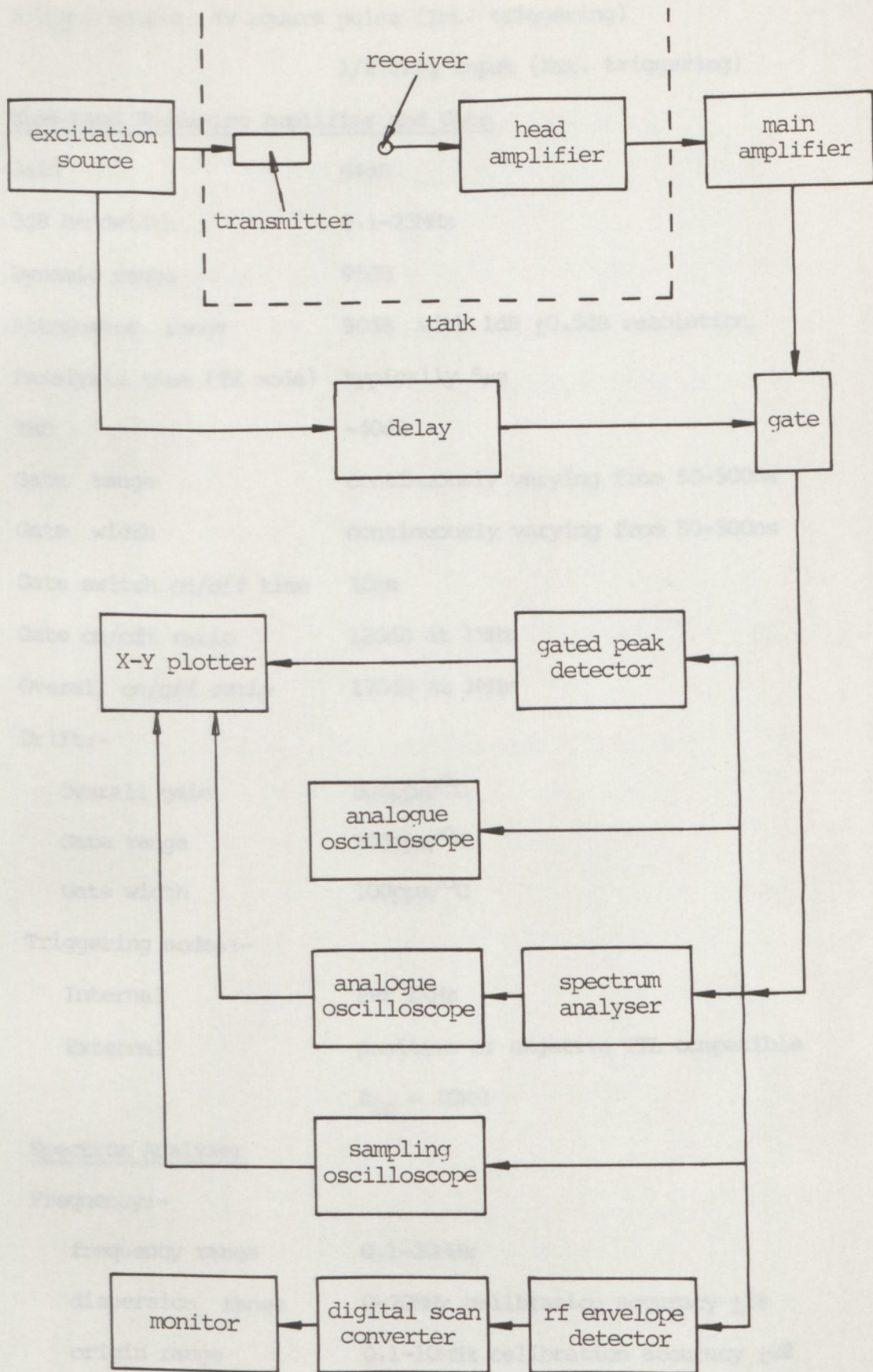


**Figure 3-8** A schematic illustration of the wide-band, excitation and receiving system used to make measurements of the pressure waveforms, transmit-receive responses and associated spectra of both conventional, uniformly excited transducers and non-uniformly excited transducers

Trigger output: 4V square pulse (Int. triggering)

1/2 Trig input (Ext. triggering)

Wide-band Receiving Amplifier and Gate

Gain	64dB
3dB Bandwidth	0.1-25MHz
Dynamic range	95dB
Attenuator range	90dB with 1dB $\pm$ 0.5dB resolution
Paralysis time (TR mode)	typically 5 $\mu$ s
THD	-40dB
Gate range	continuously varying from 50-500ns
Gate width	continuously varying from 50-500ns
Gate switch on/off time	10ns
Gate on/off ratio	120dB at 1MHz
Overall on/off ratio	170dB at 1MHz

Drift:-

Overall gain	500ppm/ $^{\circ}$ C
Gate range	100ppm/ $^{\circ}$ C
Gate width	100ppm/ $^{\circ}$ C

Triggering modes:-

Internal	PRF 1kHz
External	positive or negative TTL compatible

$R_{in} = 10K\Omega$

Spectrum Analyser

Frequency:-

frequency range	0.1-20MHz
dispersion range	0-20MHz calibration accuracy $\pm$ 2%
origin range	0.1-10MHz calibration accuracy $\pm$ 2%
frequency linearity	$\pm$ 0.05MHz
resolution	25kHz (3dB bandwidth)
drift	10kHz/ $^{\circ}$ C (after 1 hour)

### Amplitude:-

dynamic range	60dB
logarithmic	40dB display; 10dB/div $\pm 2$ dB
drift	0.1% (after 1 hour)

### General:-

input impedance	75 $\Omega$
sweep rate	internally/externally swept from zero to a maximum of 1MHz/ms

### Head Amplifier

Type	dual-gate MOSFET input
Gain	10dB ( $\pm 200$ ppm/ $^{\circ}$ C)
Input capacitance	6pF
Input resistance	10M $\Omega$
Output impedance	50 $\Omega$
Output voltage swing	2V peak to peak (1MHz, 1k $\Omega$ )
3dB Bandwidth	2kHz-80MHz

## CHAPTER 4

### RESULTS

This chapter presents both calculated and measured results. These describe non-uniformly excited, plane- and edge-wave only transducers as well as conventional, uniformly excited transducers.

The chapter begins with detailed calculations of pulsed pressure waveforms, transmit-receive mode responses and their associated spectra. Pressure and transmit-receive mode beam profiles are also shown. The calculations were made using adaptations of computer programs originally written by Weight(1982b). These contain suitable subroutines for performing time domain differentiations and convolutions. The results of these calculations show ideal and theoretical forms of excitation as well as practically attainable approximations to these results.

After these calculated results, the results of the experimental work undertaken to produce practical transducers are presented. These begin with the poling and depoling characteristics of the materials used for the active elements of the transducers and continue through the effect of the backing used to produce highly damped, wide-band transducers. Methods of investigating the ultrasonic fields of these transducers using a specially constructed miniature receiving probe are also presented. Experimental work to investigate the relationship between the poling regime applied to the transducer element and the pressure as measured by a miniature receiving probe at points in the field of the finished transducer is also presented.

Some B-scan images are presented as a further aid to the evaluation of the finished transducers.

All the calculations and measurements shown were for transducers operating in water.

#### 4.1 Computer Calculated Results

Computer calculated waveforms, transmit receive mode responses and beam profiles (pressure and transmit-receive mode) for circular transducers were made using the impulse response method described in section 2.2. The programs used were originally written by Weight (1982b) but for the purposes of this project have been adapted to model transducers of the appropriate sizes and frequencies.

Pressure waveforms were calculated by performing a direct, time-domain convolution of the impulse response with a velocity function. Transmit-receive mode responses were made by using a double convolution of the impulse pressure response assuming an idealized point target. Beam profiles, both pressure and transmit-receive mode, were produced from these results by taking the envelope of the peak pressure across the beam at various ranges. It should be noted that full wave detection has been used in making these calculations. This means that the largest half cycle of any waveform i.e. positive or negative has been used in the calculation.

The impulse pressure was found by differentiating the velocity potential which was calculated as a function of time from analytical expressions (Weight, 1982b). Simple velocity functions such as one cycle of a sine wave could be used or alternatively a measured waveform could be digitized and used for a direct comparison with experimental results.

The frequency spectra of the waveforms at each field point were also calculated by using a fast Fourier transform (FFT) algorithm. The waveforms were sampled over an interval given by the sampling theorem as

$$\delta t = 1/(2f_{\max}) \quad (4-1)$$

where  $f_{\max}$  is the highest frequency in the spectrum of the waveform. In theory the spectrum of a short pulse of sine waves extends to infinity but for a single cycle pulse negligible information is lost

by calculating the sampling interval (equation 4-1) with  $f_{\max}$  taken as

$$f_{\max} = 3f_0 \quad (4-2)$$

where  $f_0$  is the frequency of the (continuous) sine wave. A frequency  $f_0 = 2\text{MHz}$  was used in all the calculations presented here. If  $\delta t$  is too fine,  $\delta f$  becomes too coarse with a fixed number of data points i.e.  $N_p$  and this leads to truncation in the frequency domain function. This is especially noticeable in the time separated pulses (Weight, 1982b).

In the FFT algorithm utilized the frequency domain calculation used the range

$$-f_{\max} \leq f \leq f_{\max} \quad (4-3)$$

where

$$f_{\max} = 1/(2\delta t) \quad (4-4)$$

Performing  $N_p$  discrete Fourier transforms on the data points means that the frequency domain increment is given in terms of  $f_{\max}$  as

$$\delta f = (2f_{\max})/N_p \quad (4-5)$$

These calculation were performed using programs written in Fortran and the graphical output was produced using the GINO-F graphics package. Using the principle of superposition, the pressure at any point in the field of an axisymmetrically, non-uniform source can be considered to originate from the sum of the pressures from a collection of concentric circular sources with various radii moving in phase but with different amplitudes. Figure 4-1 shows how various types of excitation can be produced using the method of superposition. The first example (figure 4-1a) shows how a simple annular excitation can be modelled by subtraction. In figure 4-1b a more complicated step-wise approximation to a curve is built up using the addition of several sources.

The axisymmetrical nature of circular sources means that the off axis positions along any of the source radii are sufficient to fully describe the off axis response of the source. Figure 4-2 shows an array of field points at various ranges and distances off axis for a

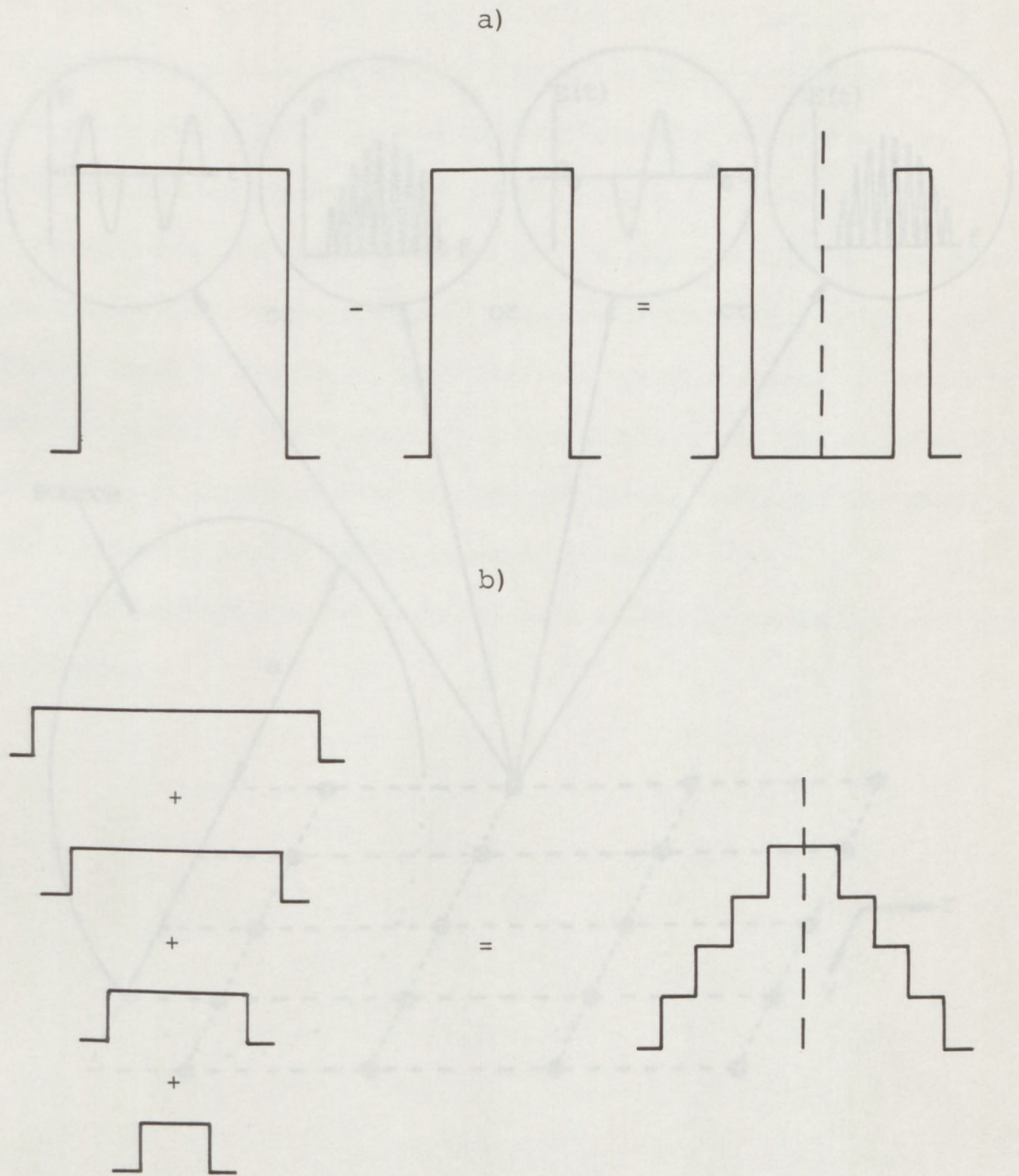


**Figure 4-1** Using the principal of superposition any axisymmetrically non-uniform source can be considered to be made up from the sum or difference of a number of concentric circular sources with various radii moving in phase but with different amplitudes.

For example:-

- a) a simple annular excitation built up by subtraction of one source from another
- b) a stepwise approximation to a curve built up by the addition of several small sources

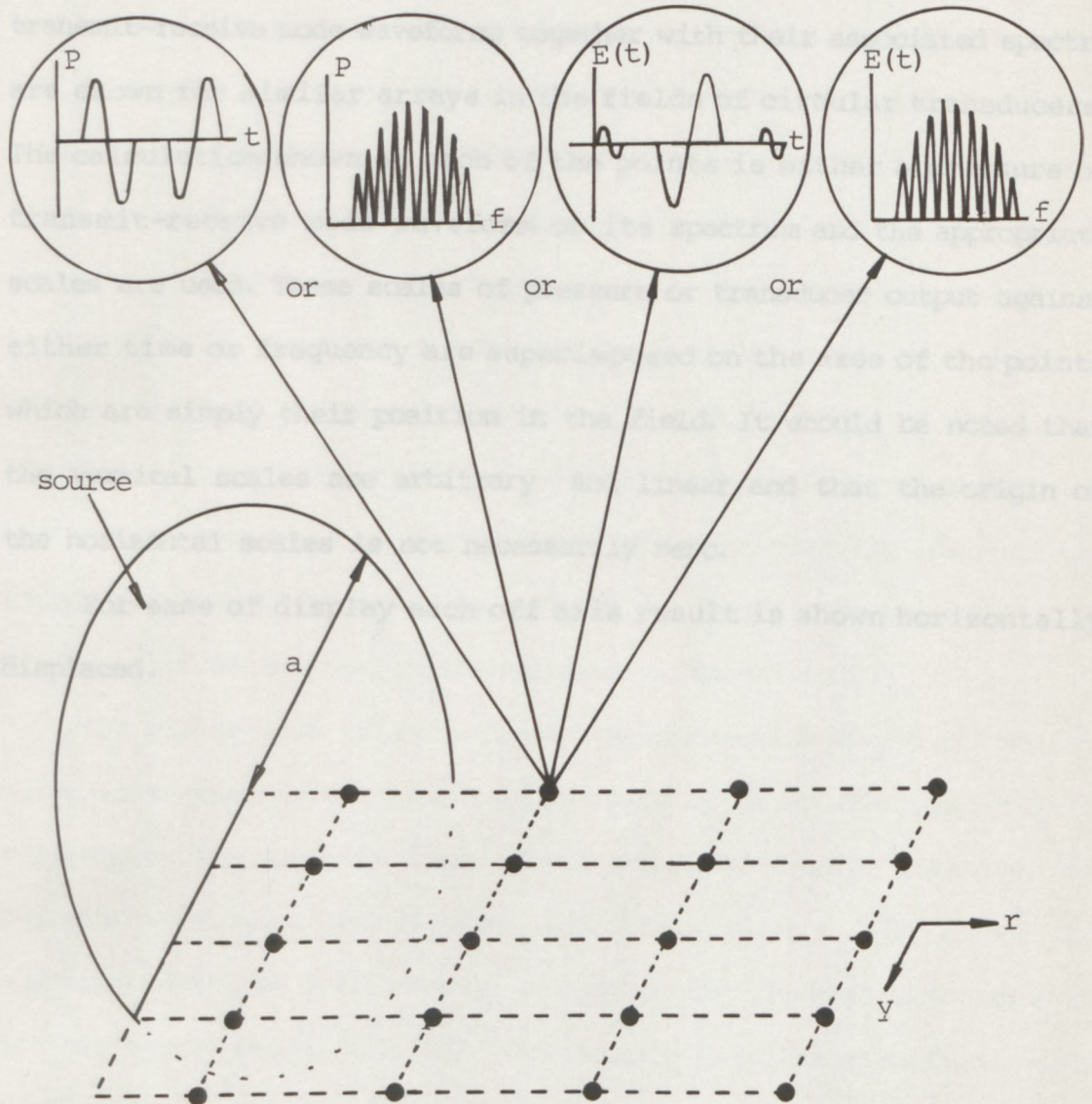


**Figure 4-2** Points in the field of a circular source where calculated or measured results were made. These points are described by their range and distance off axis. At each point the result given has its axes (i.e. pressure or transducer output against time or frequency) superimposed on the grid. The axisymmetrical nature of a circular source means that the results in this plane alone are enough to fully describe the field of the source

circular source at which calculations were made. These can be used to fully describe the field of that source. In the results which follow in sections 4-1-1 and 4-1-2 calculations of both pressure and transmit-receive mode waveforms together with their associated spectra are shown for similar arrays in the fields of circular transducers. The calculation shown at each of the points is either a pressure or transmit-receive mode waveform or its spectrum and the appropriate scales are used. These scales of pressure or transducer output against either time or frequency are superimposed on the axes of the points which are simply their position in the field. It should be noted that the vertical scales are arbitrary and linear and that the origin of the horizontal scales is not necessarily zero.

For ease of display each off axis result is shown horizontally displaced.

The plane-wave retains its shape and amplitude at all points within the geometrical beam region where it is not overlapped by an edge-wave. The same is true of the axial edge-wave although its structure is more complicated. Off axis, figure 4-3a shows the opposing phases of the inwardly and outwardly directed components of the edge-wave (section 2.1.2). The changes in pulse structure with field position described above are reflected in the spectra shown in figure 4-3b. As the pulse structure becomes simpler the modulation of the corresponding spectra decreases.

By suitably altering the program (see section 4-1) the pressure waveforms and spectra of non-uniformly excited transducers may also be calculated. Figure 4-4 shows the case for a non-uniformly excited PWD type source which possesses the weighting function described in section 2.3.1. The pulse shapes shown in figure 4-4a and the spectra shown in figure 4-4b are obviously simpler due to the smearing out of the edge-wave contributions which effectively reduce the number of

#### 4.1.1 Pressure waveforms and spectra for circular transducers

Pressure waveforms and spectra for a uniformly excited transducer are shown in figure 4-3. In figure 4-3a on axis and close to the source both the plane- and edge-waves can be seen clearly resolved. Moving towards the axial far field of the source these increasingly overlap. This produces a single pulse. In the near field this has a large negative going portion produced by the second half of the plane-wave pulse overlapping the first half of the edge-wave pulse and reinforcing it. However, eventually this overlap leads to a decrease in the amplitude of the pulse due to the opposing signs of the plane- and edge-wave components. The pulse amplitude continues to decrease with range producing a differentiating effect so that the shape of the axial far field pressure waveform is asymptotic to the time differential of the near field plane-wave (Weight,1982b).

The plane-wave retains its shape and amplitude at all points within the geometrical beam region where it is not overlapped by an edge-wave. The same is true of the axial edge-wave although its structure is more complicated. Off axis, figure 4-3a shows the opposing phases of the inwardly and outwardly directed components of the edge-wave (section 2.1.2). The changes in pulse structure with field position described above are reflected in the spectra shown in figure 4-3b. As the pulse structure becomes simpler the modulation of the corresponding spectra decreases.

By suitably altering the program (see section 4-1) the pressure waveforms and spectra of non-uniformly excited transducers may also be calculated. Figure 4-4 shows the case for a non-uniformly excited PWO type source which possesses the weighting function described in section 2.3.1. The pulse shapes shown in figure 4-4a and the spectra shown in figure 4-4b are obviously simpler due to the smearing out of the edge-wave contributions which effectively reduces the number of

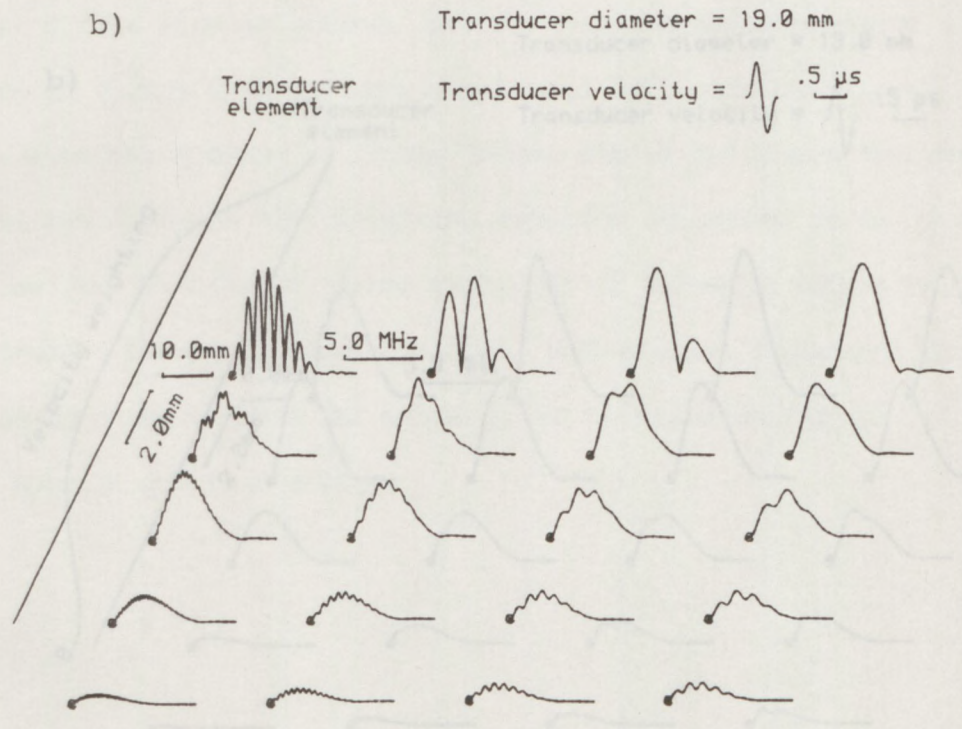
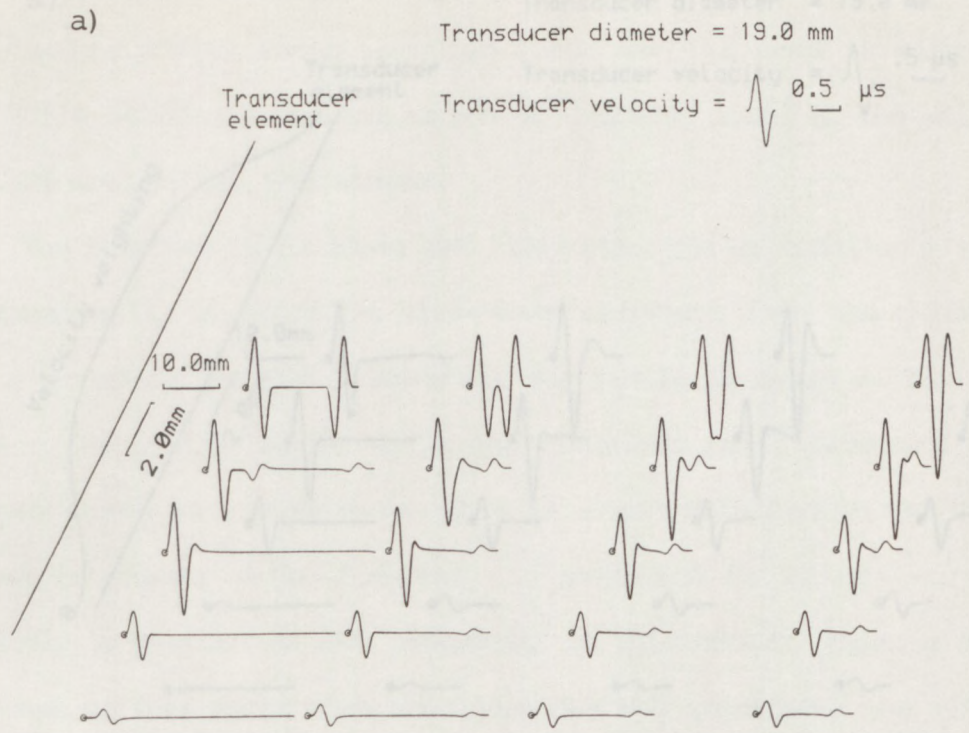
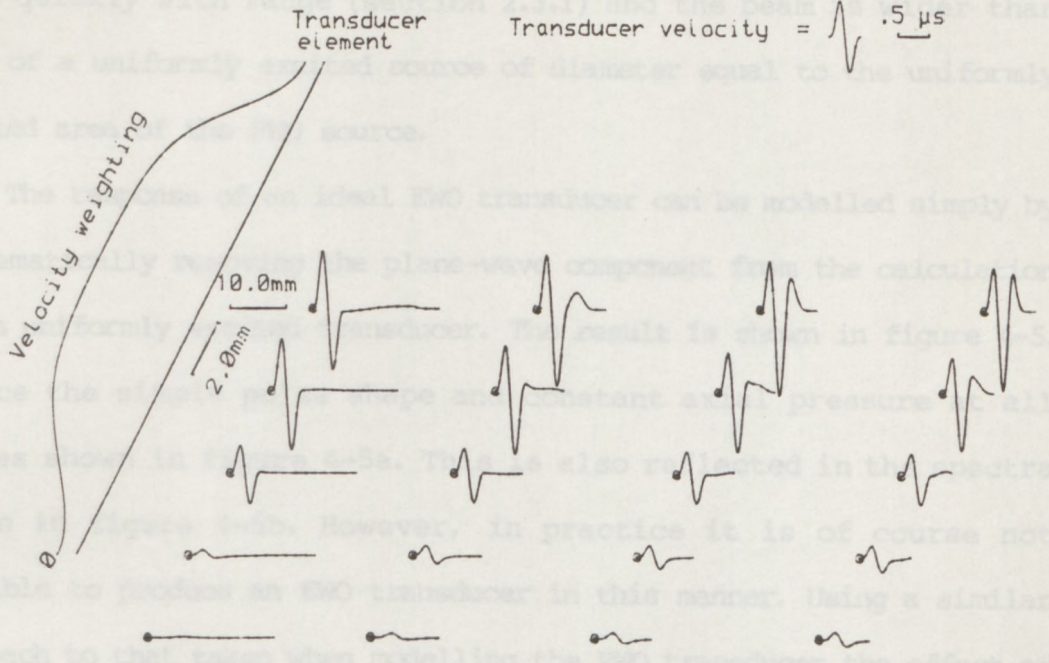


**Figure 4-3** Computer calculated results at points in the field of an ideal, uniformly-excited transducer radiating a short pulse into water showing:-  
 a) pressure waveforms b) pressure spectra

a)

Transducer diameter = 19.0 mm

Transducer velocity =  0.5  $\mu$ s



b)

Transducer diameter = 19.0 mm

Transducer velocity =  0.5  $\mu$ s

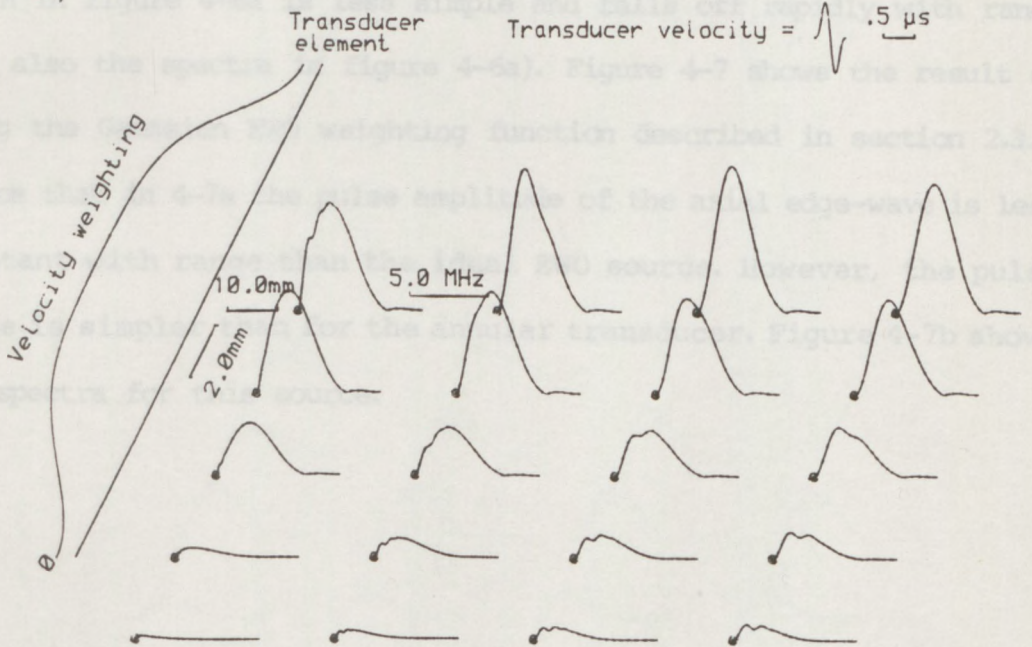


**Figure 4-4** Computer calculated results at points in the field of a non-uniformly excited PWO type transducer radiating a short pulse into water showing:-

a) pressure waveforms    b) pressure spectra

wave components present. As expected however, the pressure falls off more quickly with range (section 2.3.1) and the beam is wider than that of a uniformly excited source of diameter equal to the uniformly excited area of the PWO source.

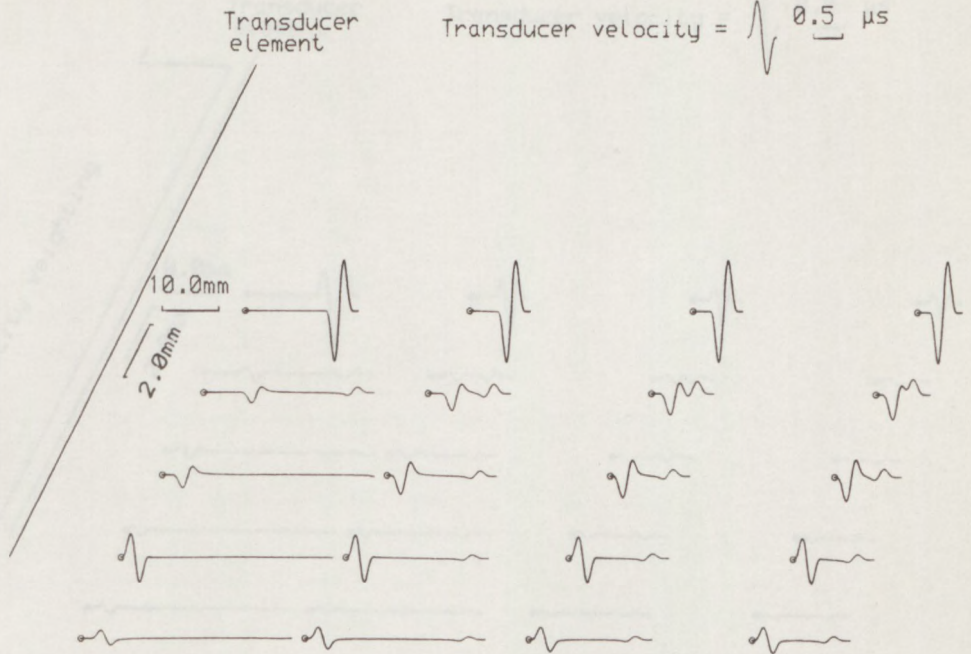
The response of an ideal EWO transducer can be modelled simply by mathematically removing the plane-wave component from the calculation for a uniformly excited transducer. The result is shown in figure 4-5. Notice the simple pulse shape and constant axial pressure at all ranges shown in figure 4-5a. This is also reflected in the spectra shown in figure 4-5b. However, in practice it is of course not possible to produce an EWO transducer in this manner. Using a similar approach to that taken when modelling the PWO transducer the effect of other EWO type weighting functions can be modelled. A result of this type is shown in figure 4-6 where a simple step function is used to model a thin annular source. In this case the axial pressure waveform shown in figure 4-6a is less simple and falls off rapidly with range (see also the spectra in figure 4-6a). Figure 4-7 shows the result of using the Gaussian EWO weighting function described in section 2.3.2. Notice that in 4-7a the pulse amplitude of the axial edge-wave is less constant with range than the ideal EWO source. However, the pulse shape is simpler than for the annular transducer. Figure 4-7b shows the spectra for this source.

Figure 4-5 Computer calculated results at points in the field of an ideal EWO type transducer radiating a short pulse into water showing: a) pressure waveforms b) pressure spectra

a)

Transducer diameter = 19.0 mm

Transducer velocity =  $\sqrt{0.5 \mu s}$



Note: Width of array = 0.75m

b)

Transducer diameter = 19.0 mm

Transducer velocity =  $\sqrt{.5 \mu s}$

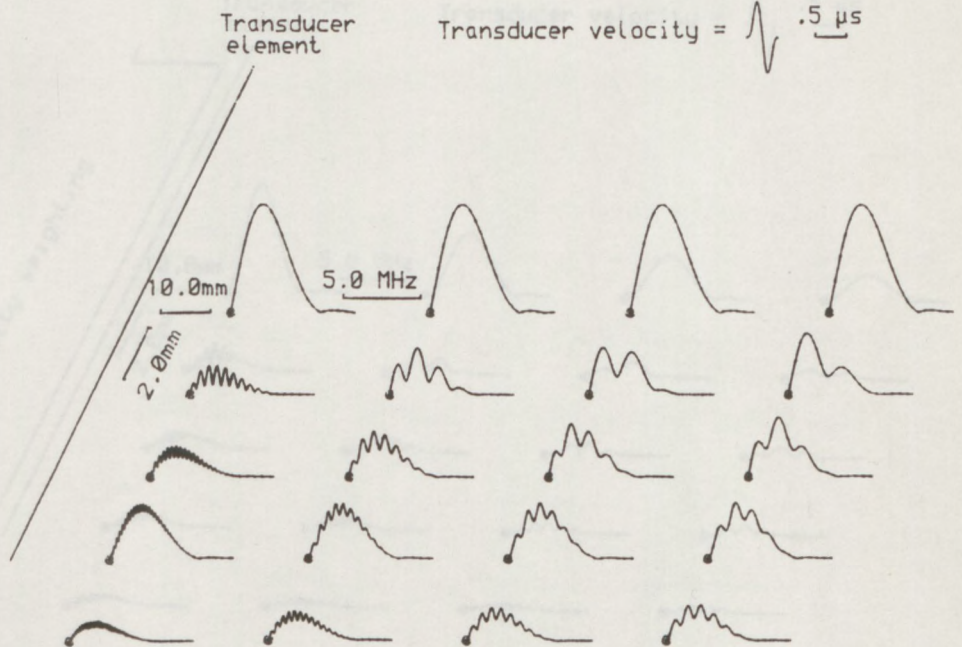
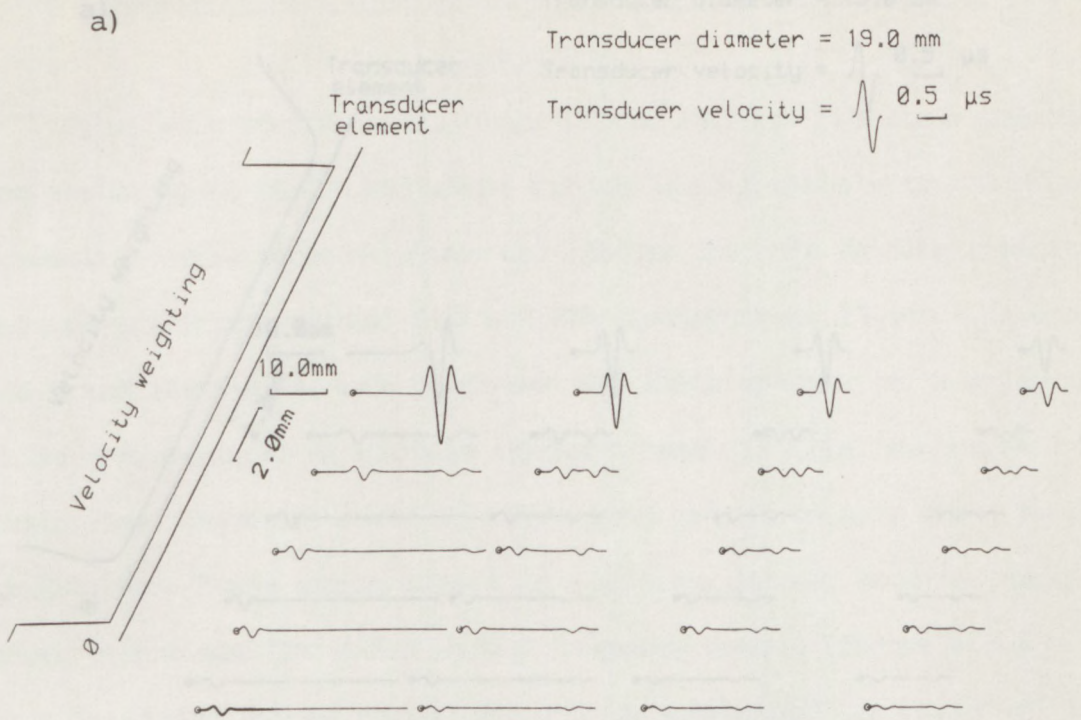
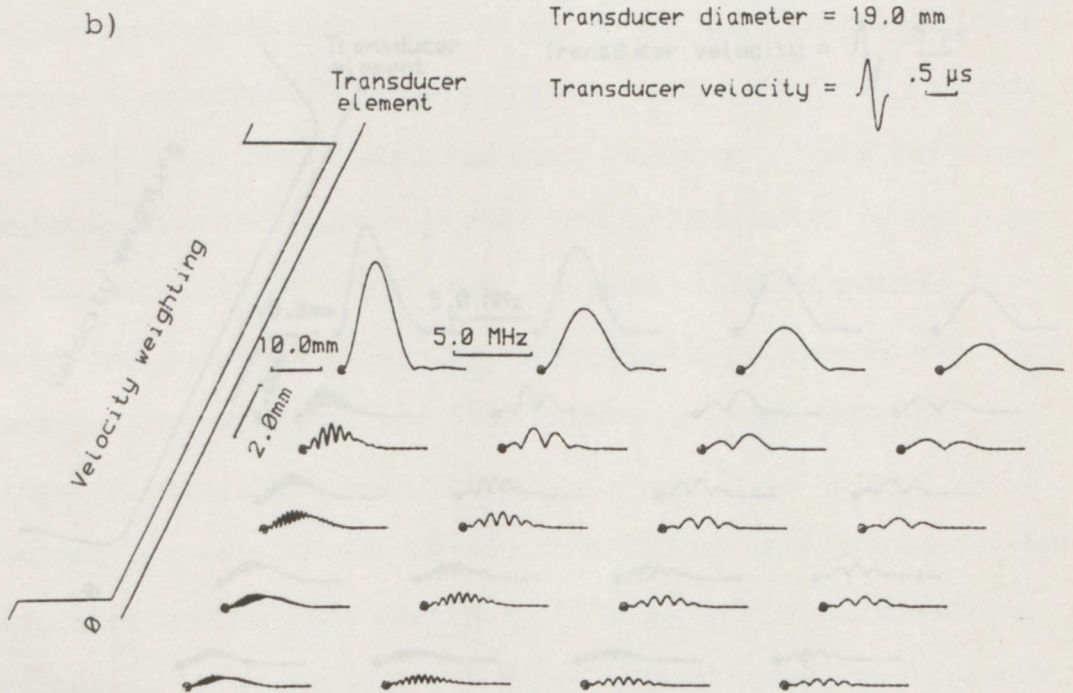


Figure 4-5 Computer calculated results at points in the field of an ideal EWD type transducer radiating a short pulse into water showing:-  
a) pressure waveforms b) pressure spectra



Note: Width of annulus = 0.75mm



**Figure 4-6** Computer calculated results at points in the field of an annular EWO type transducer radiating a short pulse into water showing:-  
 a) pressure waveforms b) pressure spectra

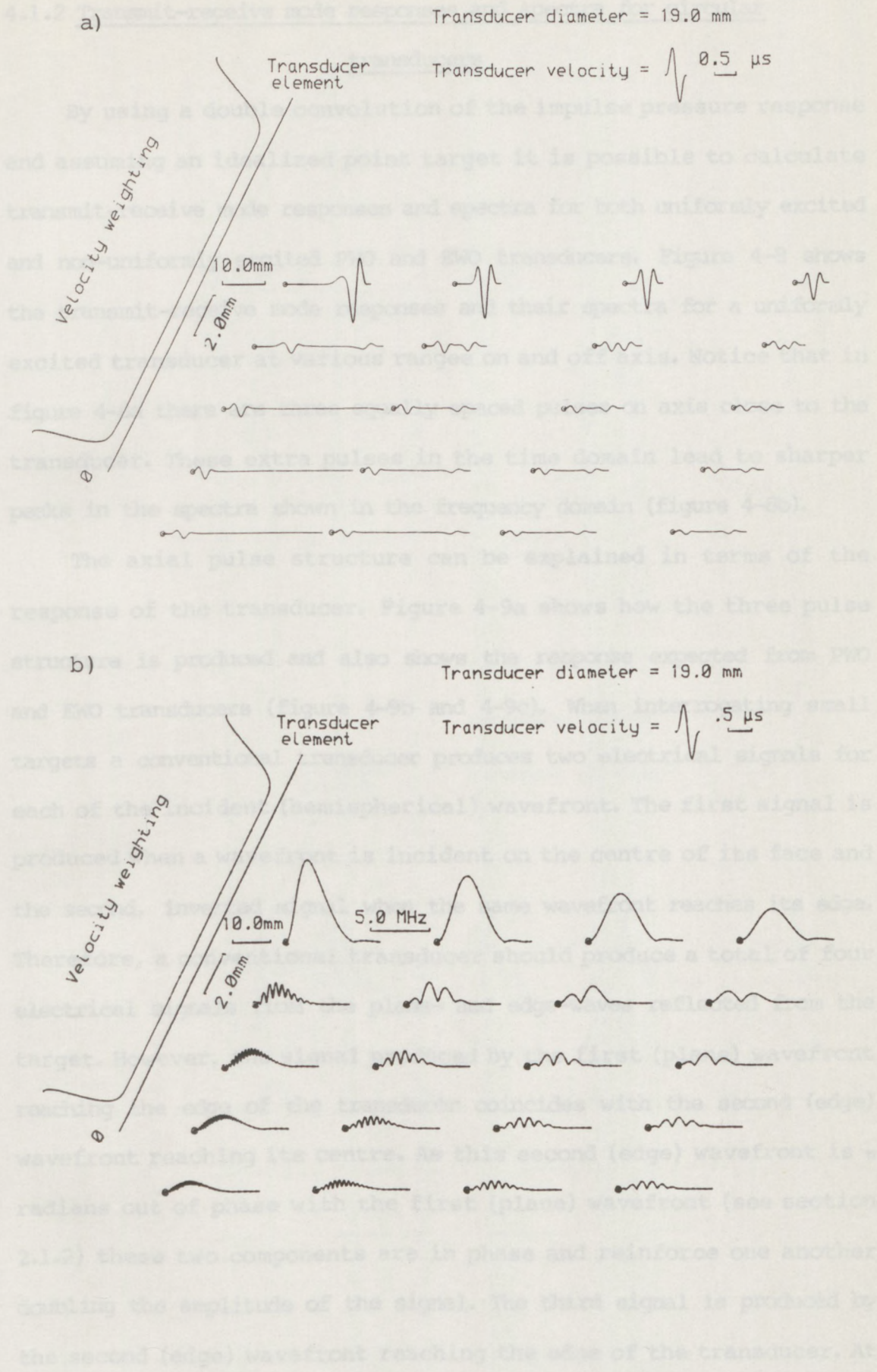


**Figure 4-7** Computer calculated results at points in the field of a non-uniformly excited, EWO type transducer radiating a short pulse into water showing:-  
 a) pressure waveforms b) pressure spectra

#### 4.1.2 Transmit-receive mode responses and spectra for circular transducers

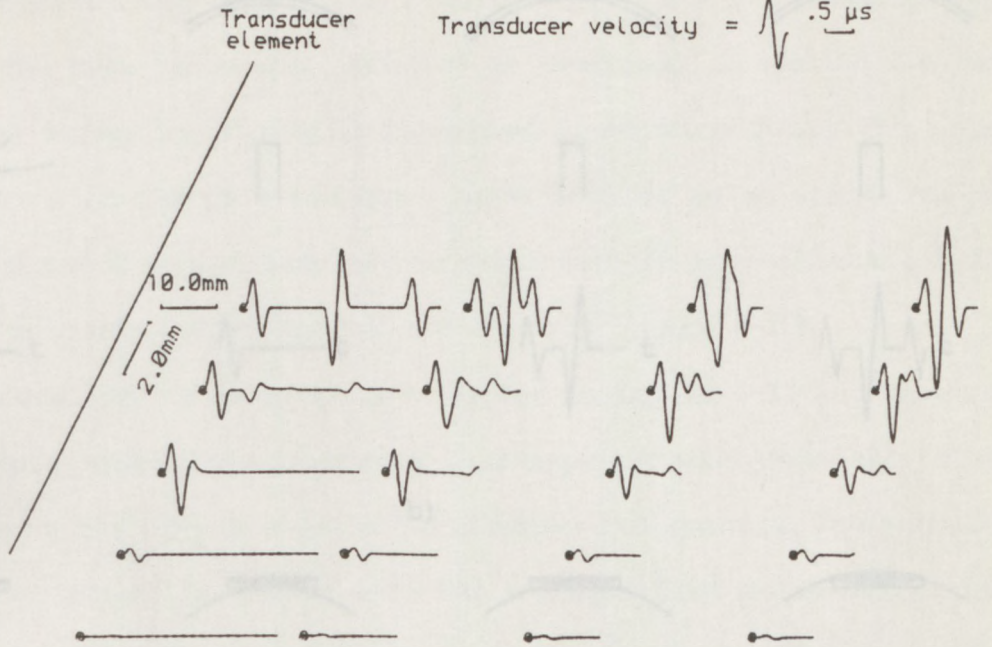
By using a double convolution of the impulse pressure response and assuming an idealized point target it is possible to calculate transmit-receive mode responses and spectra for both uniformly excited and non-uniformly excited PWO and EWO transducers. Figure 4-8 shows the transmit-receive mode responses and their spectra for a uniformly excited transducer at various ranges on and off axis. Notice that in figure 4-8a there are three equally spaced pulses on axis close to the transducer. These extra pulses in the time domain lead to sharper peaks in the spectra shown in the frequency domain (figure 4-8b).

The axial pulse structure can be explained in terms of the response of the transducer. Figure 4-9a shows how the three pulse structure is produced and also shows the response expected from PWO and EWO transducers (figure 4-9b and 4-9c). When interrogating small targets a conventional transducer produces two electrical signals for each of the incident (hemispherical) wavefront. The first signal is produced when a wavefront is incident on the centre of its face and the second, inverted signal when the same wavefront reaches its edge. Therefore, a conventional transducer should produce a total of four electrical signals from the plane- and edge-waves reflected from the target. However, the signal produced by the first (plane) wavefront reaching the edge of the transducer coincides with the second (edge) wavefront reaching its centre. As this second (edge) wavefront is  $\pi$  radians out of phase with the first (plane) wavefront (see section 2.1.2) these two components are in phase and reinforce one another doubling the amplitude of the signal. The third signal is produced by the second (edge) wavefront reaching the edge of the transducer. At larger axial ranges these signals are no longer time resolved and appear as a single pulse of continuously changing shape and amplitude.

a)

Transducer diameter = 19.0 mm

Transducer velocity =  $\sqrt{\quad} .5 \mu\text{s}$



b)

Transducer diameter = 19.0 mm

Transducer velocity =  $\sqrt{\quad} .5 \mu\text{s}$

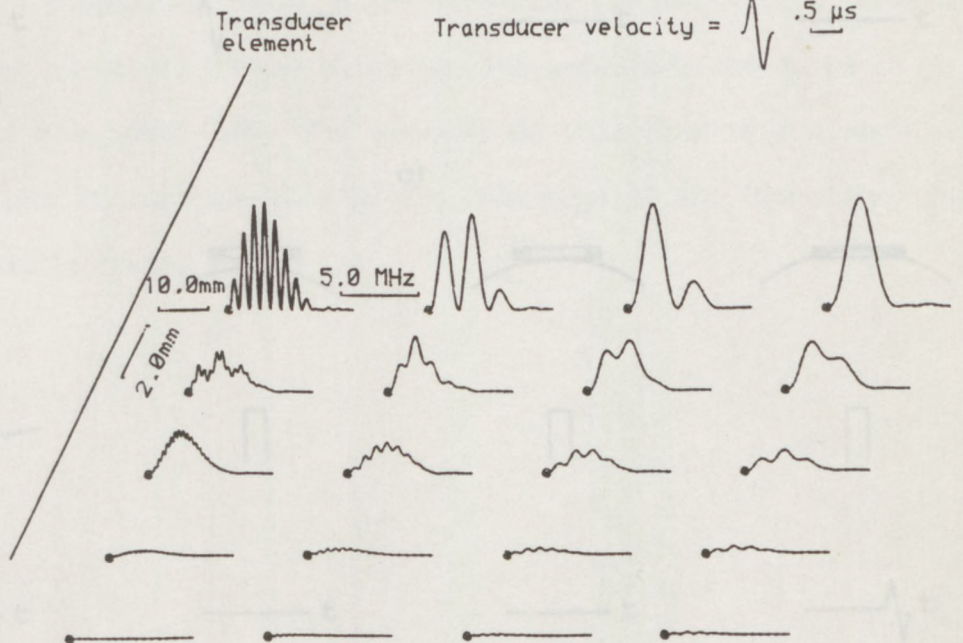
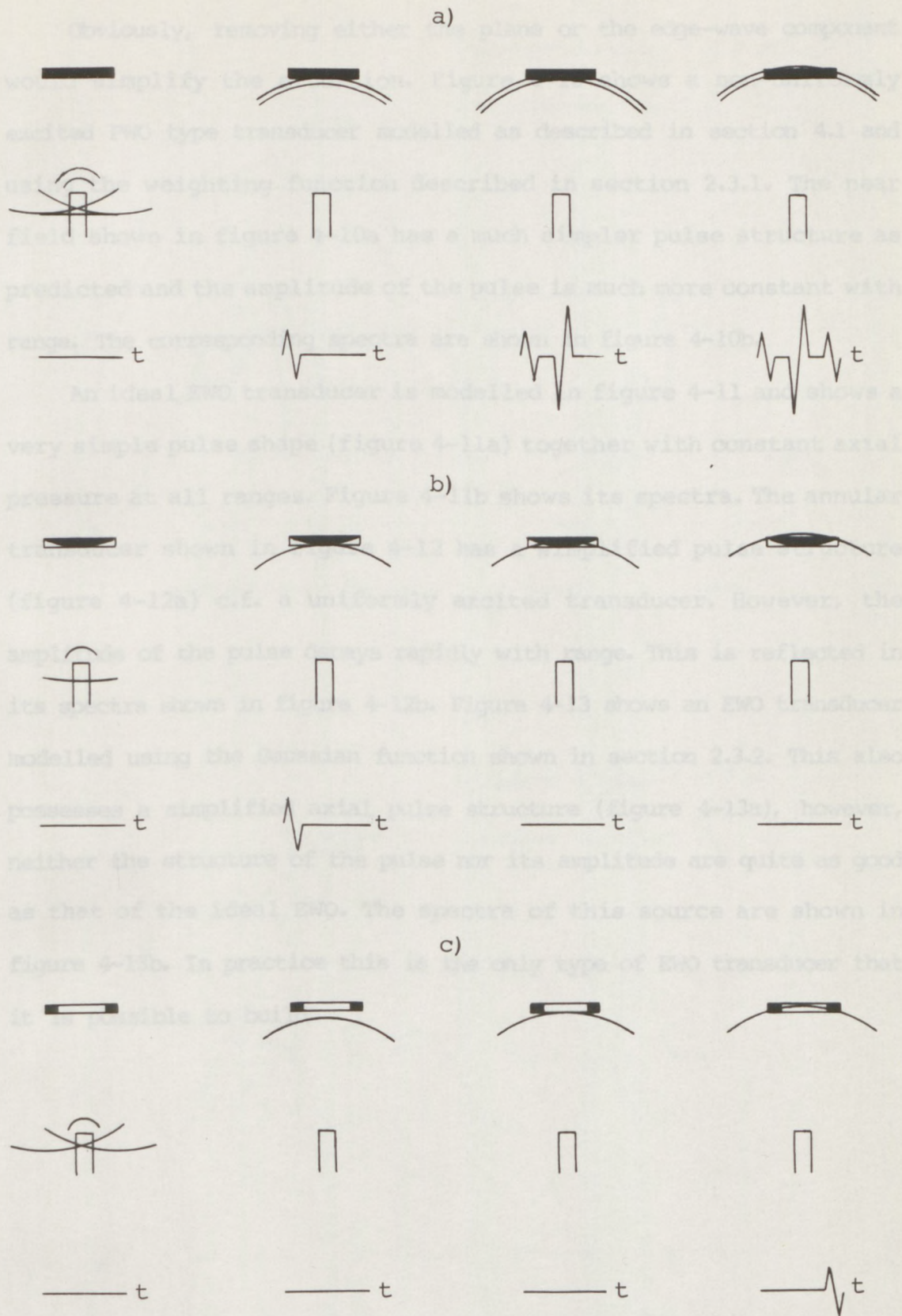


Figure 4-8 Computer calculated transmit-receive mode results for an ideal, uniformly excited transducer interrogating a small target in water showing:-

- a) transmit-receive mode responses
- b) transmit-receive mode spectra



**Figure 4-9** A schematic representation of the transmit-receive mode responses produced by transducers with various excitations interrogating a small (point-like), axial target in the near field in water for:-

- a) a conventional, uniformly-excited transducer
- b) a non-uniformly-excited PWO type transducer
- c) a non-uniformly-excited EWO type transducer

Obviously, removing either the plane or the edge-wave component would simplify the situation. Figure 4-10 shows a non-uniformly excited PWO type transducer modelled as described in section 4.1 and using the weighting function described in section 2.3.1. The near field shown in figure 4-10a has a much simpler pulse structure as predicted and the amplitude of the pulse is much more constant with range. The corresponding spectra are shown in figure 4-10b.

An ideal EWO transducer is modelled in figure 4-11 and shows a very simple pulse shape (figure 4-11a) together with constant axial pressure at all ranges. Figure 4-11b shows its spectra. The annular transducer shown in figure 4-12 has a simplified pulse structure (figure 4-12a) c.f. a uniformly excited transducer. However, the amplitude of the pulse decays rapidly with range. This is reflected in its spectra shown in figure 4-12b. Figure 4-13 shows an EWO transducer modelled using the Gaussian function shown in section 2.3.2. This also possesses a simplified axial pulse structure (figure 4-13a), however, neither the structure of the pulse nor its amplitude are quite as good as that of the ideal EWO. The spectra of this source are shown in figure 4-13b. In practice this is the only type of EWO transducer that it is possible to build.

Figure 4-10 Computer calculated transmit-receive mode results for a non-uniformly excited PWO type transducer interrogating a small target in water shrouds:-  
a) transmit-receive mode response  
b) transmit-receive mode spectra

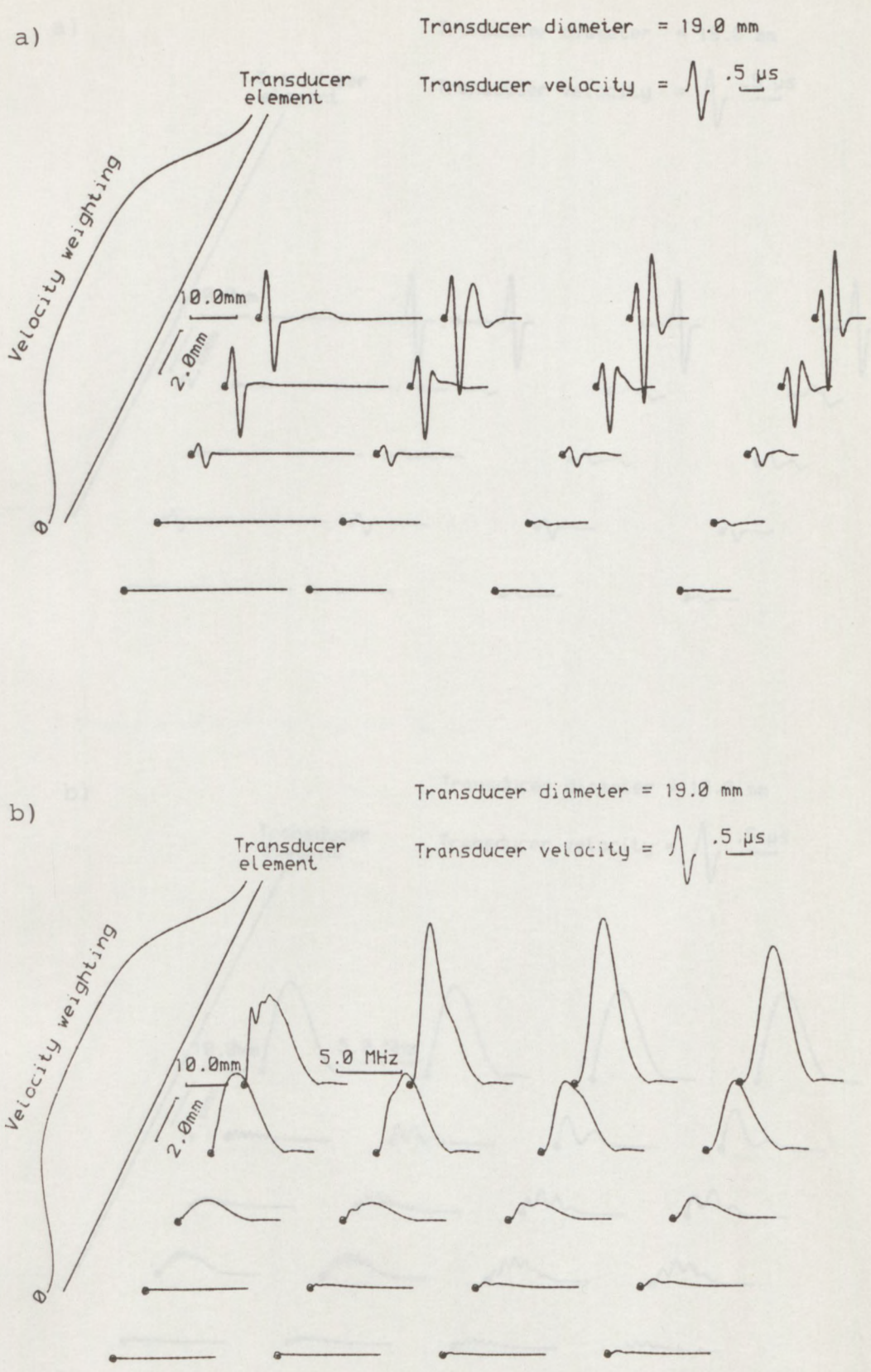
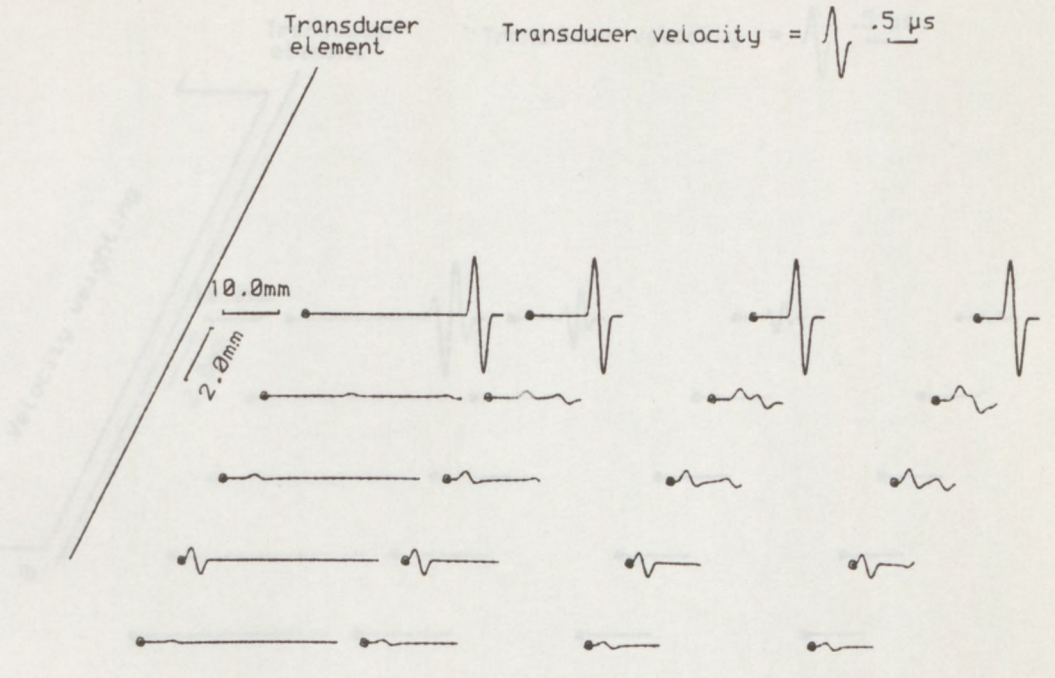


**Figure 4-10** Computer calculated transmit-receive mode results for a non-uniformly excited PWO type transducer interrogating a small target in water showing:-  
 a) transmit-receive mode responses  
 b) transmit-receive mode spectra

a)

Transducer diameter = 19.0 mm

Transducer velocity =  $\sqrt{\quad} .5 \mu s$



Note: Width of annulus = 0.75mm

b)

Transducer diameter = 19.0 mm

Transducer velocity =  $\sqrt{\quad} .5 \mu s$

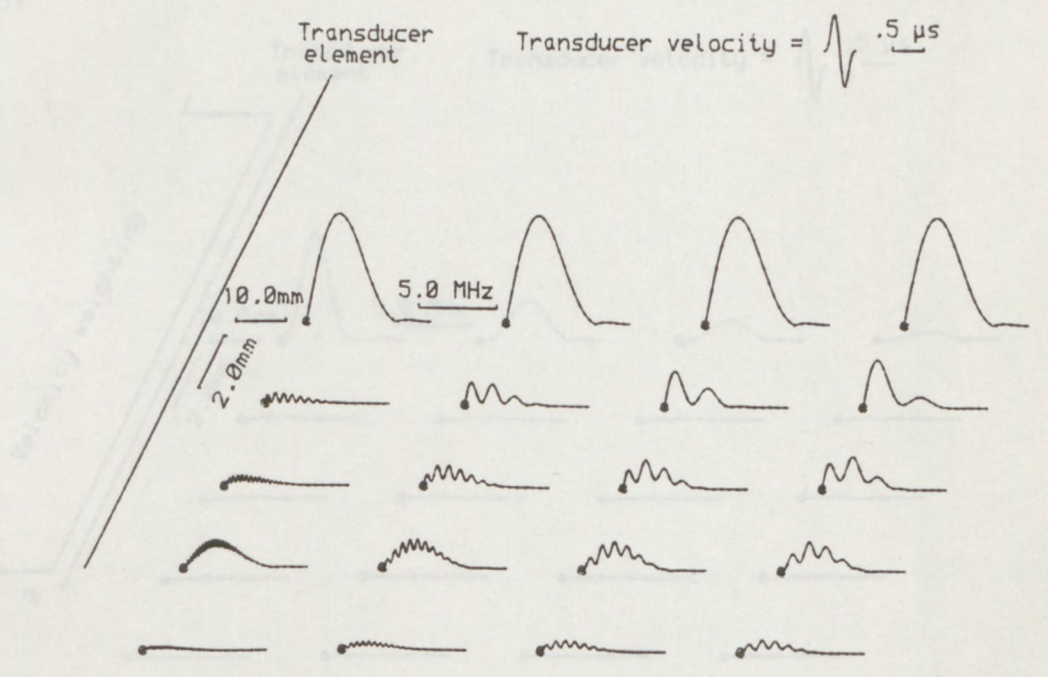


**Figure 4-11** Computer calculated transmit-receive mode results for an ideal EWO type transducer interrogating a small target in water showing:-

- a) transmit-receive mode responses
- b) transmit-receive mode spectra

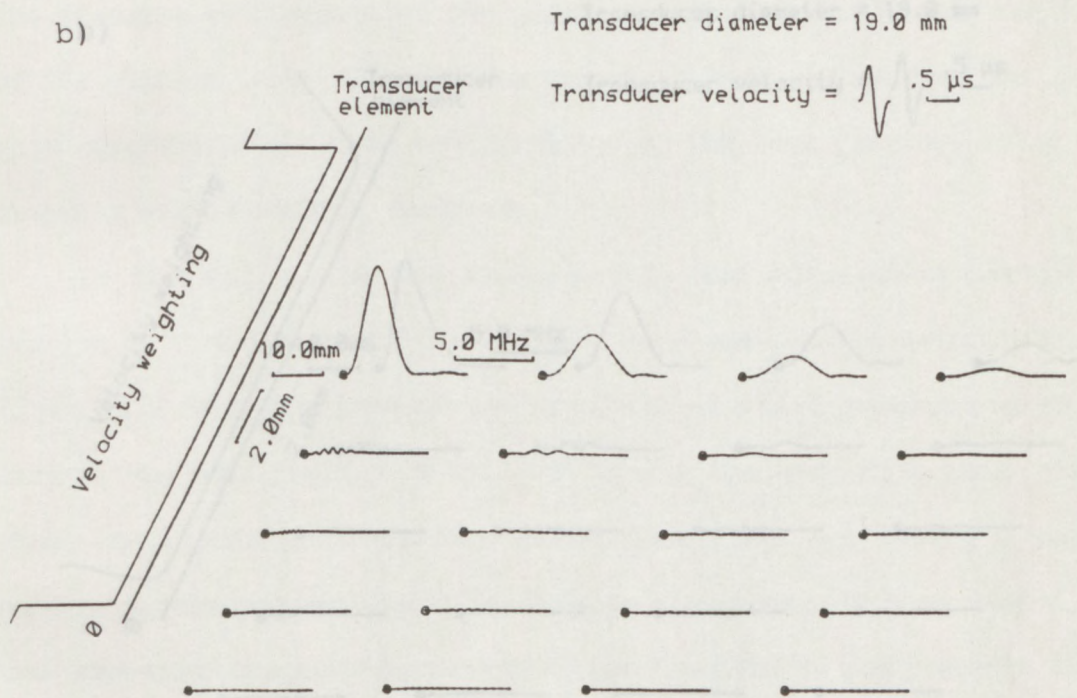
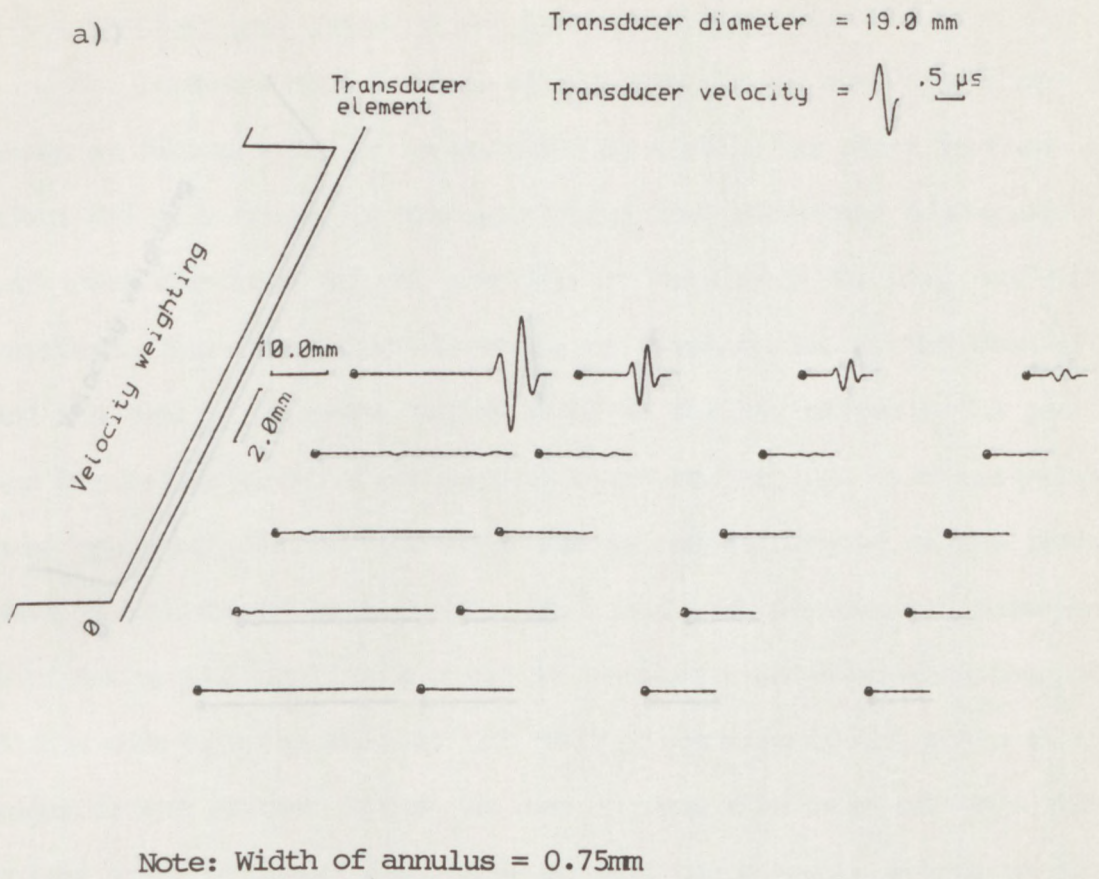


**Figure 4-12** Computer calculated transmit-receive mode results for an annular EWO type transducer interrogating a small target in water showing:-  
 a) transmit-receive mode responses  
 b) transmit-receive mode spectra

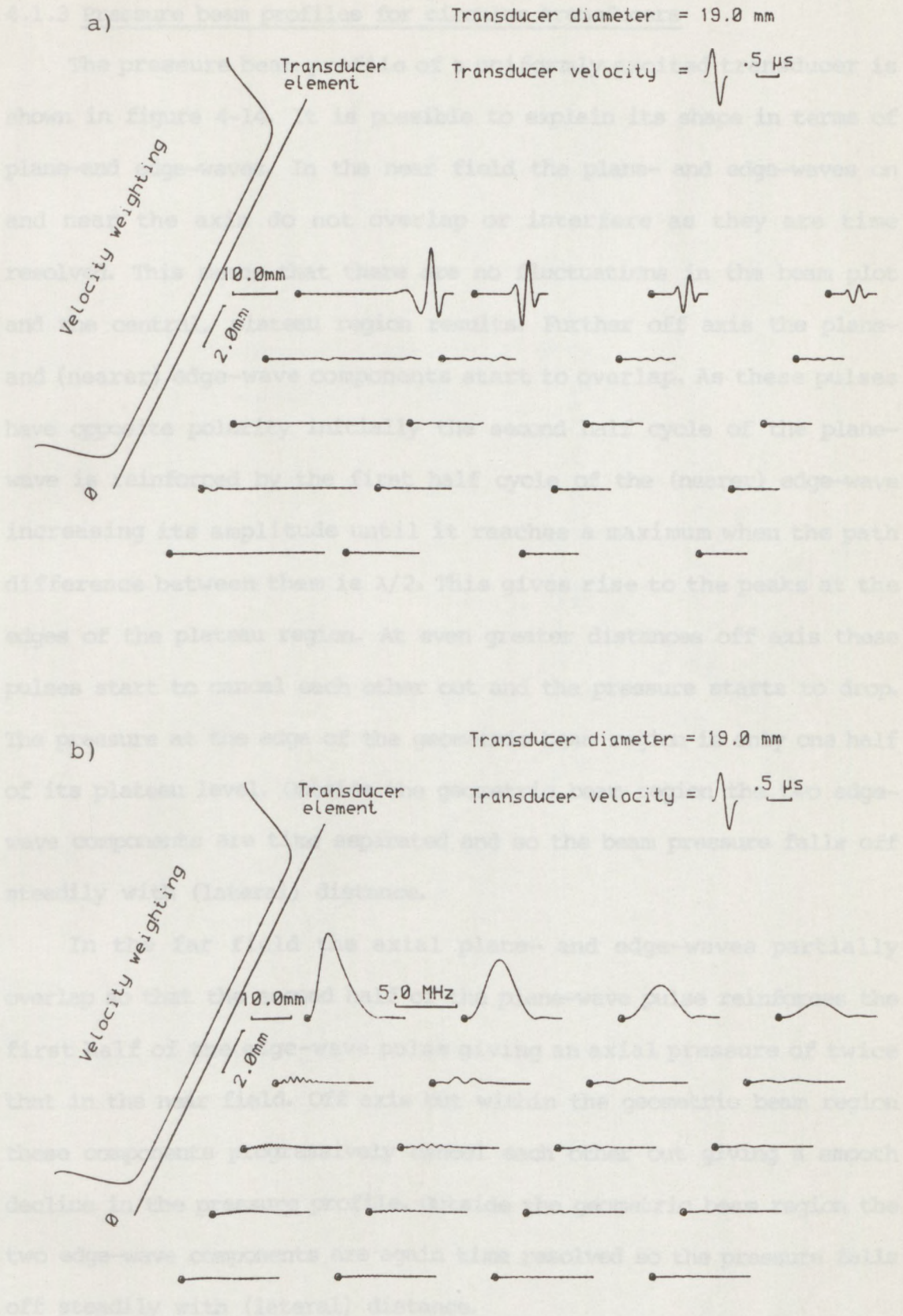


**Figure 4-13** Computer calculated transmit-receive mode results for a non-uniformly excited EWO type transducer interrogating a small target in water showing:-  
 a) transmit-receive mode responses  
 b) transmit-receive mode spectra

#### 4.1.3 Pressure beam profiles for circular transducers

The pressure beam profile of a uniformly excited transducer is shown in figure 4-14. It is possible to explain its shape in terms of plane- and edge-waves. In the near field the plane- and edge-waves on and near the axis do not overlap or interfere as they are time resolved. This means that there are no fluctuations in the beam plot and the central, plateau region results. Further off axis the plane- and (nearer) edge-wave components start to overlap. As these pulses have opposite polarity initially the second half cycle of the plane-wave is reinforced by the first half cycle of the (nearer) edge-wave increasing its amplitude until it reaches a maximum when the path difference between them is  $\lambda/2$ . This gives rise to the peaks at the edges of the plateau region. At even greater distances off axis these pulses start to cancel each other out and the pressure starts to drop. The pressure at the edge of the geometric beam region is only one half of its plateau level. Outside the geometric beam region the two edge-wave components are time separated and so the beam pressure falls off steadily with (lateral) distance.

In the far field the axial plane- and edge-waves partially overlap so that the second half of the plane-wave pulse reinforces the first half of the edge-wave pulse giving an axial pressure of twice that in the near field. Off axis but within the geometric beam region these components progressively cancel each other out giving a smooth decline in the pressure profile. Outside the geometric beam region the two edge-wave components are again time resolved so the pressure falls off steadily with (lateral) distance.

At intermediate ranges in between the near- and far-field the beam profile tends to resemble one or other of these situations as the width of the plateau region diminishes with increasing range.

Figure 4-15 shows a series of beam profiles for a non-uniformly

Transducer diameter = 19.0 mm

Transducer velocity =  .5  $\mu$ s

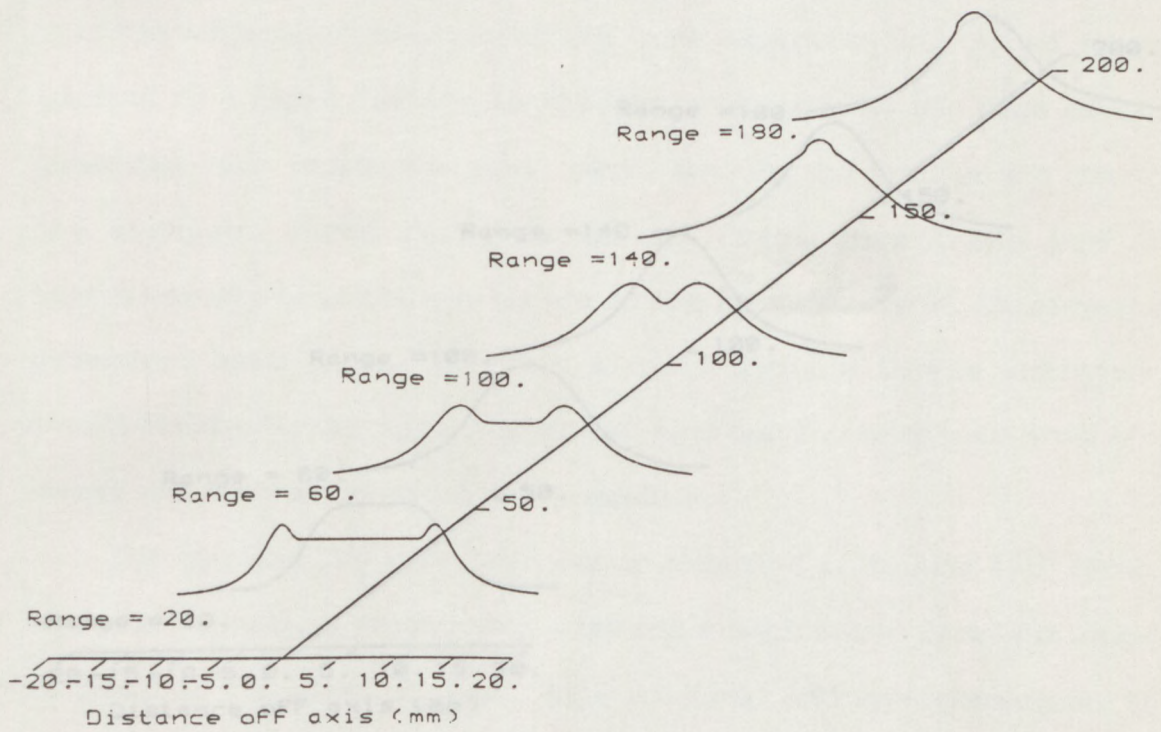


**Figure 4-14** Computer calculated pressure beam profiles for an ideal, uniformly-excited transducer, radiating a short pulse into water

excited PWO type transducer using the velocity weighting described in section 2.3.1. Removing the edge-wave component has got rid of the peaks at the edges of the plateau region in the near field. This means that the shape of the beam profile changes smoothly from a plateau with a smooth lateral decline in the near field to an axial maximum of similar amplitude.

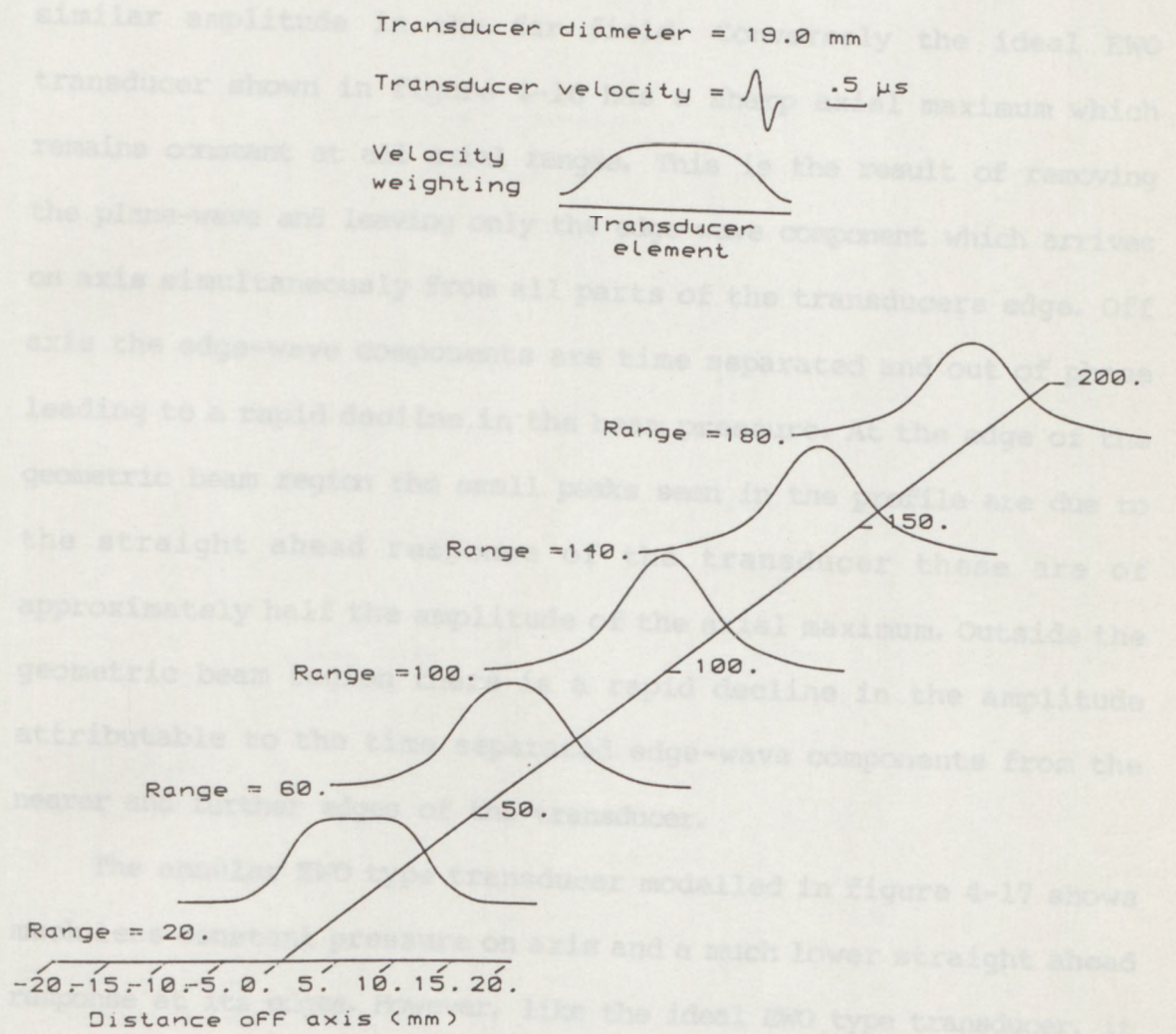


**Figure 4-15** Computer calculated pressure beam profiles for a non-uniformly excited, PWO type transducer, radiating a short pulse into water

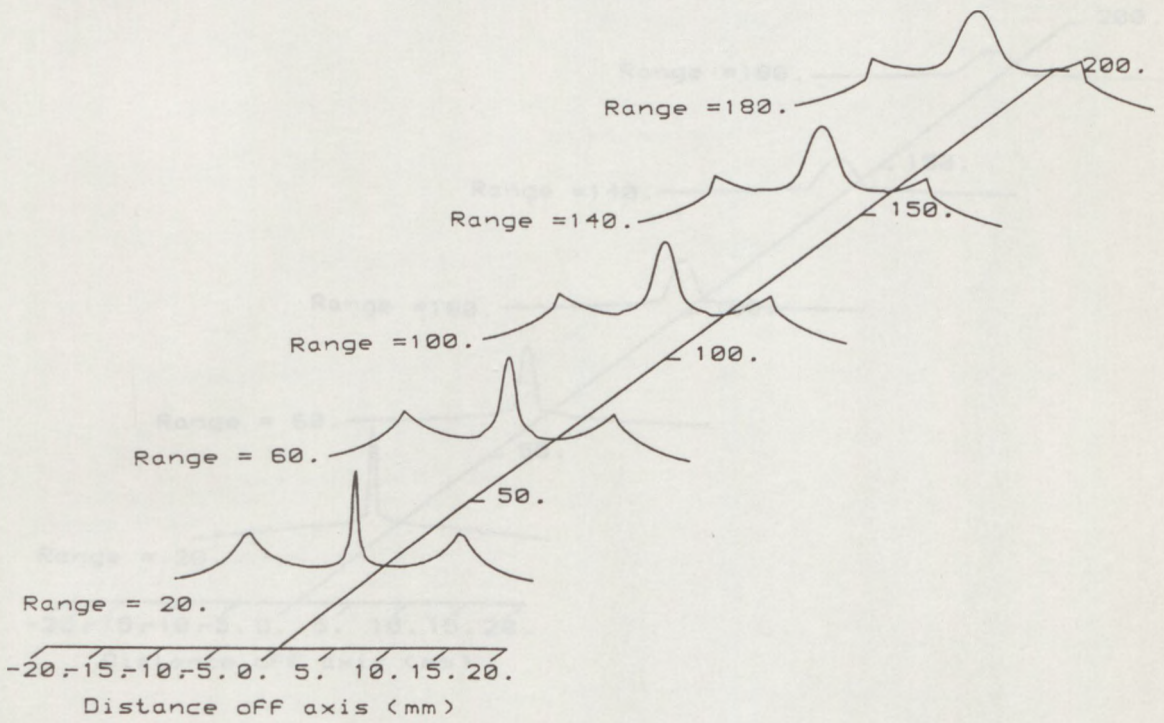
excited PWO type transducer using the velocity weighting described in section 2.3.1. Removing the edge-wave component has got rid of the peaks at the edges of the plateau region in the near field. This means that the shape of the beam profile changes smoothly from a plateau with a smooth lateral decline in the near field to an axial maximum of similar amplitude in the far field. Conversely the ideal EWO transducer shown in figure 4-16 has a sharp axial maximum which remains constant at all axial ranges. This is the result of removing the plane-wave and leaving only the edge-wave component which arrives on axis simultaneously from all parts of the transducers edge. Off axis the edge-wave components are time separated and out of phase leading to a rapid decline in the beam pressure. At the edge of the geometric beam region the small peaks seen in the profile are due to the straight ahead response of the transducer these are of approximately half the amplitude of the axial maximum. Outside the geometric beam region there is a rapid decline in the amplitude attributable to the time separated edge-wave components from the nearer and further edges of the transducer.

The annular EWO type transducer modelled in figure 4-17 shows much less constant pressure on axis and a much lower straight ahead response at its edges. However, like the ideal EWO type transducer, it cannot be realised in practice. Figure 4-18 shows a non-uniformly excited EWO type transducer using the type of excitation profile described in section 2.3.2. This has peak pressure on axis and very little "straight ahead" response at its edges. However, the axial pressure declines more quickly with range c.f. the ideal EWO transducer, although the decline is slower than for the annular transducer. In practice it is possible to make a transducer which approaches this type of excitation.

Figure 4-16 Computer calculated pressure beam profiles for an ideal EWO type transducer, raising a short pulse into wave

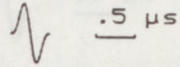
Transducer diameter = 19.0 mm

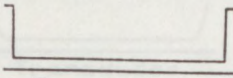
Transducer velocity =  $\sqrt{\quad}$   $.5 \mu\text{s}$

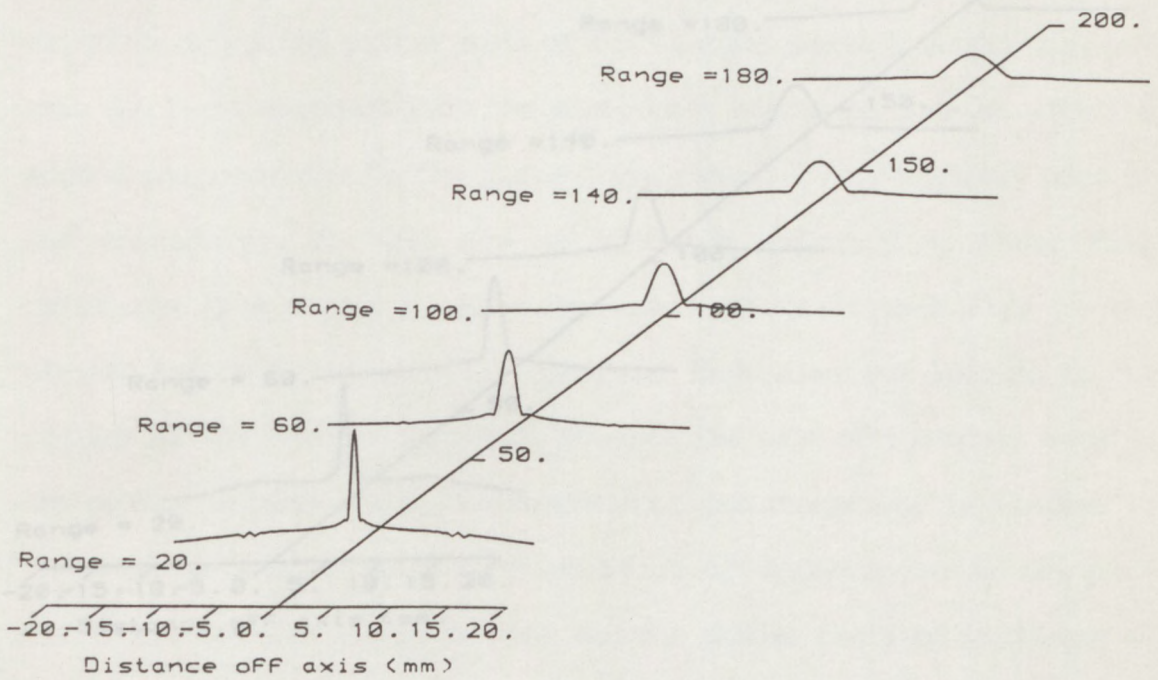


**Figure 4-16** Computer calculated pressure beam profiles for an ideal, EWO type transducer, radiating a short pulse into water

Transducer diameter = 19.0 mm

Transducer velocity =  .5 μs

Velocity weighting   
Transducer element



Note: Width of annulus = 0.75mm

Figure 4-17 Computer calculated pressure beam profiles for an annular, EWO type transducer, radiating a short pulse into water

#### 4.1.4 Transmit-receive mode beam profiles for circular transducers

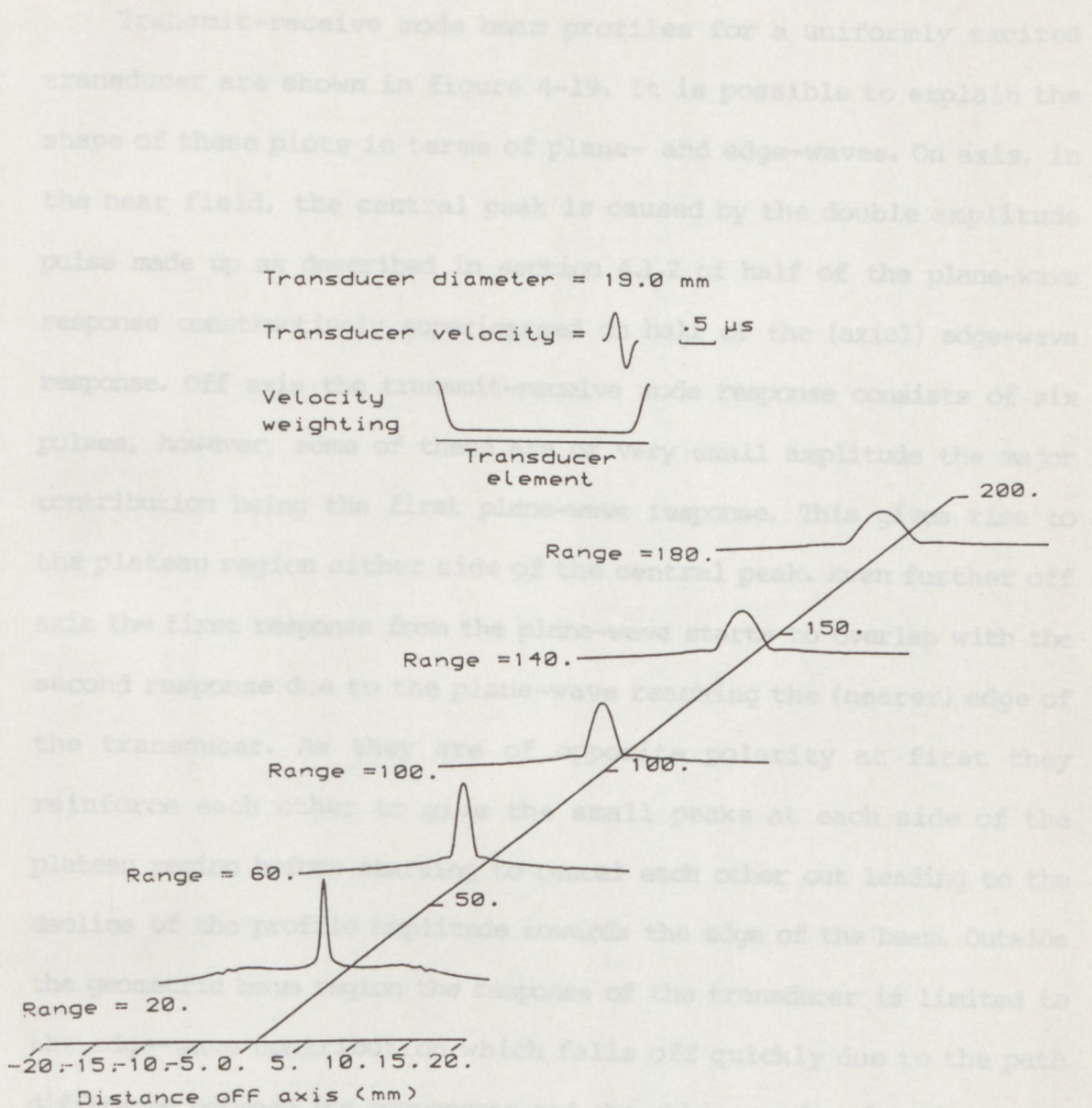


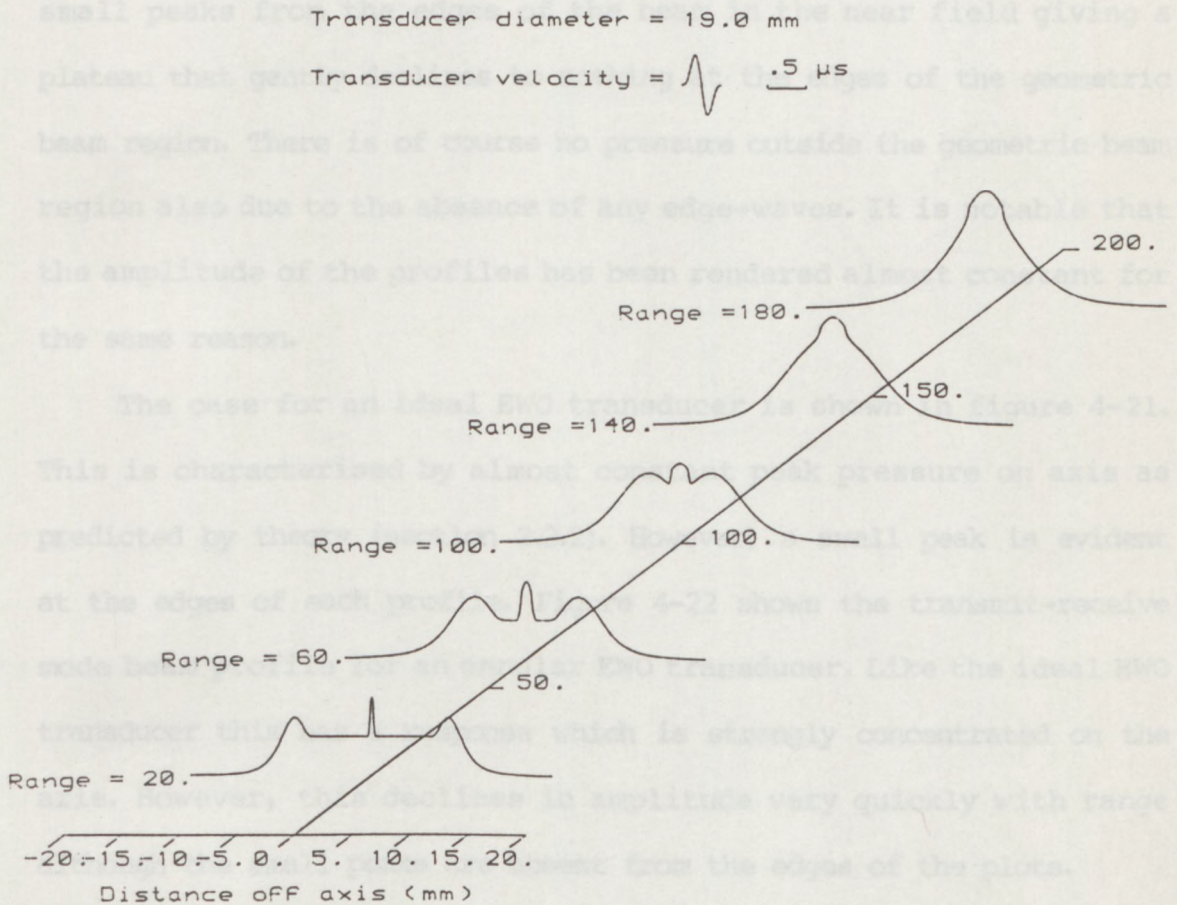
**Figure 4-18** Computer calculated pressure beam profiles for a non-uniformly excited, EWO type transducer, radiating a short pulse into water

#### 4.1.4 Transmit-receive mode beam profiles for circular transducers

Transmit-receive mode beam profiles for a uniformly excited transducer are shown in figure 4-19. It is possible to explain the shape of these plots in terms of plane- and edge-waves. On axis, in the near field, the central peak is caused by the double amplitude pulse made up as described in section 4.1.2 of half of the plane-wave response constructively superimposed on half of the (axial) edge-wave response. Off axis the transmit-receive mode response consists of six pulses, however, some of these are of very small amplitude the major contribution being the first plane-wave response. This gives rise to the plateau region either side of the central peak. Even further off axis the first response from the plane-wave starts to overlap with the second response due to the plane-wave reaching the (nearer) edge of the transducer. As they are of opposite polarity at first they reinforce each other to give the small peaks at each side of the plateau region before starting to cancel each other out leading to the decline of the profile amplitude towards the edge of the beam. Outside the geometric beam region the response of the transducer is limited to the edge-wave contribution which falls off quickly due to the path difference between its components and the obtuse angle of incidence of many of its components. In the far field the axial response is very large. It is made up of the double amplitude pulse described above which has been further reinforced by the second half of the first plane-wave response over its first half cycle and the first half of the second edge-wave response over its second half cycle. This situation occurs as the path difference and therefore the time separation between these components reduces with range. Off axis but within the geometric beam region the edge-wave components split up and overlap with the plane-wave less and less causing a steady decline in amplitude. Outside the geometric beam region the pressure is made up

of the small contributions from the edge-waves alone. Of course in going from the near to the far field the situation steadily changes from one case to the other as the plane- and edge-wave components become less time resolved.

Figure 4-20 shows the case for a non-uniformly excited PWO transducer (section 2.1.3). The absence of edge-waves has removed the small peaks from the near field giving a plateau that gives a constant pressure of the geometric beam region. There is of course no pressure outside the geometric beam region also due to the absence of any edge-waves. It is notable that the amplitude of the profiles has been rendered almost constant for the same reason.



Finally, figure 4-23 shows the response of a non-uniformly excited PWO type transducer. This has the type of excitation described in section 2.3.3 and could be made in practice. It possesses a response concentrated strongly on axis as this is the only position where all the edge-wave components arrive simultaneously and overlap. It is notable that whilst both the simple annular and the non-uniformly excited PWO transducers have no structure straight ahead of their edges the decline in the axial pressure with range is much more pronounced for the annular transducer.

**Figure 4-19** Computer calculated transmit-receive mode beam profiles for an ideal, uniformly excited transducer, interrogating a small target in water

of the small contributions from the edge-waves alone. Of course in going from the near to the far field the situation steadily changes from one case to the other as the plane- and edge-wave components become less time resolved.

Figure 4-20 shows the case for a non-uniformly excited PWO transducer (section 2.1.3). The absence of edge-waves has removed the small peaks from the edges of the beam in the near field giving a plateau that gently declines to nothing at the edges of the geometric beam region. There is of course no pressure outside the geometric beam region also due to the absence of any edge-waves. It is notable that the amplitude of the profiles has been rendered almost constant for the same reason.

The case for an ideal EWO transducer is shown in figure 4-21. This is characterised by almost constant peak pressure on axis as predicted by theory (section 2.3.2). However, a small peak is evident at the edges of each profile. Figure 4-22 shows the transmit-receive mode beam profile for an annular EWO transducer. Like the ideal EWO transducer this has a response which is strongly concentrated on the axis. However, this declines in amplitude very quickly with range although the small peaks are absent from the edges of the plots.

Finally, figure 4-23 shows the response of a non-uniformly excited EWO type transducer. This has the type of excitation described in section 2.3.2 and could be made in practice. It possesses a response concentrated strongly on axis as this is the only position where all the edge-wave components arrive simultaneously and overlap. It is notable that whilst both the simple annular and the non-uniformly excited EWO transducers have no structure straight ahead of their edges the decline in the axial pressure with range is much more pronounced for the annular transducer.

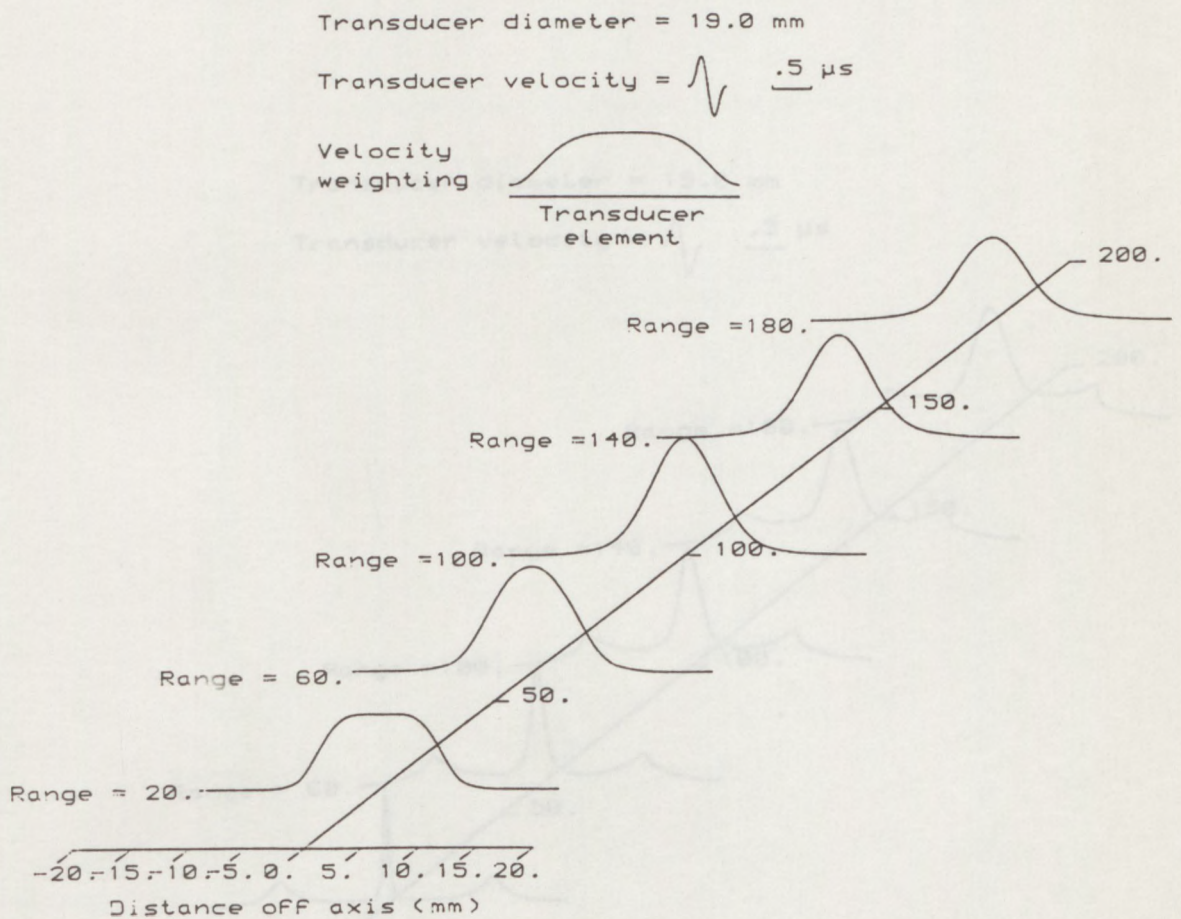
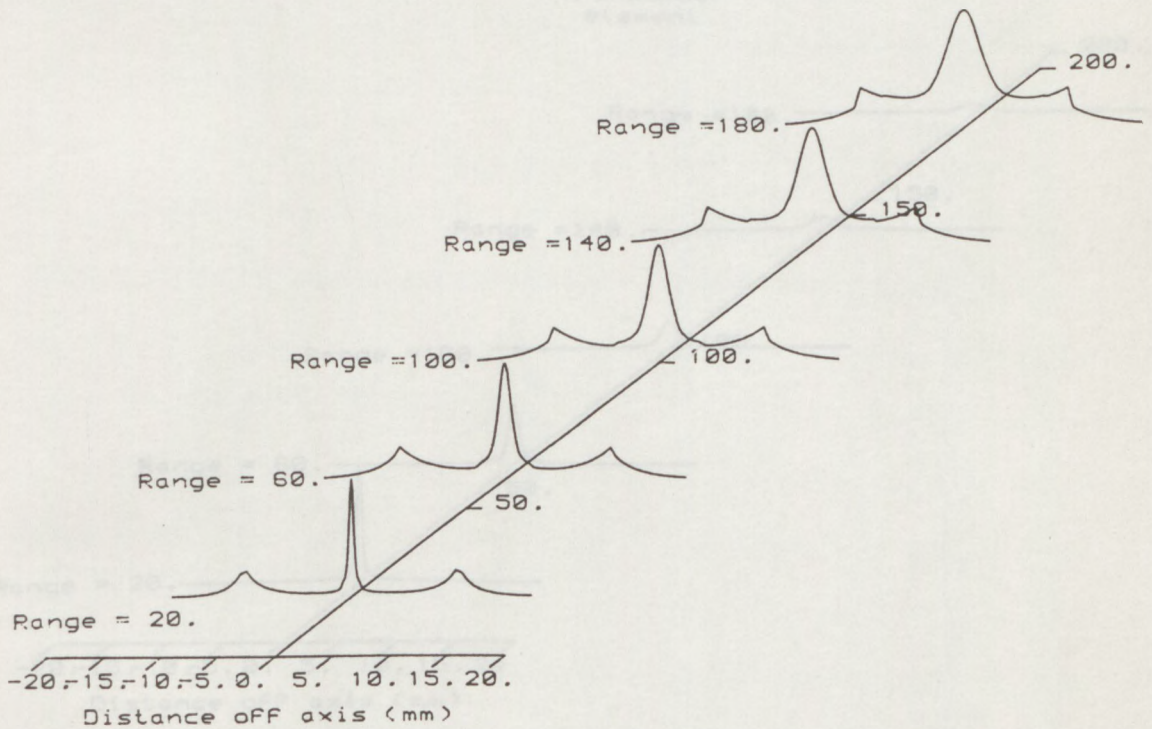


**Figure 4-20** Computer calculated transmit-receive mode beam profiles for a non-uniformly excited, PWO type transducer, interrogating a small target in water

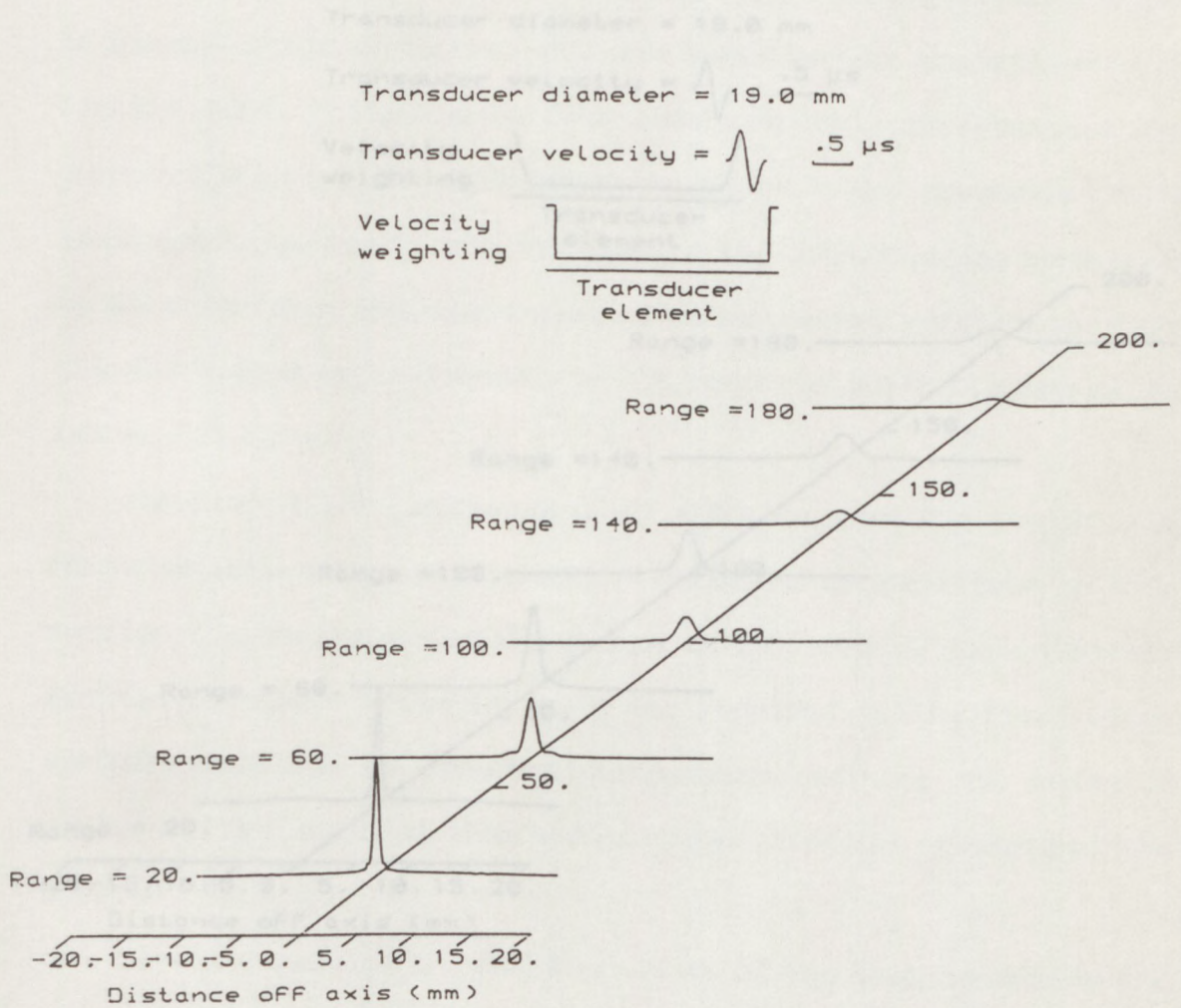
Transducer diameter = 19.0 mm

Transducer velocity =  $\sqrt{\quad}$  .5  $\mu$ s



Note: Width of beam is 0.75mm

**Figure 4-21** Computer calculated transmit-receive mode beam profiles for an ideal, EWO type transducer, interrogating a small target in water



Note: Width of annulus = 0.75mm

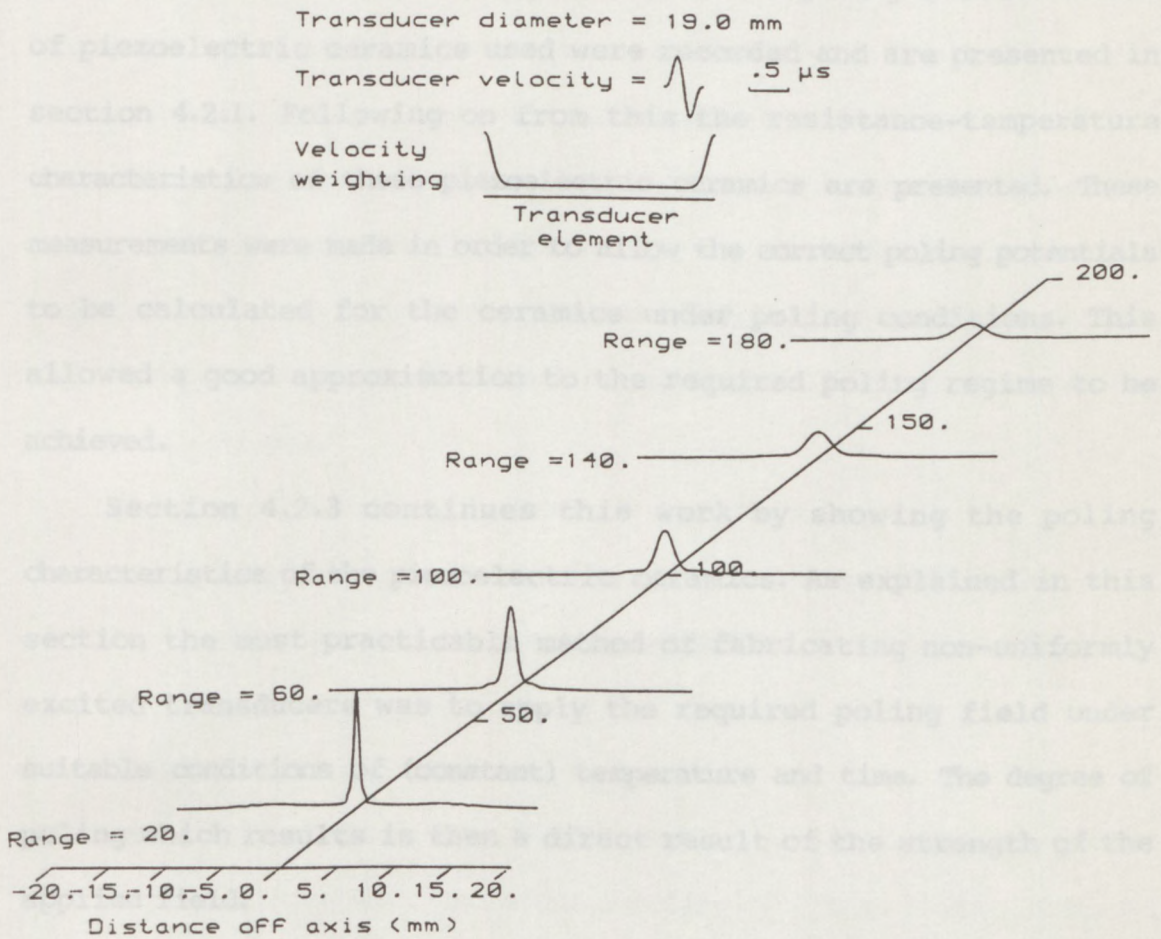
**Figure 4-22** Computer calculated transmit-receive mode beam profiles for an annular, EWO type transducer, interrogating a small target in water

#### 4.2 Poling and Fabrication of Transducers

Initial attempts at fabricating non-uniformly excited transducers at the outset of this project used thermal zoning. This method was quickly abandoned in favor of controlled zoning (section 3.3).

However, during the course of this work the zoning characteristics of piezoelectric ceramics used were investigated and are discussed in section 4.2.1. Following a review of the resistance-temperature characteristics of the ceramics, the zoning characteristics are presented. These measurements were made in order to determine the correct zoning parameters to be calculated for the ceramic zoning process.

This allowed a good approximation to the required zoning regime to be achieved. Section 4.2.3 continues this work by showing the zoning characteristics of the ceramic used in this work. This section shows the zoning characteristics of the ceramic used in this work. This section shows the zoning characteristics of the ceramic used in this work.



Finally, results showing the effect of the damping used on the shape of the pulse from the finished transducer are presented. Results showing the reproducibility of the pulse shape for this method of transducer fabrication are included.

**Figure 4-23** Computer calculated transmit-receive mode beam profiles for a non-uniformly excited, EWO type transducer, interrogating a small target in water

## 4.2 Poling and Fabrication of Transducers

Initial attempts at fabricating non-uniformly excited transducers at the outset of this project used thermal depoling. This method was quickly abandoned in favour of controlled repoling (section 3.3). However, during the course of this work the depoling characteristics of piezoelectric ceramics used were recorded and are presented in section 4.2.1. Following on from this the resistance-temperature characteristics of these piezoelectric ceramics are presented. These measurements were made in order to allow the correct poling potentials to be calculated for the ceramics under poling conditions. This allowed a good approximation to the required poling regime to be achieved.

Section 4.2.3 continues this work by showing the poling characteristics of the piezoelectric ceramics. As explained in this section the most practicable method of fabricating non-uniformly excited transducers was to apply the required poling field under suitable conditions of (constant) temperature and time. The degree of poling which results is then a direct result of the strength of the applied field.

Finally, results showing the effect of the damping used on the shape of the pulse from the finished transducer are presented. Results showing the reproducibility of the pulse shape for this method of transducer fabrication are included.

#### 4.2.1 Thermal depoling of piezoelectric ceramics

As explained earlier (section 3.3) controlled poling of isotropic, ferroelectric ceramics was the most practicable way of producing non-uniformly excited PWO and EWO transducers. Unfortunately at the outset of this project no electroded but unpoled piezoelectric ceramics were available from the manufacturers. The processes of electroding and poling are carried out simultaneously during manufacture in specially designed furnaces. Further, no facilities were available at The City University for sintering electrodes onto unpoled ceramics. This meant that the only way to obtain electroded but unpoled piezoelectric ceramics was to depole discs obtained from the manufacturers.

The three fundamental methods of depoling were:-

- (i) Field depoling using either dc fields applied in the reverse sense to the original poling field or ac fields.
- (ii) Hydrostatic pressure.
- (iii) Thermal depoling.

Of these the latter was the least destructive and the most reliable. The graph in figure 4-24 shows the depoling of PZT as a drop in  $k_p$  the electromechanical coupling factor (sections 1.2.2 and 3.1) after exposure to various temperatures up to and slightly exceeding the Curie point ( $370^{\circ}\text{C}$  for PZT type PC5). Specimens of piezoelectric ceramic were subject to these temperatures in a temperature controlled muffle furnace (section 3.3). Firstly their electrodes were shorted and connected to earth. They were then placed in a closed porcelain crucible in the furnace. This was heated to the required temperature and 30 minutes were allowed for the specimens to reach thermal equilibrium. The crucible was then removed from the furnace and allowed to cool to room temperature before a measurement of  $k_p$  was made. Notice how  $k_p$  drops sharply to zero at about the Curie point.

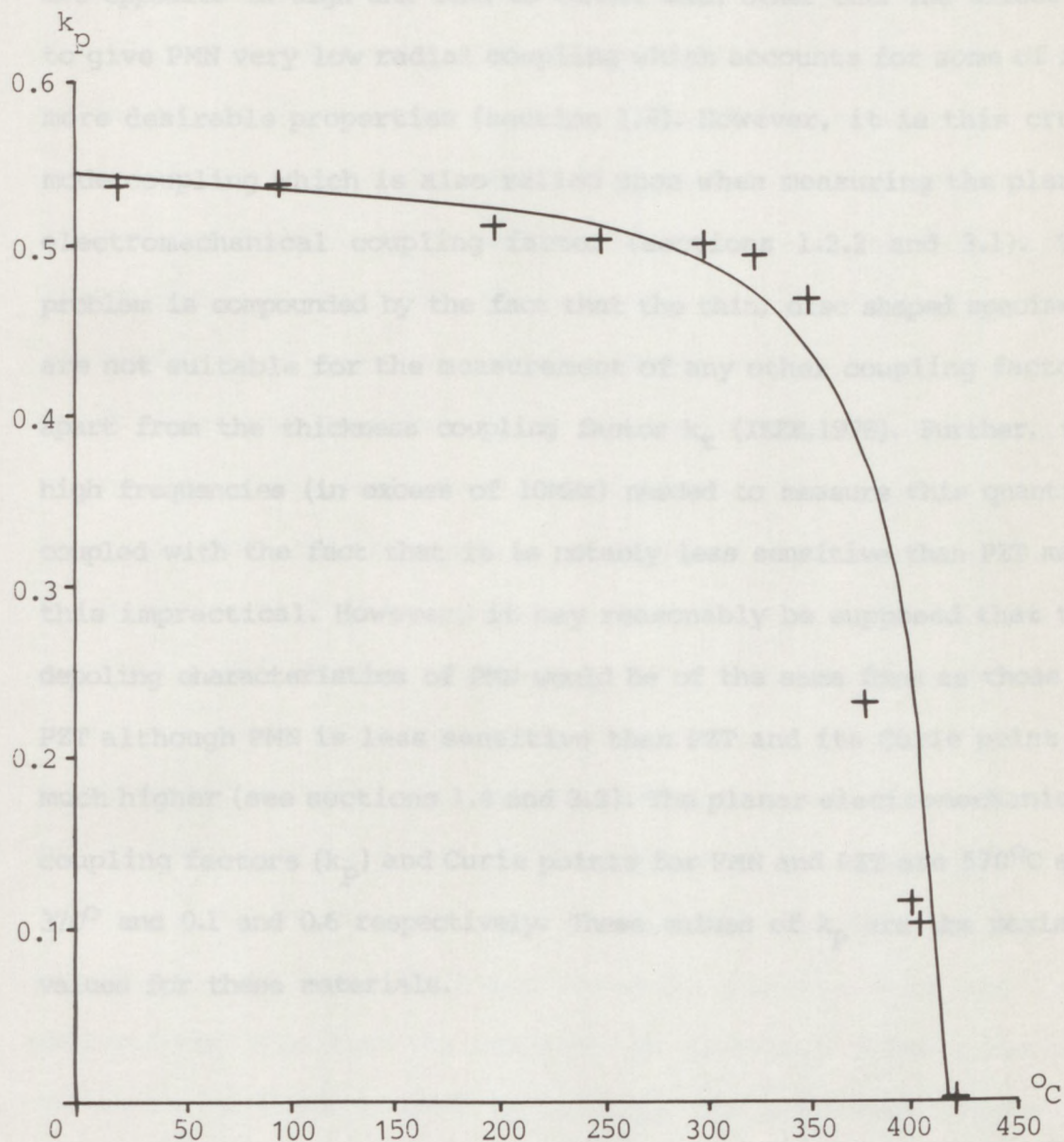


**Figure 4-24** Planar electromechanical coupling factor( $k_p$ ) against depoling temperature for PZT ceramic (type PC5)

4-2 The thermal depoling characteristics of PMN were not measured due to the difficulties in measuring its planar electromechanical coupling factor. As explained earlier (section 1.4) the  $d_{31}$  and  $d_{32}$  constants are opposite in sign and tend to cancel each other out. The effect is to give PMN very low radial coupling which accounts for some of its more desirable properties (section 1.4). However, it is this cross mode coupling which is also relied upon when measuring the planar electromechanical coupling factor (sections 1.2.2 and 3.1). The problem is compounded by the fact that the thin, disc shaped specimens are not suitable for the measurement of any other coupling factors apart from the thickness coupling factor  $k_t$  (IEEE,1978). Further, the high frequencies (in excess of 10MHz) needed to measure this quantity coupled with the fact that it is notably less sensitive than PZT make this impractical. However, it may reasonably be supposed that the depoling characteristics of PMN would be of the same form as those of PZT although PMN is less sensitive than PZT and its Curie point is much higher (see sections 1.4 and 3.3). The planar electromechanical coupling factors ( $k_p$ ) and Curie points for PMN and PZT are 570°C and 370°C and 0.1 and 0.6 respectively. These values of  $k_p$  are the maximum values for these materials.

#### 4.2.2 Resistance-temperature characteristics of piezoelectric ceramics

Piezoelectric ceramics have, like all dielectrics, a negative temperature coefficient of resistance. As the conductivity of these materials increases with temperature it is necessary to make allowance for this when calculating the voltages needed to produce the desired poling regime. The resistance-temperature characteristics of these materials were measured using a temperature controlled hot plate (Gallenkamp HPL500-050M) and a Mega-meter (Evershed and Vignoles Ltd. LONDON model 70145). Discs of both PZT and PMN with their major faces electroded were placed on a metal plate on top of the hot plate. The metal plate (and therefore one of the disc electrodes) was connected to one side of the Mega-meter. A connection was then made between the other electrode and the remaining terminal of the Mega-meter using a piece of wire held against the upper face electrode by a glass rod in a retort stand. The hot plate was then switched on and readings of resistance were taken at various temperatures ranging from room temperature to 300°C. The resistance-temperature characteristics of PZT and PMN using samples of 15mm diameter by 10MHz equivalent thickness PZT (type PC5) and 20mm diameter by 10MHz equivalent thickness PMN (type K83) are shown in figures 4-25 and 4-26 respectively. Note that the scale of the Mega-meter shows a maximum resistance of 100M $\Omega$  followed by infinity. The resistance-temperature characteristics can be clearly seen from these results. However, these results are specific to samples of these shapes and sizes so the resistivities have been calculated and plotted against temperature for PZT (type PC5) and PMN (type K83) in figures 4-27 and 4-28 respectively. Figure 4-29 shows the resistance-temperature results for both PZT (type PC5) and PMN (type K83) plotted on the same scale. It is notable that the resistivity of PZT is approximately an order of magnitude higher than that of PMN over the temperature range shown.

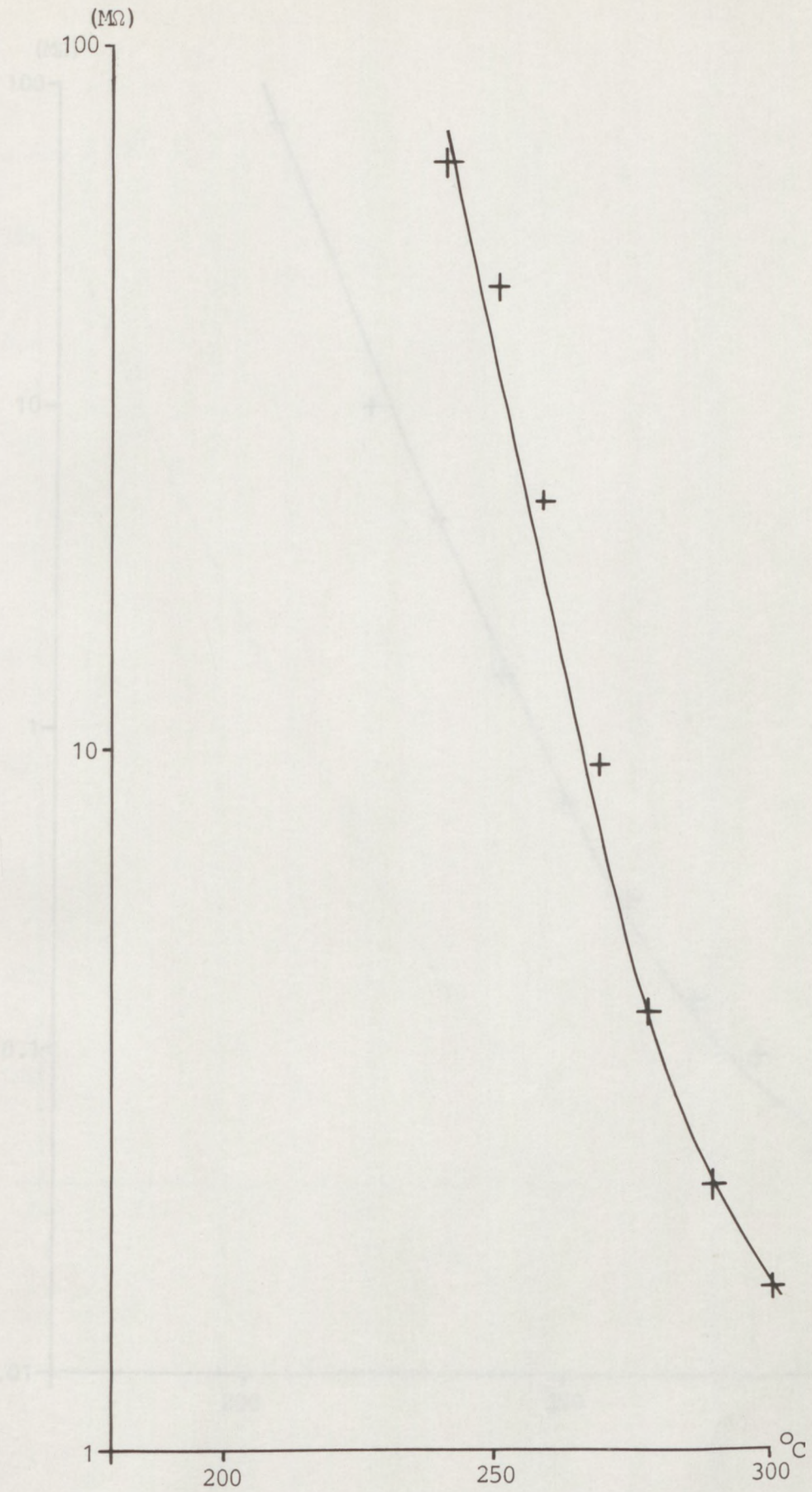


**Figure 4-25** Resistance against temperature for a sample of PZT (type PC5) 15mm in diameter by 10MHz equivalent thickness

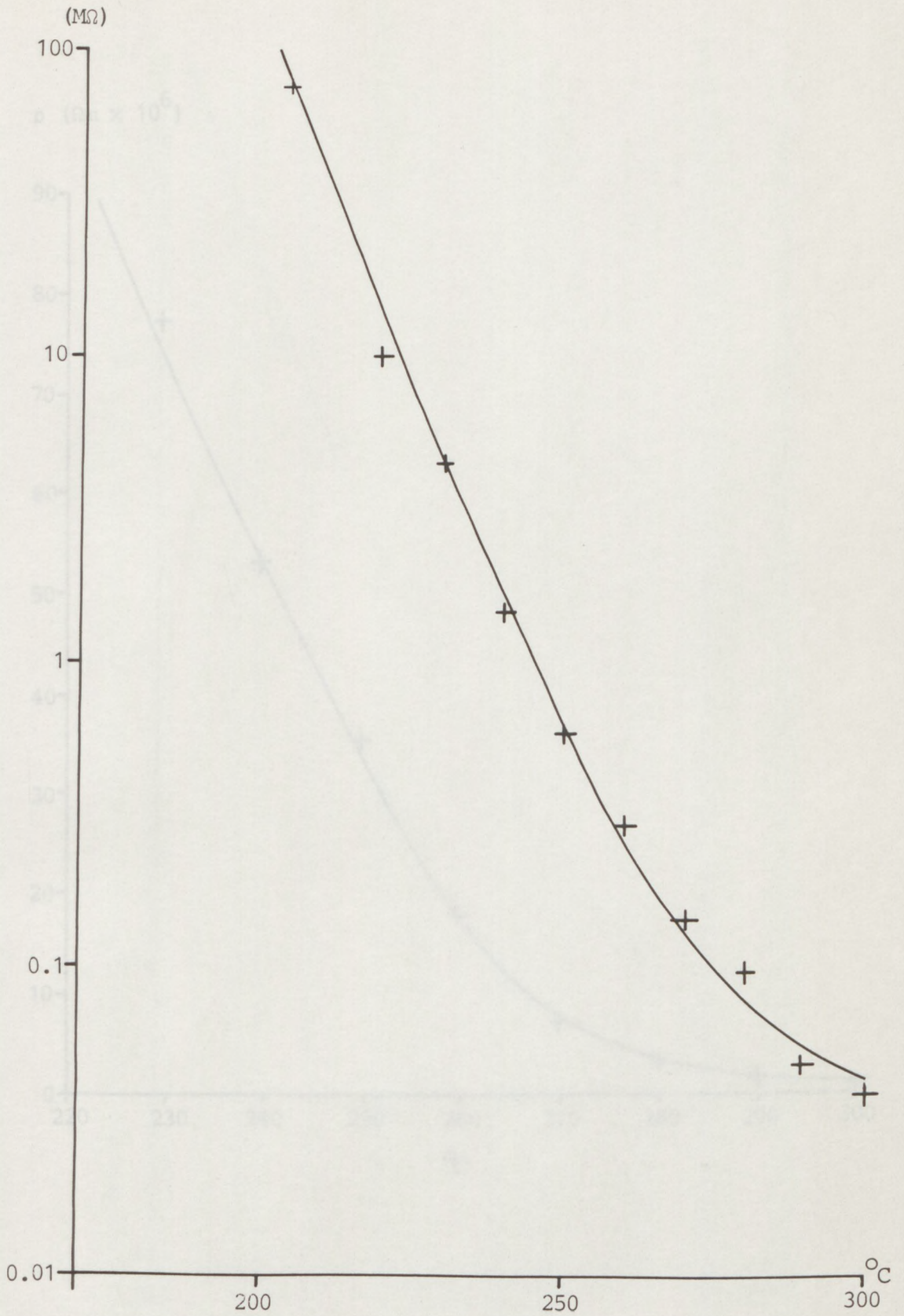


**Figure 4-26** Resistance against temperature for a sample of PMN (type K83) 20mm in diameter by 10MHz equivalent thickness

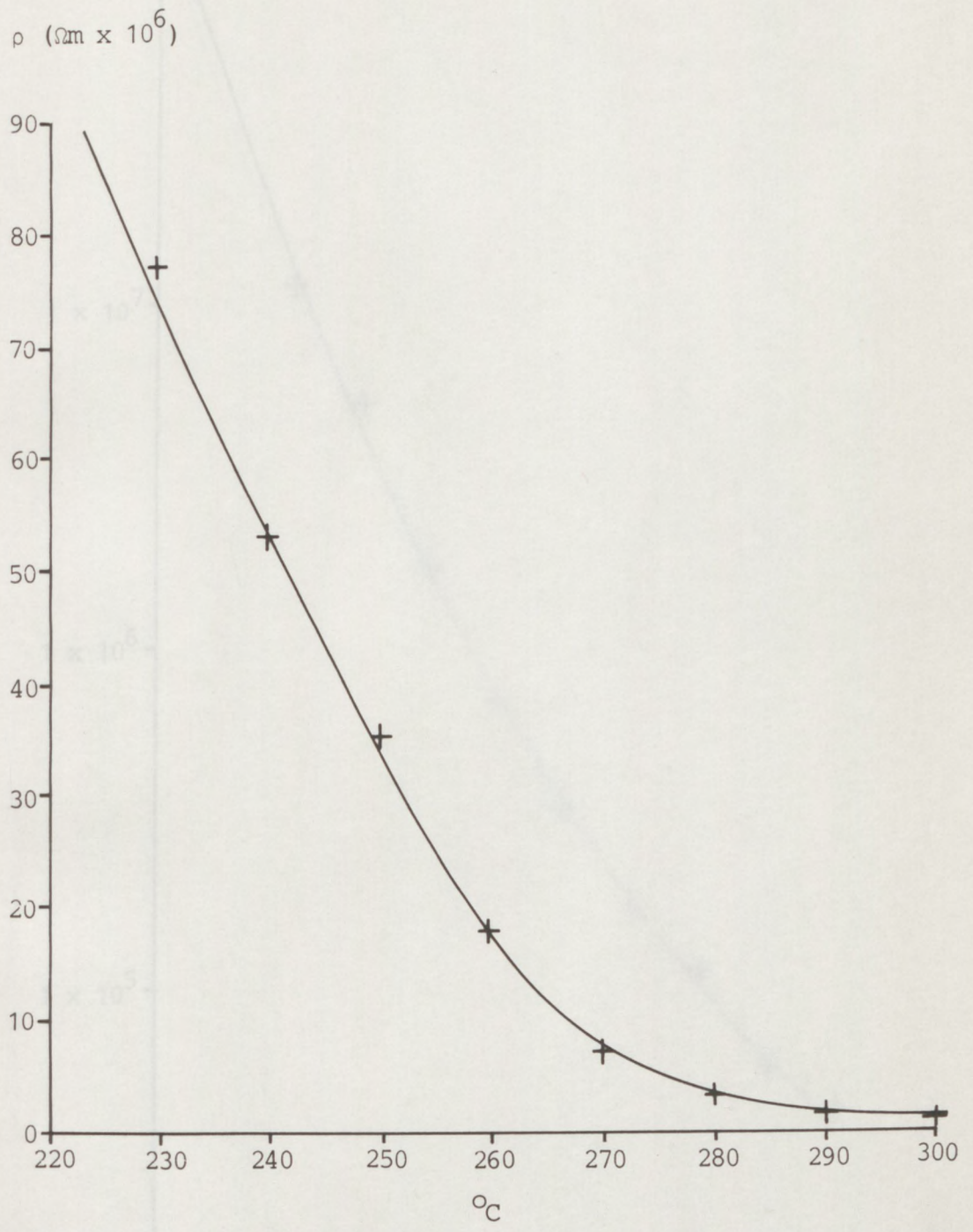


Figure 4-27 Resistivity against temperature for PZT (type PC5)

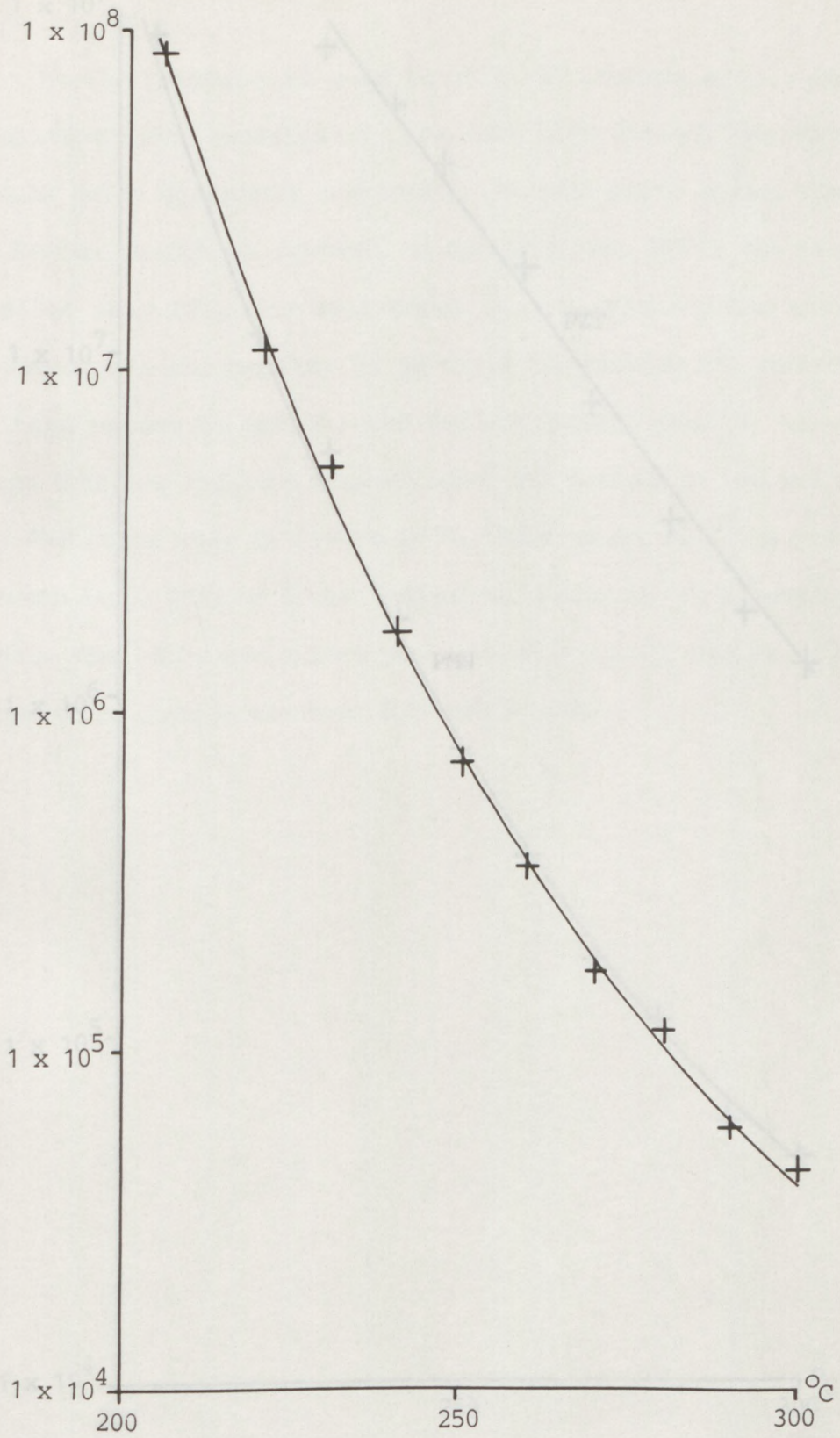
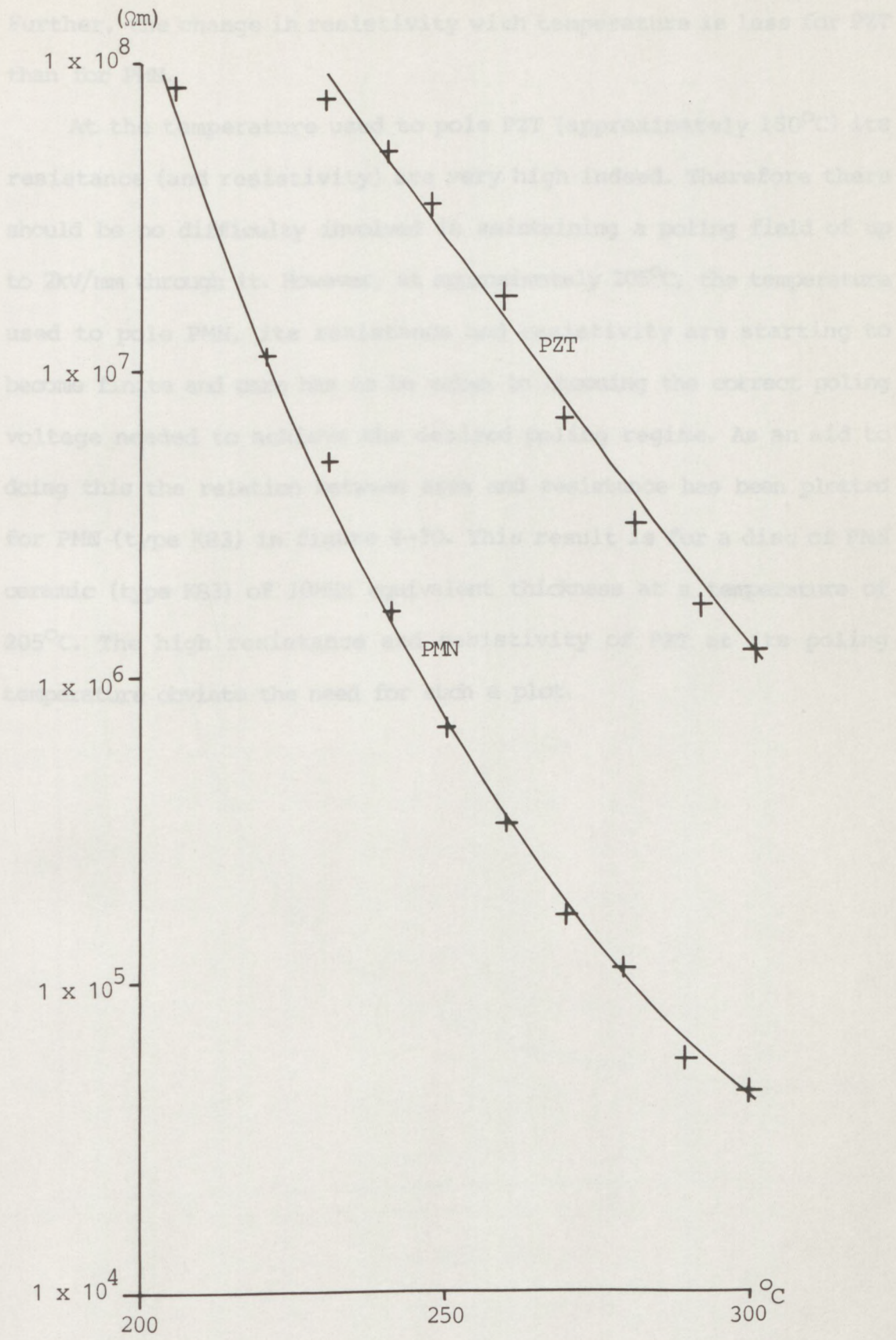


Figure 4-28 Resistivity against temperature for PMN (type K83)



**Figure 4-29** Resistivity against temperature for PZT (type PC5) and PMN (type K83)

Further, the change in resistivity with temperature is less for PZT than for PMN.

At the temperature used to pole PZT (approximately 150°C) its resistance (and resistivity) are very high indeed. Therefore there should be no difficulty involved in maintaining a poling field of up to 2kV/mm through it. However, at approximately 205°C, the temperature used to pole PMN, its resistance and resistivity are starting to become finite and care has to be taken in choosing the correct poling voltage needed to achieve the desired poling regime. As an aid to doing this the relation between area and resistance has been plotted for PMN (type K83) in figure 4-30. This result is for a disc of PMN ceramic (type K83) of 10MHz equivalent thickness at a temperature of 205°C. The high resistance and resistivity of PZT at its poling temperature obviate the need for such a plot.

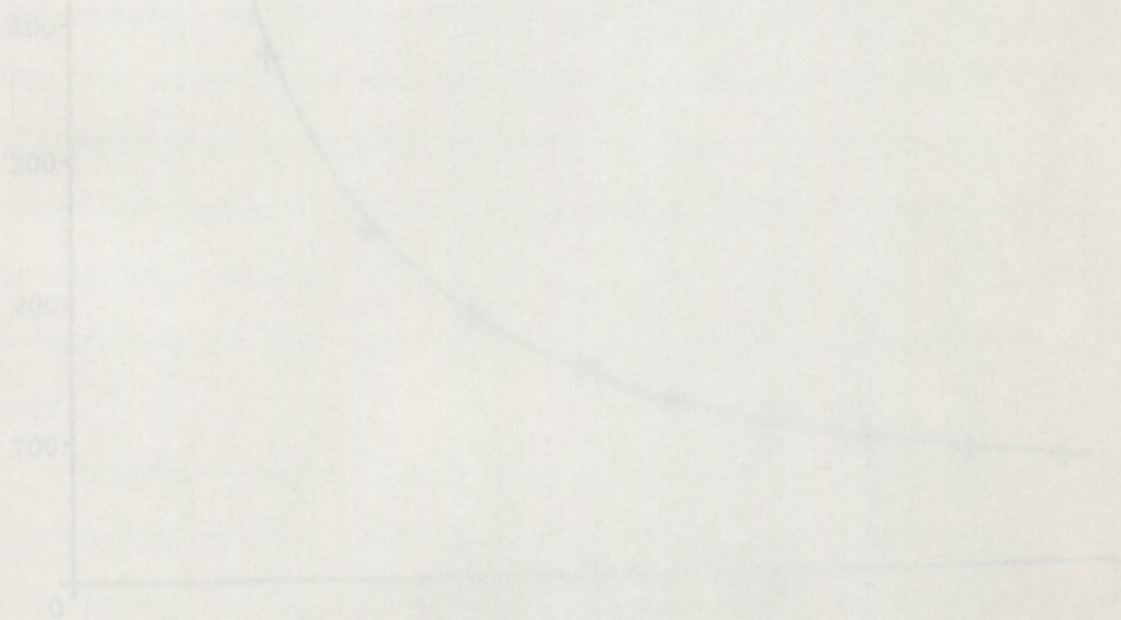
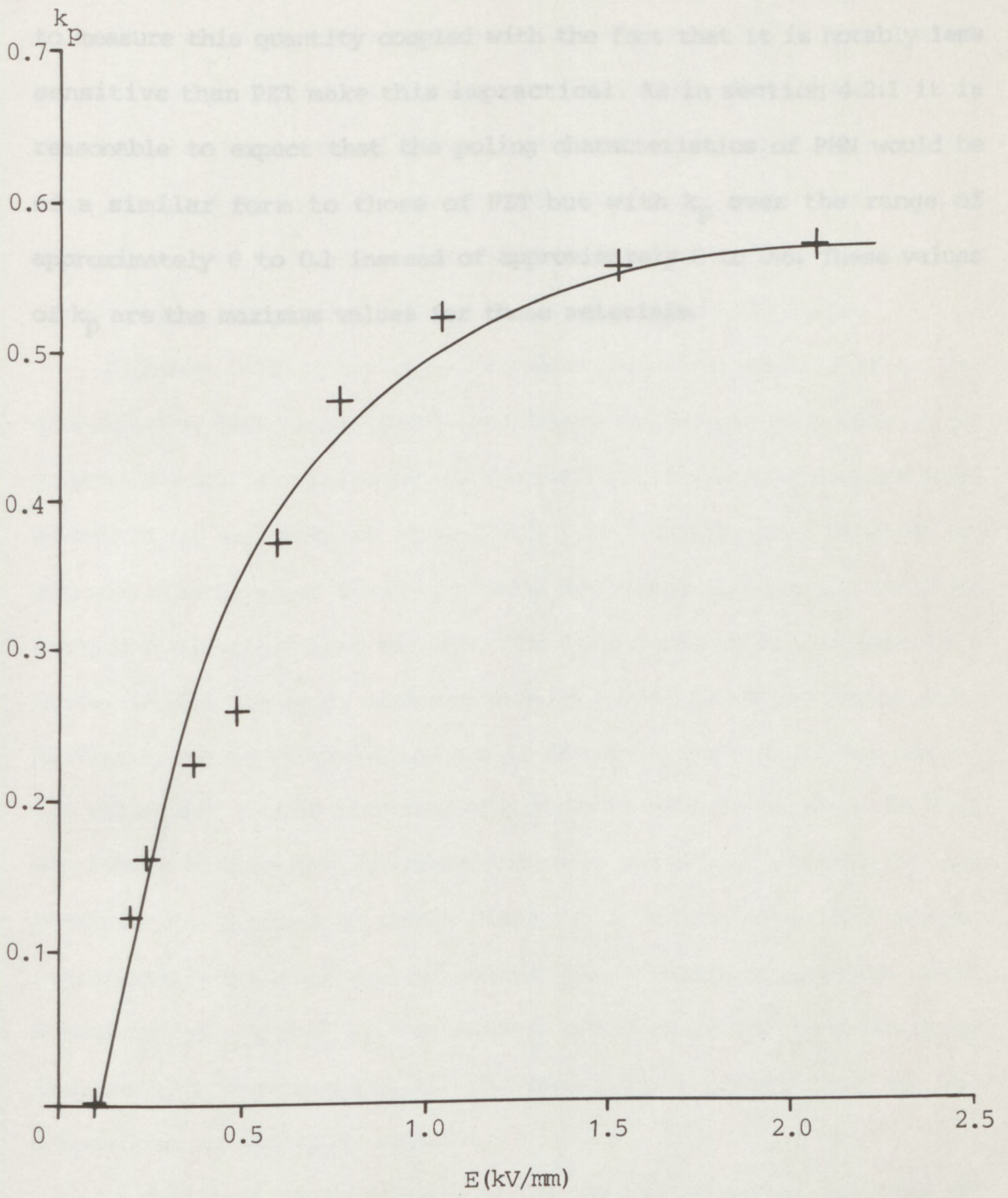


Figure 4-30 Resistance plotted area for PMN ceramic thickness 10MHz

#### 4.2.3 Poling and electromechanical coupling factor

The degree of poling achieved in a sample (up to a limit set by the material) is a function of the temperature, time and field. To a certain extent each factor may be traded off against the others to give a large combination of conditions that result in the same degree of poling. However, there are some practical limitations to the extent to which certain factors may be increased. For example if the field and/or temperature are too low the time required for poling may become indefinitely long. If the temperature is too high materials such as PMN tend to become conductive preventing the maintenance of a field across them. On the other hand PZT tends to lose some of its more volatile components and become a less effective piezoelectric material. If the temperature is too low during poling the high field required may cause dielectric breakdown of the material before poling has occurred. For these reasons it was decided to keep the temperature and time constant and vary the strength of the poling field to produce the poling regime required (see section 3.3). The graph in figure 4-31 shows the degree of poling as the planar electromechanical coupling factor ( $k_p$ ) against field for PZT. The conditions of constant temperature and time were 150°C and 20 minutes respectively (section 3.3).

Unfortunately no equivalent graph could be constructed for PMN due to difficulties in measuring  $k_p$ . As explained earlier (section 1.4) the  $d_{31}$  and  $d_{32}$  constants are opposite in sign and tend to cancel each other out. The effect is to give PMN very low radial coupling which accounts for some of its more desirable properties (section 1.4). However, this cross mode coupling which is also relied upon when measuring the planar electromechanical coupling factor (sections 1.2.2 and 3.1). The problem is compounded by the fact that the thin, disc shaped specimens are not suitable for the measurement of any other



**Figure 4-31** Planar electromechanical coupling factor ( $k_p$ ) against poling field for PZT (type PC5) under conditions of constant poling temperature and time (150°C and 20 minutes respectively)

coupling factors apart from the thickness coupling factor  $k_t$  (IEEE,1978). However, the high frequencies (in excess of 10MHz) needed to measure this quantity coupled with the fact that it is notably less sensitive than PZT make this impractical. As in section 4.2.1 it is reasonable to expect that the poling characteristics of PMN would be of a similar form to those of PZT but with  $k_p$  over the range of approximately 0 to 0.1 instead of approximately 0 to 0.6. These values of  $k_p$  are the maximum values for these materials.

Figure 4-22 shows how the pulse shape and spectra of a 15mm diameter by 5MHz equivalent thickness PZT (type PCS) transducer improves with the matching of the backing. These transducers were constructed as detailed in section 3.4. Briefly, the fabrication process consisted of casting a tungsten loaded epoxy resin onto the back of a piezoelectric element. The tungsten was in the form of a powder whilst the epoxy took the form of a mixture of two resins and a hardener. One of these resins set to the hardness of a rubber whilst the other set to the hardness of a plastic such as perspex. As they were both completely miscible and used the same hardener it was possible to produce a cured resin with a hardness that ranged continuously between that of either one of these components. Each transducer was backed with a similar quantity of the tungsten/epoxy mixture and the hardness of the backing was controlled by the composition of the epoxy resin.

In the first result (figure 4-22a) the transducer is under damped and shows some "ringing" or overshoot at its resonant frequency. This produces the pulse shape and causes a sharp peak in the spectrum. The backing of this transducer was made up of an epoxy mixture which consisted of 90% CY20 (the soft resin) and 10% araldite (the hard resin) by volume together with a suitable quantity of hardener (see section 3.4). The second result (figure 4-22b) shows much better damping and a

#### 4.2.4 The effect of backing characteristics on pulse shape and reproducibility

The results presented here show the effect of the characteristics of the backing on the pulse shape of a transducer. The reproducibility of the pulse shape has also been tested. The results in this section were obtained using uniformly-excited transducers in transmit-receive mode at a range of approximately 20mm from a large, plane reflector in water. The reflector was a large block of polished aluminium.

Figures 4-32 shows how the pulse shape and spectra of a 15mm diameter by 5MHz equivalent thickness PZT (type PC5) transducer improves with the matching of the backing. These transducers were constructed as detailed in section 3.4. Briefly, the fabrication process consisted of casting a tungsten loaded epoxy resin onto the back of a piezoelectric element. The tungsten was in the form of a powder whilst the epoxy took the form of a mixture of two resins and a hardener. One of these resins set to the hardness of a rubber whilst the other set to the hardness of a plastic such as perspex. As they were both completely miscible and used the same hardener it was possible to produce a cured resin with a hardness that ranged continuously between that of either one of these components. Each transducer was backed with a similar quantity of the tungsten/epoxy mixture and the hardness of the backing was controlled by the composition of the epoxy resin.

In the first result (figure 4-32a) the transducer is under damped and shows some "ringing" or resonance at its resonant frequency. This prolongs the pulse shape and causes a sharp peak in the spectrum. The backing of this transducer was made up of an epoxy mixture which consisted of 90% CY208 (the soft resin) and 10% MY750 (the hard resin) by volume together with a suitable quantity of hardener (see section 3.4). The second result figure 4-32b shows much better damping and a

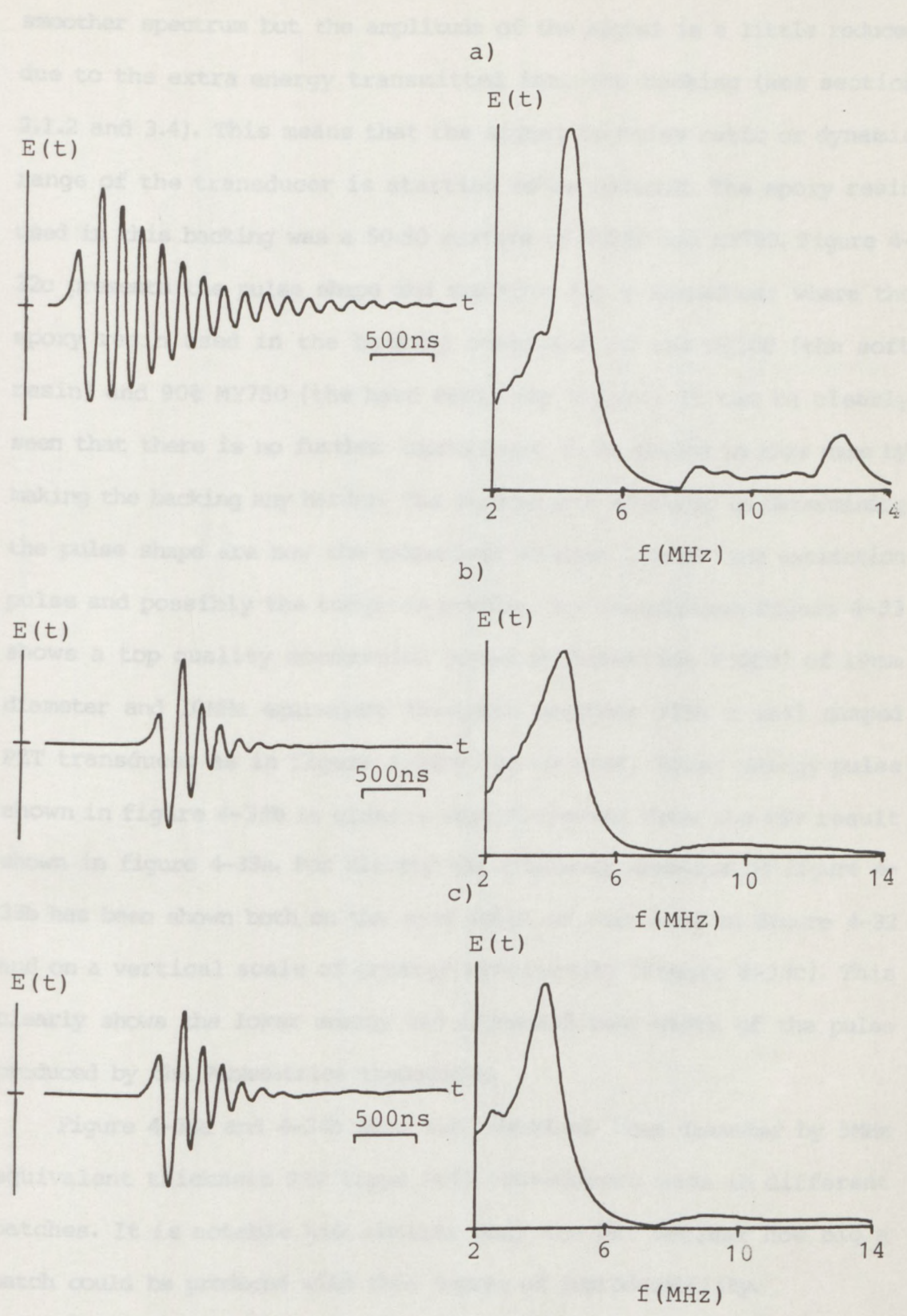


**Figure 4-32** Transmit-receive mode responses and spectra for PZT transducers (type PC5, 19mm diameter by 5MHz equivalent thickness) with various backings at a range of 20mm from a large, plane, aluminium-reflector in water showing the effect of backing characteristics on pulse shape for:-  
 a) a soft backing (90% CY208 resin and 10% MY750 by volume)  
 b) a medium hard backing (equal parts of resins CY208 and MY750 by volume)  
 c) a hard backing (10% CY208 resin and 90% MY750 by volume)

smoother spectrum but the amplitude of the signal is a little reduced due to the extra energy transmitted into the backing (see section 2.1.2 and 3.4). This means that the signal to noise ratio or dynamic range of the transducer is starting to be reduced. The epoxy resin used in this backing was a 50:50 mixture of CY208 and MY750. Figure 4-32c presents the pulse shape and spectrum for a transducer where the epoxy resin used in the backing consisted of 10% CY208 (the soft resin) and 90% MY750 (the hard resin) by volume. It can be clearly seen that there is no further improvement to be gained in this case by making the backing any harder. The predominant features in determining the pulse shape are now the transducer element itself, the excitation pulse and possibly the tungsten powder. For comparison figure 4-33 shows a top quality commercial probe (Panametrics V3289) of 19mm diameter and 10MHz equivalent thickness together with a well damped PZT transducer as in figure 4-32b. The shorter, lower energy pulse shown in figure 4-33b is clearly very different from the PZT result shown in figure 4-33a. For clarity the frequency spectrum of figure 4-33b has been shown both on the same scale as that used in figure 4-32 and on a vertical scale of greater sensitivity (figure 4-33c). This clearly shows the lower energy and increased band-width of the pulse produced by the Panametrics transducer.

Figure 4-34a and 4-34b show two identical 15mm diameter by 5MHz equivalent thickness PZT (type PC5) transducers made in different batches. It is notable how similar they are but unclear how big a batch could be produced with this degree of reproducibility.

Similar results were also obtained for PMN. The transducer elements in this case were 19mm in diameter by 10MHz equivalent thickness and were made of PMN type K83. In figure 4-35 the pulse shapes from three transducers are shown, each transducer was constructed in a similar manner and from similar materials with the

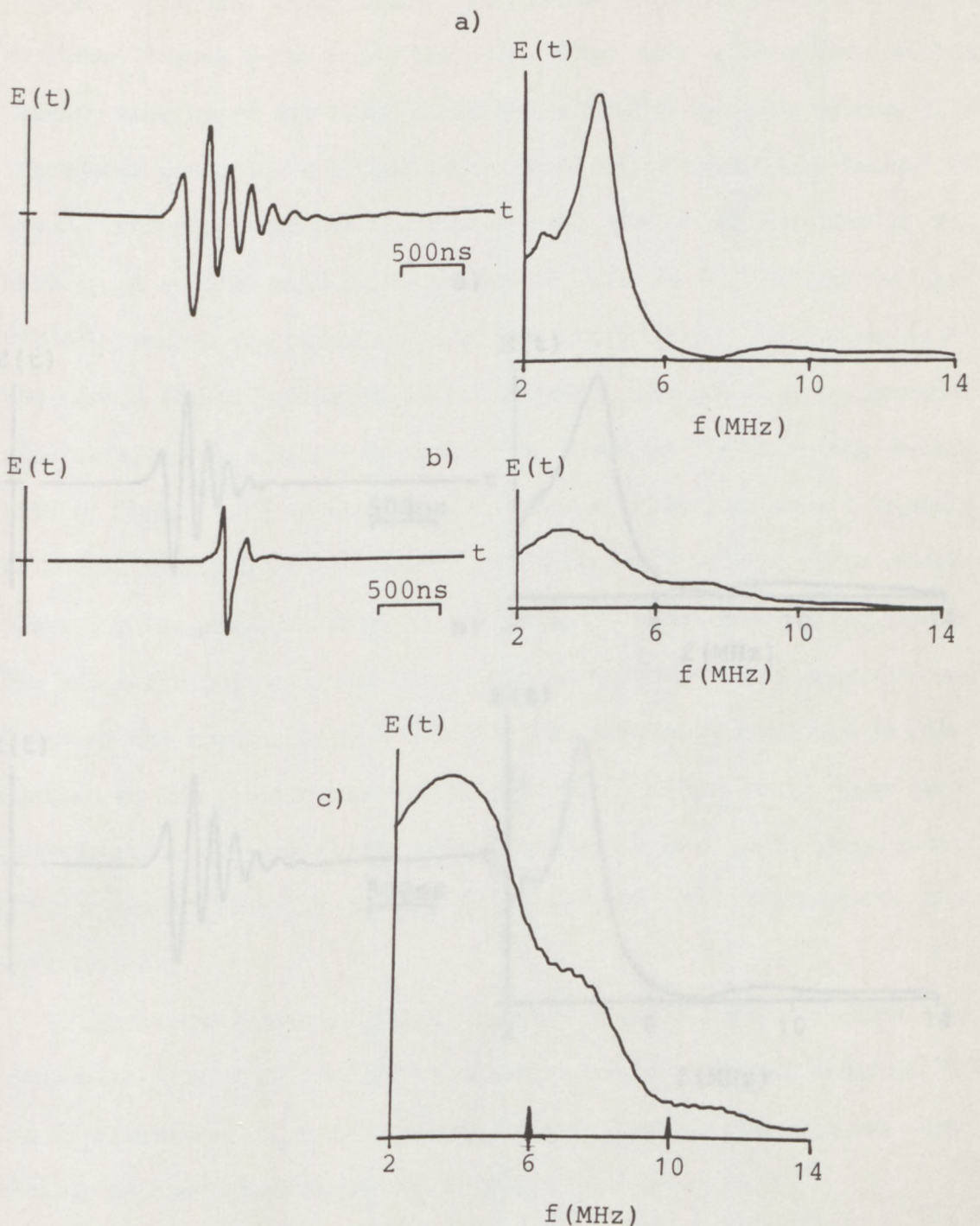


**Figure 4-33** Transmit-receive mode responses and spectra for transducers (19mm diameter by 5MHz equivalent thickness) at a range of 20mm from a large, plane, aluminium-reflector in water showing the pulse shape for:-

- a) a PZT transducer with a medium hard backing (equal parts of resins CY208 and MY750 by volume)
- b) a high quality commercial transducer made of PMN
- c) is the pressure spectrum of b) shown at greater magnification to emphasise the shape of the frequency response

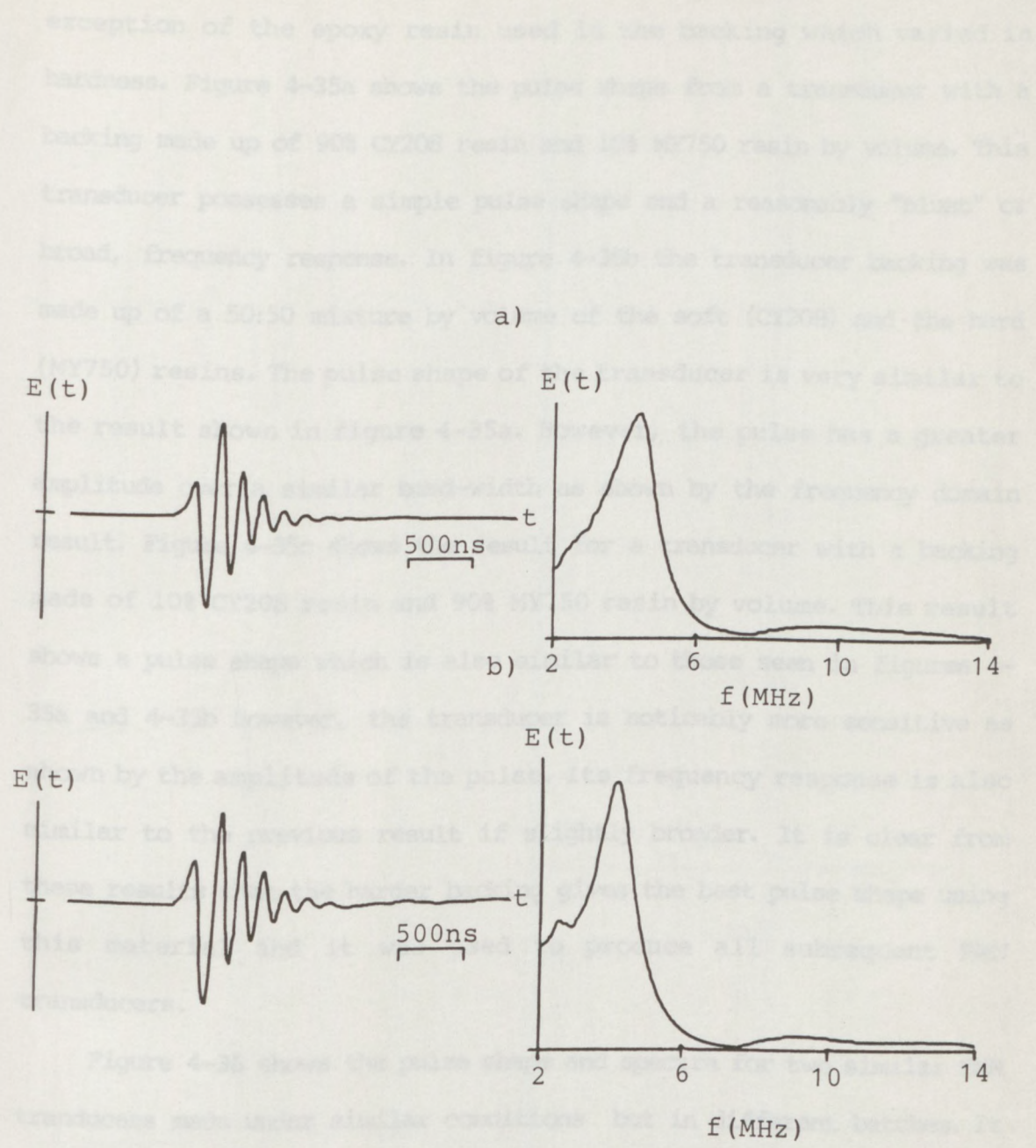


**Figure 4-34** Transmit-receive mode responses and spectra for two PZT transducers (type PC5 19mm diameter by 5MHz equivalent thickness) made by identical methods but in different batches at a range of 20mm from a large, plane aluminium-reflector in water demonstrating reproducibility of pulse shape for:-  
 a) the transducer from batch 1 (with a medium hard backing)  
 b) the transducer from batch 2 (with a medium hard backing)

exception of the epoxy resin used in the backing which varied in hardness. Figure 4-35a shows the pulse shape from a transducer with a backing made up of 90% CY208 resin and 10% MY750 resin by volume. This transducer possesses a simple pulse shape and a reasonably "blunt" or broad, frequency response. In figure 4-35b the transducer backing was made up of a 50:50 mixture by volume of the soft (CY208) and the hard (MY750) resins. The pulse shape of the transducer is very similar to the result shown in figure 4-35a. However, the pulse has a greater amplitude over a similar band-width as shown by the frequency domain result. Figure 4-35c shows the result for a transducer with a backing made of 10% CY208 resin and 90% MY750 resin by volume. This result shows a pulse shape which is also similar to those seen in figures 4-35a and 4-35b however, the transducer is noticeably more sensitive as shown by the amplitude of the pulse. Its frequency response is also similar to the previous result if slightly broader. It is clear from these results that the harder backing gives the best pulse shape using this material and it was used to produce all subsequent PMN transducers.

Figure 4-36 shows the pulse shape and spectra for two similar PMN transducers made under similar conditions but in different batches. It can be clearly seen, as in the case of PZT, that the results are very similar in both pulse shape and frequency content.

For comparison the results in figure 4-35 are repeated in figure 4-36a to 4-36c whilst the pulse shape and spectrum of a top quality commercial transducer (Panametrics V3289) made of the PMN of the same dimensions and type are shown in figure 4-37d. The commercial transducer has a similar pulse shape and band-width but greater sensitivity. This is largely due to the carefully designed and constructed matching layer which is attached to the front face. The transducers constructed during the course of this project were not

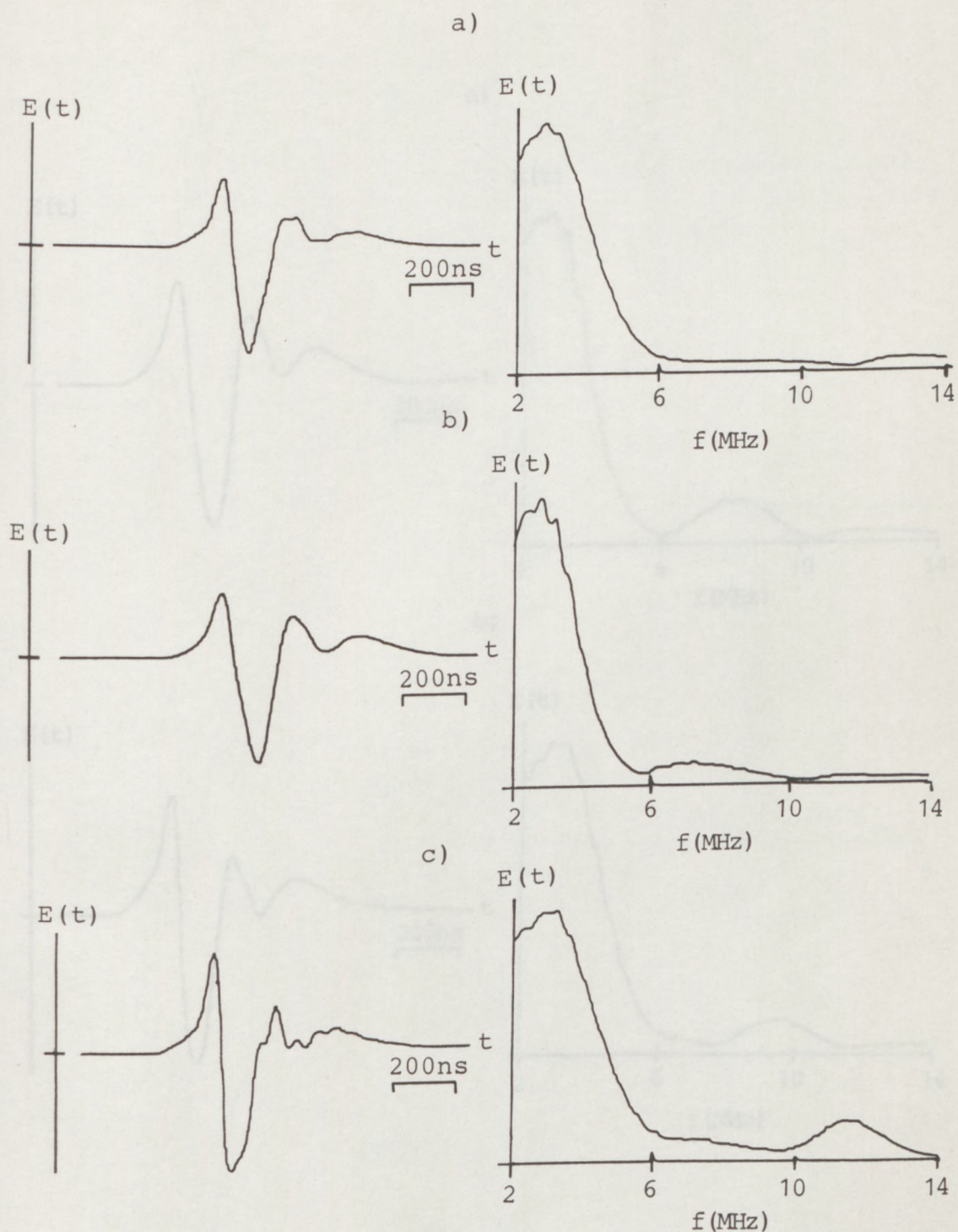


**Figure 4-35** Transmit-receive mode responses and spectra for PMN transducers (type K83, 19mm diameter by 10MHz equivalent thickness) with various backings at a range of 20mm from a large, plane, aluminium-reflector in water showing the effect of backing characteristics on pulse shape for:-

- a) a soft backing (90% CY208 resin and 10% MY750 by volume)
- b) a medium hard backing (equal parts of resins CY208 and MY750 by volume)
- c) a hard backing (10% CY208 resin and 90% MY750 by volume)

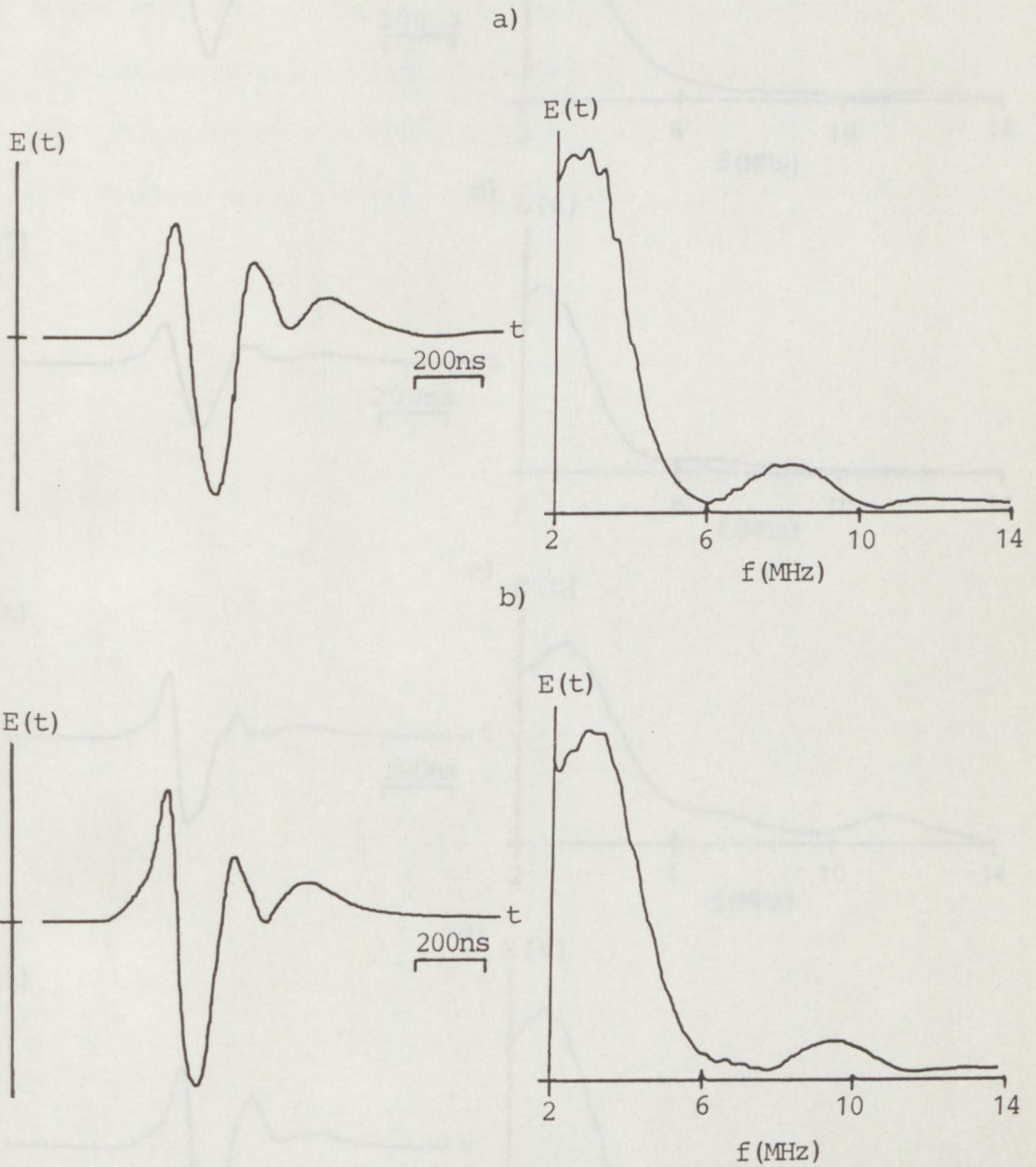


**Figure 4-36** Transmit-receive mode responses and spectra for two PMN transducers (type K83 19mm diameter by 10MHz equivalent thickness) made by identical methods but in different batches at a range of 20mm from a large, plane aluminium-reflector in water demonstrating reproducibility of pulse shape for:-  
a) the transducer from batch 1 (with a medium hard backing)  
b) the transducer from batch 2 (with a medium hard backing)

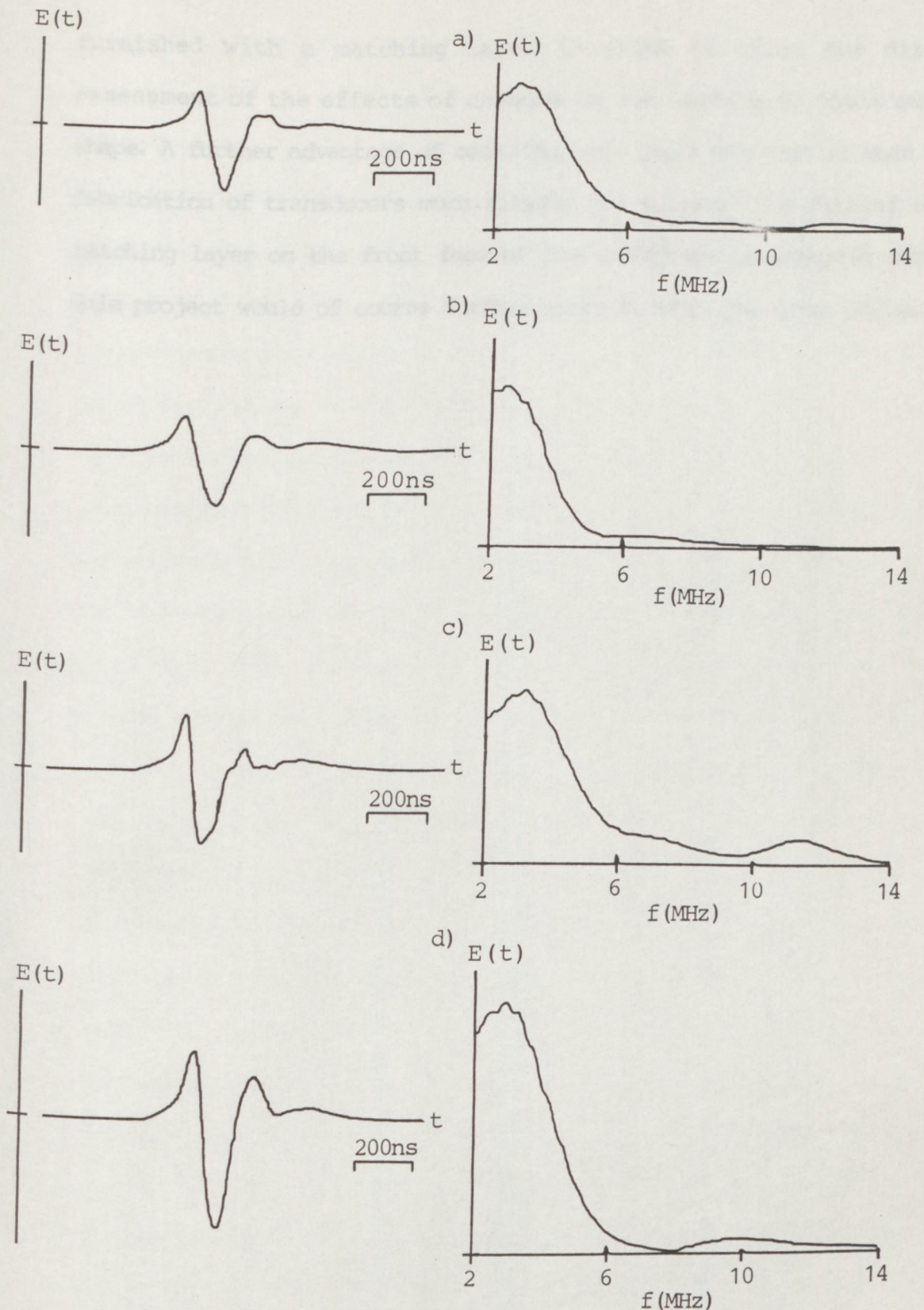


**Figure 4-37** Transmit-receive mode responses and spectra for PMN transducers (type K83, 19mm diameter by 10MHz equivalent thickness) with various backings at a range of 20mm from a large, plane, aluminium-reflector in water showing the effect of backing characteristics on pulse shape for:-

- a) a soft backing (90% CY208 resin and 10% MY750 by volume)
- b) a medium hard backing (equal parts of resins CY208 and MY750 by volume)
- c) a hard backing (10% CY208 resin and 90% MY750 by volume)
- d) a high quality commercial transducer made of PMN

furnished with a matching layer in order to allow the direct assessment of the effects of changes in the backing on their pulse shape. A further advantage of omitting this layer was that it made the fabrication of transducers much simpler and quicker. The fitting of a matching layer on the front face of the transducer constructed during this project would of course further improve their characteristics.

#### 4.2.5 Calibration of a miniature probe

In order to assess the excitation of non-uniformly excited transducers a miniature receiving probe (constructed within the ultrasonics research group at The City University - Weight, 1982b) was specially calibrated. The object was to link the amplitude of the output voltage  $A(P)$  (which is proportional to pressure) to the electromechanical coupling factor ( $k_p$ ) of an element and the poling field applied to it. To do this it was necessary to go through a careful calibration procedure. This involved taking transducer elements that had been poled to various degrees (as measured by  $k_p$ ) and mounting them onto similar backings in similar cases to produce a set of transducers that were as similar as possible in all respects apart from their sensitivity. This set of transducers were then excited by similar excitation pulses whilst a small probe was scanned laterally across their diameters. The probe passed about 1mm from the front face of each transducer and the experiment resulted in a set of beam plots in the form of a "top hat" with various plateau heights. The advantage of plotting these beam profiles as opposed to simply making point pressure measurements in the field of these transducers was that it immediately demonstrated how uniform the excitation was over the face of each transducer. These were recorded on a chart recorder (section 3.5). By keeping all the settings on the apparatus the same for each scan the height of the plateau could be linked to the electromechanical coupling factor (sections 1.2.2 and 3.1) of the element and therefore to the poling field (sections 1.5 and 3.3)

The results are for 0.5mm diameter PZT probe and 15mm diameter by 5MHz equivalent thickness PZT transducers. In figure 4-38  $A(P)$  is plotted against  $K_p$  and it can be clearly seen that there is an almost linear relationship between the degree of poling and the sensitivity of the transducer. Figure 4-39 shows the more fundamental relationship

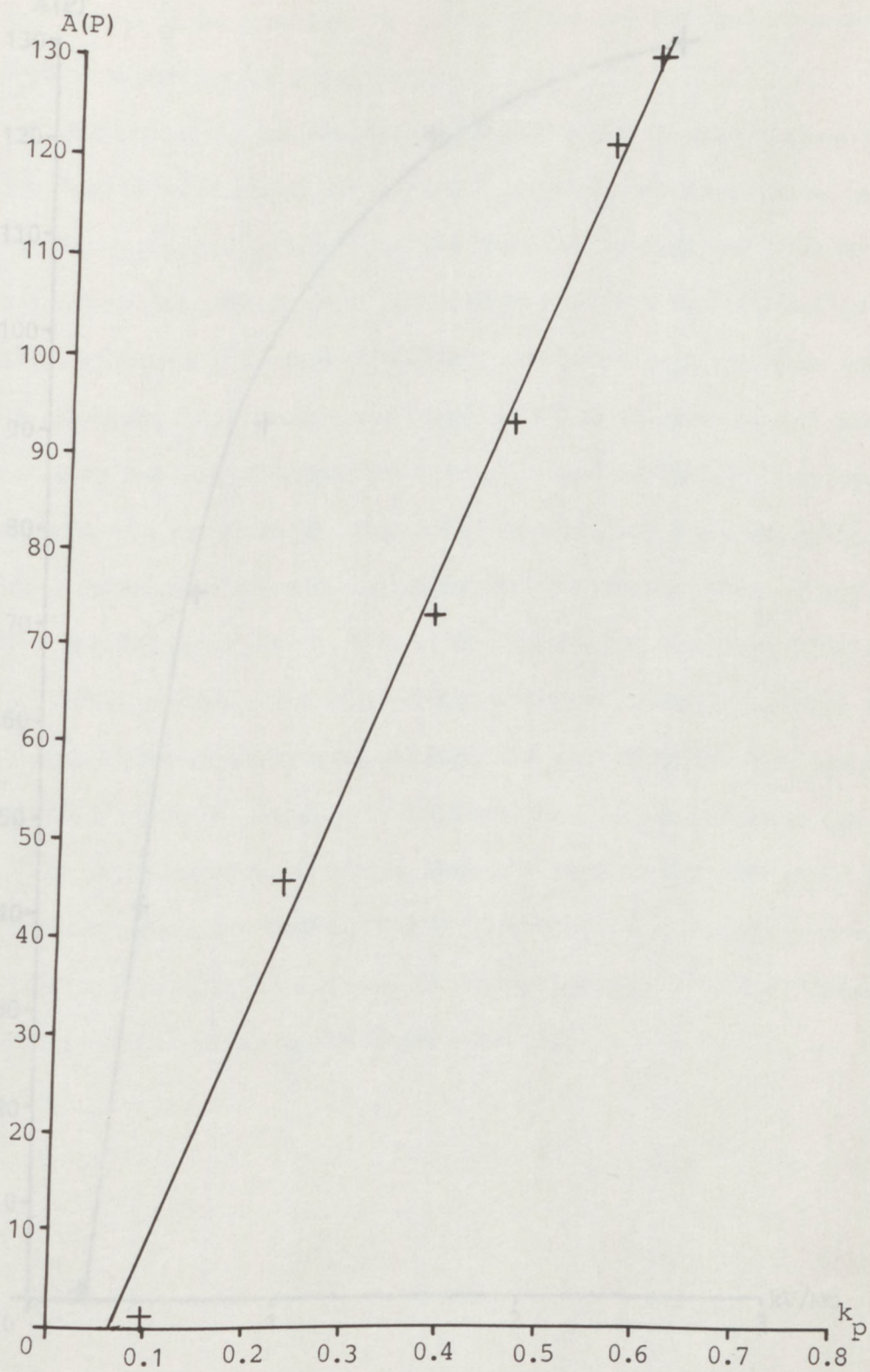


**Figure 4-38** Acoustic pressure as measured by a miniature receiving probe in water against electromechanical coupling factor for PZT

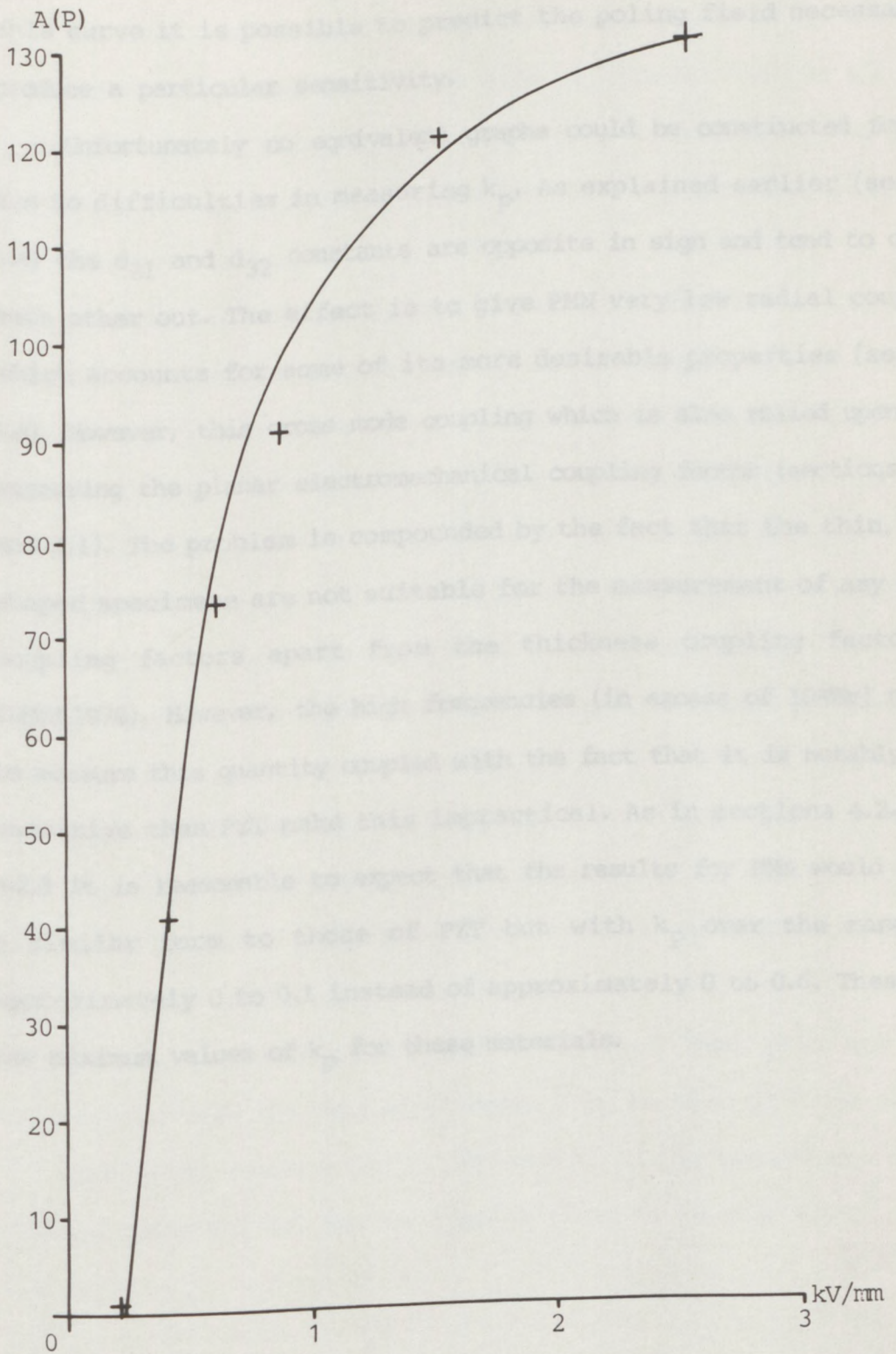


**Figure 4-39** Acoustic pressure as measured by a miniature receiving probe in water against poling field for PZT (type PC5) under conditions of constant poling temperature and time (150°C and 20 minutes respectively)

between the poling field and the sensitivity of the transducer. From this curve it is possible to predict the poling field necessary to produce a particular sensitivity.

Unfortunately no equivalent graphs could be constructed for PMN due to difficulties in measuring  $k_p$ . As explained earlier (section 1.4) the  $d_{31}$  and  $d_{32}$  constants are opposite in sign and tend to cancel each other out. The effect is to give PMN very low radial coupling which accounts for some of its more desirable properties (section 1.4). However, this cross mode coupling which is also relied upon when measuring the planar electromechanical coupling factor (sections 1.2.2 and 3.1). The problem is compounded by the fact that the thin, disc shaped specimens are not suitable for the measurement of any other coupling factors apart from the thickness coupling factor  $k_t$  (IEEE,1978). However, the high frequencies (in excess of 10MHz) needed to measure this quantity coupled with the fact that it is notably less sensitive than PZT make this impractical. As in sections 4.2.1 and 4.2.3 it is reasonable to expect that the results for PMN would be of a similar form to those of PZT but with  $k_p$  over the range of approximately 0 to 0.1 instead of approximately 0 to 0.6. These are the maximum values of  $k_p$  for these materials.

### 4.3 Field Measurements in Water

Pressure and transmit-receive mode measurements in the fields of non-uniformly excited transducers made of both PZT and PMN are given here. For comparison similar measurements from a conventional, uniformly-excited transducer in the form of a top quality, commercial, PMN transducer are also given.

A miniature receiving probe, constructed within the ultrasonics research group at The City University London (Weight, 1982b), was used to make the pressure waveform measurements. The fields of these transducers were investigated by using the miniature receiving probe to make measurements at various ranges both on and off axis. These measurements were pressure waveforms at points in the fields of the transducers. The pressure spectra of these waveforms are also given. These results are compared with the calculated results in section 4.1.1.

Transmit-receive mode responses and spectra were measured using a small, point-like target at various ranges both on and off axis in the fields of these transducers. The results given are compared with the calculated results in section 4.1.2.

Finally, pressure and transmit-receive mode beam plots are given and compared with the calculated results in section 4.1.3 and 4.1.4.

From these results the poling regimes of the transducers can be assessed using the calibration results given in section 4.2.5.

#### 4.3.1 Pressure waveform measurements

The results in this section show measured pressure waveforms for both non-uniformly excited and conventional, uniformly-excited transducers at various ranges both on and off axis. The ranges are the same as those in section 4.1 i.e. 20mm, 60mm, 100mm and 140mm. These ranges were chosen to show the near and far field features of the transducers. Some intermediate ranges are also shown.

These measurements were made in water using the miniature receiving probe. Figure 4-40 shows axial pressure waveforms and spectra for a uniformly-excited, PMN transducer of 19mm diameter by 10MHz equivalent thickness. In the near field, at an axial range of 20mm (figure 4-40a), the edge-waves from the source all arrive simultaneously to produce a pulse that is time resolved from the plane-wave. The plane-wave arrives on axis before the edge-wave as its path length is shorter. According to theory the plane- and edge-wave pulses should be of equal amplitude and opposing phase as shown in the calculated results (figure 4-3a section 4.1.1). In the measured results the plane- and edge-wave pulses are clearly of opposite phase, however, the amplitude of the edge-wave pulse is slightly greater than that of the plane-wave pulse. This is due to interference between the head-waves and the edge-waves leading to the "focusing effect" described in section 2.4. The pressure spectrum at an axial range of 20mm also shows modulation due to the time separated plane- and edge-wave components similar to the calculated result (figure 4-3b section 4.1.1). At the greater axial ranges shown in figures 4-40b and 4-40c the time separation of the plane- and edge-wave pulses gradually diminishes until as shown in figure 4-40d, at an axial range of 140mm they overlap to form a single pulse. This represents the beginning of the far field of the transducer and the single pulse formed here has a simple, single-peak pressure spectrum as shown in figure 4-40d. The

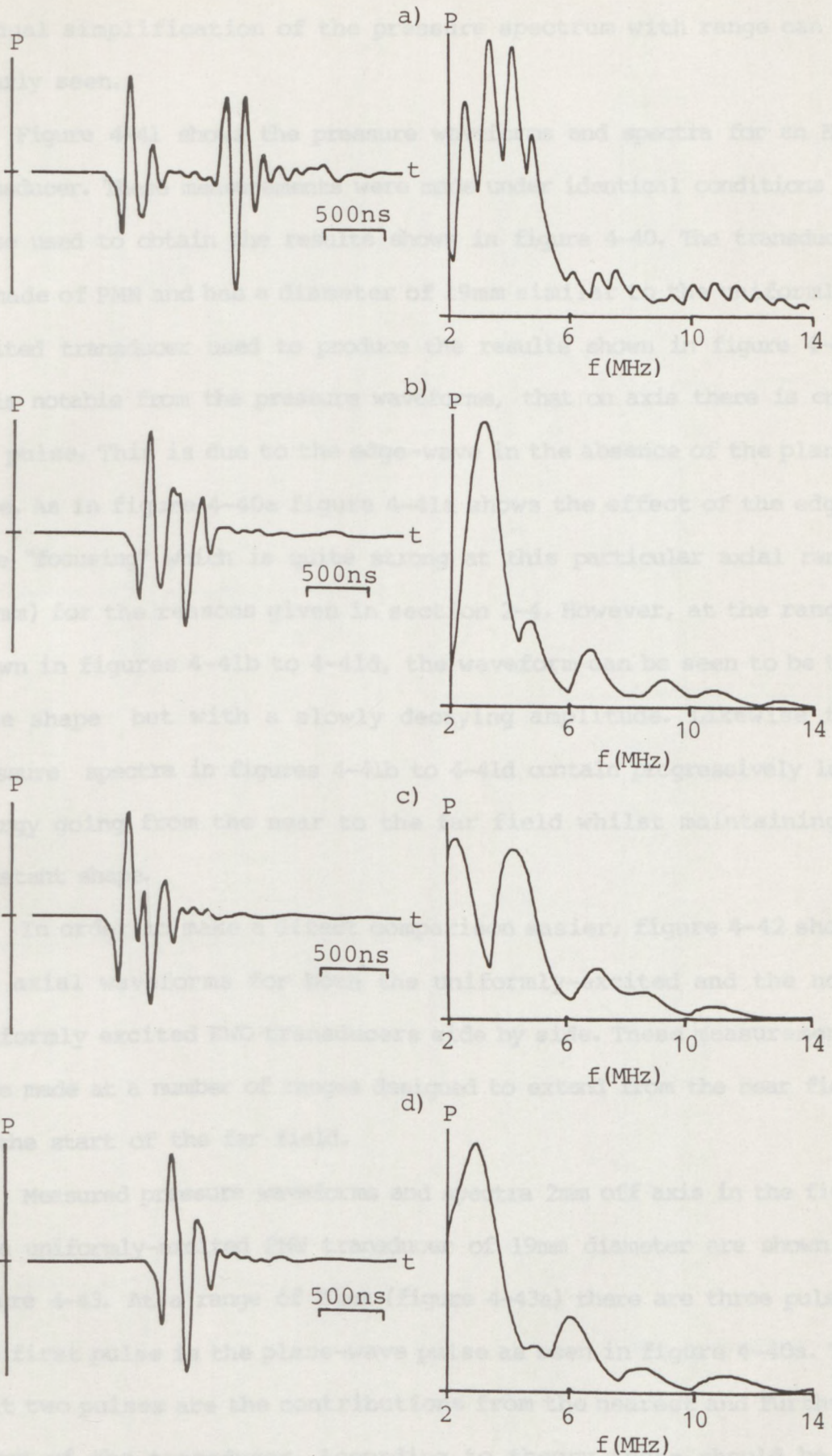


**Figure 4-40** Pressure waveforms and spectra measured on the axis of a conventional, uniformly-excited, circular transducer 19mm diameter by 10MHz equivalent thickness (Panametrics V3289) with a miniature (point-like) receiver in water at ranges of:-  
a) 20mm b) 60mm c) 100mm d) 140mm

gradual simplification of the pressure spectrum with range can be clearly seen.

Figure 4-41 shows the pressure waveforms and spectra for an EWO transducer. These measurements were made under identical conditions to those used to obtain the results shown in figure 4-40. The transducer is made of PMN and has a diameter of 19mm similar to the uniformly-excited transducer used to produce the results shown in figure 4-40. It is notable from the pressure waveforms, that on axis there is only one pulse. This is due to the edge-wave in the absence of the plane-wave. As in figure 4-40a figure 4-41a shows the effect of the edge-wave "focusing" which is quite strong at this particular axial range (20mm) for the reasons given in section 2-4. However, at the ranges shown in figures 4-41b to 4-41d, the waveform can be seen to be the same shape but with a slowly decaying amplitude. Likewise the pressure spectra in figures 4-41b to 4-41d contain progressively less energy going from the near to the far field whilst maintaining a constant shape.

In order to make a direct comparison easier, figure 4-42 shows the axial waveforms for both the uniformly-excited and the non-uniformly excited EWO transducers side by side. These measurements were made at a number of ranges designed to extend from the near field to the start of the far field.

Measured pressure waveforms and spectra 2mm off axis in the field of a uniformly-excited PMN transducer of 19mm diameter are shown in figure 4-43. At a range of 20mm (figure 4-43a) there are three pulses. The first pulse is the plane-wave pulse as seen in figure 4-40a. The next two pulses are the contributions from the nearest and furthest edges of the transducer. According to theory these should be of opposing phase. However, due to the "edge-wave focusing" described earlier the phase has been altered. At the greater ranges shown in

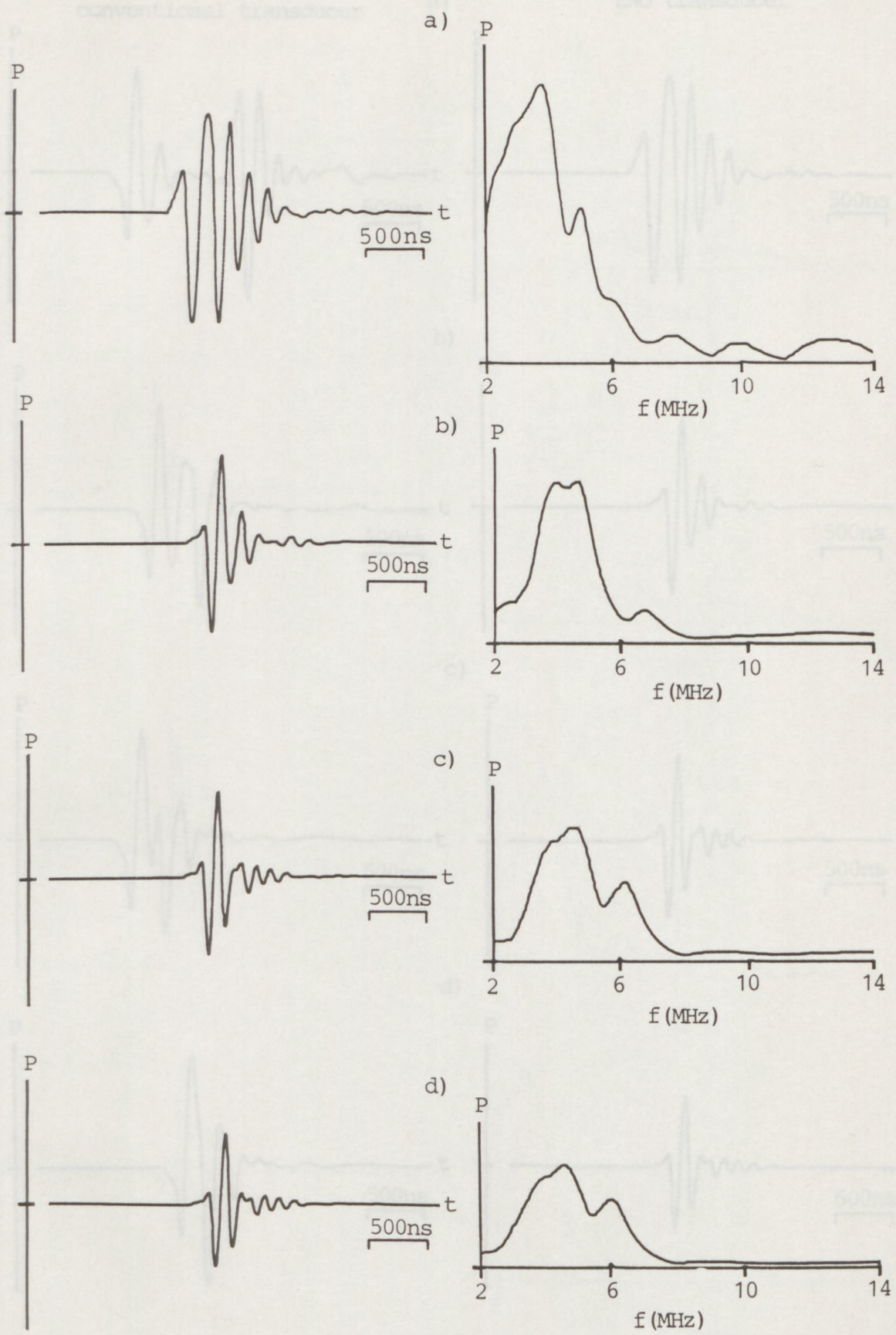


**Figure 4-41** Pressure waveforms and spectra measured on the axis of an EWO transducer 19mm diameter by 10MHz equivalent thickness) with a miniature (point-like) receiver in water at ranges of:-  
 a) 20mm b) 60mm c) 100mm d) 140mm

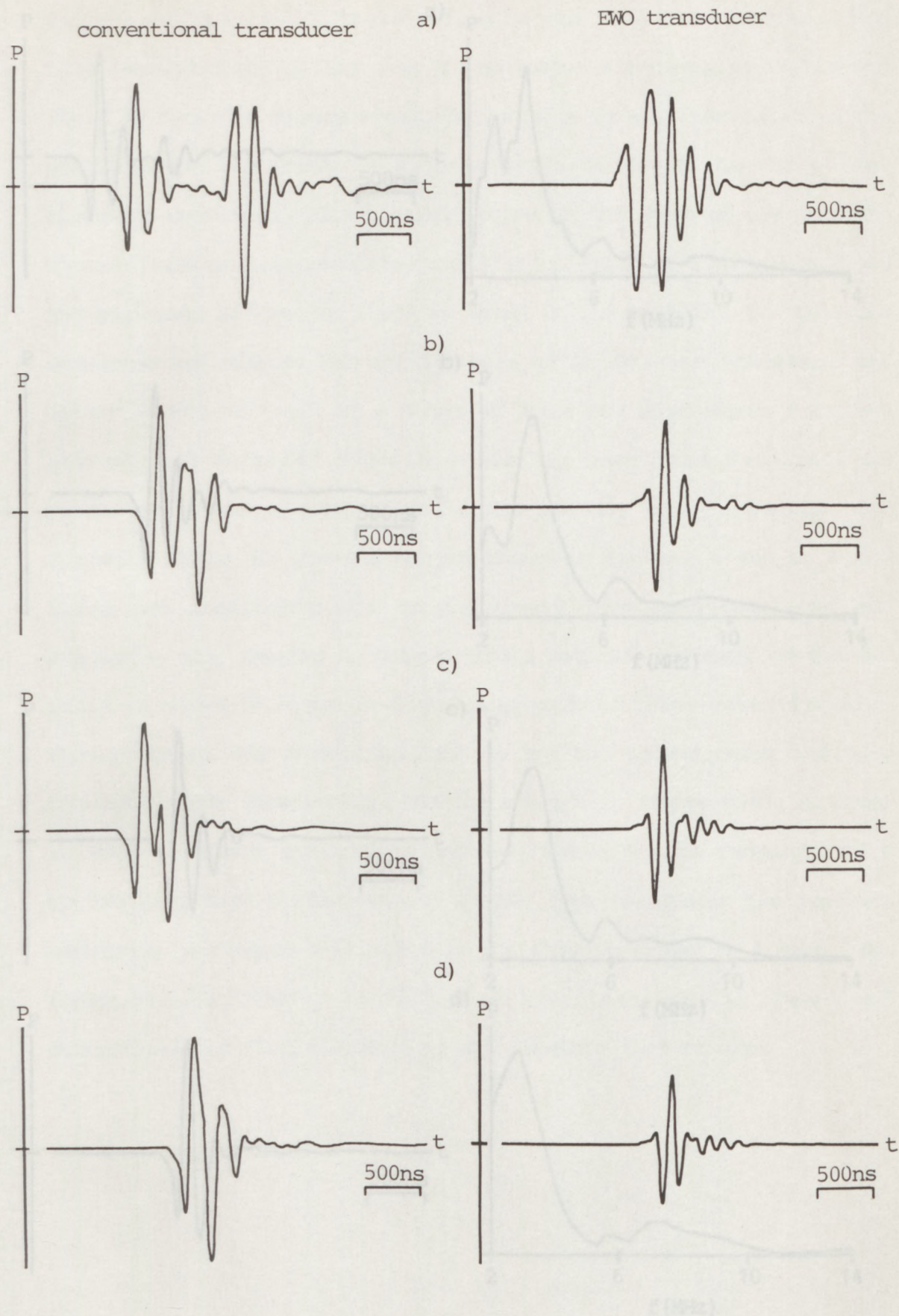


**Figure 4-42** Axial Pressure waveforms for a conventional, uniformly-excited, circular transducer and an EWO transducer (both 19mm diameter by 10MHz equivalent thickness) made with a miniature (point-like) receiver in water at ranges of:-  
a) 20mm b) 60mm c) 100mm d) 140mm

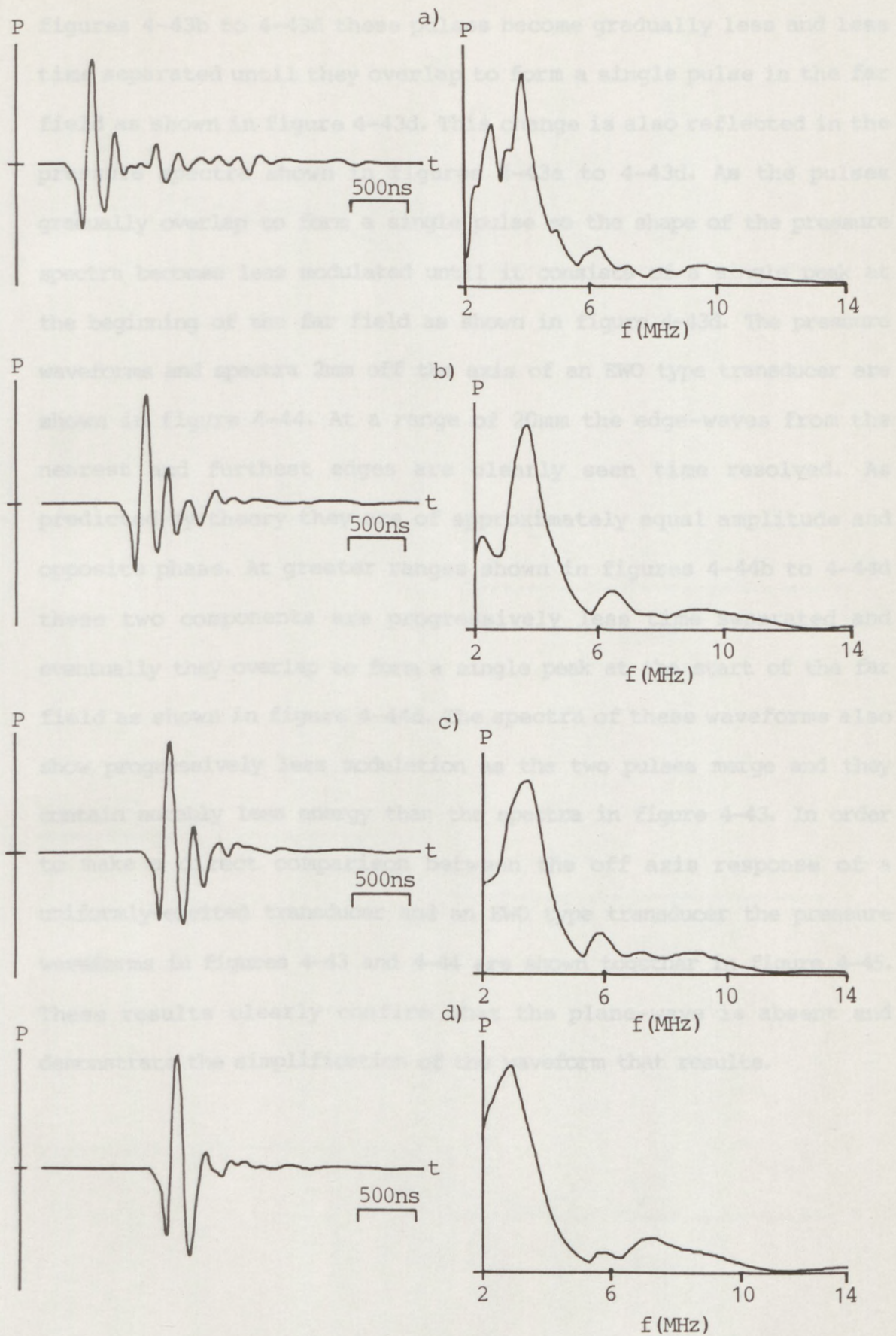


**Figure 4-43** Pressure waveforms and spectra measured 2mm off the axis of a conventional, uniformly-excited, circular transducer, 19mm diameter by 10MHz equivalent thickness (Panametrics V3289) with a miniature (point-like) receiver in water at ranges of:-  
a) 20mm b) 60mm c) 100mm d) 140mm

figures 4-43b to 4-43d these pulses become gradually less and less time separated until they overlap to form a single pulse in the far field as shown in figure 4-43d. This change is also reflected in the pressure spectra shown in figures 4-43a to 4-43d. As the pulses gradually overlap to form a single pulse so the shape of the pressure spectra becomes less modulated until it consists of a single peak at the beginning of the far field as shown in figure 4-43d. The pressure waveforms and spectra 2mm off the axis of an EWO type transducer are shown in figure 4-44. At a range of 20mm the edge-waves from the nearest and furthest edges are clearly seen time resolved. As predicted by theory they are of approximately equal amplitude and opposite phase. At greater ranges shown in figures 4-44b to 4-44d these two components are progressively less time separated and eventually they overlap to form a single peak at the start of the far field as shown in figure 4-44d. The spectra of these waveforms also show progressively less modulation as the two pulses merge and they contain notably less energy than the spectra in figure 4-43. In order to make a direct comparison between the off axis response of a uniformly-excited transducer and an EWO type transducer the pressure waveforms in figures 4-43 and 4-44 are shown together in figure 4-45. These results clearly confirm that the plane-wave is absent and demonstrate the simplification of the waveform that results.

Figure 4-44 Pressure waveforms and spectra measured 2mm off the axis of an EWO transducer. The distance from the equivalent distance with a miniature (point-like) receiver is shown at ranges of: a) 20mm b) 40mm c) 60mm d) 80mm

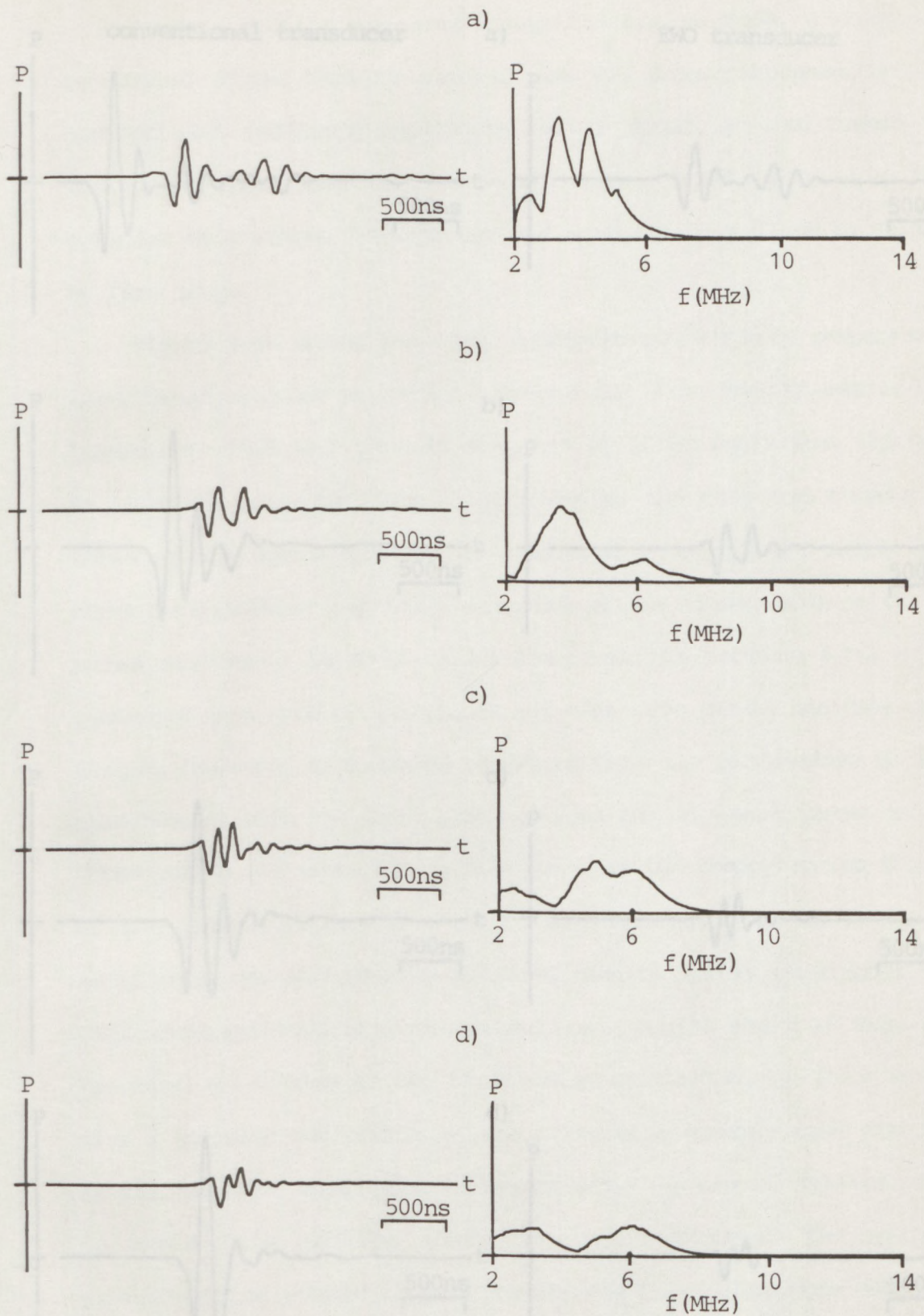
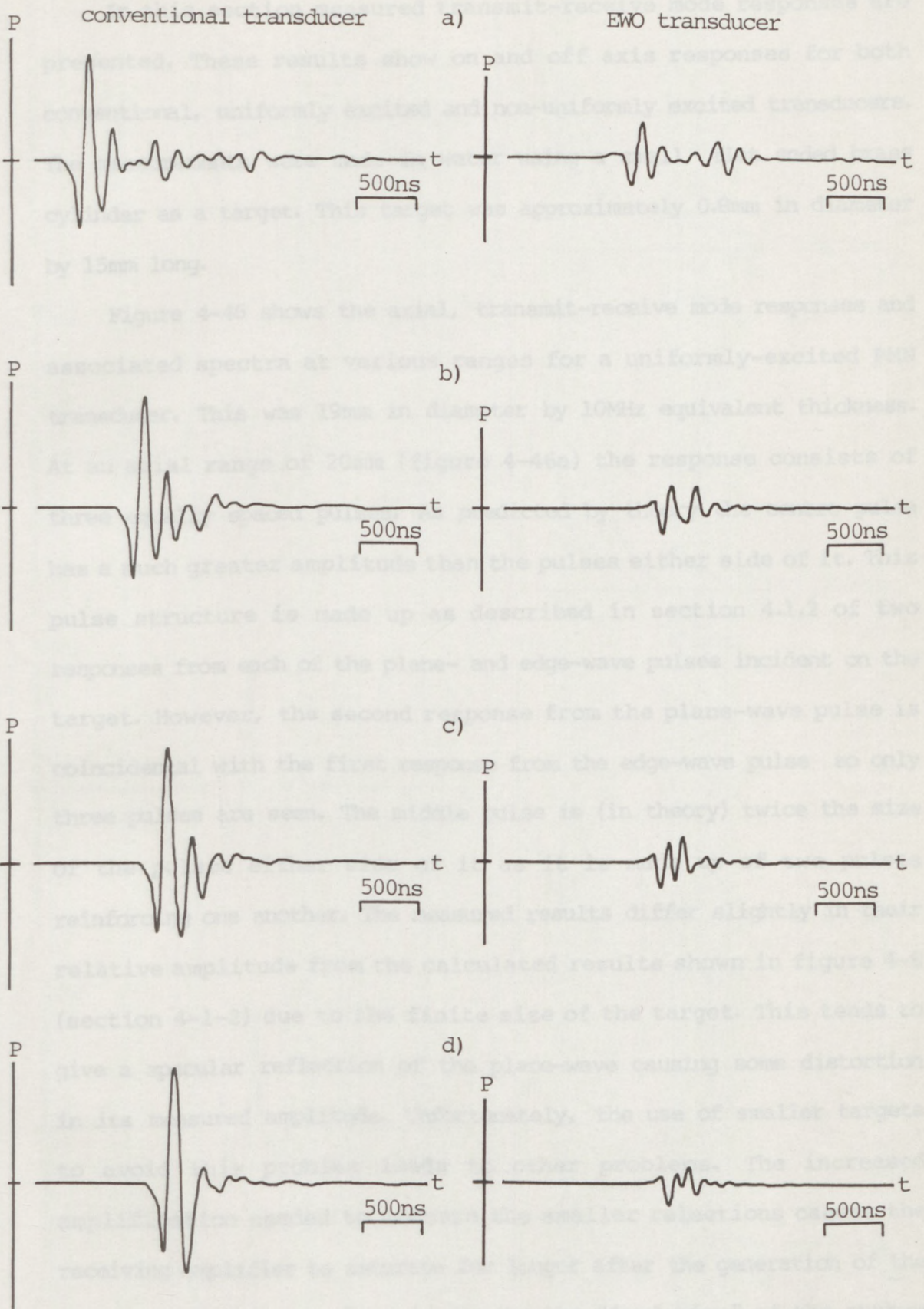


Figure 4-44 Pressure waveforms and spectra measured 2mm off the axis of an EWO transducer, 19mm diameter by 10MHz equivalent thickness with a miniature (point-like) receiver in water at ranges of:-  
 a) 20mm b) 60mm c) 100mm d) 140mm



**Figure 4-45** Pressure waveforms 2mm off axis for a conventional, uniformly-excited, circular transducer and an EWO transducer (both 19mm diameter by 10MHz equivalent thickness) made with a miniature (point-like) receiver in water at ranges of:-  
 a) 20mm b) 60mm c) 100mm d) 140mm

#### 4.3.2 Transmit-receive mode measurements

In this section measured transmit-receive mode responses are presented. These results show on and off axis responses for both conventional, uniformly excited and non-uniformly excited transducers. The measurements were made in water using a small, flat ended brass cylinder as a target. This target was approximately 0.8mm in diameter by 15mm long.

Figure 4-46 shows the axial, transmit-receive mode responses and associated spectra at various ranges for a uniformly-excited PMN transducer. This was 19mm in diameter by 10MHz equivalent thickness. At an axial range of 20mm (figure 4-46a) the response consists of three equally spaced pulses. As predicted by theory the centre pulse has a much greater amplitude than the pulses either side of it. This pulse structure is made up as described in section 4.1.2 of two responses from each of the plane- and edge-wave pulses incident on the target. However, the second response from the plane-wave pulse is coincidental with the first response from the edge-wave pulse so only three pulses are seen. The middle pulse is (in theory) twice the size of the pulses either side of it as it is made up of two pulses reinforcing one another. The measured results differ slightly in their relative amplitude from the calculated results shown in figure 4-8 (section 4-1-2) due to the finite size of the target. This tends to give a specular reflection of the plane-wave causing some distortion in its measured amplitude. Unfortunately, the use of smaller targets to avoid this problem leads to other problems. The increased amplification needed to measure the smaller reflections causes the receiving amplifier to saturate for longer after the generation of the interrogating pulse. This increases the "dead time" of the system during which no measurements can be made and prevents measurements from being made at the short ranges where the responses of the

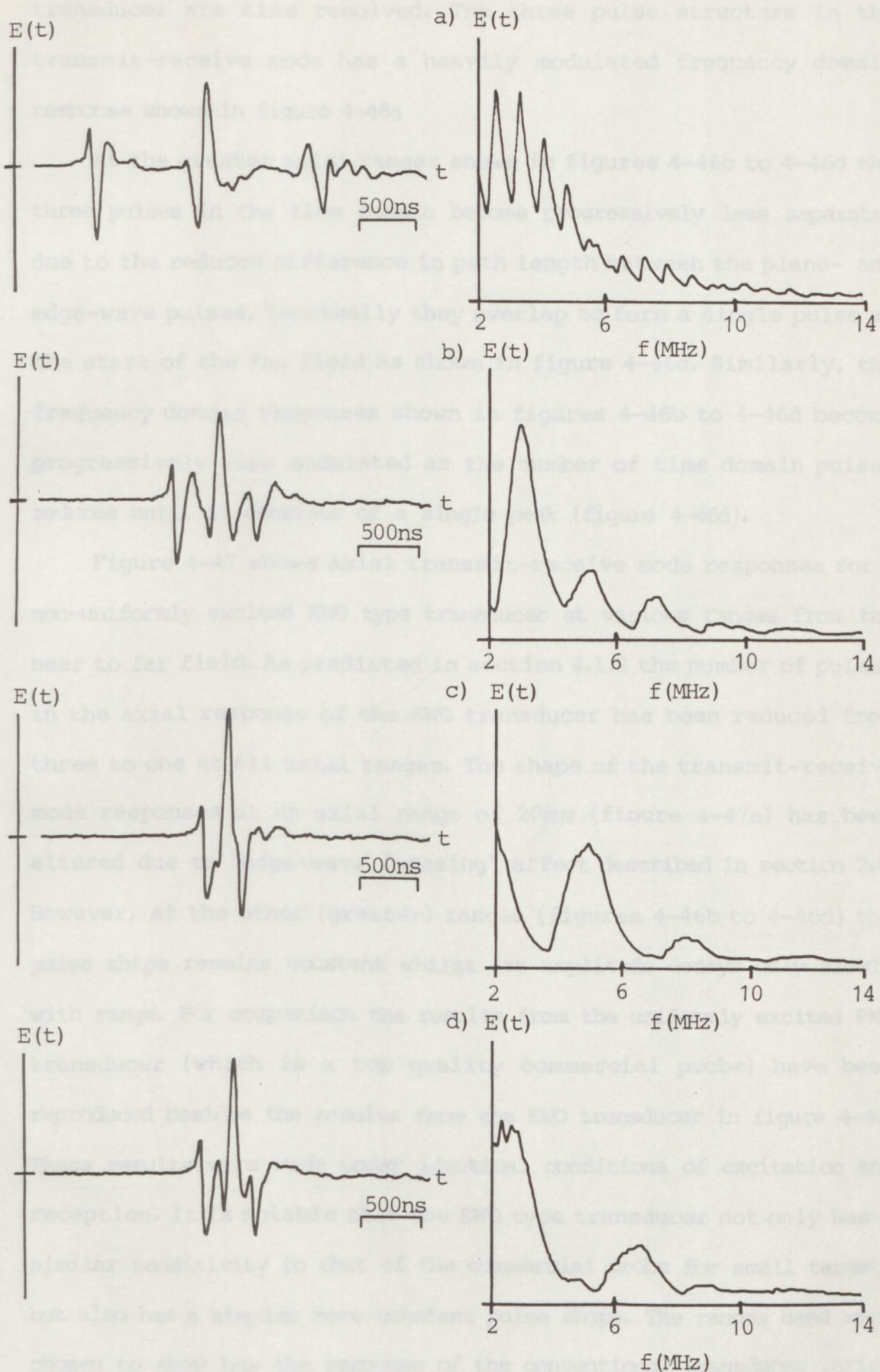


**Figure 4-46** Transmit-receive mode responses and spectra for a conventional, uniformly-excited, circular transducer (19mm diameter by 10MHz equivalent thickness) interrogating a small brass target approximately 0.8mm in diameter in water at axial ranges of:-  
a) 20mm b) 60mm c) 100mm d) 140mm

transducer are time resolved. The three pulse structure in the transmit-receive mode has a heavily modulated frequency domain response shown in figure 4-46a

At the greater axial ranges shown in figures 4-46b to 4-46d the three pulses in the time domain become progressively less separated due to the reduced difference in path length between the plane- and edge-wave pulses. Eventually they overlap to form a single pulse at the start of the far field as shown in figure 4-46d. Similarly, the frequency domain responses shown in figures 4-46b to 4-46d become progressively less modulated as the number of time domain pulses reduces until it consists of a single peak (figure 4-46d).

Figure 4-47 shows axial transmit-receive mode responses for a non-uniformly excited EWO type transducer at various ranges from the near to far field. As predicted in section 4.1.2 the number of pulses in the axial response of the EWO transducer has been reduced from three to one at all axial ranges. The shape of the transmit-receive mode responses at an axial range of 20mm (figure 4-47a) has been altered due to "edge-wave focusing" effect described in section 2.4. However, at the other (greater) ranges (figures 4-46b to 4-46d) the pulse shape remains constant whilst its amplitude decays only slowly with range. For comparison the results from the uniformly excited PMN transducer (which is a top quality commercial probe) have been reproduced besides the results from the EWO transducer in figure 4-48. These results were made under identical conditions of excitation and reception. It is notable that the EWO type transducer not only has a similar sensitivity to that of the commercial probe for small targets but also has a simpler more constant pulse shape. The ranges used were chosen to show how the response of the conventional transducer varies from the near field to the far field; intermediate positions are also shown.

a) 20mm b) 50mm c) 100mm d) 140mm

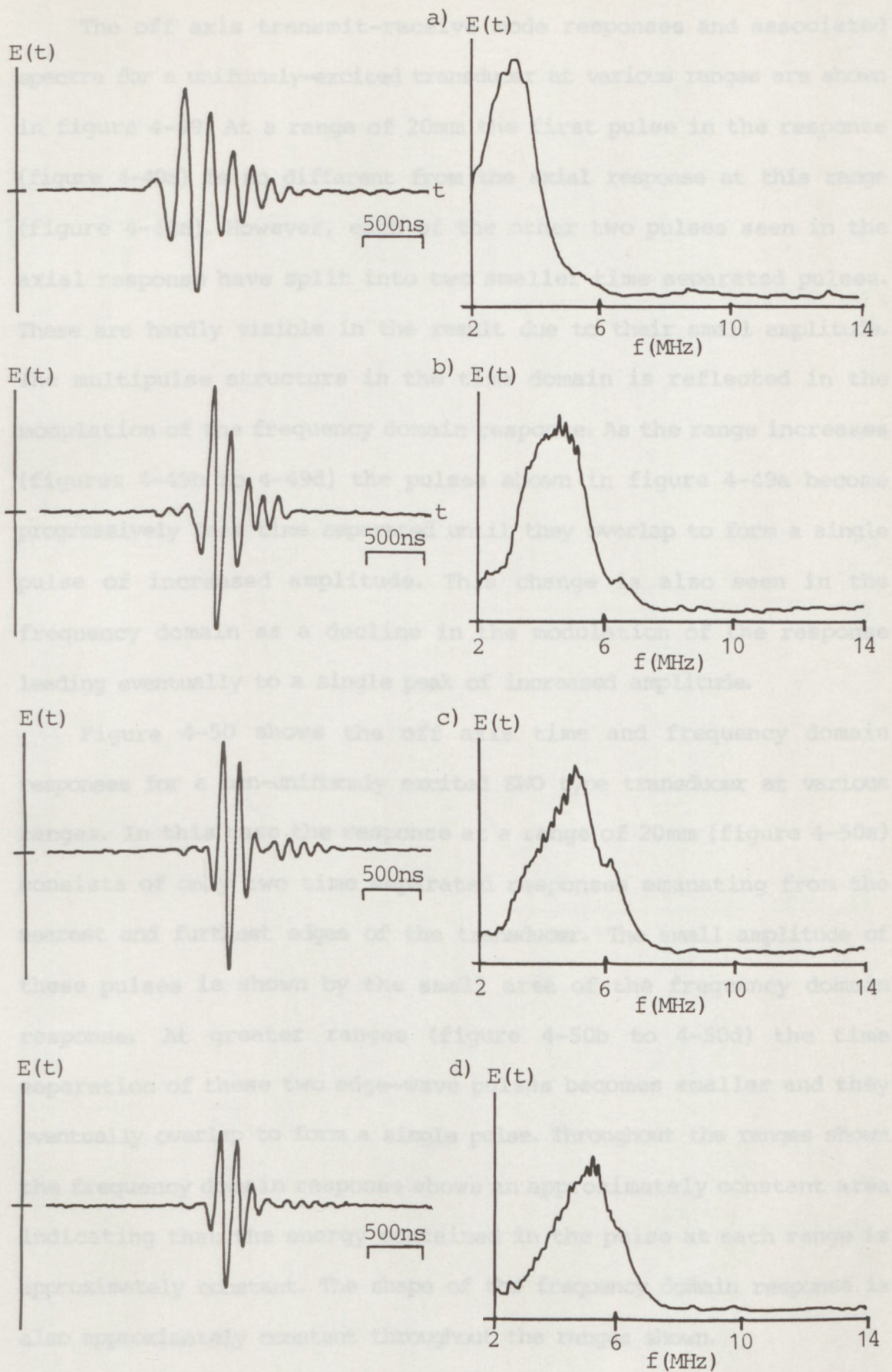
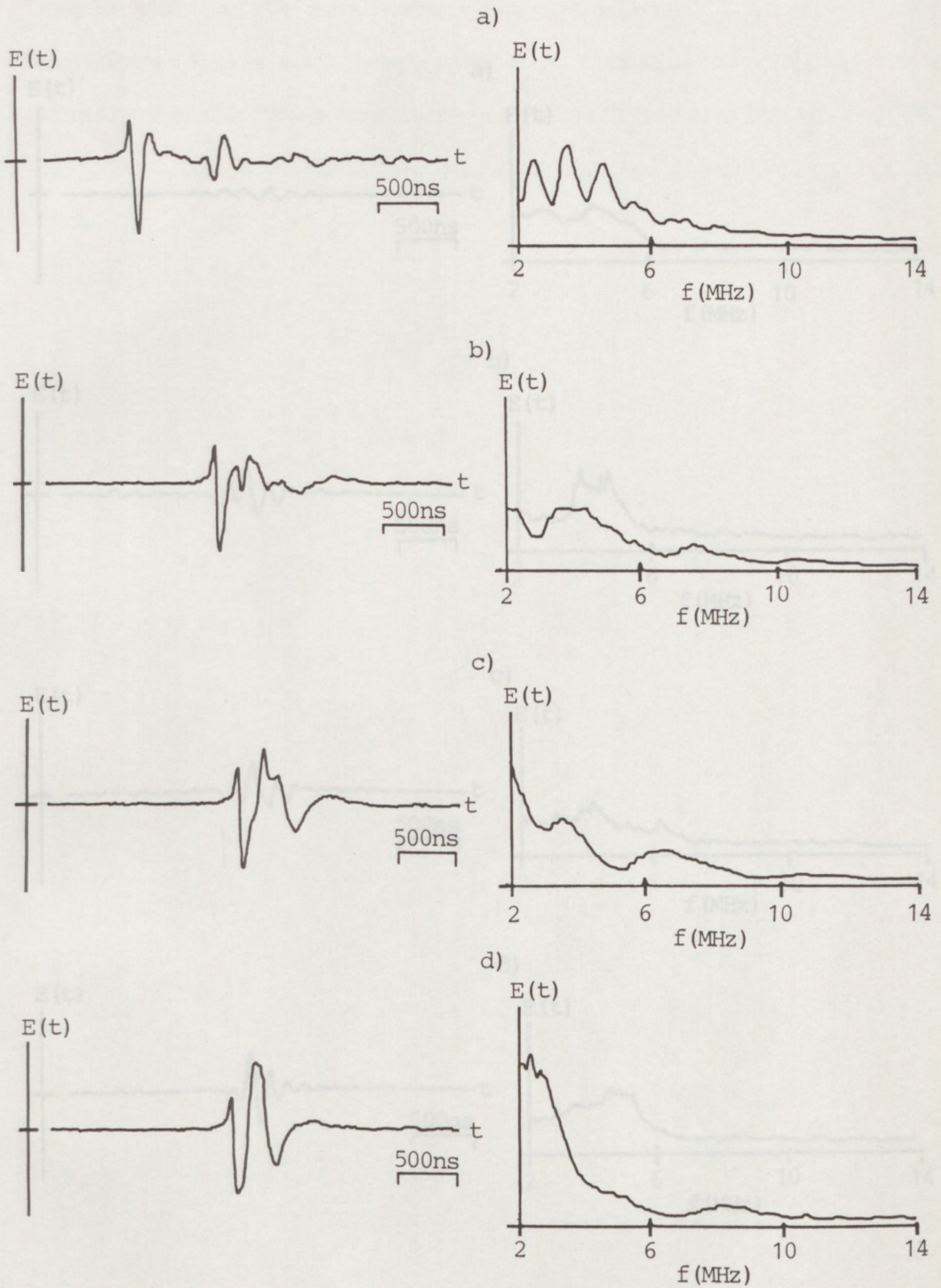


**Figure 4-47** Transmit-receive mode responses and spectra for an EWO transducer (19mm diameter by 10MHz equivalent thickness) interrogating a small brass target approximately 0.8mm in diameter in water at axial ranges of:-  
 a) 20mm b) 60mm c) 100mm d) 140mm

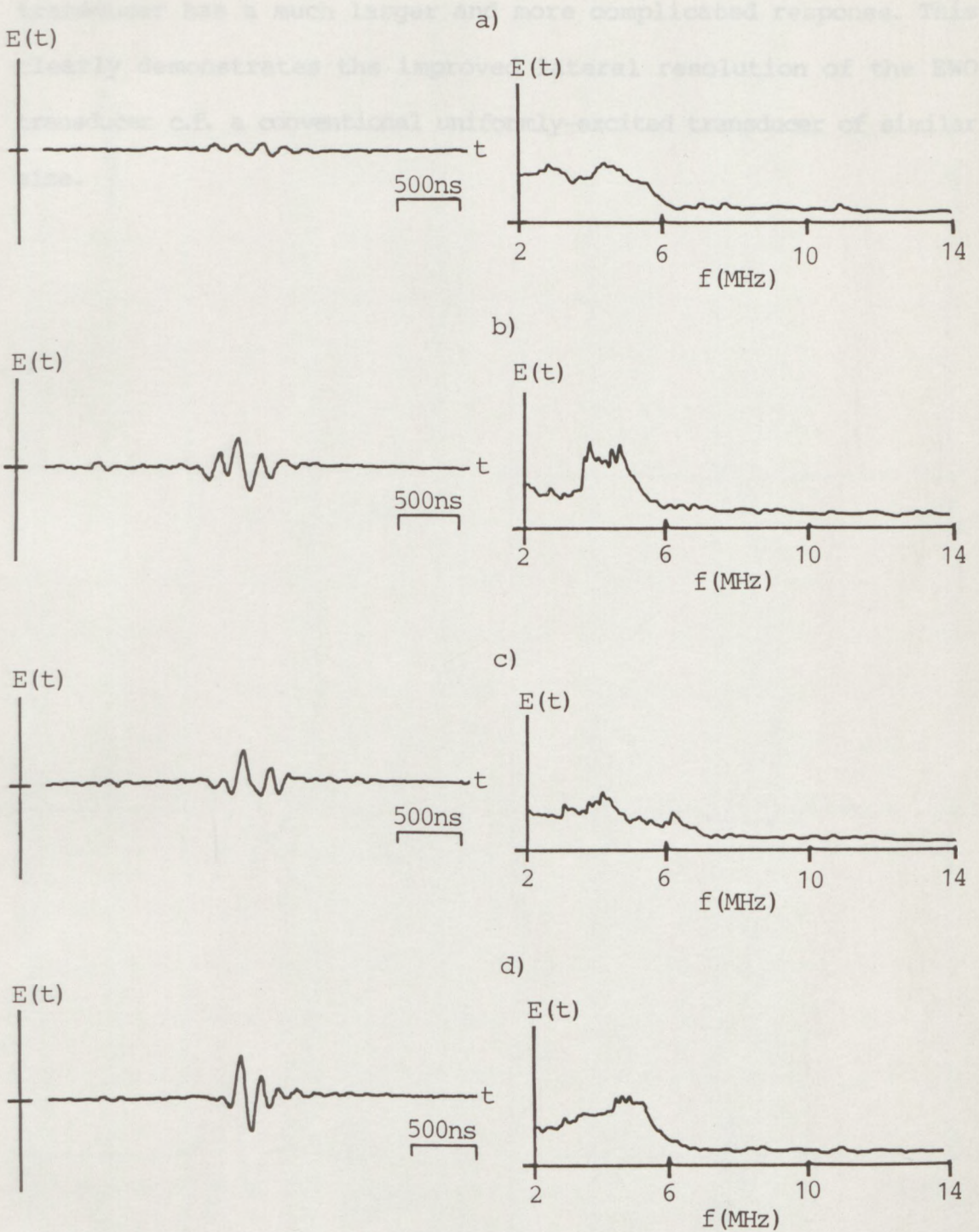
The off axis transmit-receive mode responses and associated spectra for a uniformly-excited transducer at various ranges are shown in figure 4-49. At a range of 20mm the first pulse in the response (figure 4-49a) is no different from the axial response at this range (figure 4-48a). However, each of the other two pulses seen in the axial response have split into two smaller time separated pulses. These are hardly visible in the result due to their small amplitude. The multipulse structure in the time domain is reflected in the modulation of the frequency domain response. As the range increases (figures 4-49b to 4-49d) the pulses shown in figure 4-49a become progressively less time separated until they overlap to form a single pulse of increased amplitude. This change is also seen in the frequency domain as a decline in the modulation of the response leading eventually to a single peak of increased amplitude.

Figure 4-50 shows the off axis time and frequency domain responses for a non-uniformly excited EWO type transducer at various ranges. In this case the response at a range of 20mm (figure 4-50a) consists of only two time separated responses emanating from the nearest and furthest edges of the transducer. The small amplitude of these pulses is shown by the small area of the frequency domain response. At greater ranges (figure 4-50b to 4-50d) the time separation of these two edge-wave pulses becomes smaller and they eventually overlap to form a single pulse. Throughout the ranges shown the frequency domain response shows an approximately constant area indicating that the energy contained in the pulse at each range is approximately constant. The shape of the frequency domain response is also approximately constant throughout the ranges shown.

A comparison between the off axis responses of a conventional, uniformly-excited transducer and a non-uniformly excited EWO type transducer of the same diameter, also made of PMN is given in figure



**Figure 4-49** Transmit-receive mode responses and pressure spectra for a conventional, uniformly-excited, circular transducer (19mm diameter by 10MHz equivalent thickness) interrogating a small brass target approximately 0.8mm in diameter 2mm off axis in water at ranges of:-  
a) 20mm b) 60mm c) 100mm d) 140mm



**Figure 4-50** Transmit-receive mode responses and pressure spectra for an EWO transducer (19mm diameter by 10MHz equivalent thickness) interrogating a small brass target approximately 0.8mm in diameter in water 2mm off axis at ranges of:-  
 a) 20mm b) 60mm c) 100mm d) 140mm

4-51. It can be clearly seen that the response of the EWO is small and simple just 2mm off axis whereas the conventional, uniformly-excited transducer has a much larger and more complicated response. This clearly demonstrates the improved lateral resolution of the EWO transducer c.f. a conventional uniformly-excited transducer of similar size.

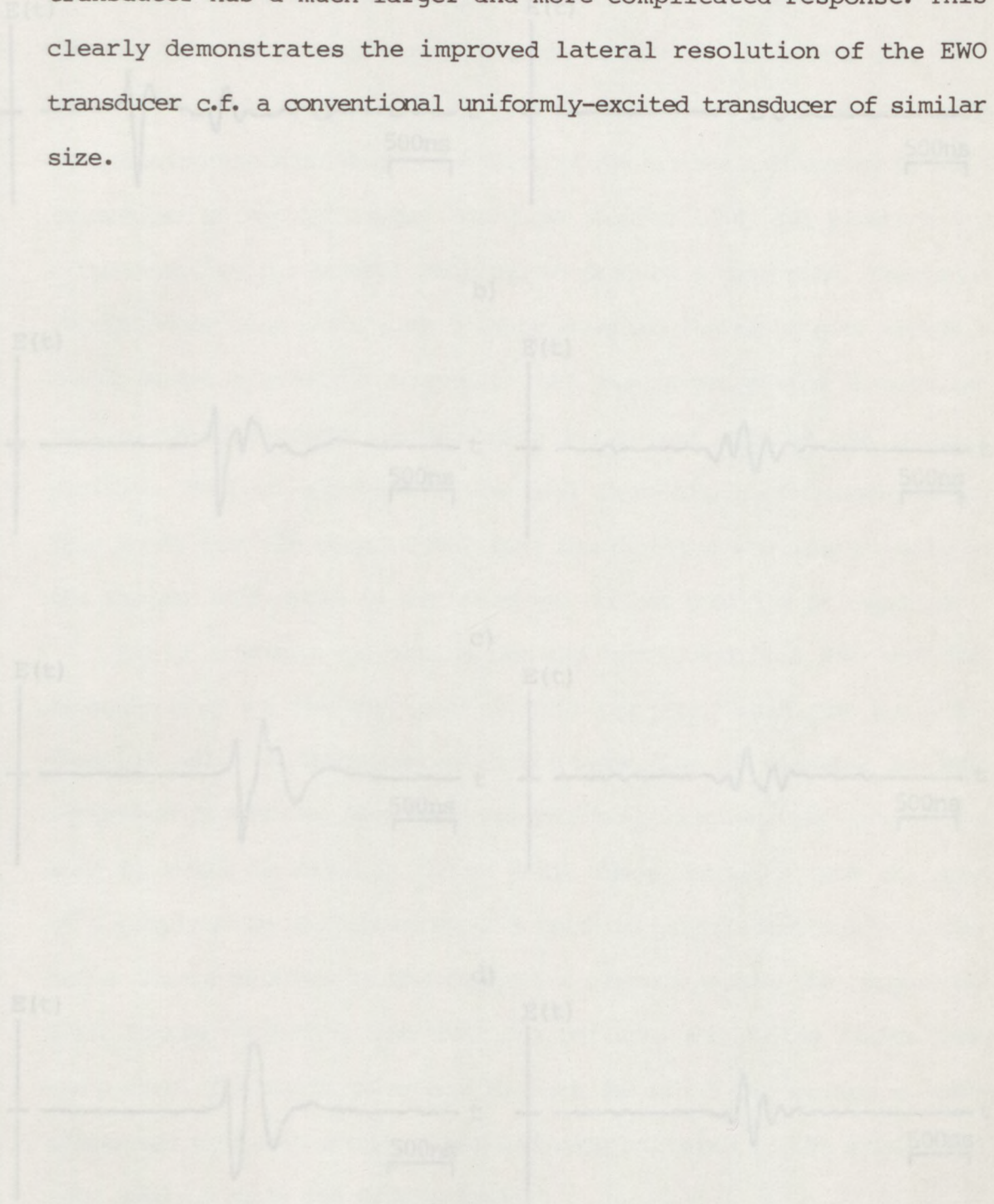
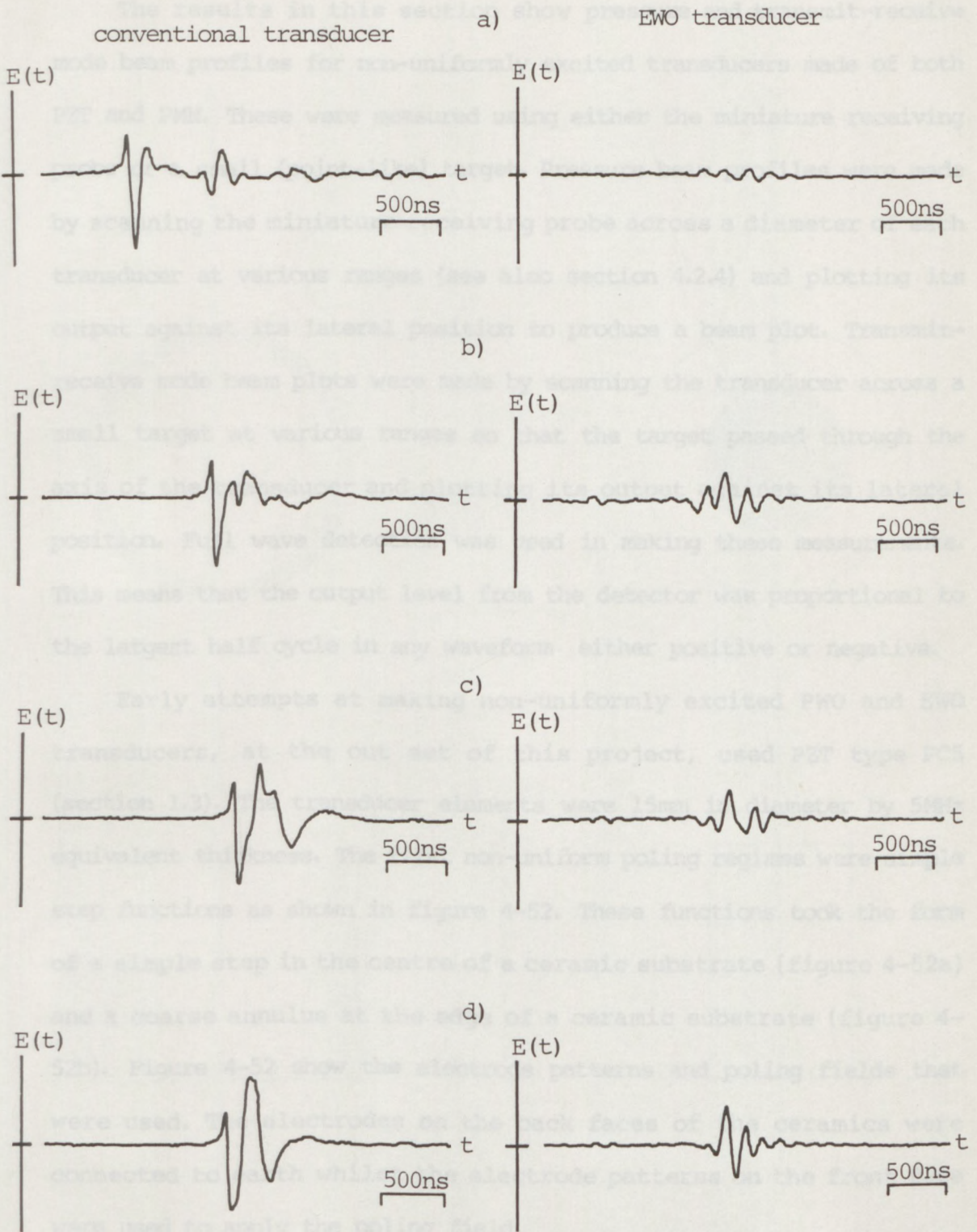


Figure 4-51 Transmit-receive mode responses 2mm off the axis of a conventional, uniformly-excited, circular transducer and an EWO transducer (both 19mm diameter by 10MHz equivalent thickness) interrogating a small brass target approximately 0.8mm in diameter in water at ranges of:-  
a) 30mm b) 60mm c) 100mm d) 140mm

### 4.3.3 Beam profiles

The results in this section show that the transmit-receive mode responses of both conventional and EWO transducers are similar. These were measured using either the miniature receiving PZT and PML. These were measured using either the miniature receiving PZT and PML. These were measured using either the miniature receiving PZT and PML.



**Figure 4-51** Transmit-receive mode responses 2mm off the axis of a conventional, uniformly-excited, circular transducer and an EWO transducer (both 19mm diameter by 10MHz equivalent thickness) interrogating a small brass target approximately 0.8mm in diameter in water at ranges of:-  
a) 20mm b) 60mm c) 100mm d) 140mm

### 4.3.3 Beam profiles

The results in this section show pressure and transmit-receive mode beam profiles for non-uniformly excited transducers made of both PZT and PMN. These were measured using either the miniature receiving probe or a small (point-like) target. Pressure beam profiles were made by scanning the miniature receiving probe across a diameter of each transducer at various ranges (see also section 4.2.4) and plotting its output against its lateral position to produce a beam plot. Transmit-receive mode beam plots were made by scanning the transducer across a small target at various ranges so that the target passed through the axis of the transducer and plotting its output against its lateral position. Full wave detection was used in making these measurements. This means that the output level from the detector was proportional to the largest half cycle in any waveform either positive or negative.

Early attempts at making non-uniformly excited PWO and EWO transducers, at the outset of this project, used PZT type PC5 (section 1.3). The transducer elements were 15mm in diameter by 5MHz equivalent thickness. The first non-uniform poling regimes were simple step functions as shown in figure 4-52. These functions took the form of a simple step in the centre of a ceramic substrate (figure 4-52a) and a coarse annulus at the edge of a ceramic substrate (figure 4-52b). Figure 4-52 show the electrode patterns and poling fields that were used. The electrodes on the back faces of the ceramics were connected to earth whilst the electrode patterns on the front face were used to apply the poling field.

From the results obtained it became clear that in order to achieve non-uniform poling it was necessary to "tie down" as great an area of the element as possible to a fixed potential. The high dielectric constant of the ceramic element and the appearance of surface charge during poling and due to fringing fields (see sections

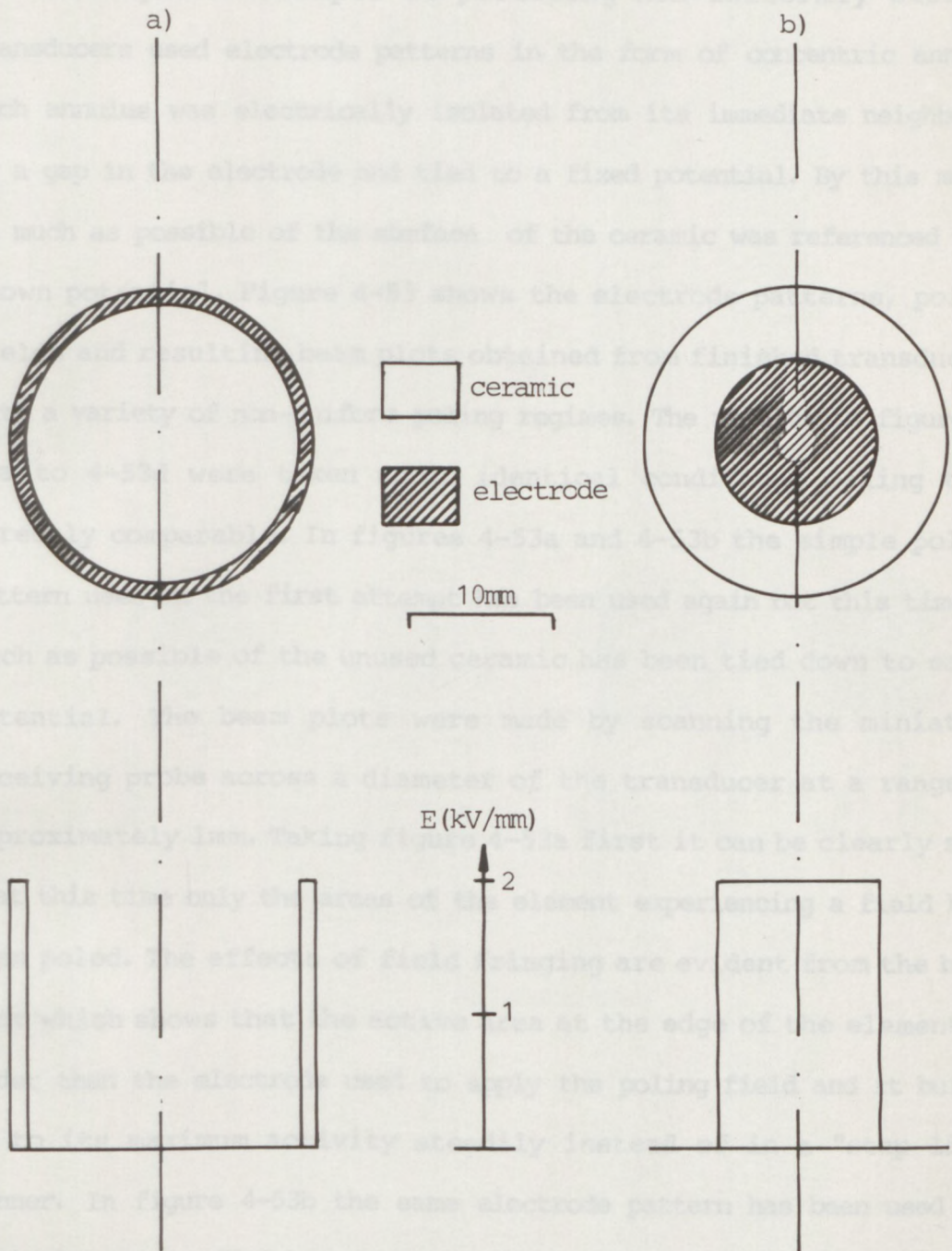


**Figure 4-52** The electrode patterns and poling fields used in an early attempt (at the beginning of this project) to produce non-uniform excitation in the form of:-

- a) a simple, step-like annulus at the edge of a disc of PZT
- b) a simple step in the centre of a disc of PZT

1.5 and 3.3) caused all unreferenced areas to float up to the highest potential present on any adjacent area and become poled.

Subsequent attempts at producing non-uniformly excited transducers used electrode patterns in the form of concentric annuli. Each annulus was electrically isolated from its immediate neighbours by a gap in the electrode and tied to a fixed potential. By this means as much as possible of the surface of the ceramic was referenced to a known potential. Figure 4-53 shows the electrode patterns, poling fields and resulting beam plots obtained from finished transducers with a variety of non-uniform poling regimes. The results in figure 4-53a to 4-53d were taken under identical conditions making them directly comparable. In figures 4-53a and 4-53b the simple poling pattern used in the first attempt has been used again but this time as much as possible of the unused ceramic has been tied down to earth potential. The beam plots were made by scanning the miniature receiving probe across a diameter of the transducer at a range of approximately 1mm. Taking figure 4-53a first it can be clearly seen that this time only the areas of the element experiencing a field have been poled. The effects of field fringing are evident from the beam plot which shows that the active area at the edge of the element is wider than the electrode used to apply the poling field and it builds up to its maximum activity steadily instead of in a "step like" manner. In figure 4-53b the same electrode pattern has been used but with the poling field applied to the opposite areas of the pattern from those used in figure 4-53a. It can be seen that what has been produced is effectively is a circular source in the centre of a larger circular substrate. The effects of field fringing are also evident in this result.

Figure 4-53c and 4-53d show the results for a series of concentric annuli on the front face of a transducer element. The

poling field increases in steps in steps in figure 4-53a and decreases in steps in figure 4-53b. The lower poling potentials were derived from the maximum poling potential using a simple, multi-tapped, resistive potential divider. As well as the maximum poling potential (2kV/mm) the following fractions of it were produced:- 0.75, 0.5 and 0.25.

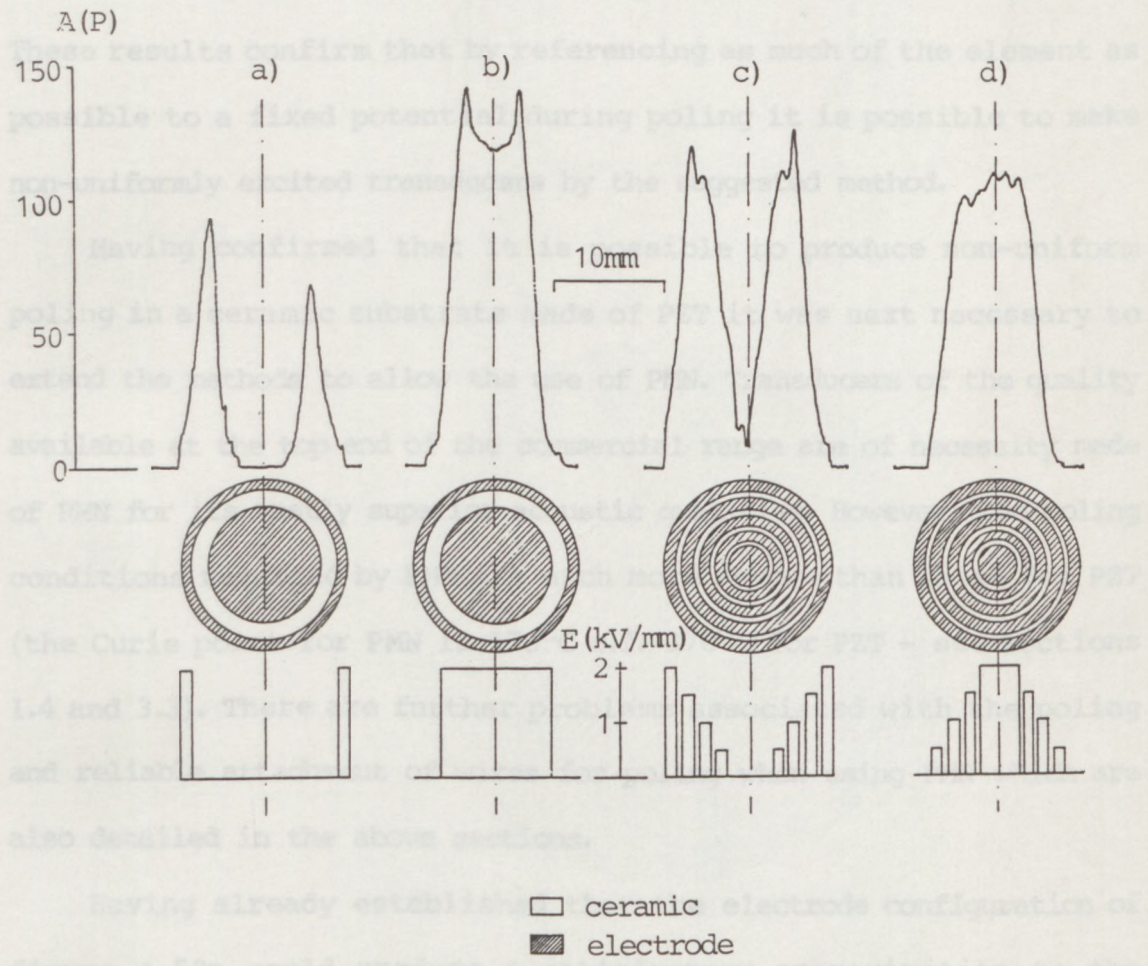


**Figure 4-53** Beam profiles, electrode patterns and poling fields for non-uniformly excited PZT transducers 15mm diameter by 5MHz equivalent thickness:-  
 a) a simple EWO b) a simple PWO  
 c) a step-wise approximation to an EWO  
 d) a step-wise approximation to a PWO

poling field increases in steps in figure 4-53c and decreases in steps in figure 4-53d. The lower poling potentials were derived from the maximum poling potential using a simple, multi-tapped, resistive potential divider. As well as the maximum poling potential (2kV/mm) the following fractions of it were produced:- 0.75, 0.5 and 0.25. These results confirm that by referencing as much of the element as possible to a fixed potential during poling it is possible to make non-uniformly excited transducers by the suggested method.

Having confirmed that it is possible to produce non-uniform poling in a ceramic substrate made of PZT it was next necessary to extend the methods to allow the use of PMN. Transducers of the quality available at the top end of the commercial range are of necessity made of PMN for its vastly superior acoustic qualities. However, the poling conditions required by PMN are much more severe than those for PZT (the Curie point for PMN is 570°C c.f. 370°C for PZT - see sections 1.4 and 3.3). There are further problems associated with the poling and reliable attachment of wires for poling when using PMN which are also detailed in the above sections.

Having already established that the electrode configuration of figure 4-53a could produce a satisfactory approximation to the Gaussian excitation profile required for an EWO type transducer it was then necessary to try and produce as fine an annulus and gap as possible in order to mimic the EWO characteristics shown in the computer modelling results. Finally a 19mm diameter disc of PMN (type K83) was poled according to the pattern shown in figure 4-54a. In this case the outer annulus and gap had dimensions 0.3mm and 0.1mm respectively. These represented the finest dimensions that could be produced using the experimental techniques that were available. Figure 4-53a shows how the activity of the disc rises sharply at its edges but not in a "step" fashion as might be predicted from a simple

analysis of the applied field. The smoothing effect of the field itself which is exploited here causes the approximation to a Gaussian fall off which is required.

Figure 4-55 shows a pressure beam profile for a non-uniformly excited EWO type transducer. It can be seen that as predicted by theory and shown in the calculated results of section 4-1-5 the peak pressure is concentrated along the axis and falls off rapidly with range. Further, the width of the axial response increases with range as shown in these calculated results. For comparison figure 4-56 shows the measured result together with a computer calculated result produced without charge transfer.

Figure 4-57 shows a cross-sectional plot for this transducer. The ceramic is shown with a white fill and the electrode with a hatched pattern. The diameter is 19mm.

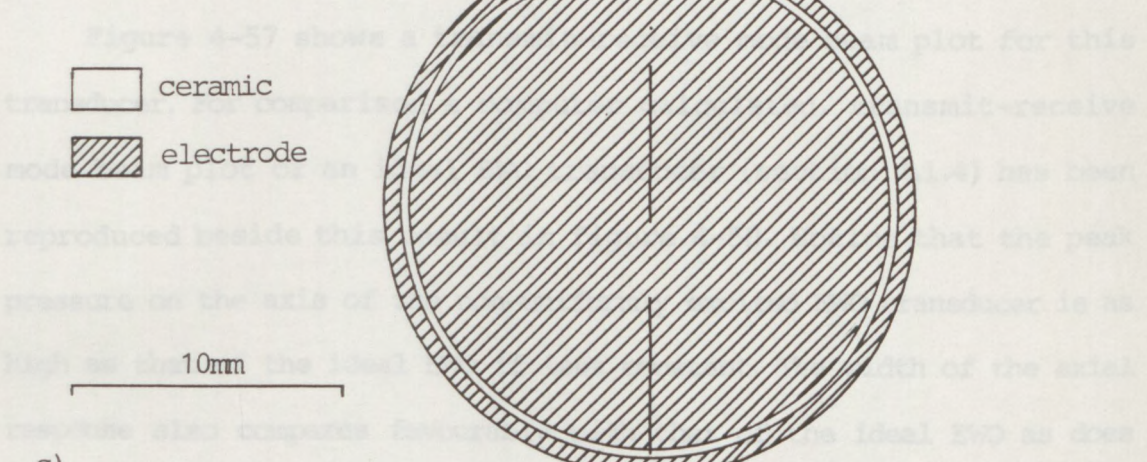
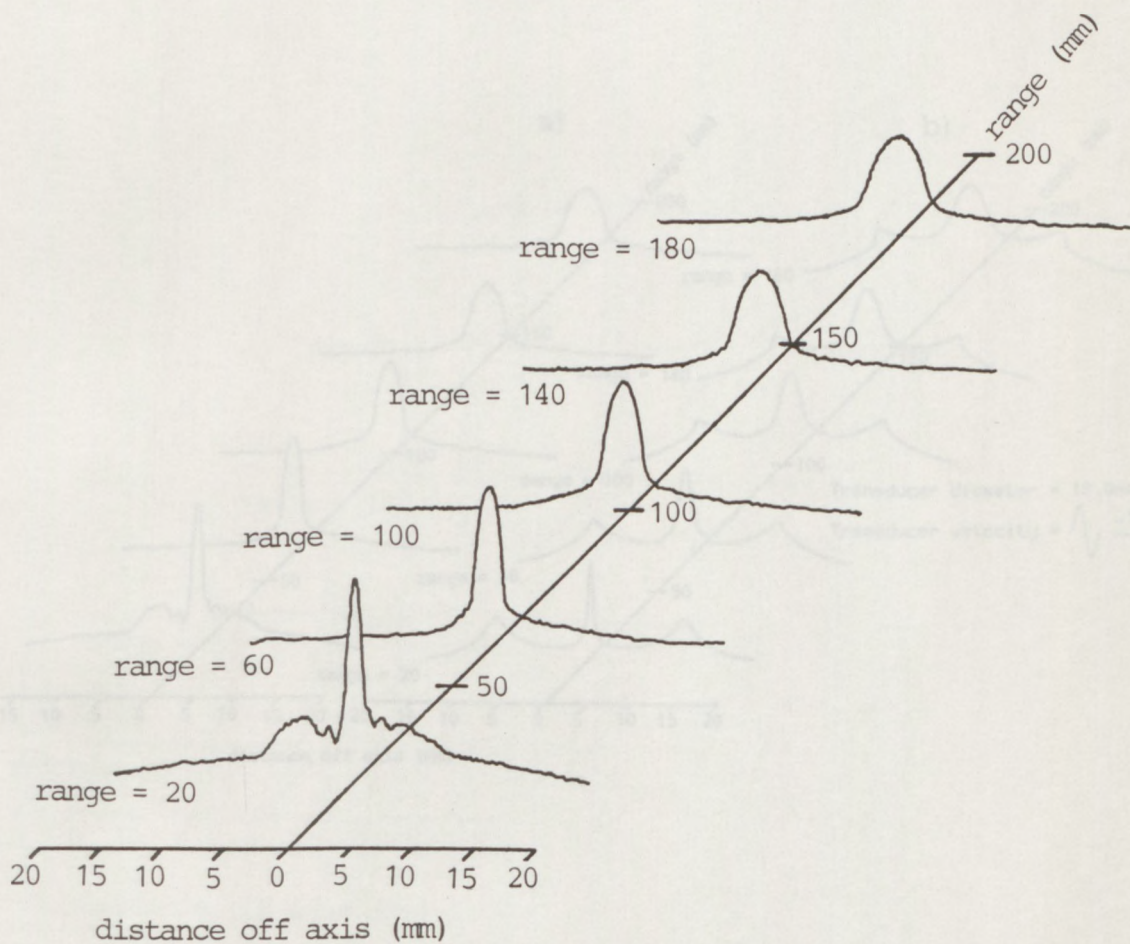


**Figure 4-54** Results for a non-uniformly excited, EWO type transducer, 19mm diameter by 10MHz equivalent thickness made of PMN (type K83), showing:- a) beam profile b) electrode pattern c) poling field

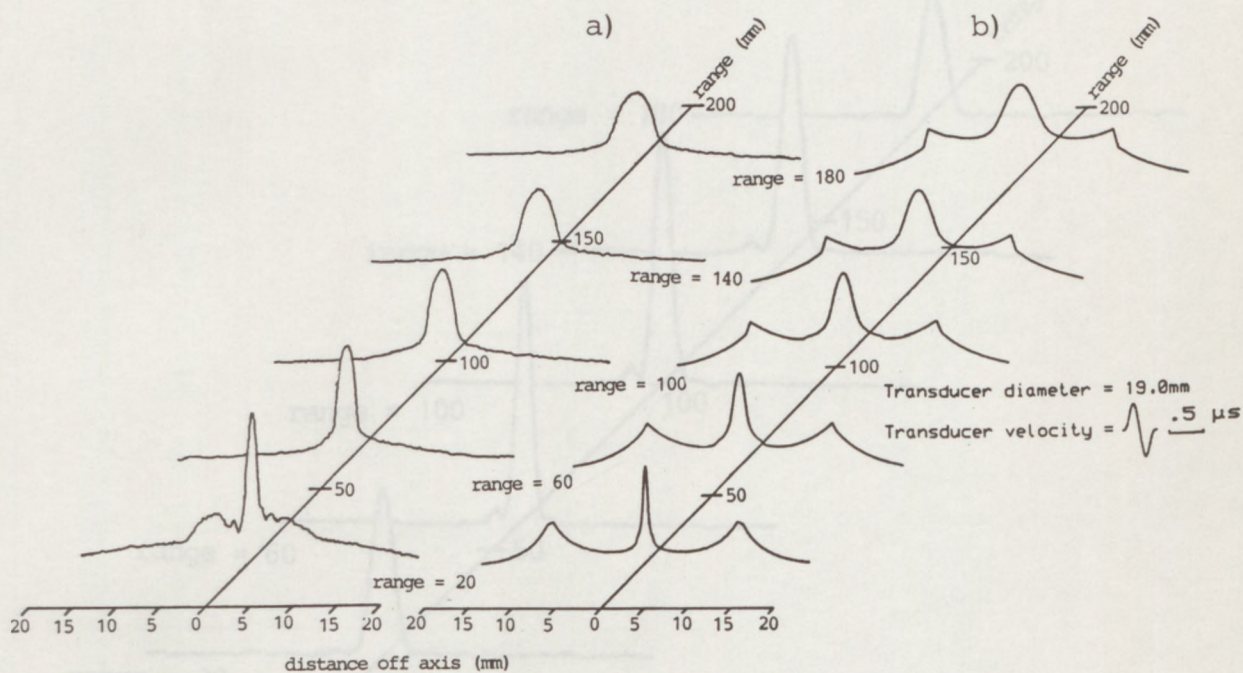
analysis of the applied field. The smoothing effect of the field fringing which is exploited here causes the approximation to a Gaussian fall off which is required.

Figure 4-55 shows a pressure beam profile for a non-uniformly excited EWO type transducer. It can be seen that as predicted by theory and shown in the calculated results of section 4-1-5 the peak pressure is concentrated along the axis and falls off only slowly with range. Further, the width of the axial response increases with range as shown in these calculated results. For comparison figure 4-56 shows the measured result together with a computer calculated result reproduced without change from section 4.1.3.

Figure 4-57 shows a transmit-receive mode beam plot for this transducer. For comparison a computer calculated, transmit-receive mode beam plot of an ideal EWO transducer (section 4.1.4) has been reproduced beside this result in figure 4-58. Notice that the peak pressure on the axis of the non-uniformly excited EWO transducer is as high as that of the ideal EWO if less constant. The width of the axial response also compares favourably with that of the ideal EWO as does the lack of side structure in the non-uniformly excited EWO.



**Figure 4-55** Measured pressure beam profiles at various ranges in water for a non-uniformly excited, EWO type transducer, 19mm in diameter by 10MHz equivalent thickness made of PMN (type K83)



**Figure 4-56** Measured and calculated pressure beam profiles at various ranges in water for a non-uniformly excited, EWO type transducer:-  
 a) measured      b) calculated

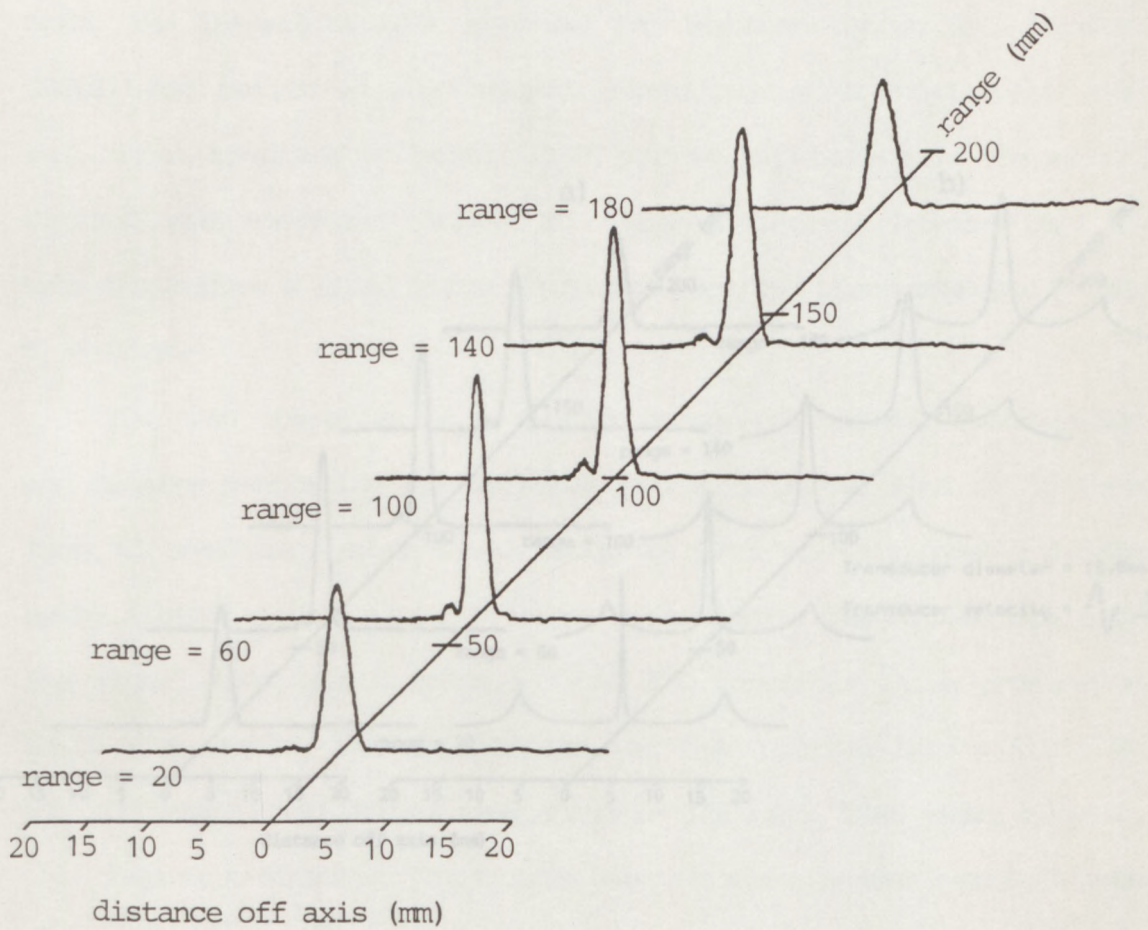


**Figure 4-57** Measured transmit-receive mode beam profiles at various ranges in water for a non-uniformly excited, EWO type transducer, 19mm in diameter by 10MHz equivalent thickness made of PMN type (K83)

#### 4.4 B-Scan Images

To further evaluate the non-uniformly excited transducers produced during this project, B-scan images were produced. These used the positional information from a scanning, ultrasonic inspection tank and the signal from a transducer operating in the transmit-receive mode. The inspection tank (Systems and Instrumentation Ltd. Pershore WORCS.) had motion in 2 orthogonal directions with positional read out to an accuracy of better than  $\pm 0.5\text{mm}$  anywhere over its area. A digital scan converter (Anamatic 80 - Diver Aircraft Cooper USA) was used to produce a video image which was recorded photographically on a monitor.

The scan converter was used to produce a video image which was recorded photographically on a monitor. The scan converter was used to produce a video image which was recorded photographically on a monitor. The scan converter was used to produce a video image which was recorded photographically on a monitor.

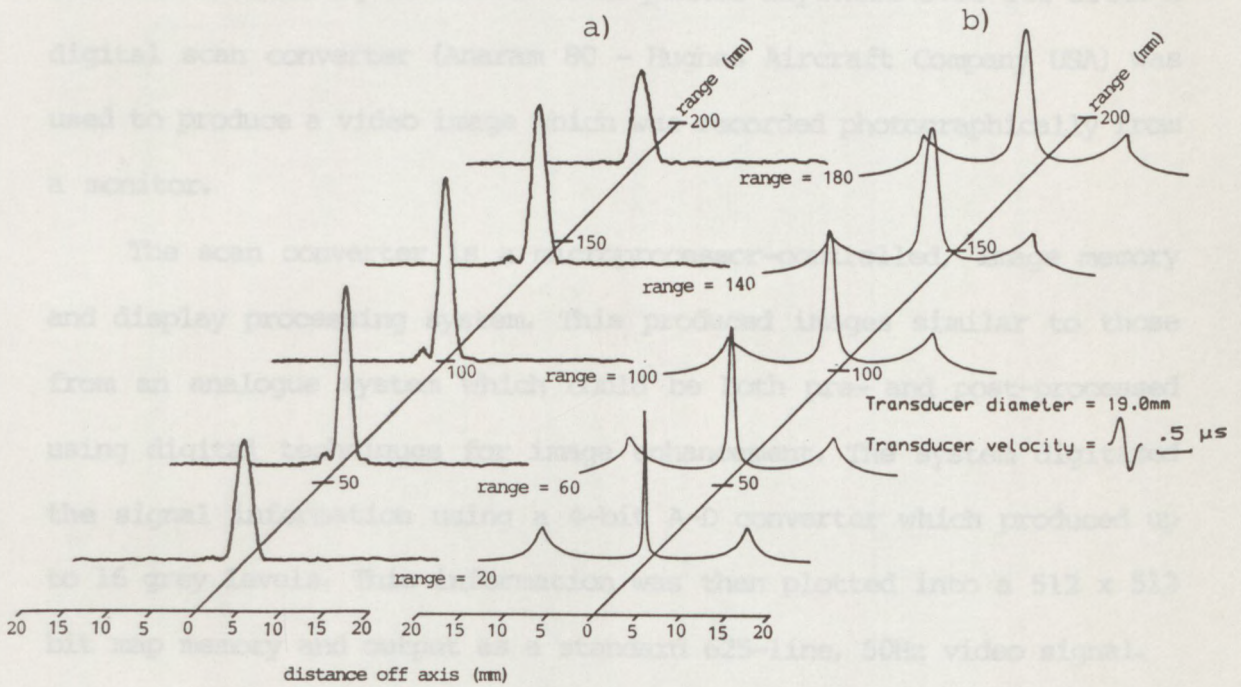


Figure 4-59 shows the target used to produce the B-scan images shown in figures 4-58a and 4-58b. It consisted of a block of mild steel containing a row of flat bottomed holes. These were 2mm in diameter and varied in depth from 12 to 60μm as shown in figure 4-59; the horizontal and vertical scales are the same as shown in figures 4-58a and 4-58b. Imaging was under water and both figures 4-58a and 4-58b were taken under identical conditions. However, figure 4-58a was produced using a top quality, uniformly excited, conventional transducer of 13mm diameter (Sonotronics VIII) whilst figure 4-58b was produced using a non-uniformly excited EWO transducer of 19mm diameter. In

**Figure 4-58** Measured and calculated transmit-receive mode, beam profiles at various ranges in water from a small (point-like) target for a non-uniformly excited, EWO type transducer:-  
a) measured b) calculated

#### 4.4 B-Scan Images

To further evaluate the non-uniformly excited transducers produced during this project, B-scan images were produced. These used the positional information from a scanning, ultrasonic inspection tank and the signal from a transducer operating in the transmit-receive mode. The inspection tank (Systems and Instrumentation Ltd. Pershore WORCS.) had motion in 2 orthogonal directions with positional read out to an accuracy of better than  $\pm 0.5\text{mm}$  anywhere over its area. A digital scan converter (Anaram 80 - Hughes Aircraft Company USA) was used to produce a video image which was recorded photographically from a monitor.

The scan converter is a microprocessor-controlled, image memory and display processing system. This produced images similar to those from an analogue system which could be both pre- and post-processed using digital techniques for image enhancement. The system digitized the signal information using a 4-bit A-D converter which produced up to 16 grey levels. This information was then plotted into a 512 x 512 bit map memory and output as a standard 625-line, 50Hz video signal.

Figure 4-59 shows the target used to produce the B-scan images shown in figures 4-60a and 4-60b. It consisted of a block of mild steel containing a row of flat bottomed holes. These were 2mm in diameter and varied in depth from 12 to 60mm as shown in figure 4-59; the horizontal and vertical scales are the same as shown in figure 4-60. Imaging was under water and both figures 4-60a and 4-60b were taken under identical conditions. However, figure 4-60a was produced using a top quality, uniformly excited, conventional transducer of 13mm diameter (Panametrics V111) whilst figure 4-60b was produced using a non-uniformly excited EWO transducer of 19mm diameter. In figure 4-60a the depths of the bottoms of the holes are resolved but the lateral resolution of the conventional transducer is of the order

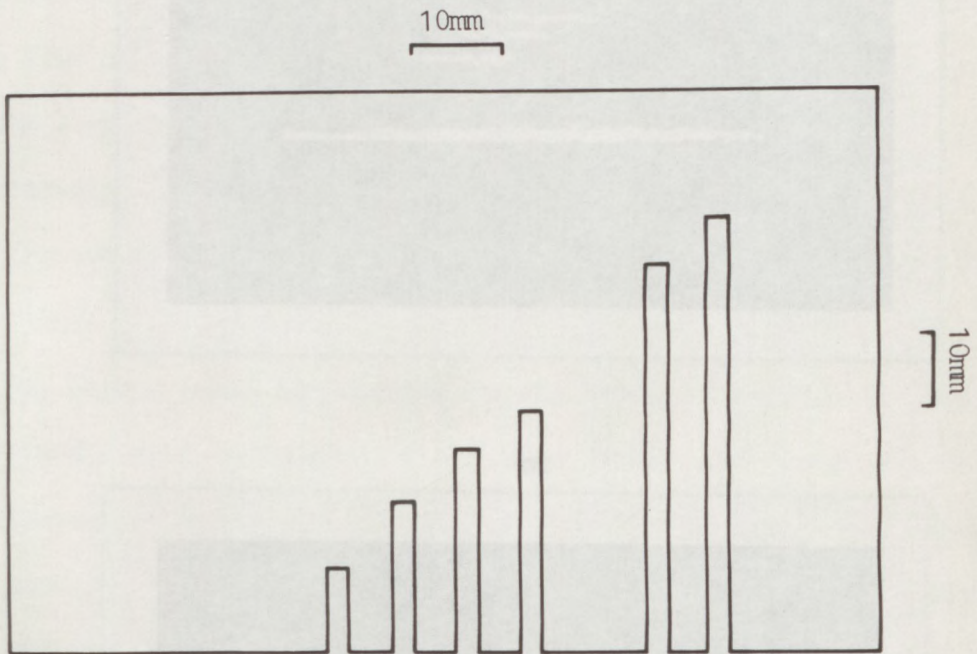


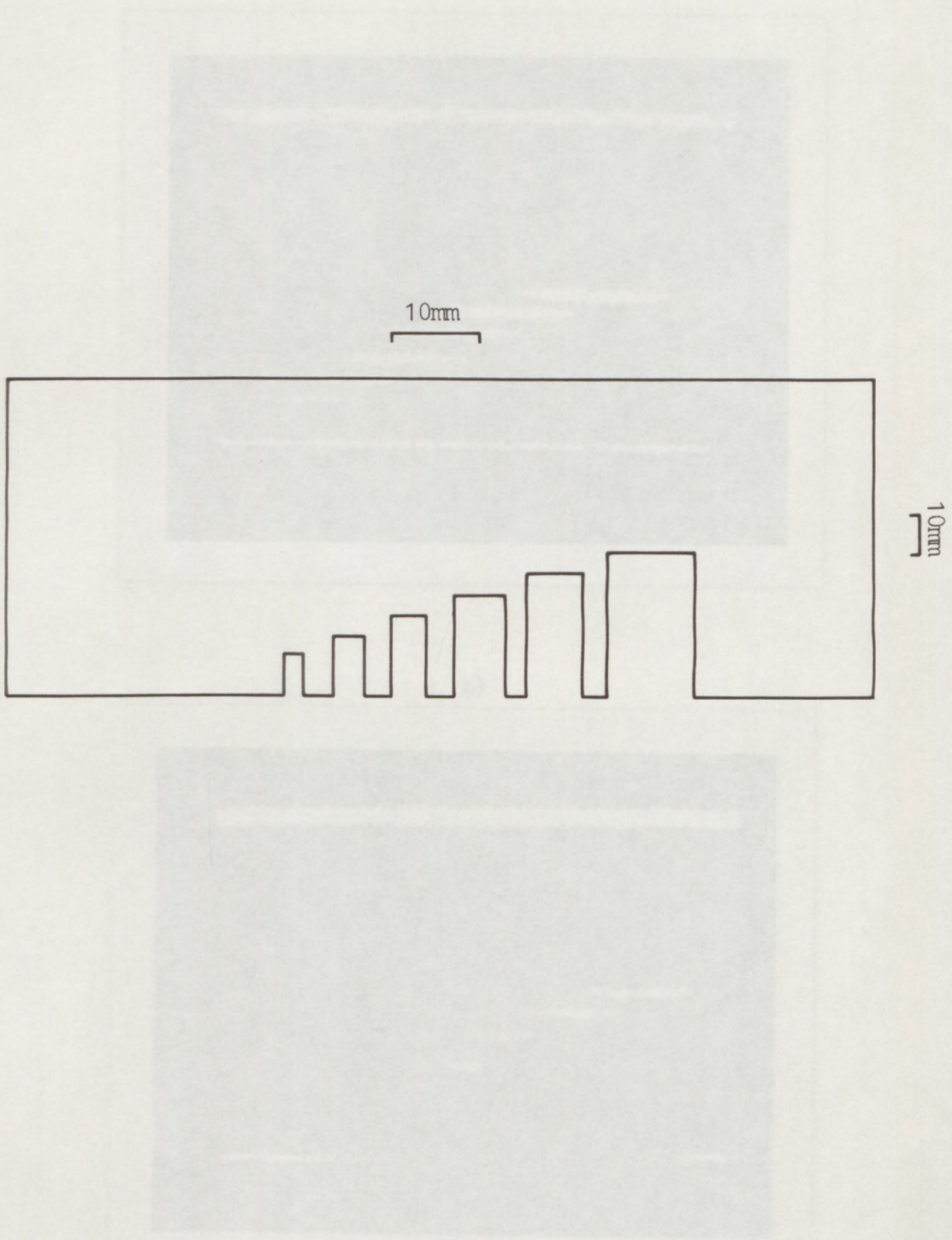
Figure 4-59 To scale schematic of the target imaged in the B-scans shown in figure 4-60



of its aperture so the hole diameters are not accurately represented. In figure 4-60b the bottoms of the holes are clearly resolved in time and their diameter can be clearly ascertained to an accuracy of better than 0.3mm. It is also notable that the gaps in the back wall of the target where the holes begin are visible in this figure. Since, as explained in section 2.3.2, there is a non-linear time-range (from the plane of the transducer) relationship with the EWO transducer and since the same linear time-base ramp was used in producing both figures 4-60a and 4-60b, the depths of the holes as indicated in the EWO transducer scan will not be exactly correct. However, at the coupling range used here, the error in the depth of any of the holes due to this is less than 1mm and can be allowed for if required.

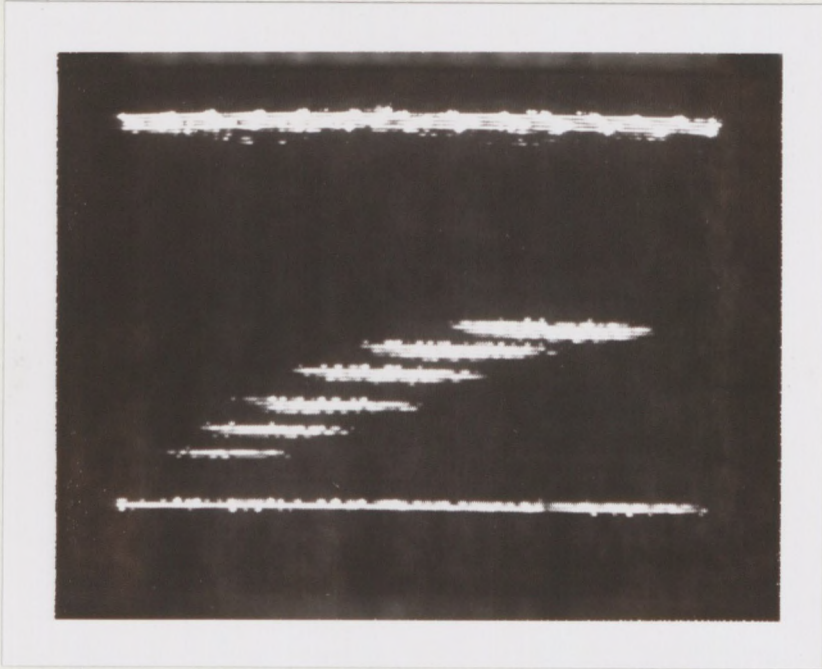
The target used to produce figure 4-62a and 4-62b is shown in figure 4-61. This consisted of a row of holes which varied in both diameter and depth as shown in figure 4-61. The block was made of aluminium and the horizontal and vertical scales were the same as those shown in figure 4-62. The scans shown in figure 4-62a and 4-62b were also taken under identical conditions. In figure 4-62a the holes are just resolved in relation to depth, but again the (lateral) resolution is of the order of the transducers diameter (13mm) so the hole diameters are not accurately represented. However, in figure 4-62b the bottoms of the holes are clearly resolved and their diameters can be ascertained to an accuracy of better than 1mm. The gaps in the back wall of the block are again becoming visible in the scan.

Figure 4-63 also shows B-scan images, again taken under identical conditions but using a commercial probe and an EWO transducer of the same aperture (19mm). In this case the target consists of a group of nylon monofilaments. Each one was 0.2mm in diameter and round in cross section. These were arranged at various positions in a jig to produce a pattern which gave rise to two rows of letters, The top row (TCU)



**Figure 4-61** To scale schematic of the target imaged in the B-scans shown in figure 4-62

a)



b)

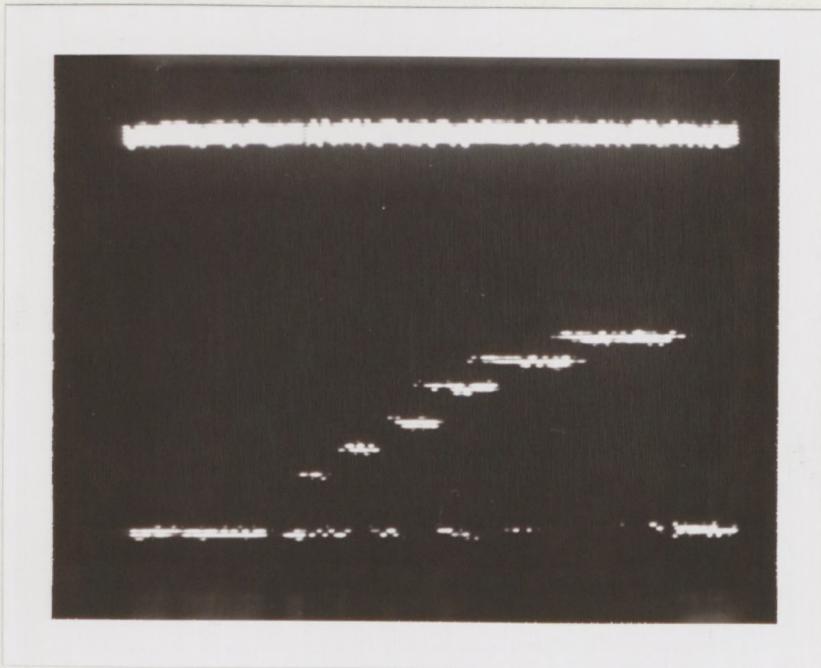
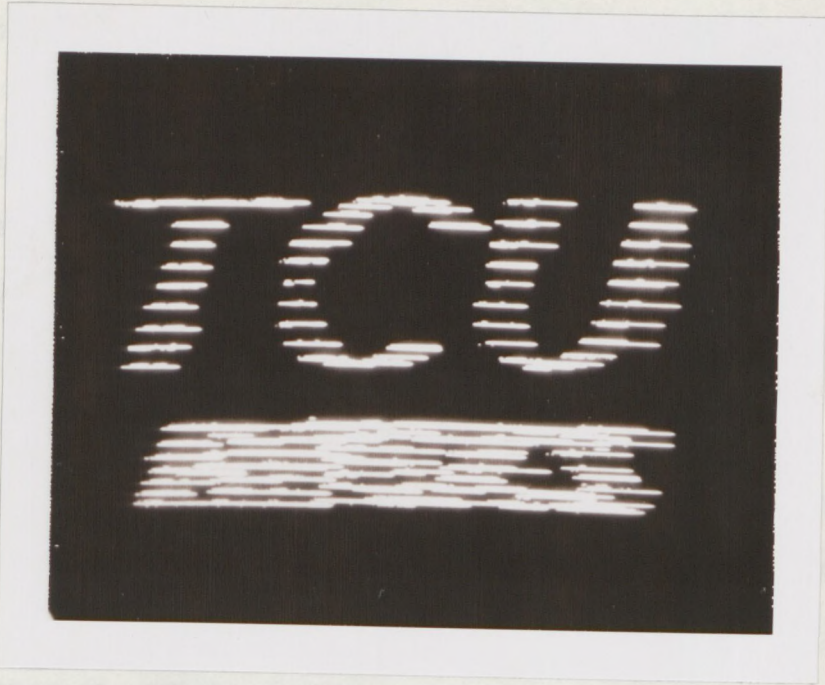


**Figure 4-62** B-scan images of the target shown in figure 4-61 imaged in water with:-  
a) a conventional transducer of 13mm diameter  
b) an EWO type transducer of 19mm diameter

a)



b)

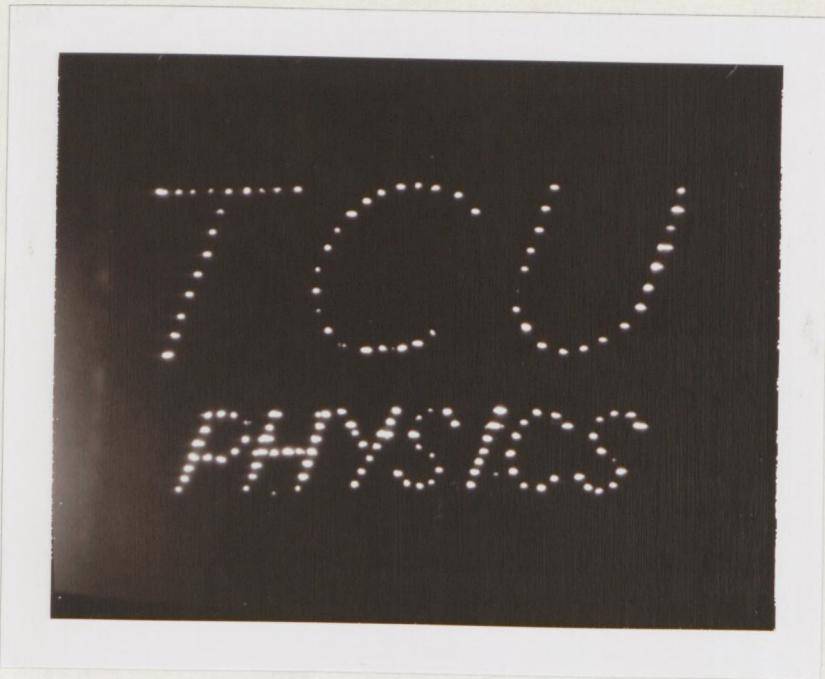


**Figure 4-63** B-scan images of a group 0.2mm diameter nylon threads, held in a plastic jig to produce a matrix pattern that gives rise to the words TCU (top row) and PHYSICS (bottom row). These are imaged in water using:-

- a) a conventional transducer of 19mm diameter
- b) an EWO type transducer of 19mm diameter

being much more widely spaced than the bottom row (PHYSICS). In figure 4-63a the top row of letters can be clearly recognized. However, the poor lateral resolution of the conventional transducer is very evident, the lower row of letters being illegible. With the EWO transducer (figure 4-63b) the lower row of letters are easily read and each thread is clearly imaged as a dot. This test is similar to that used to test medical imaging systems and is quite stringent, the small threads being weak scatterers spread over a depth range of approximately 80mm.

These pictures demonstrate the improved resolution of the EWO transducer compared to that of a top quality commercial probe, as well as the advantages of the simpler, more compact pulse shape for imaging small targets at various depths.

DISCUSSION, CONCLUSIONS AND SUGGESTIONS FOR FURTHER WORK

This work has confirmed that it is possible to produce non-uniformly excited transducers by apodising the strength of the piezoelectric effect in a ceramic transducer element. The work began with controlled depoling of PZT elements which were supplied electroded and poled by the manufacturers. It soon became clear that the methods of depoling available were either too destructive or not controllable enough to produce the apodisation required. The work quickly progressed to controlled repoling of thermally depoled PZT. This was followed by work on PMN. Whilst this material is much superior to PZT in many of its transducer properties, such as its low cross mode coupling and mechanical quality factor  $Q_m$ , it is much harder to work with. The high coercivity and Curie point together with a tendency to become conductive at the elevated temperatures used for poling, meant that special and more stringent techniques had to be developed to exploit the advantages of this material.

The final results were obtained by controlled repoling of electroded but unpoled PMN. This was obtained by special order from manufacturers in the USA. Non-uniformly excited transducers made from this material underwent fewer process steps and therefore experienced less handling. This reduced the risk of degrading the element and its electrodes and edges particularly at the relatively high temperatures required for depoling.

The resolution of the poling pattern on the transducer electrode(s) was limited primarily by practical considerations including:-

- i) The intrinsic roughness of the surface of the ceramic element.
- ii) The quality of the disc edge (which limits the minimum size

of the outer annulus).

- iii) The maximum field that can be developed across the gap between two electrodes before the poling voltage starts to track across it.

A comprehensive range of computer calculated results show the effect of various apodisation regimes. These include the purely theoretical (e.g. the ideal EWO) and the practicably unobtainable (e.g. the simple annular EWO). However, some good, practical compromises are also shown. Fortunately, in practice it was possible to produce the smooth changes in piezoelectric polarization required for these compromise regimes. The method employed used simple electrode geometries and exploited the smoothing due to field fringing.

The results presented in chapter 4 show that non-uniformly excited wide-band transducers have been produced by the method chosen. It has also been shown that these transducers have the characteristics predicted by the plane- and edge-wave model. For the case of the EWO transducer, for example, a simple, constant pulse-shape at all axial ranges. From these results it can be clearly concluded that non-uniform excitation is a viable method of producing transducers with useful and novel characteristics. Further, the use of photofabrication methods based on photoresist have been shown to be suitable for producing the required electrode pattern(s) on the metallized surfaces of the transducer elements. This includes working right up to and including the edges of the comparatively rough substrates. Despite problems with the irregular surfaces and edges of the substrates as supplied by the manufacturers, excellent results have been achieved. The application of suitable poling regimes via these patterns under suitable conditions of constant temperature and time so that the degree of poling can be controlled directly from the strength of the

poling field has also been shown to be a practical method of fabrication.

Like the predictions made by the plane and edge-wave model, the computer calculated results shown at the beginning of chapter 4 have also been verified. In particular a non-uniformly excited transducer which produces primarily edge-waves has been shown to possess a high lateral resolution over an extended depth of field.

The non-uniformly excited transducers have been produced in a format similar to that found in commercial transducers. This enables them to directly replace conventional transducers in all situations from contact testing to medical applications which use high-speed scanning to produce real time images. Figure 5-1 shows a photograph of a top quality, uniformly-excited commercial transducer beside a non-uniformly excited EWO transducer of the same diameter (19mm).

Tests with a miniature piezoelectric probe, developed within the ultrasonics group at The City University have confirmed that it is possible to produce a direct and predictable correlation between the ultrasonic pressure in the field of a transducer and the poling regime applied to its element. Hence it has been possible to calibrate a miniature probe for use in directly assessing the excitation of non-uniform transducers.

Whilst the work shown here has proved beyond doubt the viability of the methods used for the fabrication of non-uniformly excited wide-band transducers there is still of scope for further work. For example, other poling methods may be used to avoid problems such as the arcing of high voltages between the various tracks in the electrode pattern and the problem of conductivity experienced in PMN at elevated temperatures. Poling may also be made easier by the use of pulsed or other novel types of poling field to avoid some of the problems associated with the use of high dc fields for protracted

periods. This of course would require that more or less  
characterization and calibration work presented here should be  
repeated.

Should non-uniformly excited transducers such as those described  
here be manufactured, the required electrode pattern would be prepared  
prior to rolling. In these circumstances the photoresistive pattern  
used here may well be replaced by some type of a polymer pattern.

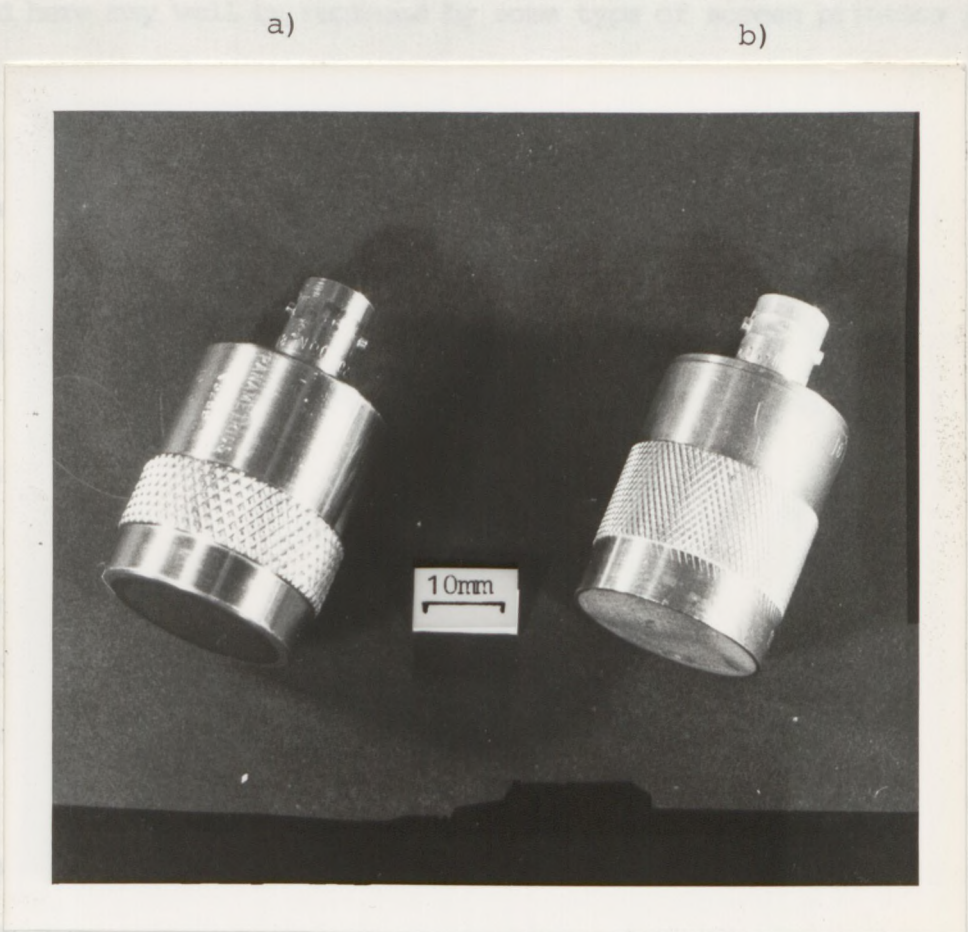


**Figure 5-1** A photograph showing a non-uniformly excited, EWO type transducer, together with a uniformly-excited, top quality, commercial probe of the same diameter  
a) a conventional, uniformly-excited, top quality, commercial probe  
b) a non-uniformly excited EWO type transducer

periods. This of course would require that much of the characterization and calibration work presented here should be repeated.

Should non-uniformly excited transducers such as those described here be manufactured, the required electrode pattern would be applied prior to poling. In these circumstances the photofabrication method used here may well be replaced by some type of screen printing process for applying the required electrode pattern directly to the ceramic surface. This type of technology is commonly employed in the fabrication of hybrid microwave circuits on ceramic substrates. It is not yet clear which method would be the most commercially viable, the final choice between them involves commercial considerations.

A majority of the measurements given were made on the EWO type transducer. However, the results also confirm that it is possible to make transducers of the opposite configuration i.e. PWO transducers. In the future there is scope for further work to be done on the optimisation of the poling regime used in the production of these transducers.

As the work presented here is based on the plane and edge-wave model of action of a transducer the computer calculations were based firmly on the study of the propagation of acoustic pulses from the front face of the transducer forward. There is no doubt that a significant amount of work remains to be done on computer modelling of the action of non-uniformly excited transducers starting from the electro-mechanical properties of the transducer element itself.

Another extension of this work would be the use of piezoelectric polymers for the elements of non-uniformly excited, wide-band, ultrasonic transducers. Materials such as poly(vinylidene) (PVDF) offer useful wide-band properties and are rendered piezoelectric by processes analogous those used to pole piezoelectric ceramics. Like

PZT and PMN, PVDF is not a true piezoelectric, however, it has a very much lower acoustic impedance which makes up for its lower sensitivity. PVDF also offers the possibility of avoiding some of the problems encountered with the head-waves which are generated by ceramic elements. There would obviously be a completely new set of practical problems involved with the use of PVDF. The solution of these and the other problems described above is left as material for future work.

BACON, J. C., LAKSHMINI, P and PERREUX, M (1984). Theoretical and experimental study of the contribution of radial waves to the pulsed ultrasonic field radiated by a thick piezoelectric disk. Journal of the Acoustical Society of America 75 (6):1722-1731.

BEHRNDT, H. D (1967). Thermodynamic theory of ferroelectric ceramics. Physical Review 105 (2): 480 - 486.

BIRNBAUM, K. F and SILK, M. G (1980). Some factors which affect the performance of ultrasonic transducers. British Journal of Appl Phys 31 (1): 15-20.

BEAVERS, W. D (1974). Size near-field of a pulsed piston radiator. Journal of the Acoustical Society of America 56 (4): 1043-1046.

BERLINGUET, D. A., BRILL, C and SMARSKI, P. T (1960a). Polymorphism of titanate ceramics. United States Patent number 2,938,163.

BERLINGUET, D. A., JAYE, E and SCHMIDT, R. H. A (1960b). Piezoelectric properties of lead titanate zirconate ceramics. IRE Transactions on Ultrasonics Engineering US-7 (1): 1-6.

BERLINGUET, D. A., CIPMAN, D. R and JAYE, A (1964). Piezoelectric and piezomagnetic materials and their function in transducers. In Physical acoustics, ed. by W. P. Mason (London: Academic Press).

BERLINGUET, D. A (1964). Variation of electromechanical constants of polycrystalline lead titanate zirconate with thicknesses of poling. Journal of the Acoustical Society of America 36 (3): 518.

## REFERENCES

- ALI, H A (1977). An investigation of piezoelectric torsional wave transducers for millisecond delay lines. PhD Thesis: Kings College, University of London, Department of Electrical Engineering and Electronic Engineering.
- ANDERSON, P (1960). Physics of dielectrics. (in Russian). In: FIZIKA DIELEKTRIKOV, TRUDY VSESOYUZNOI KONFERENTSII, 2D, MOSCOW 1958 SSSR INSTITUT FIZIKA pp 290-296.
- BABOUX, J C, LAKESTANI, F and PERDRIX, M (1984). Theoretical and experimental study of the contribution of radial waves to the pulsed ultrasonic field radiated by a thick piezoelectric disk. Journal of the Acoustical Society of America 75 (6):1722-1731.
- BAERWALD, H G (1957). Thermodynamic theory of ferroelectric ceramics. Physical Review 105 (2): 480 - 486.
- BAINTON, K F and SILK, M G (1980). Some factors which affect the performance of ultrasonic transducers. British Journal of NDT 22 (1): 15-20.
- BEAVER, W L (1974). Sonic near-field of a pulsed piston radiator. Journal of the Acoustical Society of America 56 (4): 1043-1048.
- BERLINCOURT, D A, FALLS, C and BRUNARSKI, F T (1960a). Polarization of titanate ceramics. United States Patent number 2,928,163.
- BERLINCOURT, D A, JAFFE, B and KRUEGER, H H A (1960b). Transducer properties of lead titanate zirconate ceramics. IRE Transactions on Ultrasonics Engineering UE-7 (1) : 1-6.
- BERLINCOURT, D A, CURRAN, D R and JAFFE, A (1964). Piezoelectric and piezomagnetic materials and their function in transducers. In: Physical acoustics, ed. by W P Mason (London: Academic Press).
- BERLINCOURT, D A (1964). Variation of electroelastic constants of polycrystalline lead titanate zirconate with thoroughness of poling. Journal of the Acoustical Society of America 36 (3): 515.

- BESS, L (1970). Sonic radiation from a circular piston with impulse excitation. NASA Electronics Research Centre Cambridge MA Unpublished report.
- BOND, L J, JAYASUNDERE, D A, SINCLAIR, D A and SMITH, I R (1982). Investigation of ultrasonic transducers as used for non-destructive testing. In: Review of Progress in Quantitative Non-Destructive Evaluation Volume 1, ed. D O Thompson and D E Chimenti (London: Plenum). pp 691-701.
- BORN, M and HUANG, K (1956). Dynamical theory of crystal lattices (Oxford: Clarendon Press).
- BRADFIELD, G (1960). The use of radially graded ultrasonic radiators to improve the uniformity of the near field. In: SECOND INTERNATIONAL CONFERENCE ON MEDICAL ELECTRONICS. Proceedings ed. C N Smyth. London: Iliffe and Son Ltd. pp 367-373.
- BREDAEL, I (1977). Characterisation of ultrasonic transducers. In: Research Techniques in NDT Volume 3, ed. R S Sharp (London: Academic Press). pp 177-215.
- BURCKHARDT, C B, GRANDCHAMP, P A and HOFFMAN, H (1975). Focusing ultrasound over a large depth with an annular transducer - an alternative method. IEEE Transactions on Sonics and Ultrasonics SU22 (1): 11-15.
- BURFOOT, J C (1967). Ferroelectrics, an introduction to the physical principles. (London: D Van Nostrand Company Inc).
- BUSCH, G and SCHERNER, P (1935). A new seignettelectric substance. (in German). Naturwissenschaften 23 (43): 737.
- CADY, W G (1946). Piezoelectricity (London: McGraw Hill Book Company Inc).
- CASPARI, M E and MERZ, W I (1950). The electromechanical behaviour of BaTiO<sub>3</sub> single domain crystals. Physical Review 80 (6): 1082-1089.

- COCHRAN, W (1961) Crystal stability and the theory of ferroelectricity II. Piezoelectric crystals. Advances in Physics 10 (40): 401-420.
- COURSEY, P R and BRAND, K G (1946). Dielectric constants of some titanates. Nature 157 (3985): 297-298.
- CROSS, L E, BIGGERS, J V and NEWNHAM, R E (1977). Ceramic piezoelectric transducers. Report number AD-A038 152.
- CROSS, L E, NEWNHAM, R E, BARSCH, G R and BIGGERS, J V (1980). Targeted basic studies of ferroelectric and ferroelastic materials for piezoelectric transducer applications. Report Number ADA 079 400/8.
- CROSS, L E, NEWNHAM, R E, BARSCH, G R and BIGGERS, J V (1981). Targeted basic studies of ferroelectric and ferroelastic materials for piezoelectric transducer applications. Report No. AD96 451/0.
- CURIE, J and CURIE, P (1880). Development of polar electricity in hemihedral crystals with inclined faces by compression. (in French). Bulletin de la Societe Mineralogique de France 3 (4): 90-93.
- DERI, M (1966). Ferroelectric ceramics (Maclaren Ltd).
- DESILETS, C S, FRASER, J and KINO, G S (1975). Transducer arrays suitable for acoustic imaging. In: 1975 ULTRASONICS SYMPOSIUM PROCEEDINGS. IEEE. pp 148-152.
- DESILETS, C S, FRASER, J and KINO, G S (1978). The design of efficient broad-band piezoelectric transducers. IEEE Transactions on Sonics and Ultrasonics SU-25 (3): 115-125.
- DEVONSHIRE, A F (1954). Theory of ferroelectrics. Advances in Physics 3 (10): 85-130.
- DIETZ, D R, PARKS, S I and LINZER, M (1979). Expanding aperture annular array. Ultrasonic Imaging 1 (1): 56-75.

- DUFFEK, E F (1970). Fine line patterning of metallized ceramics. Plating - Journal of the American Electroplaters Society 57 (1): 37-42.
- ELLIOTT, D J (1982). Integrated circuit fabrication technology (London: McGraw Hill Book Company Inc).
- FATUZZO, E and MERZ, W J (1967). Ferroelectricity (London: North - Holland).
- FOREST, W S De (1975). Photoresist - materials and processes (London: McGraw Hill Book Company Inc).
- FOSTER, F S and HUNT, J W (1978). The design and characterisation of short pulse ultrasonic transducers. Ultrasonics 16 (3) 116-122.
- FRANCOMBE, M H (1956). Polymorphism in lead metaniobate. Acta Crystallographica 9 : 683 - 685.
- FRANCOMBE, M H and LEWIS, B (1958). Structural, dielectric and optical properties of ferroelectric lead metaniobate. Acta Crystallographica 11 : 696 - 703.
- FRASER, J D (1979). The Design of Efficient, Broadband Ultrasonic Transducers PhD Thesis: Stanford University, Department of Physics.
- FREEDMAN, A (1970). Sound fields of plane or gently curved pulsed radiators. Journal of the Acoustical Society of America 48 (1) part 2: 221-227.
- GALASSO, F S (1969). Structure, properties and preparation of perovskite-type compounds. (London: Pergamon Press).
- GINZBURG, V L (1961). Some remarks on second order phase transitions and the microscopic theory of ferroelectrics. Soviet Physics Solid State 2 (9): 2031-2043. ( translated from Fizika Elektronika Tela 2 (9): 2031-2043).

- GOLDSCHMIDT, V M (1926). Geochemical distribution laws of the elements. VIII. Researches on the structure and properties of crystals. (in Norwegian). Skrifter utgitt av det Norske Videnskaps - Akademi i Oslo. 1. Matematisk - Naturvidenskapelig Klasse 2 (8): 7-156.
- GOODMAN, G (1952). Ferroelectric properties of lead niobate. American Ceramic Society Bulletin 31 (3): 113.
- GOODMAN, G (1953). Ferroelectric properties of lead metaniobate. Journal of the American Ceramic Society 36 (11): 368-372.
- GRUVER, R M, BUESSEM, W R, DICKEY, C W et al (1966). State-of-the art review on ferroelectric ceramic materials. Report number AD801027.
- HAGG, G and MAGNELI, A (1954). Recent structure investigations of oxygen compounds of molybdenum and tungsten. Review of Pure and Applied Chemistry 4 (4): 235-250.
- HAJJAR, W M (1981). Multi-focus, multi-element matrix, ultrasonic transducer for real time Doppler imaging - design, construction and evaluation. PhD Thesis: Worcester Polytechnic Institute, Department of Biomedical Engineering.
- HARRIS, G R (1981). Transient field of a baffled planar piston having an arbitrary vibration amplitude distribution. Journal of the Acoustical Society of America 70 (1): 186-204.
- HARRIS, G R, CAROME, E F and DARDY, H D (1982). Pulsed ultrasonic measurements using circular and annular polymer membrane receivers. In: 1982 IEEE ULTRASONICS SYMPOSIUM Proceedings pp 841-844.
- HASELBERG, K von and KRAUTKRAMER, J (1959). An ultrasonic transducer for materials testing with an improved near-field. (in German). Acustica 9 (5): 359-364.
- HAYMAN, A J (1977). Schlieren visualisation of focussed ultrasonic images. PhD Thesis: The City University, Department of Physics.

- HAYMAN, A J and WEIGHT, J P (1979). Transmission and reception of short ultrasonic pulses by circular and square transducers. Journal of the Acoustical Society of America 66 (4): 945-951.
- HIPPEL, A von, BRECKENRIDGE, R G, CHESLEY, F G and TISZA, L. (1946). High dielectric constant ceramics. Industrial and Engineering Chemistry 38 (11): 1097 - 1109.
- HUNTER, J L (1957). Acoustics (New Jersey: Prentice Hall Inc).
- IEEE Standard number 176 (1978) Piezoelectricity.
- IKEGAMI, S and UEDA, I (1970). Polarization and piezoelectric properties of  $PbTiO_3$  ceramics. In: INTERNATIONAL MEETING OF FERROELECTRICITY, 2nd TOKYO 1969. Proceedings. Journal of the Physical Society of Japan 28 (supplement): 331-333.
- IRE Standards on piezoelectric crystals (1949): Proceedings of the IRE 37 (12): 1378-1395.
- IRE Standards on piezoelectric crystals (1957): The piezoelectric vibrator definitions and methods of measurement, 1957. Proceedings of the IRE 45 (3): 353-358.
- IRE Standards on piezoelectric crystals (1958): Determination of the elastic, piezoelectric constants - the electromechanical coupling factor, 1958. Proceedings of the IRE 46 (4): 764-778.
- IRE Standards on piezoelectric crystals (1961): Measurements of piezoelectric ceramics, 1961. Proceedings of the IRE 49 (7): 1161-1169.
- JACKSON, W and REDDISH, W (1945). High permittivity crystalline aggregates. Nature 156 (3972): 717.
- JAFFE, B, ROTH, R S and MARZULLO, S (1954). Piezoelectric properties of lead zirconate - lead titanate solid-solution ceramics. Journal of Applied Physics 25 (6): 809-810.
- JAFFE, H and BERLINCOURT, D A (1965). Piezoelectric transducer materials. Proceedings of the IEEE 53 (10) : 1372 - 1386.

- JAFFE, B, COOK, W R and JAFFE, H (1971). Piezoelectric ceramics (London: Academic Press).
- JONA, F and SHIRANE, G (1962). Ferroelectric crystals. (London: Pergamon Press).
- KANSEY, R J (1975). Acoustic generation by non-uniform polarization in ferroelectric ceramics. PhD Thesis: University of Illinois at Urbana-Champaign, Department of Electrical Engineering.
- KASPAR'YANTS, A A (1960). Non-stationary radiation of a sound by a piston. Soviet Physics Acoustics 6 (1): 47-51. (translated from Akusticheskii Zhurnal 6 (1): 52-56).
- KERAMOS INC PIEZOELECTRICS, Lizton, Indiana. USA. Kesite Bulletins on Lead meta-Niobate.
- KERVEL, S J H van and THYSSEN, J H (1973). A calculation scheme for the optimum design of ultrasonic transducers. Ultrasonics 21 (3): 134-140.
- KODAK Ltd Hemel Hempstead (1979). Photofabrication methods with Kodak photoresists. Kodak Publication No. P-246.
- KONDRAT'EV, Yu A and KARPEL'SON, A E (1978). Formation of narrow slightly diverging ultrasonic beams. Soviet Journal of NDT 14 (10): 938-943. (translated from Deftoskopiya 14 (10): 95-102).
- KOSSOFF, G (1966). The effects of backing and matching on the performance of piezoelectric ceramic transducers. IEEE Transactions on Sonics and Ultrasonics SU13 (1): 20-30.
- KOSSOFF, G (1971). A transducer with uniform intensity distribution. Ultrasonics 9 (4): 196-200.
- KOZINA, O G and MAKAMOV, G I (1961). Transient processes in the acoustic fields generated by a piston membrane of arbitrary shape. Soviet Physics Acoustics 7 (1): 39-43. (translated from Akusticheskii Zhurnal 7 (1): 53-58).

- KRIMHOLTS R, LEEDOM, D A and MATTHAEI, G L (1970). New equivalent circuits for elementary piezoelectric transducers. Electronics Letters 6 (13): 398-399.
- LAND, C E, SMITH, G W and WESTGATE, C R (1964). The dependence of the small-signal parameters of ferroelectric ceramic resonators upon state of polarization. IEEE Transactions on Sonics and Ultrasonics SU-11 (1): 8-19.
- LEEDOM, D A, KRIMHOLTS, R, and MATTHAEI, G L (1971). Equivalent circuits for transducers having even or odd symmetry piezoelectric excitation. IEEE Transactions on Sonics and Ultrasonics SU18 (3): 128-141.
- LEES, S and DAVIDSON, C L, (1977). Ultrasonic measurement of some mineral filled plastics. IEEE Transactions on Sonics and Ultrasonics SU24 (3): 222-225.
- LOCKWOOD, J C and WILLETE, J G (1973). High speed method for computing the exact solution for the pressure variation in the near field of a baffled piston. Journal of the Acoustical Society of America 53 (3): 735-791.
- LOW, G C (1975). An Investigation into ultrasonic probes for high resolution non-destructive testing. PhD Thesis: Aberdeen University, Department of Natural Philosophy.
- LOW, G C and JONES R V (1984). Design and construction of short pulse ultrasonic probes for non-destructive testing. Ultrasonics 22 (22): 85-95.
- MAGNELI, A (1949). Some aspects on the crystal structure of tetragonal potassium tungsten bronze. Arkiv for Kemi 1 (24) : 213-221.
- MAGNELI, A. (1956). The crystal chemistry of oxygen compounds of molybdenum and tungsten containing the structural elements of  $\text{ReO}_3$  or perovskite type. Journal of Inorganic and Nuclear Chemistry 2 (5/6): 330-339.

- MALDONADO, J R and MEITZLER, A H (1971). Strain based ferroelectric-photoconductor image storage and display devices. Proceedings of the IEEE 59 (3): 368-382.
- MARTIN, F D and BREAZEALE, M A (1971). A simple way to eliminate diffraction lobes emitted by ultrasonic transducers. Journal of the Acoustical Society of America 49 (5) part 2: 1668-1669.
- MASON, W P (1948). Electromechanical transducers and wave filters 2nd edition (Princeton New Jersey: Van Nostrand Reinhold).
- MASON, W P (1950). Piezoelectric crystals and their application to ultrasonics. (London: D. Van Nostrand Company Inc).
- MASON, W P (1971). Fifty years of ferroelectricity. Journal of the Acoustical Society of America 50 (5): 1281-1298.
- MATTIAT, O E ed. (1971). Ultrasonic transducer materials (London: Plenum Press).
- MEGAW, H D (1945). Crystal structure of barium titanate. Nature 155 (3938): 484-485.
- MEGAW, H D (1946). Crystal structure of double oxides of the perovskite type. Proceedings of the Physical Society 58 (326) part 2: 133-152.
- MIYAKE, S and UEDA, R (1946). On polymorphic change of BaTiO<sub>3</sub>. Journal of the Physical Society of Japan 1 (1): 32-33.
- MORTON, N (1979). Thomas Young and the theory of diffraction. Physics Education 14: 450-453.
- NARAY-SZABO, I (1943). The structure of compounds ABO<sub>3</sub> "sister structures". (in German). Naturwissenschaften 31 (39/40): 466.
- NYE, J F (1957). Physical properties of crystals (their representation by tensors and matrices). (Oxford: Clarendon Press).
- O'CALLAGHAN, M (1974). A study of the microstructure and poling characteristics of lead zirconate titanate ceramic. PhD thesis: Brighton Polytechnic, Department of Applied Physics.

- PEERCY, P S and LAND, C E (1981). Ion-implanted PLZT ceramics: a new high sensitivity image storage medium. IEEE Transactions on Electron Devices 28 (6): 756-762.
- POHLMAN, R, DAVIDTS, D and SEMIENIUK L, (1977). A novel ultrasonic radiator with interference suppressed near field. (in German). Archiv fuer das Eisenhuettenwes 48 (3): 185-190.
- POSAKONY, G J (1975). Engineering aspects of ultrasonic piezoelectric transducer design In: 1975 ULTRASONICS SYMPOSIUM PROCEEDINGS. New York: Institute of Electrical and Electronics Engineers pp 1-9.
- RANDERAAT, J van and SETTERINGTON R E ed. (1974). Piezoelectric ceramics 2nd edition (Mullard Ltd).
- ROBINSON, D E, LEES, S and BESS, L (1974). Near field transient radiation patterns for circular pistons. IEEE Transactions on Acoustics, Speech and Signal Processing ASSP 22 (6): 395-403.
- RODERICK, R L (1951). The radiation patterns from a rotationally symmetric stress source on a semi-infinite baffle. PhD Thesis (part 2): Brown University, Department of Applied Mathematics.
- ROOKSBY, H P (1945). Compounds of the structural type of calcium titanate. Nature 155 (3938): 484-485.
- ROTH, R S (1957a). Classification of perovskite and other  $ABO_3$  type compounds. Journal of Research of the National Bureau of Standards 58 (2): 75-88.
- ROTH, R S (1957b). Unit cell data of the lead niobate  $PbNb_2O_6$ . Acta Crystallographica 10 : 437.
- ROTH, R S (1959). Phase equilibrium relations in the binary systems lead oxide-niobium pentoxide. Journal of Research of the National Bureau of Standards 62 (1): 27-38.
- SAWAGUCHI, E MANIWA, H and HOSHINO, S (1951). Antiferroelectric structure of lead zirconate. Physical Review 83 (5): 1078.

- SAWYER, C B and TOWER, C H (1930). Rochelle salt as a dielectric. Physical Review 35 (3): 269-273.
- SAYERS, C M and TAIT, C E (1984). Ultrasonic properties of transducer backings Ultrasonics 22 (2): 75-60.
- SCHOCH, A (1941). Studies of the sound field of a carbon membrane. (in German). Akustische Zeitschrift 6: 318-326.
- SHIPLEY EUROPE Ltd Coventry (1985). Shipley photoresist technical manual.
- SHIRANE, G and HOSHINO, S (1951). On the phase transition in lead titanate. Journal of the Physical Society of Japan 6 (4): 265-270.
- SHIRANE, G, SUZUKI, K and TAKEDA, A (1952). Phase transitions in solid solutions of  $PbZrO_3$  and  $PbTiO_3$  II X-ray study. Journal of the Physical Society of Japan 7 (1): 12-18.
- SHNYREV, P D and SEMIOVOVA, Z S (1980). Study of a heat treatment method for piezoelectric radiators to improve their resolution. Soviet Journal of NDT 15 (10): 912-914. (translated from Defektoskopiya 15 (10): 104-106).
- SILK, M G (1983). Prediction of the effect of some constructional variables on the performance of ultrasonic transducers. Ultrasonics 21 (1): 27-33.
- SKUDRZYK, E (1971). The foundations of acoustics (New York: Springer Verlag).
- SMITH, A, WILKINSON, S J and REYNOLDS, W N (1974). The Elastic Constants of Some Epoxy Resins. Journal of Materials Sciences 9 (4): 547-550.
- STEPANISHEN, P R (1971). Transient radiation from pistons in an infinite planar baffle. Journal of the Acoustical Society of America 49 (5) part 2: 1629-1638.

- STEPANISHEN, P R (1981). Acoustic transients from planar axisymmetric vibrators using the impulse response approach. Journal of the Acoustical Society of America 70 (4): 1176-1181.
- STRUTT, J W (Lord Rayleigh) (1945). Theory of sound - Volume 2 chapters 11 and 14 (New York Dover).
- SUBBARAO, E C (1960). X-ray studies of phase transitions in ferroelectric  $\text{PbNb}_2\text{O}_6$  and related materials. Journal of the American Ceramic Society 43 (9): 439-442.
- SWARTZ, R G, PLUMMER, J D and MEINDL, J D. (1979). An improved wedged-type backing for piezoelectric transducers. IEEE Transactions on Sonics and Ultrasonics SU62 (2): 140-142.
- SZABO, T L (1975). Acoustic beam shaping and diffraction from tapered amplitude distributions. In: 1975 IEEE ULTRASONICS SYMPOSIUM Proceedings pp 116-119.
- TUPHOLME, G E (1969). Generation of acoustic pulses by baffled plane pistons. Mathematica 16: 209-224.
- VALASEK, J (1921). Piezoelectric and allied phenomena in Rochelle salt. Physical Review 17 (4): 475-481.
- VALASEK, J (1922). Piezoelectric activity of Rochelle salt under various conditions. Physical Review 19 (5): 478-491.
- VALASEK, J (1924). Dielectric anomalies in Rochelle salt crystals. Physical Review 24 (5): 560-568.
- WADSLEY, A D (1955). Crystal chemistry of stoichiometric compounds. Review of Pure and Applied Chemistry 5 (3): 165-193.
- WEIGHT, J P (1975). Instrumentation associated with the development of wide-band ultrasonic techniques (ultrasonic spectroscopy). MPhil Thesis: The City University, Department of Physics.

- WEIGHT, J P and HAYMAN, A J (1978). Observations of the propagation of very short ultrasonic pulses and their reflection by small targets. Journal of the Acoustical Society of America 63 (2): 396-404.
- WEIGHT, J P (1982a). Improved resolution transducers, systems and methods for the transmission and/or reception of waves propagated by vibration. United Kingdom Patent number 2094100.
- WEIGHT, J P (1982b). The propagation and reception of wide-band ultrasonic pulses PhD Thesis: The City University, Department of Physics.
- WEYNS, A (1980). Radiation field calculations of pulsed ultrasonic transducers. Ultrasonics 18 (4): 183-188.
- WILLSON, K, LEEMAN, S and LLOYD, E A (1977). Etched arrays for medical imaging. In: CONFERENCE ON THE EVALUATION AND CALIBRATION OF ULTRASONIC TRANSDUCERS, LONDON 1977. Proceedings, IPC Science and Technology Press (Guildford).
- WUL, B and GOLDMAN, I M (1945). Dielectric constant of barium titanate as a function of strength of an alternating field. Comptes Rendus (Doklady) de l'Academie de Sciences de l'USRR 49 (3): 177-180. (translated from Doklady Akademii Nauk SSSR 49 (3): 179-182).
- YING, C F, Li M X and ZHANG H L (1981). Computations and measurements of transient stress waves and electrical voltages generated by transmitting ultrasonic piezoelectric transducers. Ultrasonics 19 (4): 155-158.